1984

Heat transfer enhancement downstream of vortex generators on a flat plate

Aly Youssef Turk
Iowa State University

8505877

Turk, Aly Youssef

HEAT TRANSFER ENHANCEMENT DOWNSTREAM OF VORTEX GENERATORS ON A FLAT PLATE

Iowa State University PH.D. 1984

PLEASE NOTE:

In all cases this material has been filmed in the best possible way from the available copy. Problems encountered with this document have been identified here with a check mark ✓.

1. Glossy photographs or pages ______
2. Colored illustrations, paper or print ______
3. Photographs with dark background ______
4. Illustrations are poor copy ______
5. Pages with black marks, not original copy ______
6. Print shows through as there is text on both sides of page ______
7. Indistinct, broken or small print on several pages ✓
8. Print exceeds margin requirements ______
9. Tightly bound copy with print lost in spine ______
10. Computer printout pages with indistinct print ______
11. Page(s) ______ lacking when material received, and not available from school or author.
12. Page(s) ______ seem to be missing in numbering only as text follows.
13. Two pages numbered ______. Text follows.
14. Curling and wrinkled pages ______
15. Other ______

Heat transfer enhancement downstream of vortex generators on a flat plate

by

Aly Youssef Turk

A Dissertation Submitted to the

Graduate Faculty in Partial Fulfillment of the

Requirements for the Degree of

DOCTOR OF PHILOSOPHY

Major: Mechanical Engineering

Approved:

Signature was redacted for privacy.

In Charge of Major Work

Signature was redacted for privacy.

For the Major Department

Signature was redacted for privacy.

For the Graduate College

Iowa State University
Ames, Iowa

1984

TABLE OF CONTENTS

NOMENCLATURE

A_s	Area of strip surface, ft^2.
C_p	Specific heat of air, Btu/lbm°F.
c_0, c_1	Constants, equation (22).
$D_{u(x,z)}$	Mean velocity decay factor, equation (24).
E_m	The dc voltage output from hot-film anemometer, volts.
e_g	Height of a vortex generator blade, in.
g_c	Dimensional constant, 32.2 lbm-ft/lbf-sec^2.
$\bar{h}_g$	Overall convective heat transfer coefficient with vortex generators present, Btu/hr-°F-ft^2.
$\bar{h}_o$	Overall convective heat transfer coefficient with no vortex generators present, Btu/hr-°F-ft^2.
$h_{(x)g}$	Local span-averaged heat transfer coefficient with vortex generators present.
$h_{(x)o}$	Local heat transfer coefficient with no vortex generators present.
$h_{(x,z)g}$	Local heat transfer coefficient with vortex generators present.
I	Current, amp.
k_a	Thermal conductivity of air evaluated at the mean boundary layer temperature, Btu/hr-°F-ft.
k_p	Thermal conductivity of the plate material, Btu/hr-°F-ft.
L	The tested plate length, in.
l_g	Length of a vortex generator blade, in.
m_0, m_1, m_2	Constants, equation (23).
P_{atm}	Atmospheric pressure, in. Hg.
P_o	Total pressure of air inside the wind tunnel, in. water.

$P_{s(x)}$	Static pressure of air at x-distance from the plate leading edge, in. water.
Q	Heat rate input to a strip, Btu/hr.
Q_c	Energy loss by conduction.
Q_n	Net energy loss by convection.
Q_r	Energy loss by radiation.
R_{air}	The gas constant for air.
$Re_{(x)}$	Reynolds number based on a x-distance from the leading edge.
R_r	Resistance of the strip at temperature t_s, ohm.
R_s	Resistance of the strip at reference temperature t_r, ohm.
S	The hot-film sensitivity factor, volt/(ft/sec).
S_g	Pitch between pairs of the blades forming a pair of counter-rotating vortex generator blades, in.
s_g	Space between vortex generator blades, in.
$St_{(x)g}$	Local span-averaged Stanton number with vortex generators present.
$St_{(x)o}$	Local Stanton number with no vortex generators present.
T	Absolute temperature, °R.
Tu %	Turbulence intensity, %.
t_b	Temperature of the back side of the working surface, °F.
t_s	Temperature of the heated strip surface, °F.
U_m	The effective mean velocity, ft/sec.
U_o	Free-stream velocity at the leading edge, ft/sec.
$U_{o(x)}$	Free-stream velocity at a distance x from the the leading edge, ft/sec.
u	Velocity in x-direction in boundary layer.

$\tilde{u}$ — Root mean square of fluctuating velocity in x-direction in boundary layer, ft/sec.

W_{ϕ} — Uncertainty in any quantity ϕ, equation (25).

x — Distance measured parallel to the surface of plate, distance from leading edge, coordinate direction.

x_g — Location of vortex generator blades.

y — Distance measured perpendicular to surface of plate, coordinate direction.

y_p — Thickness of the plate working surface, in.

z — Distance measured spanwise to the surface of plate, coordinate direction.

α_g — Angle between a vortex generator blade and the on coming flow, degree.

α_s — Temperature coefficient of resistivity for the strip, 1/°F.

δ — Boundary layer thickness.

δ_g — Laminar boundary layer thickness edtimated at the location of vortex blades.

ϵ_s — Emissivity of the strip material.

ζ_g — Thickness of a vortex generator blade.

Λ_x — Pohlhausen's parameter defined in equation (21).

ν_a — Kinematic viscosity of air evaluated at the mean boundary layer temperature.

ξ — Unheated length of the plate.

ρ_a — Density of air.

σ — Stefan-Boltzmann constant.

Φ_p — Nonedimensional pressure gradient parameter, $[(\nu_a/U^2_{o(x)})(dU_o/dx)]$

I. INTRODUCTION

A. Rationale for Investigation

The main object of heat transfer analysis is to find ways of predicting heat transfer rates. Prediction of convective heat transfer rates requires calculation of heat transfer coefficients, values of which are governed by the type and the flow conditions of fluid involved in the heat transfer process and by the geometrical aspects of the containing walls. For convective processes involving heat transfer to or from a surface exposed to a fluid stream, the coefficient of heat transfer h is defined by the equation

$$Q = h A_s (t_s - t_o) \quad (1)$$

where Q is the heat transfer rate to or from the surface, A_s is the area of the surface, t_s is the surface temperature and t_o is the fluid temperature. For a given temperature difference, high heat transfer coefficients require less surface area and reduce the size, weight and cost of an exchanger. Improving convection heat transfer coefficients by various means is usually called augmentation or enhancement of convective heat transfer.

There are many techniques for augmenting convective heat transfer [1]. The work described in this thesis is directed at single-phase flows over flat surfaces with constant-heat-flux on which boundary layers exist, similar to the flows in many types of heat exchange equipment. Technically, constant-heat-flux problems arise in a number of situations: electric resistance heating, radiant heating and in counter flow heat exchangers when the heat capacity rates are the same. Recent work on plates and plate arrays suggests improvements in convection heat transfer are possible by creating unsteady or turbulent flows to alter the boundary layer.

Surface geometry modification such as surface protrusions or vortex generators alters the ordinary flow pattern and fluid distribution along the wall surface and enables mixing of slower fluid near the wall surface with the faster fluid from the outer region of the boundary layer. The 'akes downstream of the geometry modifications introduce longitudinal trailing vortices into the boundary layer which sweep the surface, and break up the laminar sublayer and increase the turbulence near the plate surface. In other words, if the level of mixing within the boundary layer is raised artificially by a vortex generator it leads to a thinner or more turbulent boundary layer [2]. Heat transfer coefficient for the surface is also increased because the motion of the external stream fluid toward the wall, reducing the temperature difference for a constant heat flux surface.

The work presented in this study is directed toward use of vortex generators attached to a plate surface as a means to improve heat transfer coefficients by introducing boundary layer fluid mixing in laminar flows.

Vortex generators may be characterized by whether the vortices produced rotate in the same or opposite directions. A vortex generator which produces vortices that turn in the same direction is known as a co-rotating generator. If the vortices are in the opposite sense, they are called counter-rotating vortices. Both types are schematically shown in Figure 1 together with the geometric nomenclature for typical configurations. The nomenclature for the co-rotating generator includes the spacing of the blades s_g, the blade height e_g, the blade length l_g, the blade thickness ζ_g and the angle to the oncoming flow α_g. For the counter-rotating generator, the pitch S_g between pairs of the blades is an additional parameter. The blades shown are rectangularly shaped, but other shapes such as triangles or trapezoids could be used. Moreover, the plane of the blades of either type may be tilted from the vertical at an angle β_g.

B. Literature Survey

The work of Chang [2] notes that the principle of boundary layer control by vortex generators relies on the increased mixing between the external stream and the boundary layer that is promoted by streamwise vortices trailing over the surface. Fluid particles with high momentum in the stream direction are swept in along helical paths towards the surface to mix with and to replace the slower fluid at the surface, which in turn is swept out away from the surface. The main streamwise momentum of the fluid particles in the boundary layer is increased and the skin-friction coefficient will increase where high velocities occur near the surface. Reynolds' analogy then suggests that the heat

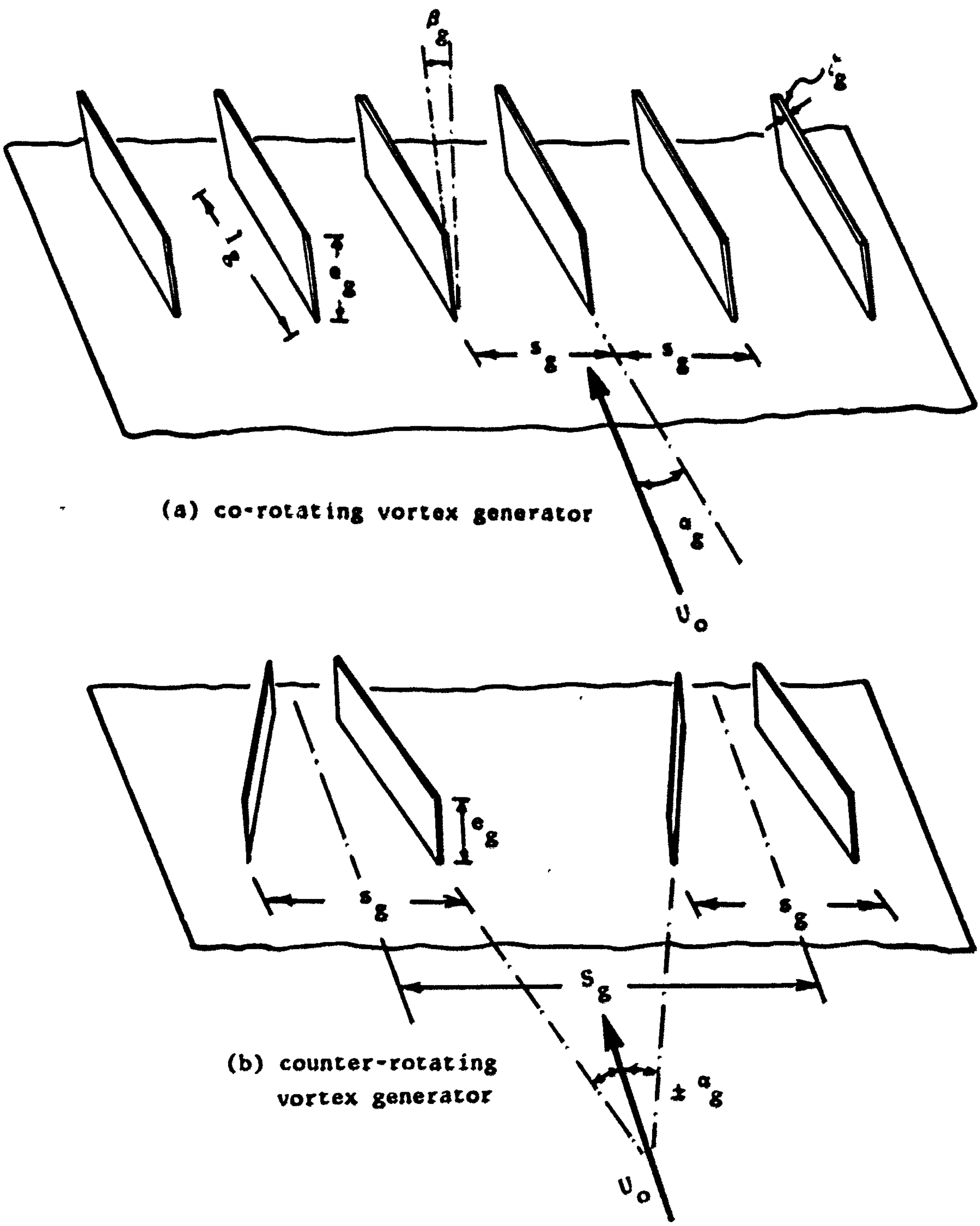

Figure 1. Schematic of vortex generators

transfer rate over the plate surface will increase due to increased skin-friction coefficient.

Pearcey [3], in studies of boundary layer control by vortex generators, found that the most important single factor in establishing an effective vortex pattern was the need to have optimum spacing of vortices. He indicated that a useful pattern could be achieved for co-rotating vortex generators if the spacing of the vortices was greater than about three times their height. For a smaller spacing, the vortices tended to damp one another and failed to maintain high velocities at any point in the cross-section of the boundary layer and vortex flow.

Pearcey indicated that the induced velocities for counter-rotating systems caused the array of vortices to change substantially as they moved downstream. In a system in which all vortices were equally spaced, it was shown that the vortices were effective in delaying boundary layer separation with extensive high energy regions occurring in which the boundary layer was kept thin between alternate pairs of vortices, and the low energy fluid was swept out between the intermediate pairs of vortices. Further downstream, the centers of vortices moved closer together in pairs and further away from the surface, and the vortices eventually damped out. Pearcey suggested a "Bi-plane" system that was essentially a combination of two or more rows of counter-rotating generators, which could be used to accelerate and improve the mixing within the boundary layer and keep the vortices adjacent to the surface further downstream.

Pearcey [3] discussed contributions to the drag due to the vortex blades, including the drag on the blades themselves and the increased skin friction on the surface due to the vortex action. These contributions were, to a greater or smaller extent, offset by the reduction in form drag of the surface because of the reduction in the boundary layer displacement effect. The net drag penalty was a balance between the opposing contributions and this was probably why it was usually reasonably small, and also why observations of its magnitude vary widely from one application to another.

Schubauer and Spangenberg [4] investigated the importance of mixing in boundary layers and in particular of forced mixing produced by vortex generators and other mixing devices. This investigation was conducted on a two-dimensional turbulent boundary layer formed on the wind tunnel floor in a special wind tunnel able to produce a variety of free-stream adverse pressure gradients. Each type of mixing device was arranged in a row perpendicular to the main flow direction on the bottom of the wind tunnel with a mixing device height of the order of the boundary layer thickness at the installation postion. The main objective was to compare the effect of increasing the mixing within the boundary layer with the effect of reducing the pressure gradient on boundary layer development and separation.

The conclusions reached from this investigation were that the mixing devices could be used to assist flow against an opposing pressure gradient by delaying the separation and giving the same effect on the boundary layer as a general reduction in pressure gradient. A spanwise variation in boundary layer longitudinal velocities was observed in the region downstream of the mixing devices. The amount of spanwise variation decreased with increasing distance downstream. The boundary layer displacement thickness with the mixing devices is generally less than that without mixing devices obtained at the same location. A small increase in momentum thickness over that obtained at the same location in the absence of the mixing devices was observed.

A conclusion of Schubauer and Spangenberg [4] is that use of vortex generators will lead to a thinner boundary layer and increased skin-friction coefficient where high velocities occur near the wall. As noted previously, according to Reynolds' analogy, the rate of heat transfer is also expected to increase.

Recently, vortex generators have been a parameter in investigations concerning enhancement of heat transfer coefficients. After an extensive literature search, only a few studies on heat transfer enhancement downstream of vortex generators were found.

It is common practice to treat heat transfer over a cylinder with very large diameter as being a close approximation to heat transfer over a flat surface. An early heat transfer investigation by Johnson and Joubert [5] was a starting point for use of vortex generators as an aid to enhancement heat transfer rate over a flat plate surface.

Johnson and Joubert [5] presented data for an experimental investigation of the effect of vortex generators on drag and heat transfer for a 6-inch diameter circular cylinder in crossflow in a wind tunnel. Two cylinders were used, one for measurement of drag and the other for measurement of heat transfer. The cylinder used for drag tests was supported on a strain gauge drag balance for measuring total drag, and had 36 pressure taps for measuring form drag. The outer surface of the cylinder used for heat transfer tests was electrically heated by a strip of Nichrome ribbon, and the inner surface was maintained at a constant temperature by using condensing steam at atmospheric pressure inside the cylinder. The heat input to the strip was controlled to adjust the strip temperature to correspond with that of the inner surface of the cylinder so that the total heat generated in the strip was convected to the air. Local coefficients were obtained from the circumferential temperature distributions and the electrical power input to the strip.

One configuration of a row of triangular co-rotating vortex generator blades was used. The blades were cut and bent from a continuous strip of 0.020 in. tinplated steel to form equally spaced right triangular blades with an angle of incidence $\alpha_g = 10$ degrees to the flow direction. The blade geometry based on the nomenclature in Figure 1 had a blade height $e_g = 0.20$ in., and a transverse space between the vortex generator blades $s_g = 0.80$ in. The cylinder was fitted with two similar rows of vortex generators which were symmetrically placed parallel to the front stagnation line. The angular postion of the rows from the front stagnation line was varied.

Meaurements were made both with and without vortex generator blades on the outer surface of the cylinder. The results showed that the drag coefficient decreased when the vortex generator blades were used, and that the location of the vortices had a large effect on the drag coefficient by changing the critical Reynolds number. The further the vortex generators were from the front stagnation line of the cylinder, the lower was the critical Reynolds number, and the higher the supercritical drag coefficient.

Johnson and Joubert [5] qualitatively determined the effect the vortex generators had on the surface shear stress by using a modified oil-film technique to obtain photographs of the flow pattern over the outer surface of the cylinder. The photographs showed that immediately behind the vortex generator strip there were regions where the film was completely removed by the generated turbulence. Moreover, the presence of trailing vortices caused the separation line to become wavy with a period equal to the space between the vortex generator blades.

The heat transfer results showed that the vortex generators had a large effect on the local rates of heat transfer causing increases of 200 percent in some positions over the surface of the cylinder. The magnitude of the local heat transfer coefficient downstream of the vortex generators was found to reach a maximum in two regions, the first immediately behind the generator station, and the second in the region around the separation point. In the first region, improvement of the heat transfer coefficient was caused by the vortices transferring momentum into the boundary layer and, to some extent, by the effect of the disturbances generated in the flow as it crosses the vortex generators. Johnson and Joubert indicated that the improvement of the heat transfer coefficient which occurred at the separation was quite unusual, and they believed that the process of the separation was affected in some way by the presence of the vortices and high turbulence. However, the increase in overall heat transfer rates was limited by reduced local heat transfer at the rear of the cylinder. The net overall increase in Nusselt number varied from 7 to 17.5 percent over a range of Reynolds numbers based on cylinder diameter ranging from 4×10^4 to 3×10^5.

From the drag and heat transfer results, Johnson and Joubert suggested that the choices of the position of the vortex generators referenced to the front stagnation line had to comply with conflicting requirements. For example, the generators placed at a larger angle from the front stagnation line showed a greater improvement of heat transfer rates, while those placed close to the front of the cylinder had a larger area of surface over which the vortices swept.

Edwards and Alker [6] carried out an investigation on the improvement of forced convection heat transfer on a flat plate by using surface protrusions in the form of cubes and vortex generators. The protrusions were attached to the lower wall of a wind tunnel with a working section heated electrically with a uniform heat flux. Local heat transfer coefficients were determined by measuring the local surface temperature and the local free-stream air temperature. Spot temperature readings were made using a luminescent phosphor technique. All cubes and vortex generator blades were one inch high, and each type was arranged in a single row normal to the flow direction. The local transverse distribution of heat transfer coefficient was measured at five locations downstream of the surface protrusions.

The single row of cubes was tested at transverse spaces s_g of 3, 4 and 6 in. between cubes. A row of co-rotating vortex generator blades was formed of vertical right triangular blades with vertical rear edges and a length l_g = 2 in. on the heated surface which similar to those tested by Johnson and Joubert [5]. This configuration of co-rotating vortex generators was tested at equal transverse spaces s_g between the blades of 2, 3 and 4 in. and for two angles α_g = 12.5 and 25 degrees between the vortex blades and the oncoming flow.

Two configurations of rectangular counter-rotating vortex generator blades were also tested with a length l_g = 1.25 in. on the heated surface. The transverse space between two blades forming a vortex pair was 1.25 in., and the transverse pitches of pairs of counter-rotating vortex generators S_g were 3 and 4 in. All configurations were placed at an angle equal of ±15 degrees between the vortex blades and the duct axis.

Edwards and Alker indicated that an improvement in the local heat transfer coefficient was obtained for all types of systems. For the row of cubes, it was found that the highest local improvement was immediately downstream of the cubes, but their effect reduced rapidly further downstream. For the vortex generators, it was observed that their effect on the improvement of the local heat transfer coefficient extended further downstream. The co-rotating vortex generator with the smaller transverse spaces between the blades improved local heat transfer coefficients more than that obtained with larger spaces. The most persistent improvement was obtained with the counter-rotating vortex flow structure, especially with the the smaller pitch arrangement.

Lee [7,8,9,10] carried out investigations to study the effect of a system of vortices in the space between the plate fins of a finned cooling tube. Tests were done in a special wind tunnel in which it was possible to mount various forms of vortex generators on the plate fins and to observe and measure the vorticity field generated in the space between the fin plates and the cooling tubes to which they were attached.

As the first step in his investigations, Lee [7] performed experiments to find out whether or not vortices could be established between the cooling fins at low Reynolds numbers. He made a 6-times scale model of the fin tube pair and ran it at about 3 fps air speed.

Five types of vortex generators were tested with angles of incidence α_g = 15, 20, 25 and 30 degrees between the vortex generator and the main flow direction. The first and second types were triangular and rectangular blades respectively with e_g = 0.5 in. and l_g = 2.0 in., and each type was mounted normal to a solid aluminum fin plate. The third type was as a ramp running from one plate to the plate above it. The fourth type was two parallel rectagular blades, each with e_g = 0.625 in. and l_g = 2.0 in., punched up out of a plane which was inclined to the main flow direction. The last type was a bulge embossed on the fin plate with e_g = 0.625 in., l_g = 3.0 in. and ζ_g = 0.625 in. The embossed vortex generator was tested with two equal transverse spaces between the blades s_g = 2.5 and 4.0 in.

Each type of vortex generator was mounted in two rows, one just behind the leading edge of the fin, the second about half way back along the fin with an opposite angle of incidence to that of the first row. The second produced co-rotating vortices with a sense opposite to those produced by the first row.

A yaw vane was used to measure the average flow direction. The vane was placed a distance downstream of the vortex generator being studied, and moved cross-stream to get the angular deflection of the flow. The maximum angular deflection of the yaw vane was considered proportional to the maximum strength of the vortex. However, due to friction and imperfections of balance, the results from the vane were unreliable.

Flow observations with a smoke generator were used to see whether or not it was possible to establish a system of vortices and to study the flow pattern to confirm if the yaw vane measurements were valid. The results showed that for a range of incidence angle from 15 to 20 degrees the punched-up rectangular blade and the embossed vortex generator seemed to be the most effective types of vortex generators.

Lee's second experiments [8] were carried out to measure the amount by which heat transfer was increased due to the vortices and to measure the increase in air flow resistance. The investigation was done on two sets of aluminum fins 0.016 in. thick spaced eight to the inch, with each set soldered to a steam tube. The vortex generators tested were embossed, and the fin plate was 6 in. wide by 1 in. deep. Each embossed vortex generator had $\zeta_g = 0.03$ in., $l_g = 0.36$ in., with $s_g = 0.33$ in. between adjacent blades. The height of the vortex generator e_g was approximately half the distance between the adjacent fin plates forming a channel.

Steam was provided by an electrically heated boiler, and air was drawn through the cooling fins by means of a small adjustable speed fan. The overall rate of heat transfer for various flow rates was obtained by measuring the rise in air temperature and the air mass flow rate. The Reynolds number was based on flow velocity between the fins and on the clear distance between them. Measurements were made both with and without the embossed vortex generators.

The results indicated that at a mass velocity of 1.2 $lb_m/ft^2.sec$ the increase in heat transfer rate was approximately 50 percent over that for the plain fin. The improvement in heat transfer rate was reduced with decreasing air flow rate and reached about 30 percent at an air flow rate of 0.4 $lb_m/ft^2.sec$. It was also found that the pressure drop across the fin tubes was increased by 28 percent at an air flow rate of 1.2 lb_m/ft^2.sec.

Lee noted that the relationship between the flow pattern observed in [7] and heat transfer rate data obtained in [8] was not precise due to the effect of roughness and small irregularities produced in the manufacture of the fins. Measurements of the electrical power to the boiler were made so that it could be compared with the power represented by the heating of the cooling air, and it was found that the electrical power was approximately 30 percent greater than the energy absorbed by the air. No indications of loss calculations were given.

Lee [8] indicated that the vortices became weaker as they flowed downstream of the vortex generators and suggested the addition of two more rows of vortex generators at the middle of the fin plate similar to those at the front edge to improve the vortex pattern over the entire fin plate surface.

Lee [9] performed experiments on an array of fintubes with rectangular fins with vortex generators, to measure the improvement of heat transfer rate and the increase of the pressure loss. The array was 18 in. square in frontal area with fins 6 in. long by 1 in. wide, spaced 10 to the inch. An embossed vortex generator configuration was adopted similar to those suggested in Reference [8], with a height of 0.05 in. Steam was generated in a boiler to maintain the heat exchanger tubes at a uniform temperature. Air was drawn through the test array from a suction chamber and the heat transfer rate was calculated from the air temperature rise and the air flow rate. Pressure differentials were measured across the test array.

Heat transfer and pressure drop were measured at varying air flow rates, and the Reynolds number was calculated using the hydraulic diameter of the fin passage and the net air mass flow. The results obtained for the array over a range of Reynolds numbers from 300 to 2,500 showed that there was a 50 percent average increase in heat transfer rate and about 17 percent increase in pressure loss.

Further tests were done to assess the effects on heat transfer and pressure loss of adding vortex generators to rectangular plate fins such as might be used in an automotive radiator [10]. Low-conductivity models of the plate fins were made at about five times full scale, each with a set of vortex generators. The vortex generator blades were rectangular blades and their arrangement was based on the earlier investigations [7,8] for the embossed vortex generators. Each rectangular vortex blade had $e_g = 0.25$ in. and $l_g = 1.0$ in., and the space between each adjacent blade s_g was 1.4 in.

Heat transfer rates were measured using a technique of observing the melt-line of a temperature-sensitive paint applied to the plate surface. The method used was to immerse a cool, painted plate fin quickly into a hot airstream generated by a heater in the wind tunnel. The time and the progression of the melt-line across the fin plate was observed through a television camera and recorded on a video-tape recorder. By using the time-temperature data together with the solution of the unsteady conduction temperature field equation for the fin, the rate of rise of the temperature of the fin material was related to the heat transfer rate and the instantaneous local heat transfer coefficients were obtained as a function of time. Mean values of local heat transfer coefficient were estimated for different regions downstream of the vortex generators, and a value of the overall heat transfer coefficient over the fin plate surface was obtained. It was found that adding the vortex generators increased the heat transfer coefficient over the plate surface by about 40 percent, and the increase in the pressure drop was about 15 percent.

A recent investigation was carried out by Russell et al.[11] to study the effects of vortex generators on heat transfer from a rectangular plate-fin surface at a uniform temperature. The investigation was based on the results obtained by Lee [7,8,9,10]. Russell et al.[11] investigated the spanwise variation of heat transfer coefficient downstream of the vortex generators at a Reynolds number of about $2x10^3$ for the model used by Lee [10]. The spanwise distribution of the local heat transfer coefficient showed that a higher improvement of heat transfer rate was always associated with the region of lower velocity .

The purpose of the vortex generators is to provide enhancement of heat transfer on the surface to which they are attached. The previous investigators indicated agreement about the improvement in performance of vortex generators in heat transfer augmentation. However, data available in the open literature give the effects of unrelated configurations of vortex generators on heat transfer enhancement. As an example, Edwards and Alker [6] investigated enhancement of local heat transfer coefficients for only one height of vortex generator blades. Lee [7,8,9,10] and Russell et al.[11] investigated the overall heat transfer coefficient over a fin plate and arrays of rectangular fins. No complete parametric data have been found for both the local and overall heat transfer coefficients downstream of a configuration vortex generators. Moreover, in all the above investigations, the vortex generator blades were attached to the heated surface, and the heat transfer enhancement was due not only to the influence of the vortex generator, but also to the vortex generator blades acting as extended surfaces. In addition, only qualitative fluid dynamic aspects were investigated to determine how and why enhancement is obtained.

C. Scope of Investigation

The present investigation was conducted in order to better understand the augmentation of forced convective heat transfer when a single row of counter-rotating vortex generator blades is attached to a flat surface. The major emphasis of this investigation is to study the way in which vortex generators augment the heat transfer coefficient of an initially-laminar boundary layer over a flat, constant-heat-flux surface exposed to favorable free-stream pressure gradients. Particular emphasis is placed on the relationship between the geometry of vortex generators and the augmentation of local and overall heat transfer coefficients and on the behavior of the boundary layer downstream of the vortex generators.

A general expression for the parameters investigated at a local point of measurement can be written as

$$St_{(x,z)} = f\,[\,Re_{(x)},\ (dp/dx),\ (s/e)_g,\ (e/\delta)_g\,] \qquad (2)$$

where $St_{(x,z)}$ is the local Stanton number, $Re_{(x)}$ is the local Reynolds number, (dp/dx) is the free-stream pressure gradient, e_g is the height of the vortex generator blade measured from the plate surface, δ_g is the boundary layer thickness at the distance x_g from the plate leading edge, and s_g is the transverse space between the vortex generator blades. The system parameters outlined above in equation (2) are described in detail in Chapters II and III.

This dissertation includes results of an experimental investigation of the heat transfer augmentation achieved by twelve configurations of rectangular blade vortex generators with three favorable pressure gradients impressed on the plate surface.

The flow pattern within the boundary layer is investigated for certain conditions in order to understand the interaction between the flow structure and the expected improvement of the heat transfer rate and a set of guidelines for the design of more efficient surface is proposed.

II. EXPERIMENTAL APPARATUS

A. General

The investigation was carried out in the Subsonic Fluid Flow Facility of the Mechanical Engineering Department, Iowa State University.

B. Air Flow Facility

The air flow facility used was an open circuit suction type wind tunnel utilizing a centrifugal fan with a nominal flow capacity of 13,400 cfm at a head of 20.8 inches of water, and driven by a 60 horsepower motor. Figure 2 shows the general configuration of the tunnel. The air flow rate is controlled by a combination of dampers and fan inlet guide vanes. Details of the test section are shown in Figure 3. The test section of the tunnel is 14 in. square in cross-section and 66 in. long, and is constructed of Plexiglas plastic and aluminum. The test plate was mounted in the test section with its leading edge 23 in. downstream from the test section entrance. The coordinate system shown was adopted to describe locations in the flow. The test section wall facing the test plate surface had four slots located at different postions in the x-direction to permit insertion of instrument probes to survey the flow downstream of the vortex generators.

Velocity profiles at the upstream end of the test section without a model present were uniform within one percent over the range of

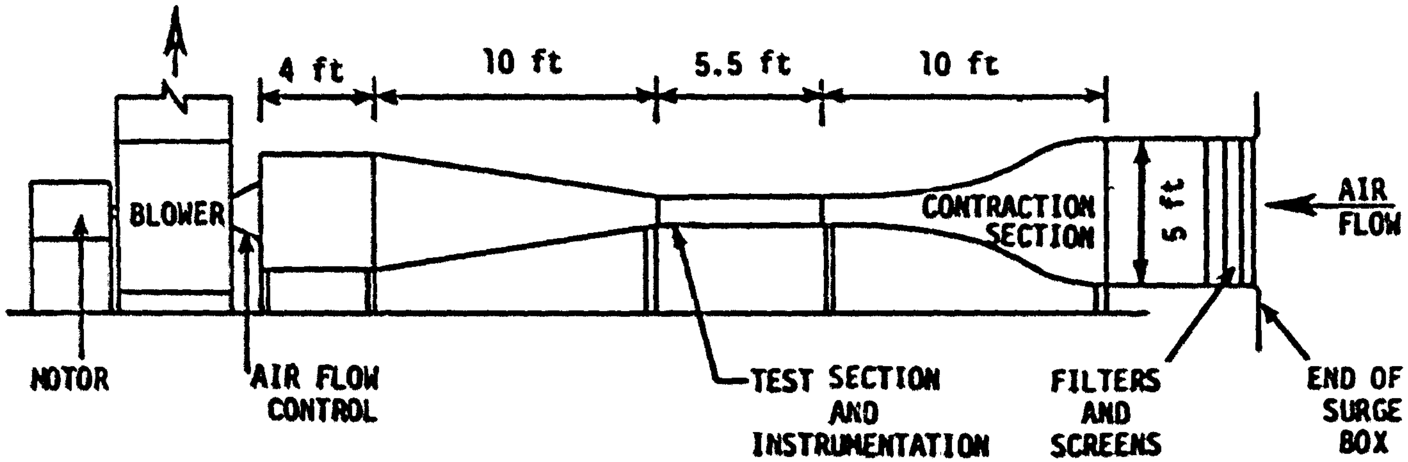

Figure 2. Air flow facility

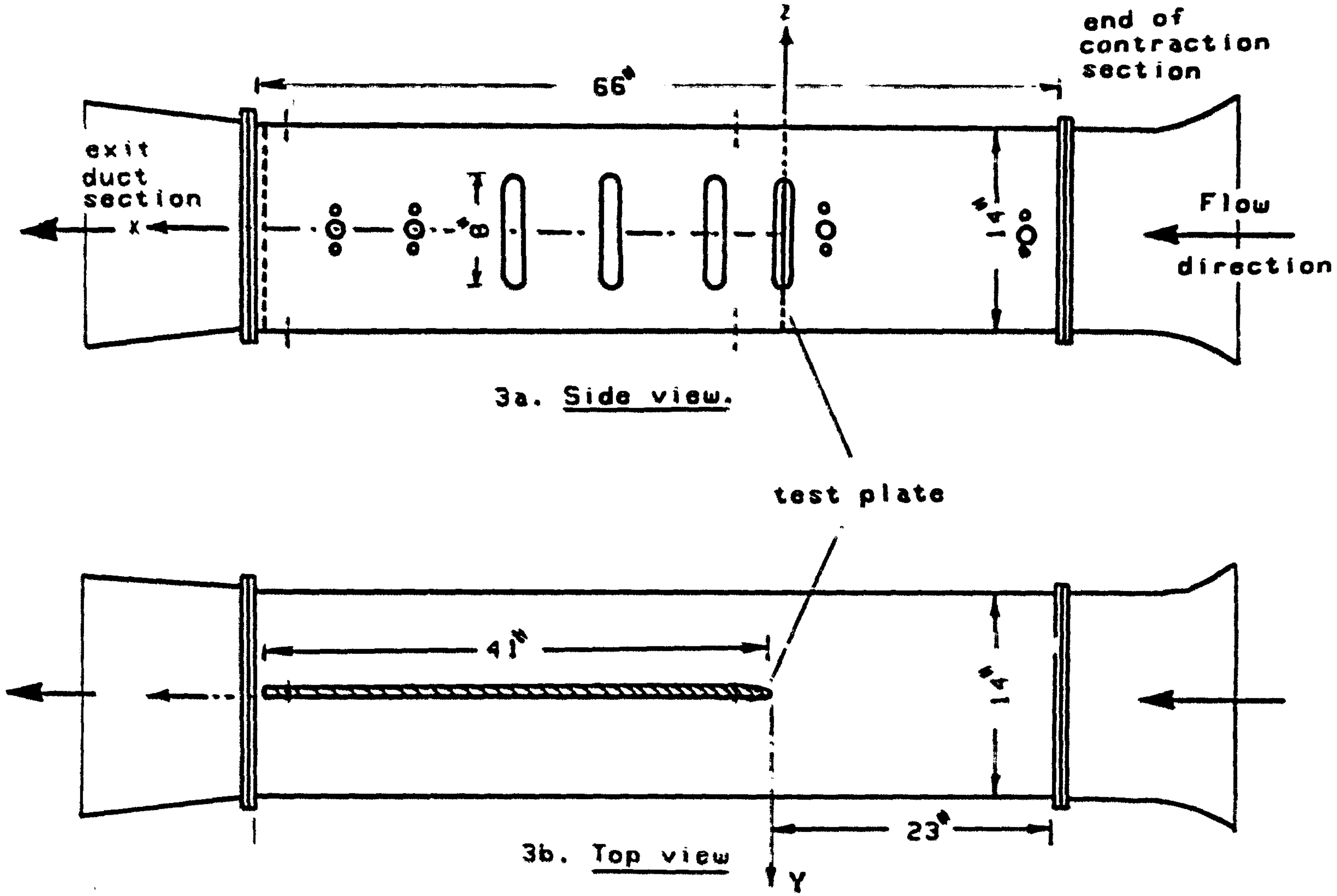

Figure 3. Test section with test plate

velocities involved in this investigation. The free tunnel had a minimum streamwise turbulence intensity of 0.35 percent at a velocity of 100 fps, and maximum streamwise turbulence intensity of 0.50 percent at a velocity of 10 fps.

C. Flat Plate

The flat plate used was similar to those used by Feiler and Yeager [12], Junkhan and Serovy [13], and Blair and Werle [14] among others. The plates in Reference [12] and [14] were approximations to constant heat flux surfaces similar to the plate described below. The assembled plate was 14 in. wide, 41 in. long and 1 in. thick. It was composed of five major parts - a nosepiece, heat transfer working surface, a plate back with supporters and ribs, and two side rails. The arrangement of these parts is shown in Figure 4.

1. Plate parts

The nosepiece was constructed of aluminum 2.25 in. long and 1 in. thick. The leading edge of the nosepiece was formed as a half ellipse section to aid in maintaining a stable stagnation point. A spanwise removable strip 1 in. wide and 0.25 in. thick was inserted in the top of the nosepiece flush with the plate surface. The spanwise strip could be replaced by a similar one with vortex generator blades mounted on it.

Electric resistance heaters were used to approximate a uniform heat flux on the surface. The metal foil heaters employed were composed of 34 transverse strips of nickel-chromium resistance alloy commercially

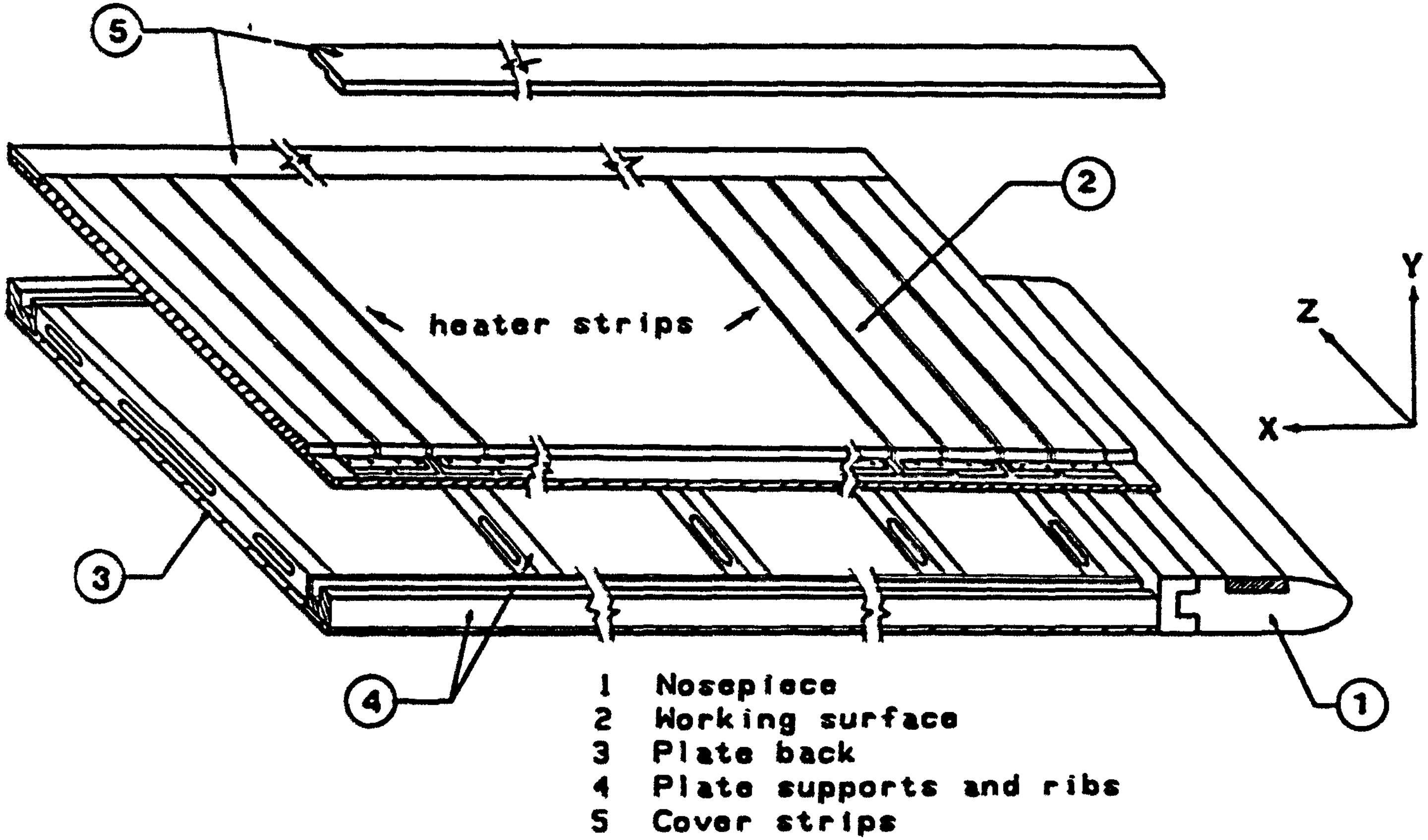

Figure 4. Expanded view of the major plate parts

known as Nichrome V, each 1 in. long, 0.002 in. thick and 12 in. wide on the working surface. The strips were mounted on the working surface, which was made from a paper-laminated phenolic commercially known as Garolite NEMA grade "C", by use of a neoprene adhesive type F-1 commercially known as Carboline. The strips were spaced 0.0625 in. apart on the working surface to allow static pressure taps of stainless steel tubing to be installed between strips. The resulting 0.0625 in. by 0.002 in. spanwise grooves were filled with a high-temperature Dekhotinsky cement and each space was carefully checked to assure a smooth working surface. These spaces are very small and occupied only a small fraction of the surface area.

The plate back, cover strips and internal spanwise ribs were made from material identical to that used for the working surface. The internal spanwise ribs and two lengthwise aluminum side rails were primarily to add structural strength to the plate assembly. The internal spanwise ribs had slots cut in them to carry the electrical wires, pressure tubing, and the thermocouple wires. The 0.50 in. thick space between the plate back and the working surface was filled with expanded polystyrene insulation balls to reduce the heat loss by conduction from the heated surface.

Two holes were drilled through each resistance strip into the edge of the working surface base, and copper bus bars, each about 2 in. long were held in position over the bent edge of the resistance strips with small copper screws to provide electrical connections. The strips were wired in series to assure that the same current passed through each of the resistance strips and were powered by a single low ripple regulated dc power supply.

The two cover strips were made from Garolite, and were designed to cover the copper bus bars and the dc power supply wires to the strips.

2. Pressure taps

Static pressure taps on the plate surface were made of 0.02 in. inside diameter stainless tubing inserted between adjacent resistance strips as shown in Figure 5. The tubing was inserted through a hole drilled in the working surface base and held in place with a spot of epoxy adhesive. Each tube was about 1 in. long and bent about 90 degrees at the middle. The tube end was connected with a plastic tube leading to the pressure measurement system. Care was taken to make sure the tubing did not cause an electrical short circuit between strips. A pressure tap was placed at the center of the stagnation line of the nosepiece.

3. Thermocouples

Local temperatures of each strip and the back side of the working surface were required for this investigation. Details of thermocouple installations are sketched in Figure 6. The thermocouples were made of 28-gage (0.0125 in.) diameter chromel-alumel wire welded in a Tigtech Inc. model 116 SRL thermocouple welder. Each of the thermocouple beads was carefully flattened by using a very fine sand paper to assure contact with the surface.

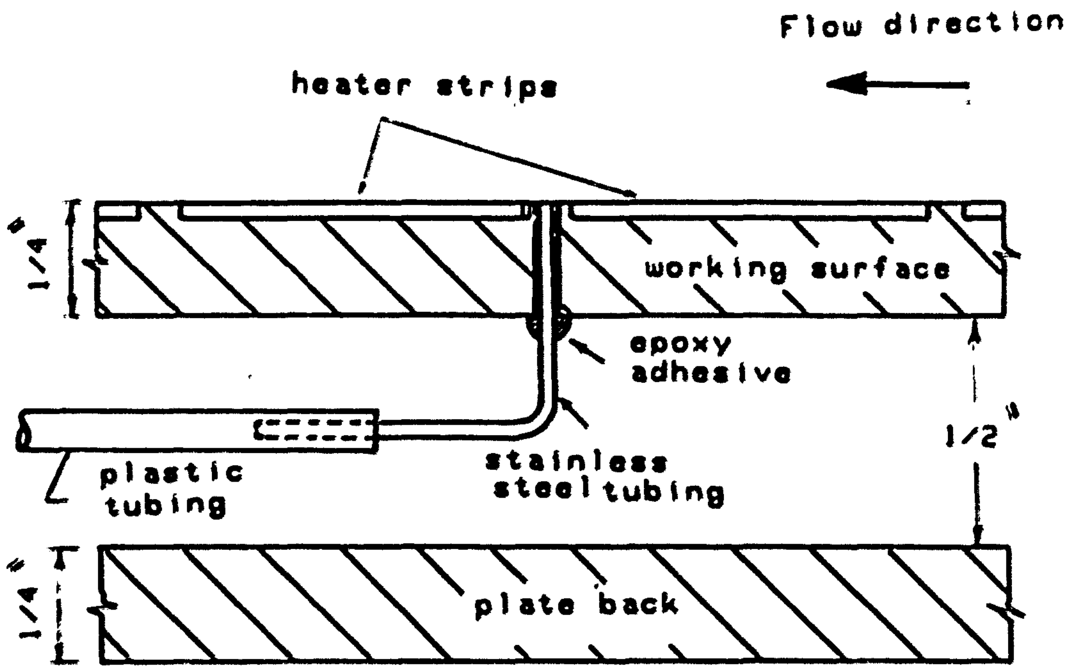

Figure 5. Detail sketch of pressure tap installation

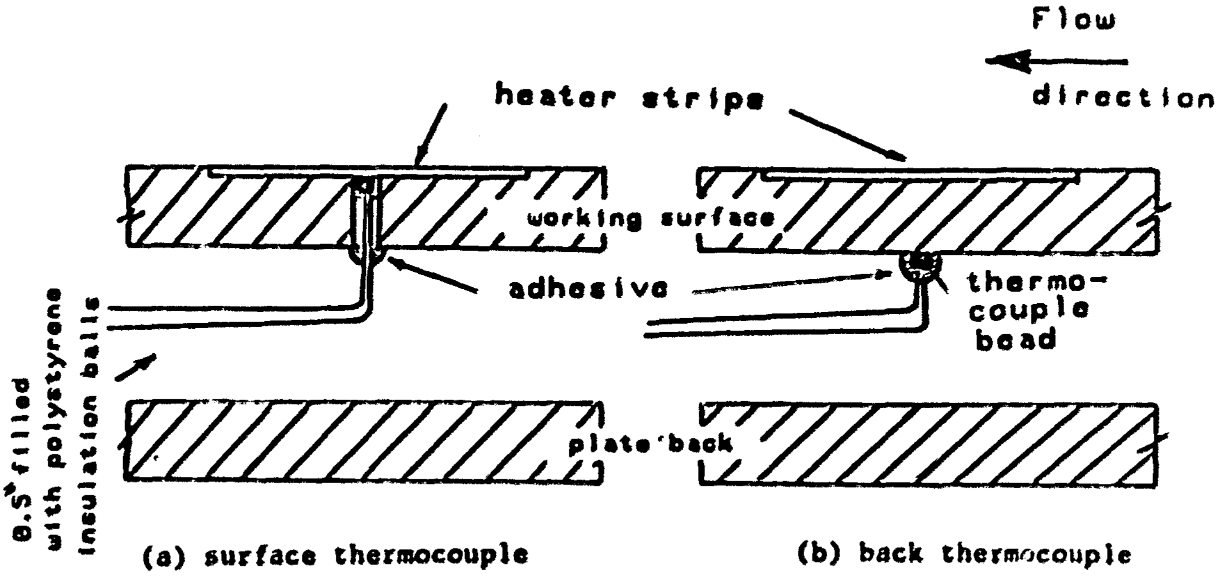

Figure 6. Detail sketch of thermocouples installation

The working surface strip temperatures were measured using a bead inserted through a small hole in the Garolite and cemented in contact with the back side of the strip as shown in Figure 6a. Omega-bond adhesive type OB-100 was used to hold the bead to the heater strip. This adhesive has good thermal conductivity and high electrical resistivity. Care was taken to be sure the thermocouple bead attached to the back side of the strip surface did not leave a rough spot on the upper surface of the strip.

Temperatures of the back side of the working surface were measured by attaching the thermocouple bead to the Garolite with the same adhesive as shown in Figure 6b.

In order to investigate the distribution of the heat transfer coefficients, twelve strips were selected for measuring the working surface temperatures. A sketch of the flat plate and the thermocouple array is shown in Figure 7. Eight of these strips were provided with seven thermocouples each, five for determining the local heated-strip surface temperatures and two for the back side of the working surface temperatures. Each of the other four strips was provided with eleven thermocouples for determining the local heated-strip surface temperature distribution and four thermocouples for measuring the temperatures of the back side of the working surface.

4. Vortex generators

An almost endless variety of vortex generators can be conceived. Because of this variety, some limitations on the vortex generator design

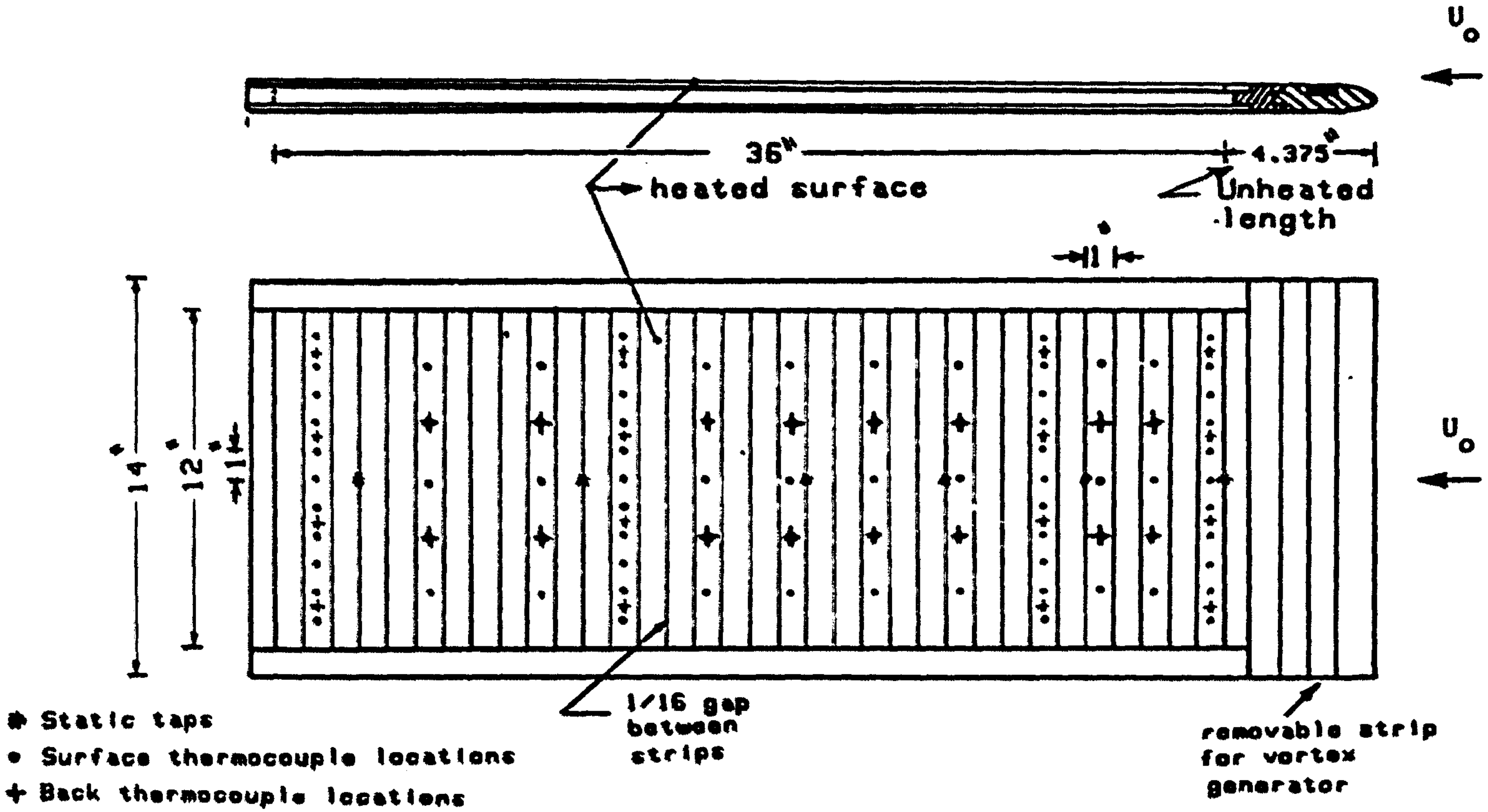

Figure 7. Instrumentation diagram for the uniform heat flux flat plate

were necessary. The general shape was limited to a rectangle and the angle β_g was fixed at 0 degrees. Details of vortex generator geometery and nomenclature are shown in Figure 8.

None of the previous workers studied the effect of vortex generator blade height e_g on the heat transfer performance. The study of boundary layer mixing devices by Schubauer and Spangenberg [4] used a vortex generator height e_g approximately equal to the boundary layer thickness δ_g estimated at the vortex generator position. However, Edwards and Alker [6] used a vortex generator height e_g greater than the boundary layer thicknes δ_g. In the present investigation, vortex generator blade heights of e_g = 0.0625, 0.125 and 0.25 in. were selected to give a range of 0.65 - 2.9 for the ratio of the vortex generator height to the boundary layer thickness.

The results obtained by Edwards and Alker [6] and Lee [7] indicate that an of an incidence angle α_g from 15 to 20 degrees is the most effective for a rectangular vortex generator blade. Pearcey [3] also indicated that a vortex generator system with a good range of vortex effectiveness could be obtained with a 20 degrees angle of incidence. A 20-degree incidence angle was used for this investigation.

Pearcey [3] found that the most important factor in establishing an effective vortex pattern was the need to keep the spacing of the adjacent vortices greater than about three times their height especially for the co-rotating vortex generator blades.

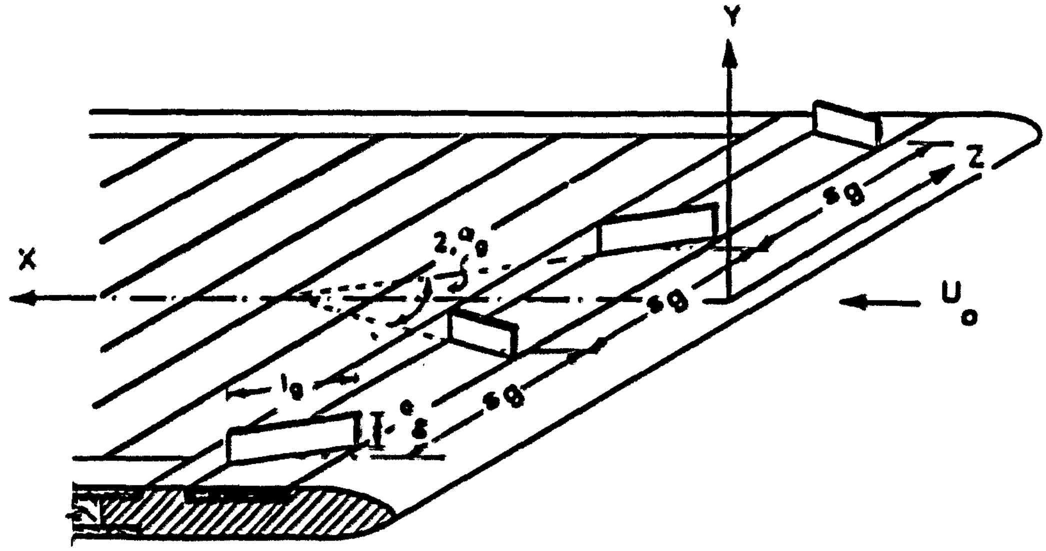

Figure 8. Counter-rotating vortex generators

In this investigation, the space/height ratio (s_g/e_g) of the vortex generator was varied from 3 to 64. The pitch S_g between vortex generator pairs and the spacing s_g between blades of the same pair were set to make $S_g = 2\ s_g$ as shown in Figure 8. Each of the rectangular vortex generator blades tested had a length $l_g = 1.0$ in. and a thickness $\zeta_g = 0.0625$ in.

D. Instrumentation

The data measured included free-stream and ambient air temperatures, the strip and back temperatures of the working surface, air velocities, free-stream static pressures, total pressure, and hot-film anemometery data.

1. Temperature sensing

Free-stream and ambient air temperature were measured using five 28-gage chromel-alumel thermocouples which were independently referenced to a Whittaker model BRJ14-50TP chromel-alumel 150 °F constant temperature junction. Free-stream air temperature measurements were obtained with three thermocouples placed at different locations downstream of the leading edge of the plate and about four inches away from the plate surface. There was almost no variation of the free-stream temperature, and the arithmetic average of the free-stream temperature reading was used in calculation. The ambient air temperature was used for the calculation of radiation losses from the strips and was obtained from the arithmetic average of two thermocouples located about 12 in. away from the test section of the wind tunnel.

A total of 120 thermocouples were attached to the plate to measure the temperatures of the working and back surfaces. However, the data acquisition system described later in this section has only a 40-channel scanner. A switch system that divided the thermocouples into four groups of 30 thermocouples each, shown in Figure 9, was used to connect banks of 30 thermocouples to the scanner at one time. The switch system was manually operated in response to prompts given by the data acquisition computer after measrements for each group was completed.

2. Pressure sensing

a. Pressure instruments   Total and static pressures were measured in the free-stream at two locations downstream of the plate leading edge at the middle distance between the plate surface and the front wall of the test section using a pitot-static tube probe. The free-stream static pressure distribution was measured with a static probe at three locations downstream of the plate leading edge. The pitot-static and static probes were connected to a Meriam model 34FB2 micromanometer capable of reading 0.001 in. water.

The static pressures on the plate surface were independently measured using the pressure taps on the plate surface. Four static pressures on the plate surface, an atmospheric reference and the stagnation pressure on the nosepiece were measured using a six channel Scanivalve and a Setra Systems model 239 pressure transducer, the output of which was connected to the data acquisition system.

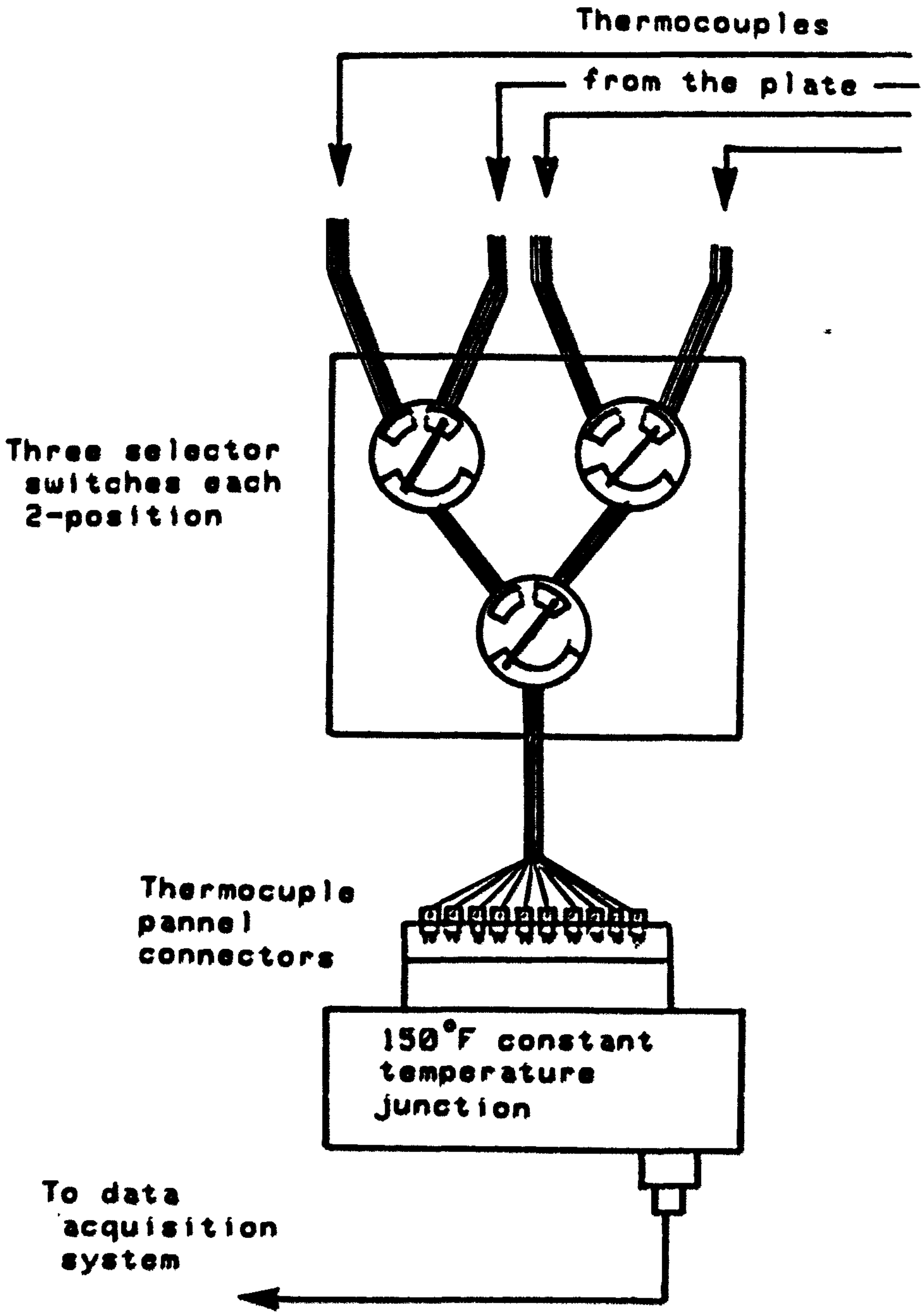

Figure 9. Sketch of the multiple selector thermocouple switches

b. Velocity-profile instruments   Boundary-layer velocity measurements were made with a total head probe constructed from stainless steel hypodermic tubing with a flattened end section to reduce the velocity gradient across the opening facing into the flow. A sketch of the probe and the micrometer probe positioner are shown in Figure 10. The opening of the tube was large enough to give a time constant for the measuring system of the order of two minutes when the pressure measurements were made with the micromanometer.

The position of the boundary-layer probe in relation to the plate surface was found by use of a 0.001 in. least count micrometer adjustment probe positioner. The zero adjustment of the probe against the plate surface was made by advancing the probe from a position some distance away from the the plate until the tip of the probe and its image, reflected in the plate surface, just touched. It was found that repeatability of the zero position was within one part in one thousand by this method.

3. Electrical instruments

a. Power input   The power input to the resistance heater was measured by obtaining the resistance of the heating strips and the dc current passing through it. The temperature coefficients of resistance of the heating strips were determined using thermocouples and a Hewlett-Packard model HP 3455A digital multimeter. Details of the heating strip charateristics are described in Chapter III.

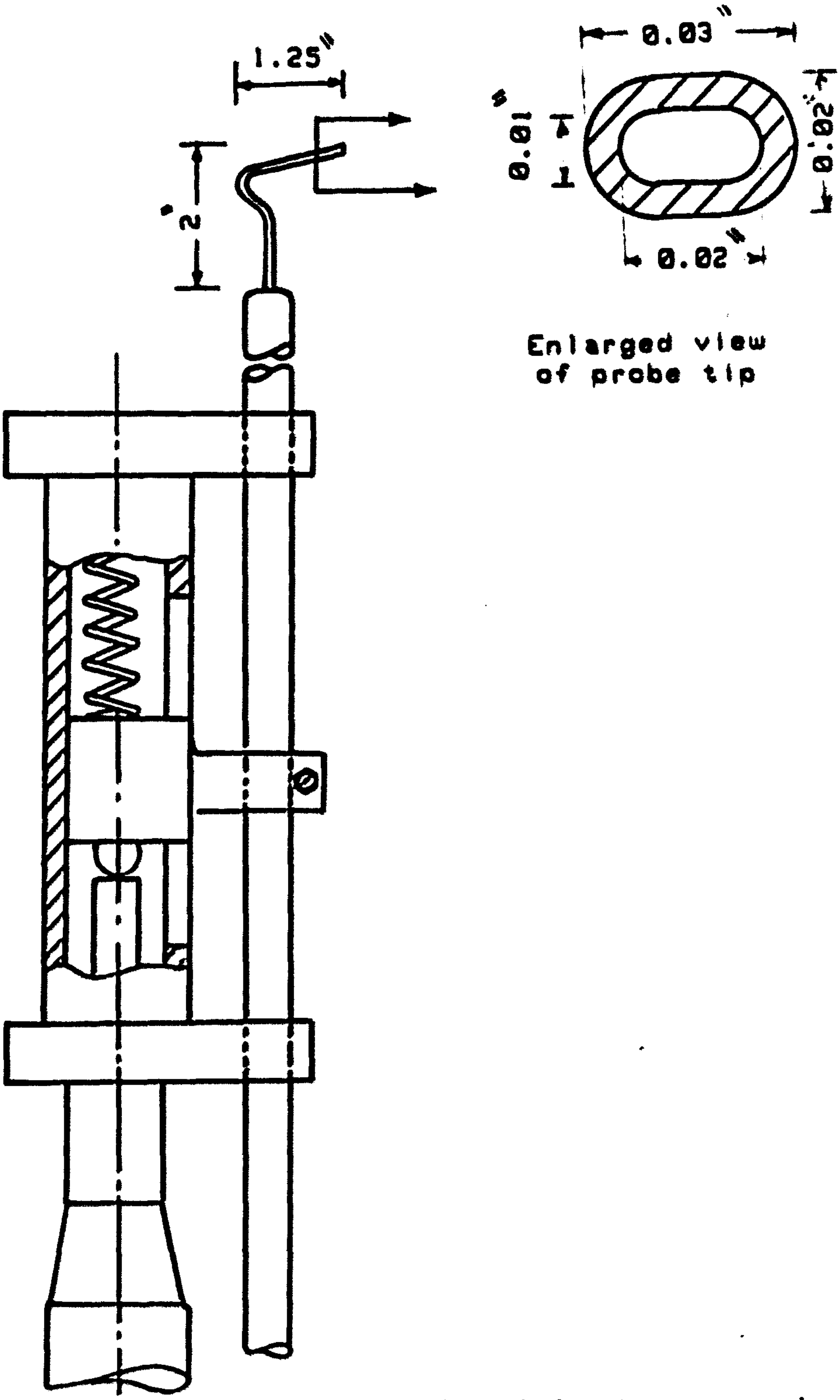

Figure 10. Sketch of the probe and the micrometer probe positioner used for boundary layer profiles

Heater strip current was supplied by an Electro model PS-5R filtered dc power supply. The dc current through the heating strips was determined by reading the voltage across a precision shunt resistance and calculating the current from Ohm's Law for the resistor.

b. Hot-film turbulence measurements Measurements of turbulence quantities downstream of selected configurations of vortex generators were obtained using a TSI model 1227 single platinum hot-film probe of 0.001 in. sensor diameter in conjunction with a TSI model 1010A constant temperature anemometer and TSI model 1072 linearizer. The circuitry involved in hot-wire anemometry is shown in Figure 11. An oscilloscope was used to visually monitor the output signal from the hot-wire as an additional check on the satisfactory operation of the anemometer equipment. The dc and true rms voltages from the linearizer were measured using the data acquisition system.

4. Data aquisition system

All voltage and resistance readings were measured using a Heat Transfer Laboratory data acquisition system consisting of a Hewlett-Packard model 9845B desktop computer, a model 3495A 40-channel scanner with low thermal offest relay contacts, and a model 3455A digital multimeter with one microvolt resolution.

Thirty-eight channels on the scanner were used for experimentation. Thirty channels were used for measuring the outputs from each thermocouple group attached to the working surface. The rest of the scanner channels were used for measuring the outputs from five

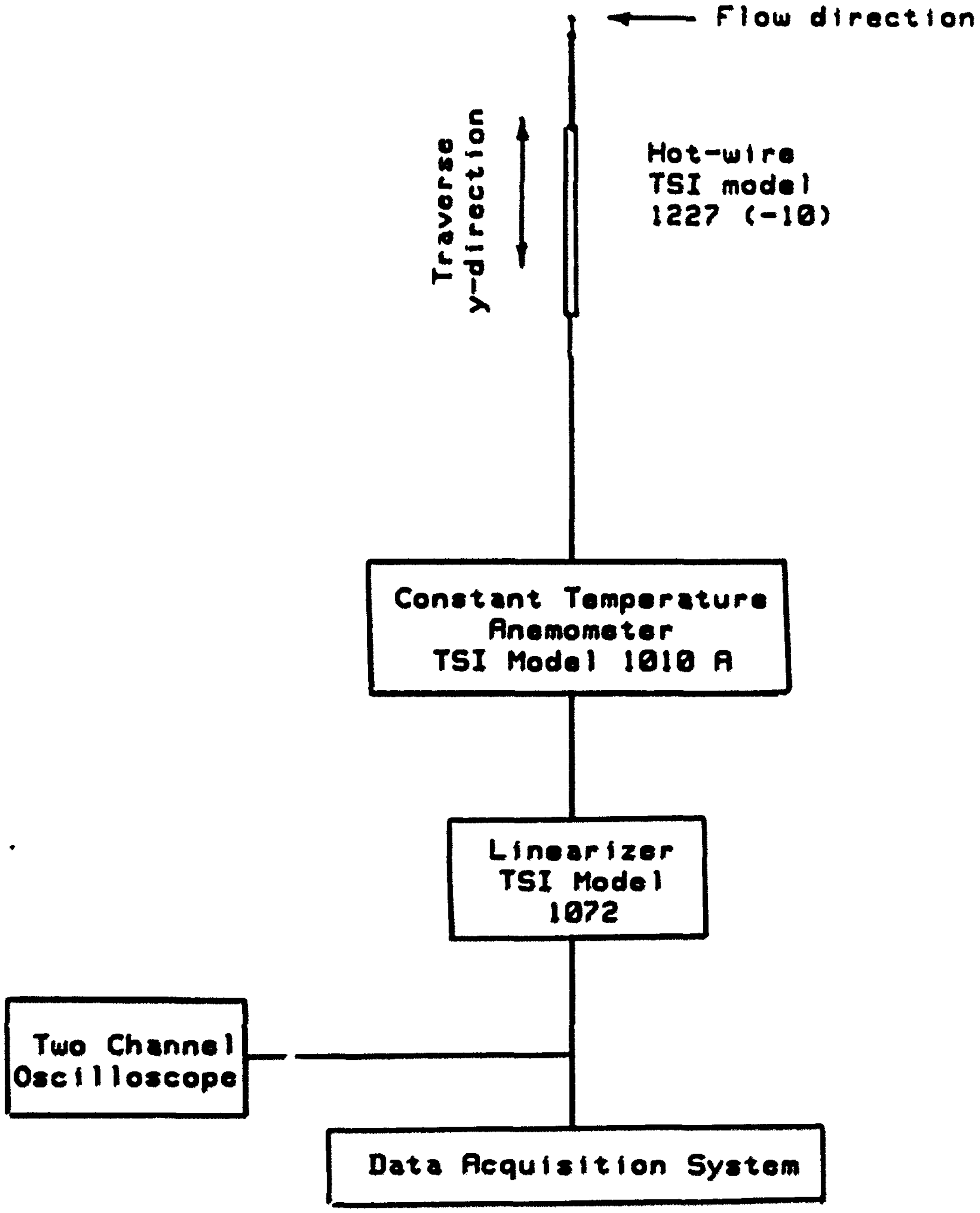

Figure 11. Hot-film anemometer circuit

thermocouples for free-stream and ambient temperatures, the pressure transducer, hot-film and the voltage drop across the precision resistor.

III. EXPERIMENTAL PROCEDURE

A. Calibration

Thermocouples, strip resistance and emissivity, the scanivalve and pressure transducer, and the hot-wire anemometer were calibrated before use. In all cases, calibrations were made using the entire system of sensors, connecting cables, data acquisition system and auxiliary equipment.

Thermocouples were calibrated by immersing them in a Haake model M-F3 constant temperature water bath having a maximum variation of 0.18 °F from the preset bath temperature. The bath temperature was measured using a calibrated mercury-in-glass thermometer with a least count of 0.1 °F. The thermocouples were calibrated over a temperature range 15 °F greater than the range of use. A linear least squares data fit was obtained for each thermocouple; the equations thus obtained were used by the data acquisition system program to reduce the thermocouple voltages to temperature values.

The pressure transducer was checked against a Meriam micromanometer with a resolution of 0.001 in. water. The transducer was referenced to atmospheric pressure so that the zero pressure intercept of the equation used to obtain the pressures from the voltage values varied with atmospheric conditions, while the slope was constant. One channel on the Scanivalve was used to determine the voltage output equivalent to atmospheric pressure.

Electrical resistance characteristics of the nickel-chromium foil strips used for the heated surface were measured at room temperature to obtain the strip length-resistance characteristics shown in Figure 12.

Three strip samples were tested to obtain the temperature-resistance characteristics of the heated strip. Temperature-resistance data obtained for the three samples are shown in Figure 13. The measurement of strip resistance was accomplished by obtaining the voltage drop across each strip and the current passing through it, while measuring the strip temperature at five locations along its length. The arithmetic average of the lengthwise temperature distribution was considered the temperature of the strip. The error analysis for these data indicates that for a given temperature the strip resistance can be calculated with an accuracy of ±0.0015 ohm using the following expression

$$R_s = R_r \, [\, 1.0 + \alpha_s(\, t_s - t_r)] \qquad (3)$$

where R_s is the strip resistance at the strip temperature t_s, R_r is the resistance of the strip at the reference temperature t_r, and α_s is the temperature coefficient of resistivity for the strip. For equation (3), the result obtained was α_s= 0.00023 1/°F referenced to R_r=0.25 ohm at t_r= 68 °F. The value obtained for the temperature coefficient of resistivity α_s agreed within a ±4.5% of that indicated by Beckwith and Buck [15] for a typical nickel-chromium material.

A TELETEMP model 44 infrared thermometer was used to estimate the emissivity of the strip material. The infrared thermometer was

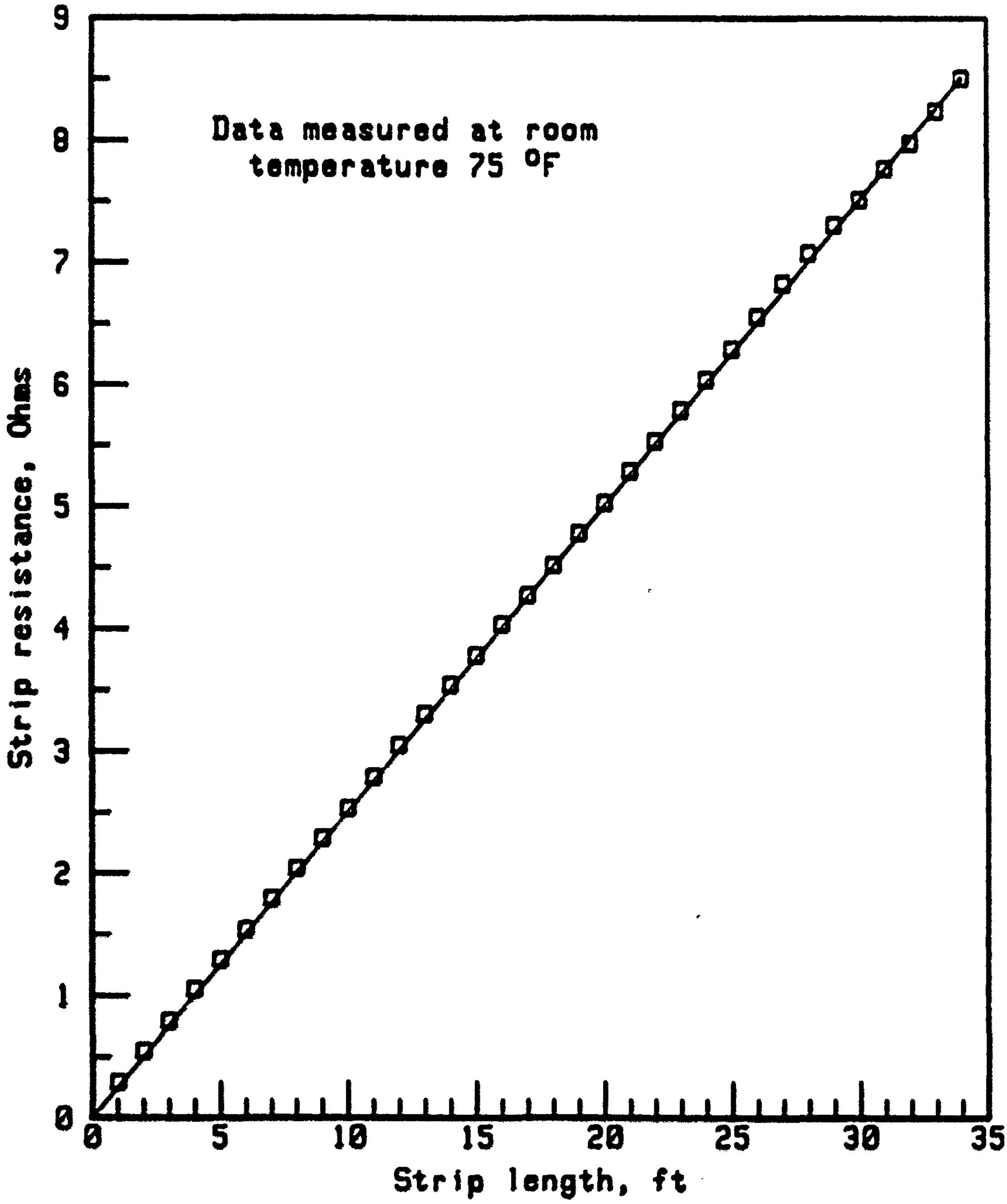

Figure 12. Strip length-resistance characteristic

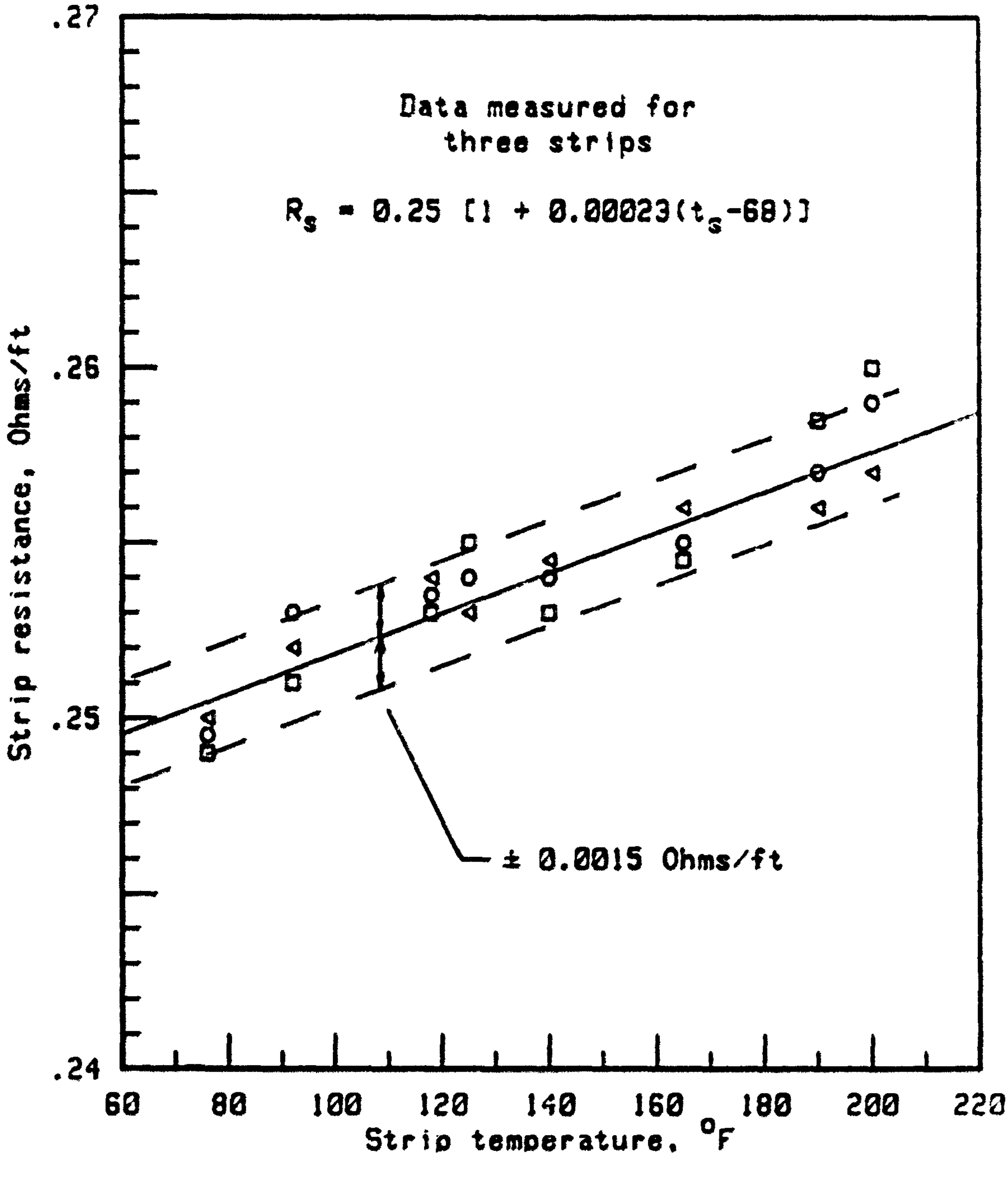

Figure 13. Strip temperature-resistance characteristic

calibrated by measuring the temperature of a strip coated with 3M type ECP-2200 high emissivity flat black paint which has a known emissivity of 0.98. The measured emissivity for the painted strip was within a ±1.0 % of that indicated by the manufacturer. The result obtained for the unpainted strips at the same temperature indicated that the heated strips had emissivity ε_s equal to 0.45.

The hot-wire system was calibrated in place in the test section to include any influences of the surroundings as discussed by Wyler [16]. A pitot-static probe was used to obtain the reference velocity at the center of the channel. Once the velocity had been adjusted, the pitot-static probe was withdrawn from the tunnel and the hot-wire was placed in the stream at the same location. Free-stream temperature was obtained from the arithmetic average of three thermocouples in the free-stream.

The relationship used to obtain the velocity from the bridge voltage output is given by

$$E_m = S\ U_m \qquad (4)$$

where E_m is the dc voltage signal output from the linearizer, U_m is the effective mean air velocity and S is the sensitivity factor to be determined from calibration. A typical calibration curve for the hot-wire is presented in Figure 14.

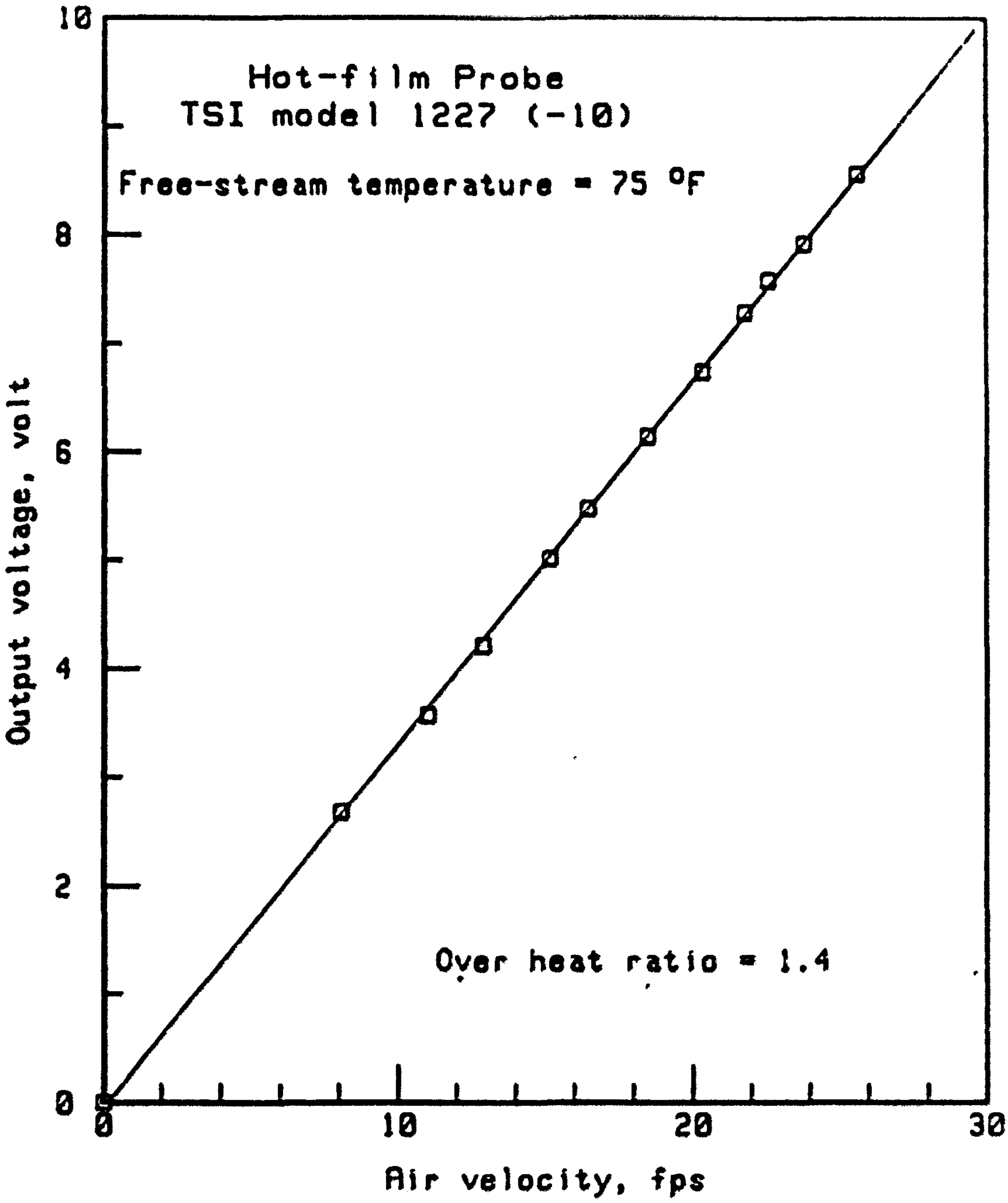

Figure 14. Calibration curve for the hot-film

B. General Operating Procedure

The sequence of the general operating procedure for taking heat transfer data is shown in detail in the flow chart in Figure 15. Initially, all electronic equipment and the thermocouple reference junction were started and allowed to stabilize. The centrifugal fan was started and fan controls were adjusted for the required operating conditions. The pitot-static and static probes were placed in the free-stream to adjust the operating conditions. Once the velocity and the pressure gradient had been adjusted, the pitot-static probe was withdrawn to a location near the front wall of the test section of wind tunnel where no possible interaction with the flow over the plate surface could occur. Perodic checks on the operating conditions were made.

The plate-heater current was adjusted until the heat input resulted in a minimum 10 °F difference between the free-stream and the heated strip surface temperatures. The maximum difference between free-stream and heated strip temperatures was about 35°F, and a majority of the tests were performed with a temperature difference about of 20°F. Monitoring of the plate temperatures and the current passing through the heated strips was required until steady-state conditions were reached. Temperature data were recorded three times over a period of about thirty minutes in order to be sure a true steady-state condition had been reached. Then, the pressure transducer output voltages were measured. The electric power input, free-stream and ambient temperatures were

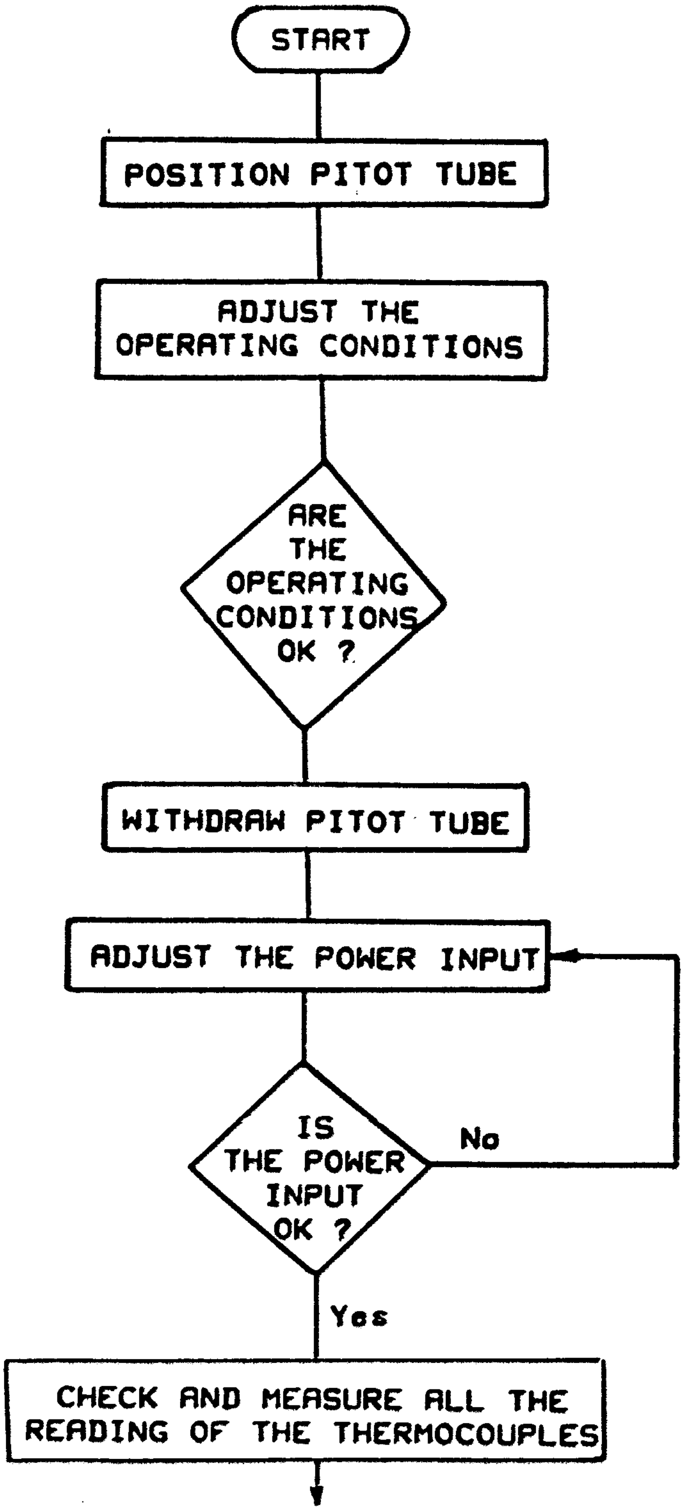

Figure 15. Flow chart for data acquisition and heat transfer reduced data

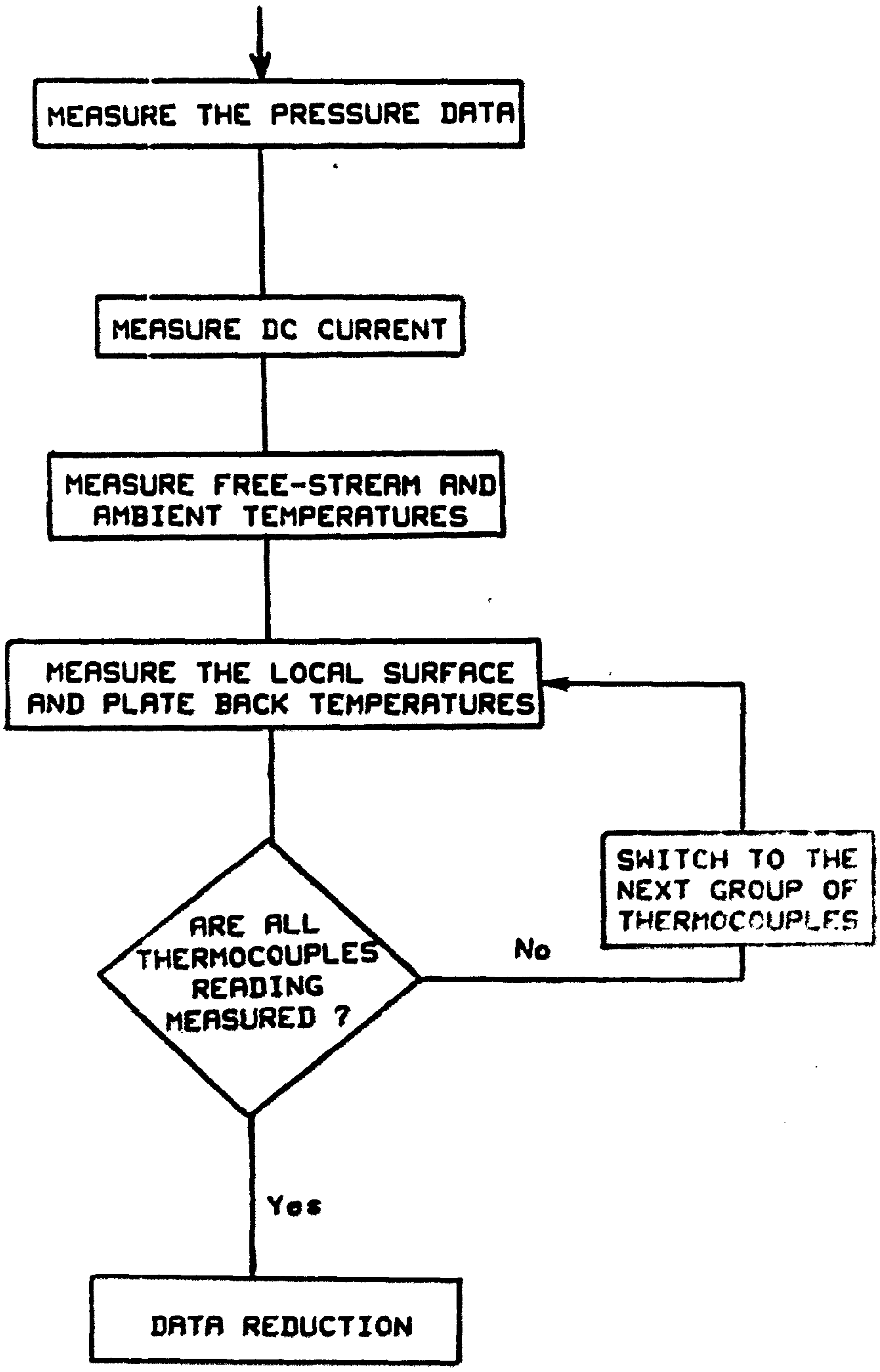

Figure 15. (continued)

rechecked before measuring the output voltages for each group of thermocouples. Then the switch was manually turned to obtain the data for the next group.

The operating procedure for obtaining hot-wire data is shown in detail in the flow chart in Figure 16. As was the case for obtaining heat transfer data, the pitot-static and static probes were used for adjusting the free-stream operating conditions. Once the operating conditions were adjusted, the pitot-static and static probes were withdrawn from the test section and the hot-film was placed in the free-stream to check its calibration. In order to study the behavior of the boundary layer and its development downstream of vortex blades, the probe was placed at three locations in the x-direction. The hot-film sensor was oriented parallel to the plate surface and perpendicular to the flow direction, as shown in Figure 17. The probe was moved through 8 in. in the z-direction and was traversed in the y-direction at five spanwise positions to obtain the mean velocity profiles and the the turbulence distributions downstream of a pair of vortex blades.

The data acquisition system measured the dc and rms voltages of the hot-wire signal ten times to obtain a true steady-state average at each point. At the same time, the osilloscope was used to check for satisfactory function of the anemometer circuit. A listing of the computer program used to acquire and reduce the hot-film data run output is given in Appendix A.

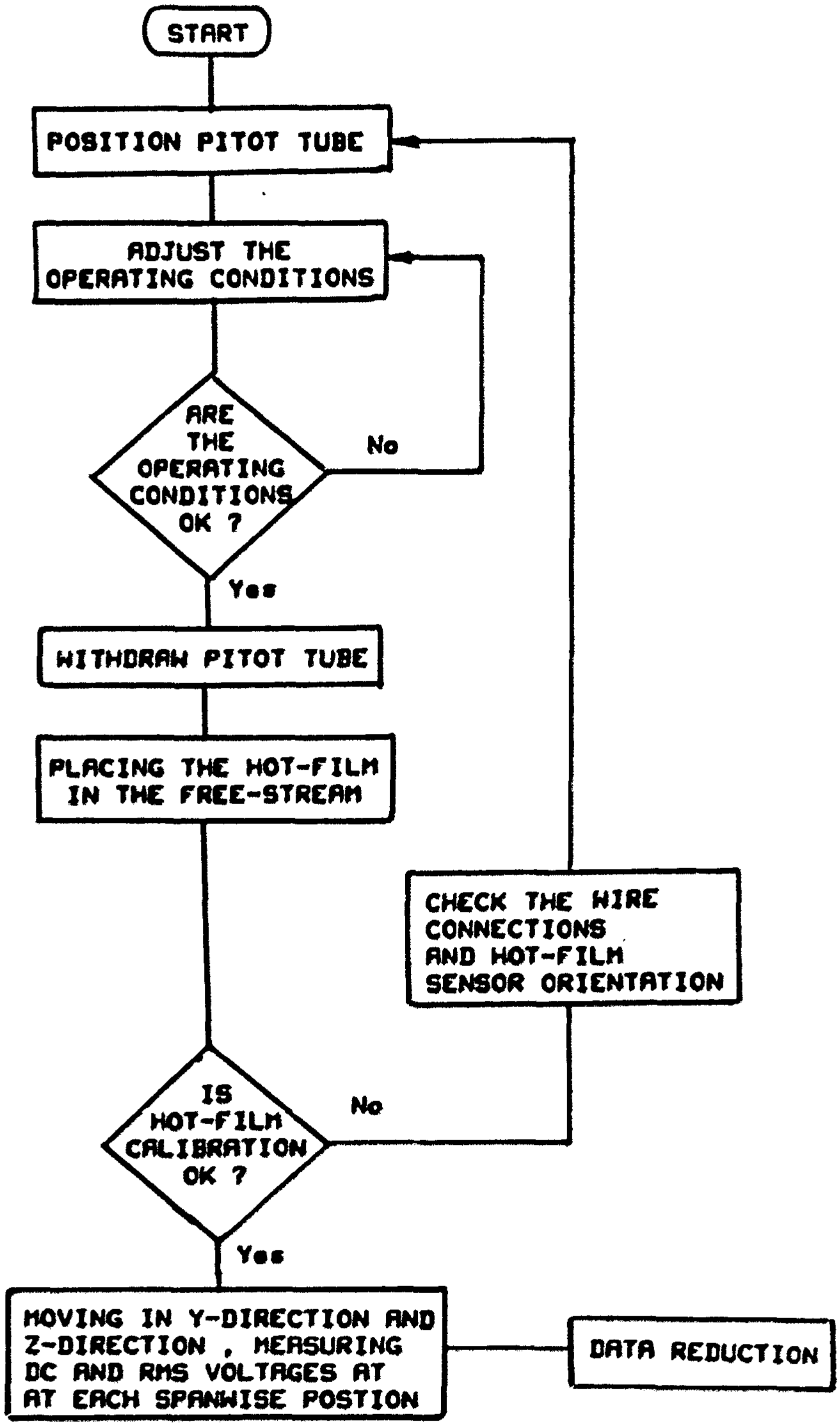

Figure 16. Flow chart for data acquisition and hot-film reduced data

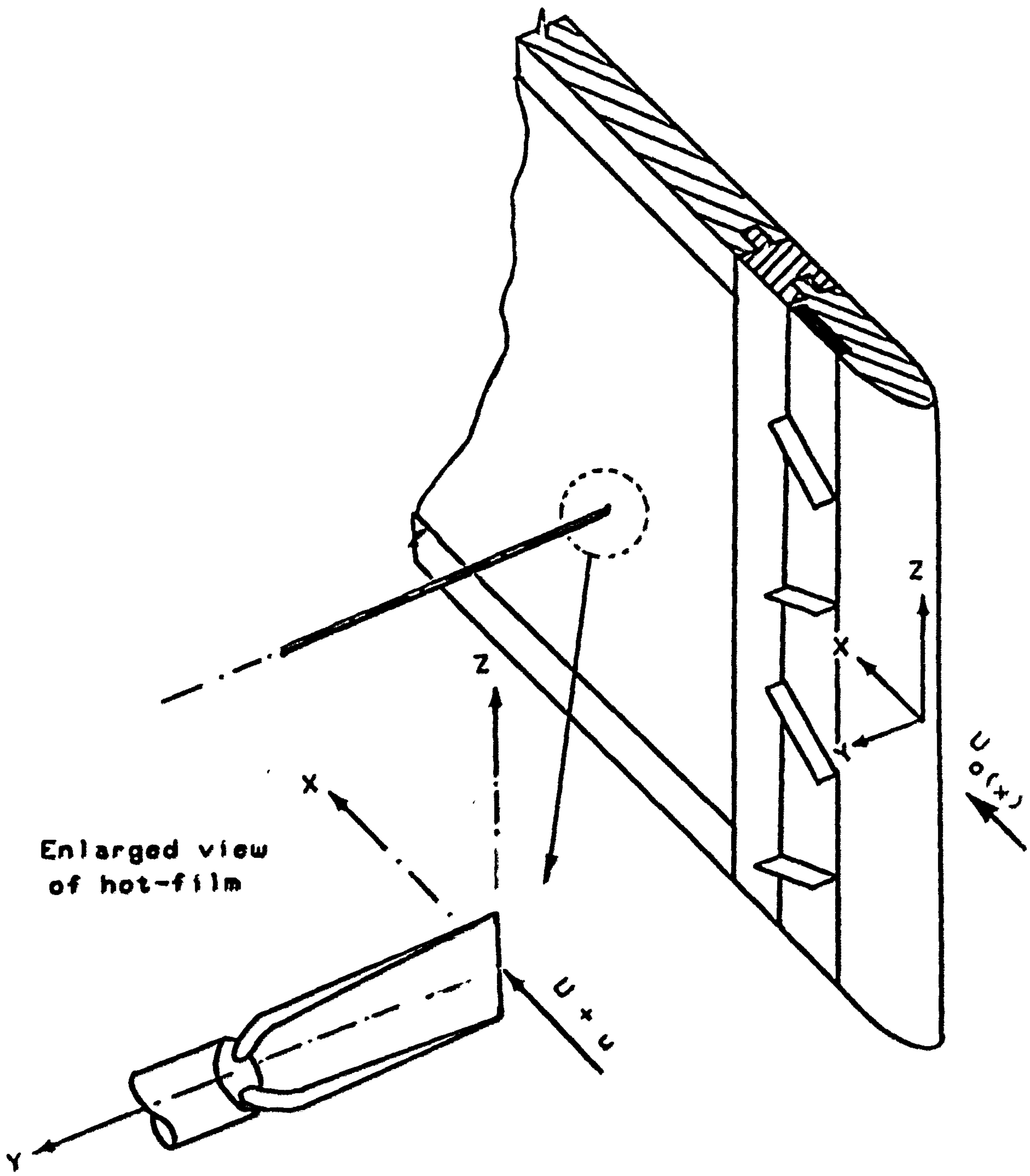

Figure 17. Hot-film and velocity components referenced to the plate axis

The raw data were reduced to obtain all required information and the results were recorded on magnetic tape and disk for use in calculation of other parameters. A listing of the computer program used to acquire and reduce the data is given in Appendix B.

C. Data Reduction

Calculation of the experimental results took place in two parts. First, the raw data were reduced to basic dimensional quantities such as free-stream velocity, local velocity and its fluctuation component, temperature, and heat transfer rate. These quantities were then combined with the plate and vortex generator geometrical data and further reduced to non-dimensional terms such as Reynolds number, Stanton number, and turbulence intensity. Basic reduction of raw data was done using the HP 9845B desk computer.

Data were subjected to an uncertainty analysis based on the method of Kline and McClintock [17]. An analysis performed for a typical set of data is given in Appendix C.

1. Plate energy equation

The conservation of energy for steady-state flow is

$$Q = \dot{Q}_n + Q_c + Q_r \qquad (5)$$

where the terms are identifed schematically in Figure 18 and where Q is the local rate of heat input to the strip, Q_c and Q_r are the local rates of heat loss from the strip by conduction and radiation respectively, and Q_n is the local rate of heat loss by convection.

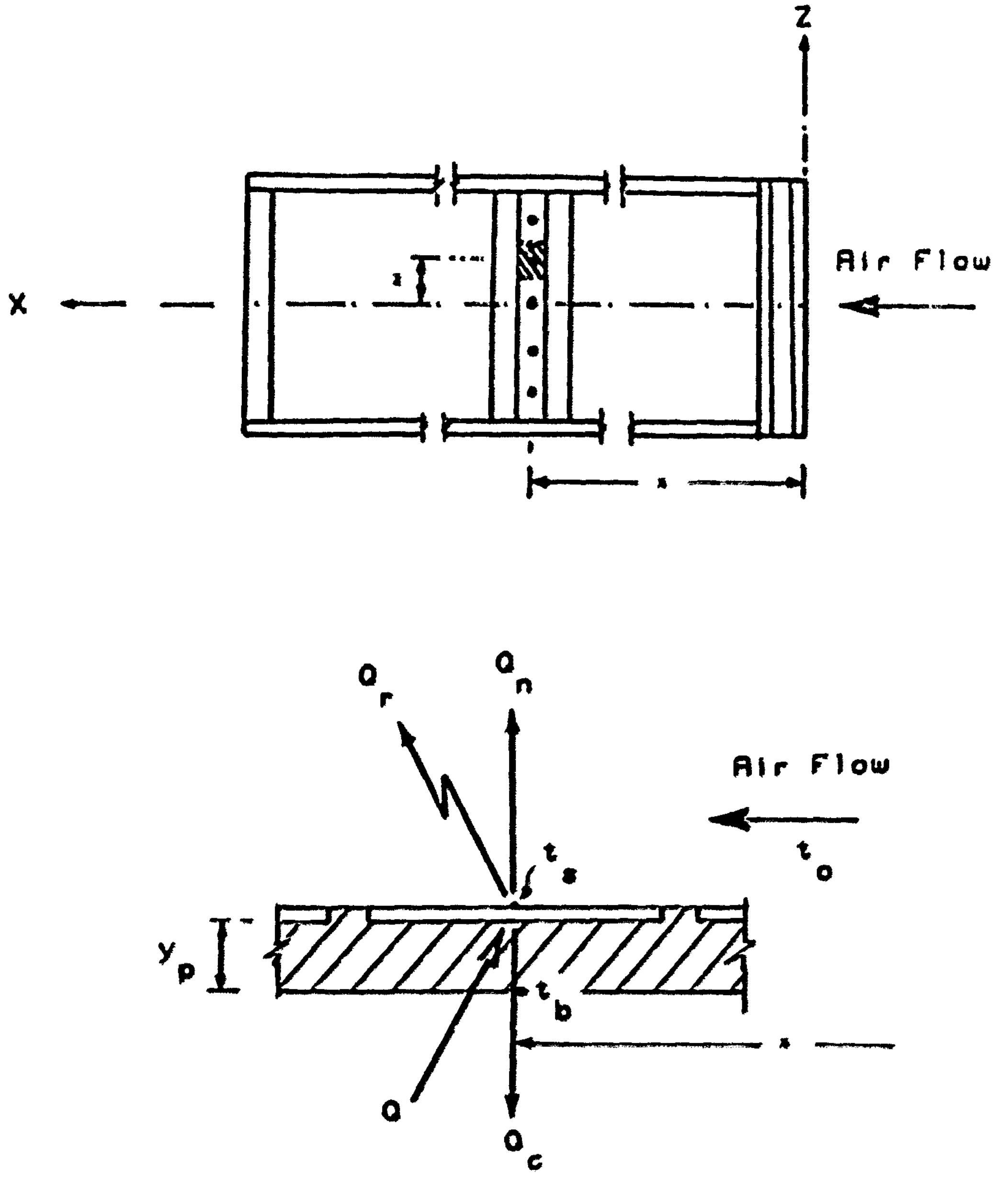

Figure 18. Schematic of energy conservation for a local point on heated strip

The generated power on the local strip surface is calculated from

$$Q = I^2 R_s \tag{6}$$

where R_s is obtained from equation (3), I is the dc strip current, and R_s is the strip resistance at the local surface temperature of the strip t_s. Equation (6) can then be written as

$$Q = I^2 R_r[1.0 + \alpha_s(t_s - t_r)] \tag{7}$$

Since the heated surface of the plate is large with relation to the thickness of the plate and because the x- and z-direction temperature gradients are small, a one-dimensional flow of energy by conduction was assumed. The local conduction loss was calculated from

$$Q_c = (k_p A_s / y_p)(t_s - t_b) \tag{8}$$

where y_p is the thickness of the plate working surface material, k_p is the thermal conductivity of the plate material, A_s is the surface area of the strip, and $(t_s - t_b)$ is the local temperature difference between the heated strip surface and the back side of the working surface.

The local rate of heat radiation loss was calculated from

$$Q_r = \varepsilon_s \sigma A_s (T_s^4 - T_a^4) \tag{9}$$

where ε_s is the emissivity of the strip material, σ is the Stefan-Boltzmann constant, T_s is the local absolute temperature of the strip surface, and T_a is the absolute temperature of the surroundings. The temperature of the surroundings was taken as the room temperature. Corrections for absorption in the room atmosphere and in the plastic tunnel wall were assumed to be negligible. The radiation geometric view factor was assumed to be unity as implied in equation (9).

The net local rate of heat loss by convection from the strip can be determined from equation (5),

$$Q_n = Q - (Q_c + Q_r) \quad (10)$$

The local heat transfer coefficient h is found from its definition

$$h = Q_n / [A_s (t_s - t_o)] \quad (11)$$

where t_o is the free-stream temperature.

2. Flow velocity and pressure

Since the plate was placed in an open suction type wind tunnel and the test section was on the suction side of the fan, the free-stream inlet density ρ_a was calculated from the ideal gas law

$$\rho_a = (p_{atm} - p_s)/(R_{air} T_o) \quad (12)$$

where p_{atm} is atmospheric pressure obtained from a barometer, p_s is the static pressure of the air at the leading edge of the plate, and R_{air} is the gas constant for air.

Using the pitot tube pressure difference between the free-stream stagnation pressure p_o and the local static pressure of air $p_{s(x)}$ and the calculated air density, the local free-stream velocity at any x-distance from the leading edge of the plate was calculated using Bernoulli's equation, given by

$$U_{o(x)} = [2g_c (p_o - p_{s(x)})/ \rho_a]^{1/2} \quad (13)$$

To obtain the velocity gradient for the free-stream, static pressures were measured at different x-locations using a static tube, and from equation (13) the local free-stream velocities were determined. The velocities were plotted as a function of x and a least squares fit was obtained to determine the velocity gradient (dU_o/dx). The pressure gradient in the free-stream can be obtained by differentiation of Bernoulli's equation,

$$(dp/dx) = - (\rho_a U_o / g_c) (dU_o / dx) \qquad (14)$$

The local Reynolds number for an experimental point at a distance x from the leading edge of the plate was calculated from

$$Re_{(x)} = [x U_{o(x)} / \nu_a] \qquad (15)$$

where ν_a is the kinematic viscosity of air evaluated at the local mean boundary layer temperature.

The value of h from equation (11) and $U_{o(x)}$ from equation (13) were used to calculate the local Stanton number for an experimental point from the Stanton number definition

$$St_{(x,z)} = [h_{(x,z)} / (\rho_a C_p U_{o(x)})] \qquad (16)$$

where C_p is the specific heat of air evaluated at the local mean boundary layer temperature.

IV. PRELIMINARY EVALUATION TESTS

A. Evaluation Tests of the Equipment and Measurement Instrumentation

A preliminary series of the evaluation tests was carried out with no vortex generators attached to the plate surface to check the wind tunnel and the plate equipment against earlier analytical and experimental work.

1. Pressure-gradient measurement

The pressure distributions for this series of tests are shown in Figure 19 as the nondimensional pressure gradient parameter ϕ_p as a function of the distance (x/L) measured from the leading edge of the plate. That data show in Figure 19 are fitted with least squares lines using values of the static pressure distribution on the plate surface measured by the pressure transducer and those measured by the static probe for the free-stream. The three average pressure gradients shown will be referred to later.

2. Heat transfer distribution

The Stanton number distribution measured on the heated surface was compared with the analytical solution presented by Kays and Crawford [18] for a zero pressure gradient, laminar boundary layer flow with a uniform convective heat flux wall and an unheated starting length,

$$St_{(x)} = 0.453\, Re_{(x)}^{-1/2} \quad Pr^{-2/3} \left[\, 1.0 - (\xi/x)^{3/4}\, \right]^{-1/3} \qquad (17)$$

For fully turbulent flow, Kays and Crawford [18] give

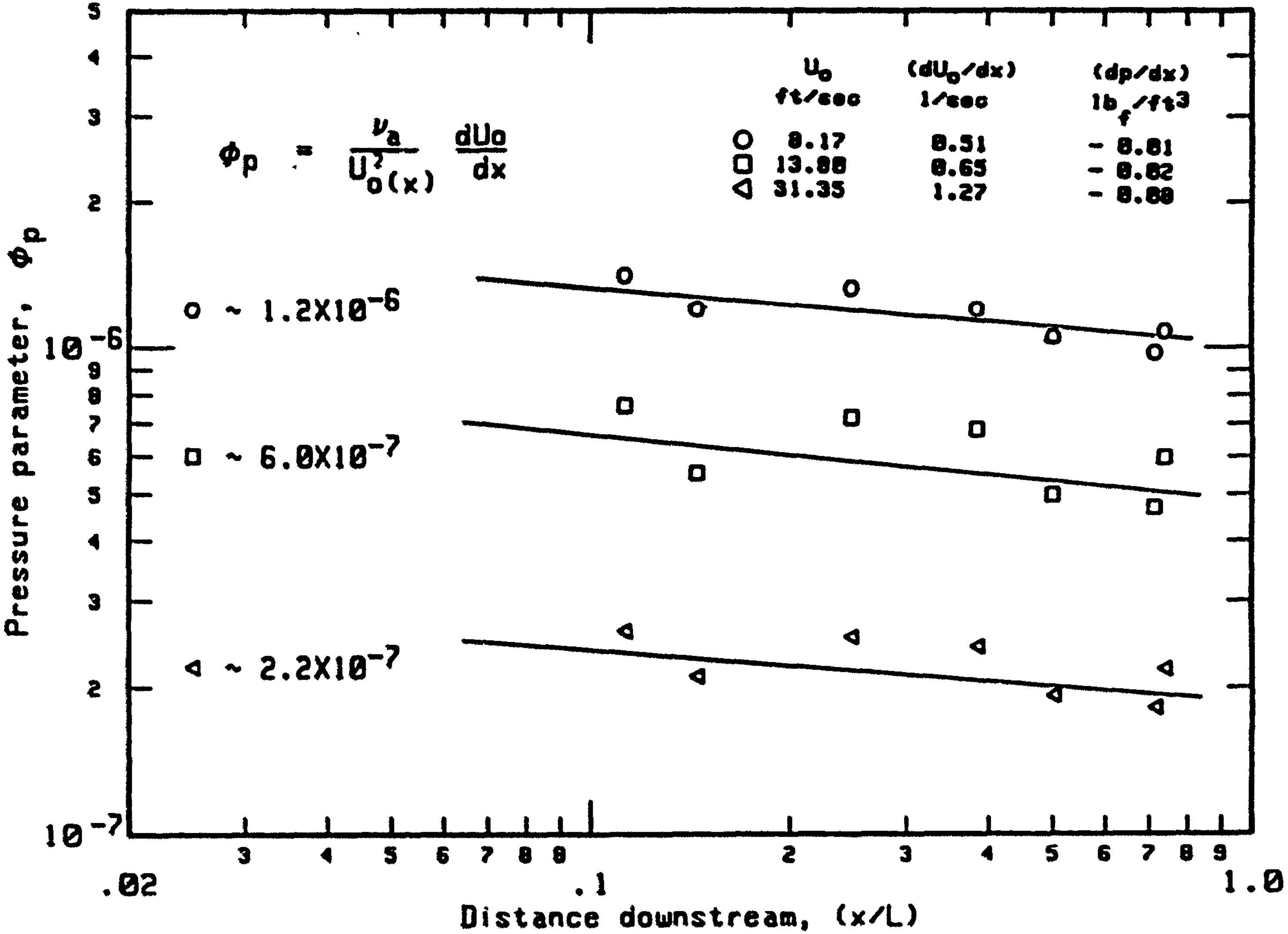

Figure 19. Static pressure distribution

$$St_{(x)} = 0.030\ Re_{(x)}^{-0.2}\ Pr^{-0.4} \tag{18}$$

where Pr is the Prandtl number and $Re_{(x)}$ is the Reynolds number based on a free-stream velocity U_o. The Reynolds number at any location x is

$$Re_{(x)} = (U_o x / \nu_a) \tag{19}$$

where ν_a is the kinematic viscosity for air, and x is measured along the plate axis from the plane of the leading edge. The distance measured from the stagnation line is different from that measured along the plate axis by about one percent; the error is included in the uncertainty analysis for Reynolds number.

The measured local span-averaged Stanton number distributions are presented in Figures 20 through 22 as the Stanton number corrected for unheated length $St_{(x)c}$ as a function of Reynolds number for the three different levels of free-stream pressure gradients. The results obtained at the lowest free-stream pressure gradient shown in Figure 20 indicate that for Reynolds number $Re_{(x)} < 10^5$ the local span-averaged Stanton numbers are in agreement within ±3 percent of that predicted from equation (17), and at $Re_{(x)} > 10^5$ they are about 10 percent higher than that given by equation (17). For $(dp/dx) = -0.02\ lb_f/ft^3$, Figure 21 shows that for $Re_{(x)} < 10^5$ the local span-averaged Stanton number was within ±2.5 percent of that predicted, and 11 percent higher for $Re_{(x)} > 10^5$. For the highest pressure gradient, Figure 22 shows that for of Reynolds number $Re_{(x)} < 3x10^5$ the local span-averaged Stanton number was within ±5 percent of that given by equation (17), and for $3x10^5 < Re_{(x)} < 6x10^5$ it was about 15 percent higher than that predicted for a laminar boundary layer with zero pressure gradient.

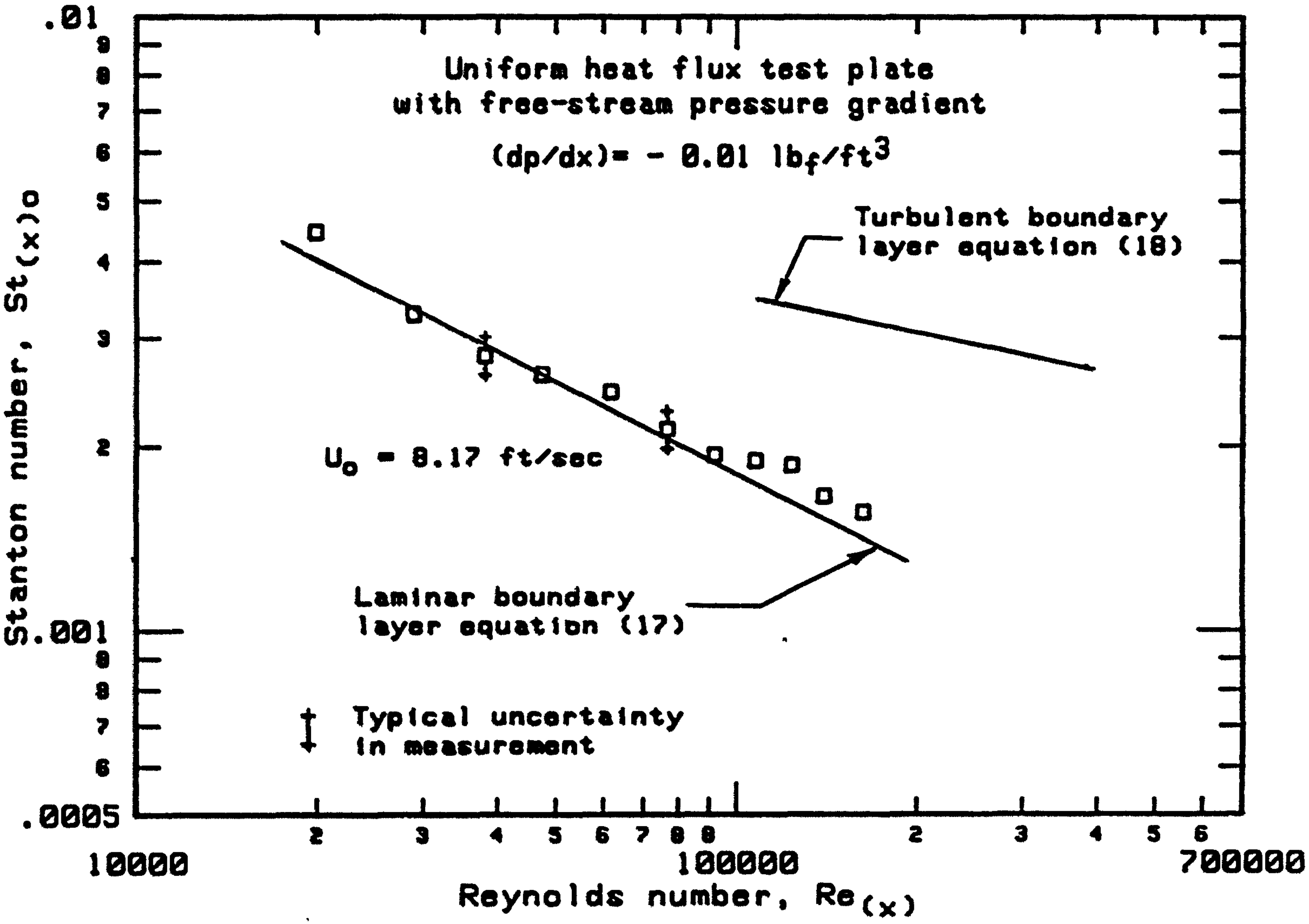

Figure 20. Heat transfer distribution along the smooth plate for $(dp/dx) = -0.01\ lb_f/ft^3$

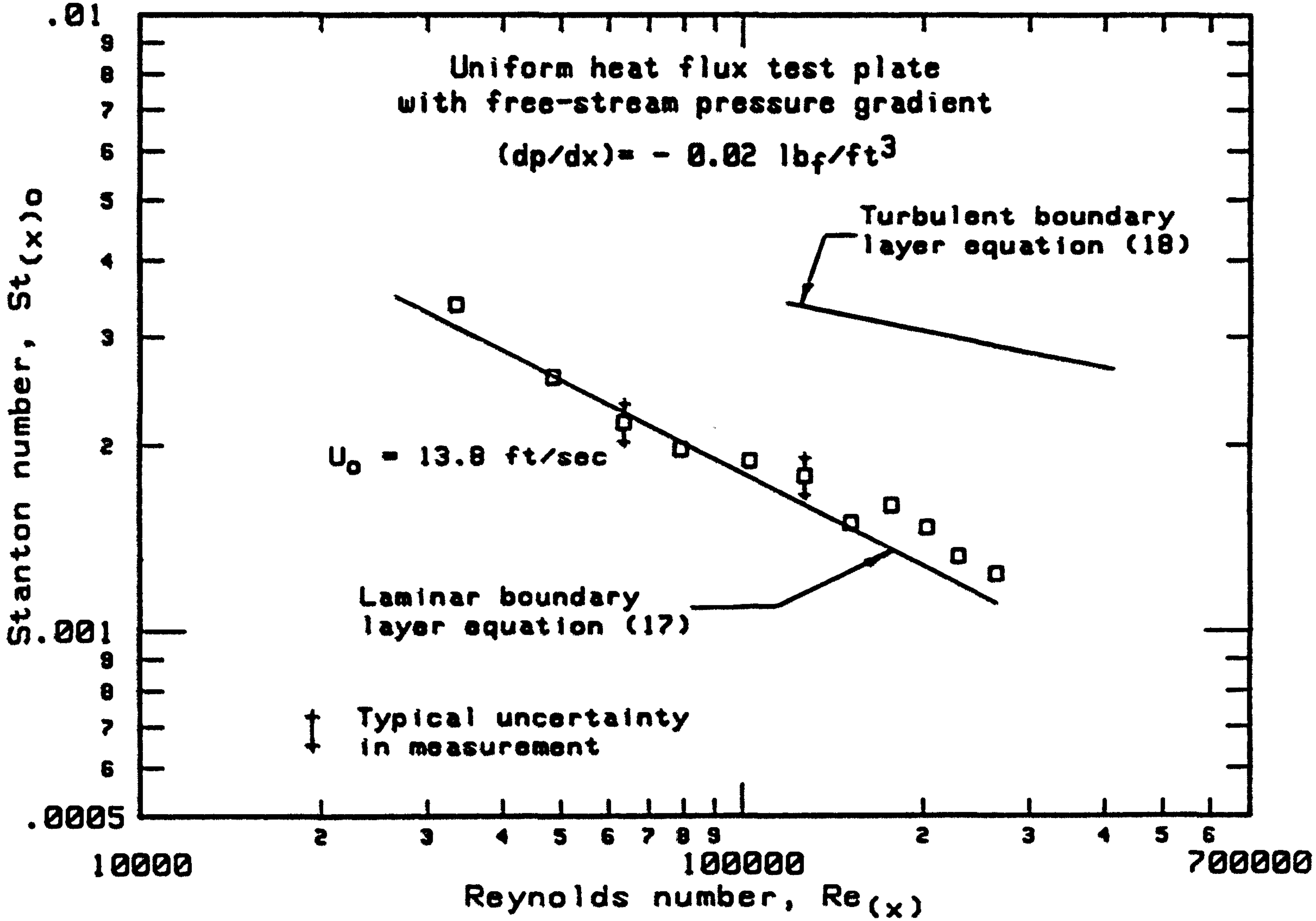

Figure 21. Heat transfer distribution along the smooth plate for $(dp/dx) = -0.02\ lb_f/ft^3$

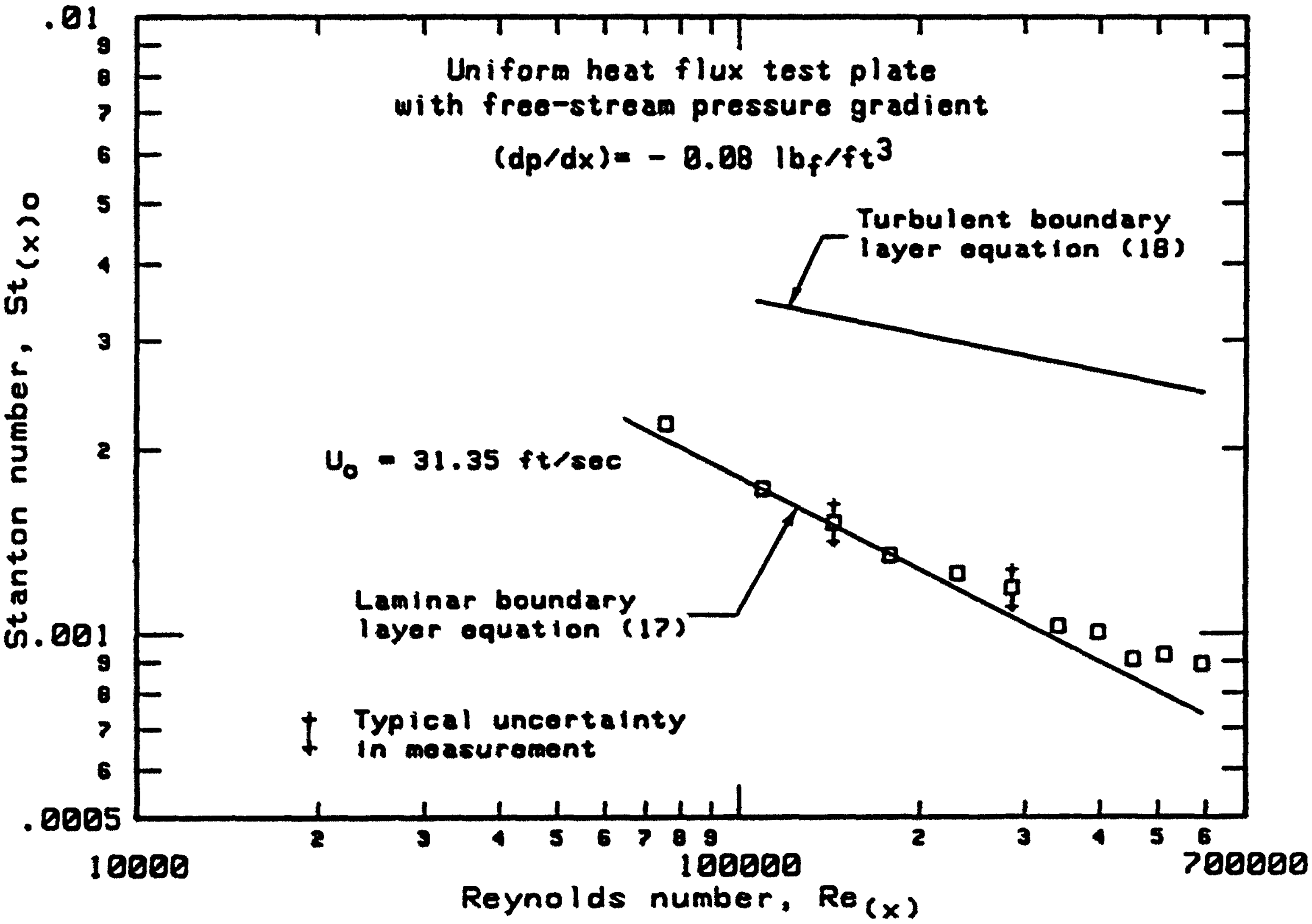

Figure 22. Heat transfer distribution along the smooth plate for $(dp/dx) = -0.08\ lb_f/ft^3$

The magnitude of the conduction and radiation losses from the heated strips varied with the strip, back side of the working surface and ambient temperatures. The radiation loss was in a range of 7% to 25% of the total heat input. The conduction loss was in a range of about 3% to 15% of the total heat input.

The conclusion reached from Figures 20 through 22 is that there is good agreement between heat transfer data measured in this facility and the analytical solution of Kays and Crawford [18], equation (17). Exact agreement should not be expected due to the approximate constant heat flux condition dictated by physical construction of the plate.

Examination of Figures 20, 21 and 22 suggest that the transition region takes place at a Reynolds number of about 10^5 for the two lower pressure gradients and at about $4x10^5$ for the highest pressure gradient.

3. Laminar boundary layer profiles

In order to check that the behavior of the boundary layer was laminar as indicated by the heat transfer results, mean velocity profile data were measured using the total head tube for each of the three favorable free-stream pressure gradients. Profile data were obtained at three positions downstream of the plate leading edge. The measurements were taken on the plate centerline as well as in the z-direction. When the experimental boundary layer thickness was required in a calculation, it was taken as the distance above the surface of the plate where the boundary layer velocity was 0.995 of the free-stream velocity. Typical profiles for Reynolds numbers in the laminar range are shown in Figures 23, 24 and 25.

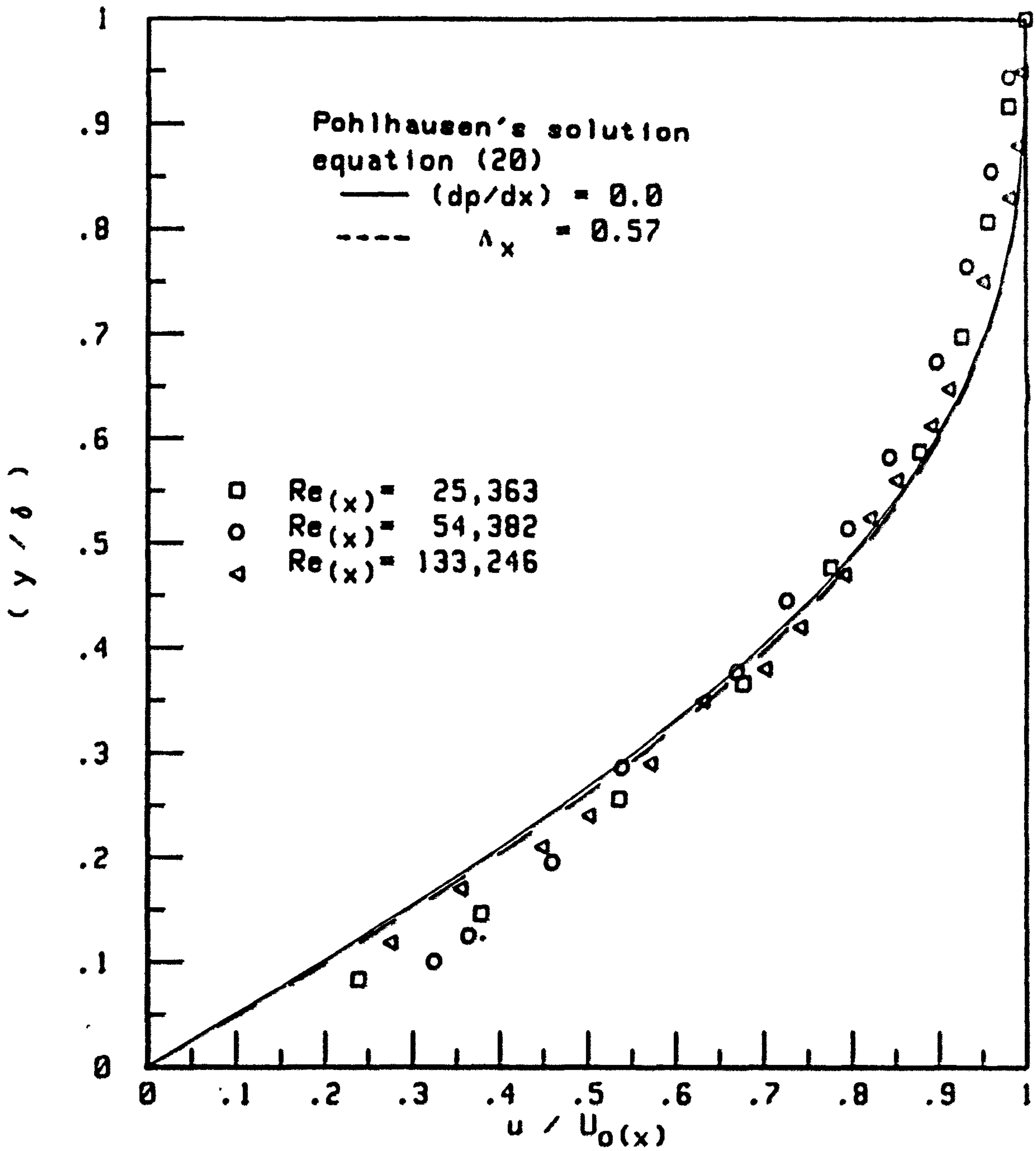

Figure 23. Laminar boundary layer profiles for (dp/dx) = -0.01 lb_f/ft^3

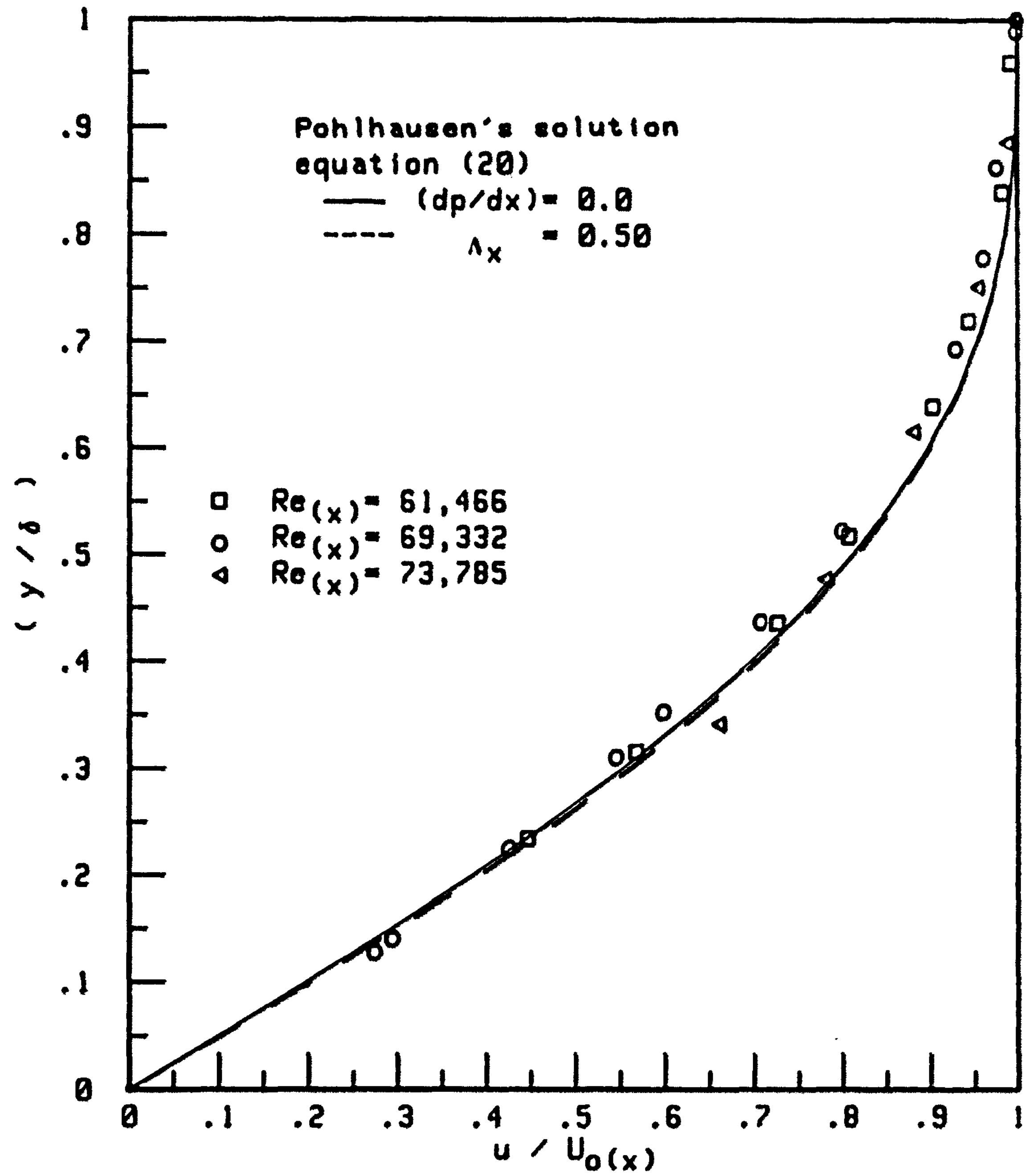

Figure 24. Laminar boundary layer profiles for $(dp/dx) = -0.02\ lb_f/ft^3$

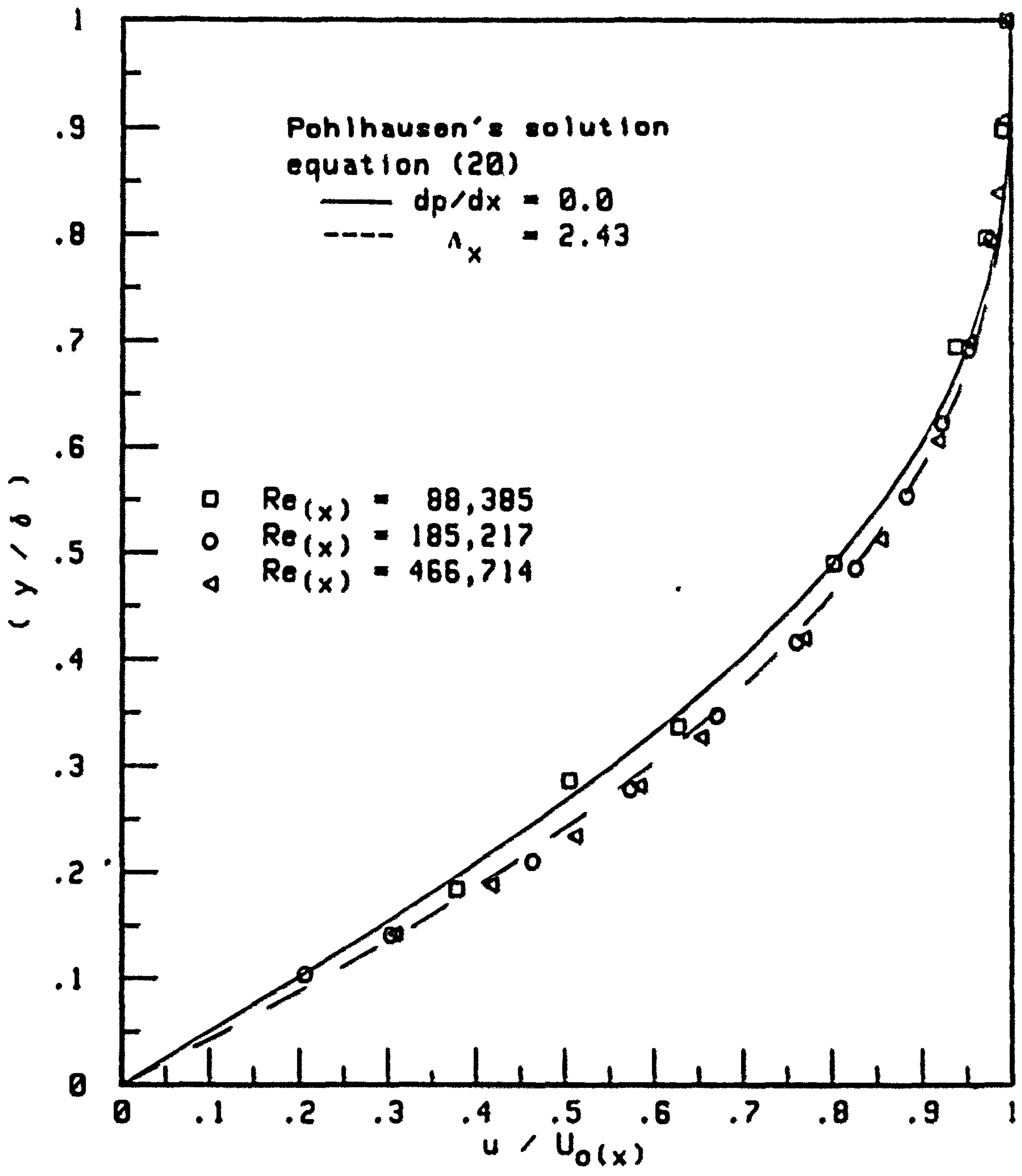

Figure 25. Laminar boundary layer profiles for $(dp/dx) = -0.08\ lb_f/ft^3$

The velocity profiles obtained were compared with the Pohlhausen polynominal approximation [19] to the laminar boundary layer over a flat plate with a free-stream pressure gradient

$$u/U_o = [\ 2\bar{y} - 2\bar{y}^3 + \bar{y}^4] + \Lambda_x\ \bar{y}\ (\ 1 - \bar{y}\ )^3 \qquad (20)$$

where, $\bar{y} = (\ y\ /\ \delta\ )$

and $\Lambda_x = (\ \delta^2 /\ 6\ \nu_a)\ (\ dU_o /\ dx\ )$ (21)

The terms in the square brackets represent zero pressure gradient conditions, while the terms proportional to Λ_x are first-order pressure gradient corrections.

The measured velocity profile data agree well with equation (20) for a laminar boundary layer with a specified free-stream pressure gradient. Little effect on the boundary layer profiles was expected in the region close to the plate surface due to the tip clearance effect of the total head tube and the temperature difference between the plate surface and the free-stream at each location of measurement. However, Figures 23 through 25 show small variations from equation (20).

Total head tube surveys were made to help establish the transition of the boundary layer from laminar to turbulent flow for the different pressure gradients. From these surveys and the heat transfer data, transition for (dp/dx) = -0.01 lb_f/ft^3 was considered to start at $Re_{(x)} = 1.5x10^5$. For (dp/dx) = -0.02 lb_f/ft^3, the transition is at $Re_{(x)} = 2x10^5$ and for the highest free-stream pressure gradient, transition occurred at $Re_{(x)} = 4.5x10^5$.

The data obtained for both heat transfer distributions and boundary layer profile tests show that the test plate boundary layer without vortex generators behaved as a highly two-dimensional laminar boundary flow over a plate surface with constant heat flux.

It was found that for the three free-stream pressure gradients the overall heat transfer coefficients for the plate were about 5, 6.1 and 6.3 percent respectively over that predicted for a laminar boundary layer at zero pressure gradient for all data. If only laminar Reynolds numbers are included, overall coefficients were 4.5, 5.1 and 5.0 percent respectively.

The overall heat transfer coefficients obtained at the three different pressure gradients show small increases over that predicted for laminar flow boundary layer at zero pressure gradients and indicate that the overall heat transfer is not a strong function of pressure gradients used. In addition, the data obtained at the lowest pressure gradient $(dp/dx) = -0.01\ lb_f/ft^3$ show that there is little difference from that predicted for a laminar boundary layer flow at zero pressure gradient. In the chapters following, the lowest pressure gradient is considered equivalent to a zero pressure gradient.

V. RESULTS AND DISCUSSION

The heat transfer data reduced using the methods described in Chapter III will be presented graphically as Stanton number versus Reynolds number for different configurations of vortex generators and three levels of favorable free-stream pressure gradient. These data are also given in tabular form in Appendix D. The earlier results obtained from the evaluation tests with no vortex generator blades confirmed that the test boundary layer was a highly two-dimensional laminar flow. Therefore, at a specified local Reynolds number the improvement of local heat transfer rates due to the vortex generators will be referenced to that obtained from the prediction of reference [18] for laminar boundary layer on a plain plate given by equation (17).

Data are presented for a row of counter-rotating vortex generator blades with pitch equal to two times the blade spacing for spacings s_g = 0.75, 1.0, 2.0 and 4.0 in., vortex blade heights e_g = 0.0625, 0.125 and 0.25 in. and three levels of free-stream pressure gradient.

The heat transfer results are used as a basis for evaluation of the effect of the different configurations of vortex generator blades on enhancement of heat transfer. The behavior of the boundary layer and its development downstream of some of the configurations of vortex generators will be presented and the interaction between the flow structure and the improvement of heat transfer rate will be discussed. The combined experimental results are used as a basis for a proposed set of guidelines for the design of more efficient surfaces with vortex generators.

A. Heat Transfer Performance at $(dp/dx) = 0$

It was determined from the series of evaluation tests with no vortex generators that there is almost no difference between the very small pressure gradient $(dp/dx) = -0.01\ lb_f/ft^3$ and a zero pressure gradient with boundary layer transition at $Re_{(x)} = 1.5x10^5$.

1. Local span-averaged heat transfer results

Data are presented in the form of the local span-averaged Stanton number corrected for unheated starting length as a function of the local Reynolds number for three different heights of vortex generator blades. Each row of vortex generator blades of the same height e_g was tested at spaces of $s_g = 0.75$, 1.0, 2.0 and 4.0 in. between the vortex blades.

a. Effect of $e_g = 0.0625$ in. Figure 26 shows the local span-averaged Stanton number distribution $St_{(x)g}$ as a function of the local Reynolds number $Re_{(x)}$ for the different spaces s_g with the smallest height of vortex generator blades, $e_g = 0.0625$ in.

The data show that the presence of the vortex generator blades has a marked effect on the heat transfer coefficients from the plate surface. Figure 26 shows that the vortex generators improve the local span-averaged Stanton number over that obtained from equation (17), in which the solid line representing for a smooth plate with a laminar boundary layer.

For all spacings between vortex blades, the local span-averaged Stanton numbers $St_{(x)g}$ show higher values in the lowest Reynolds number

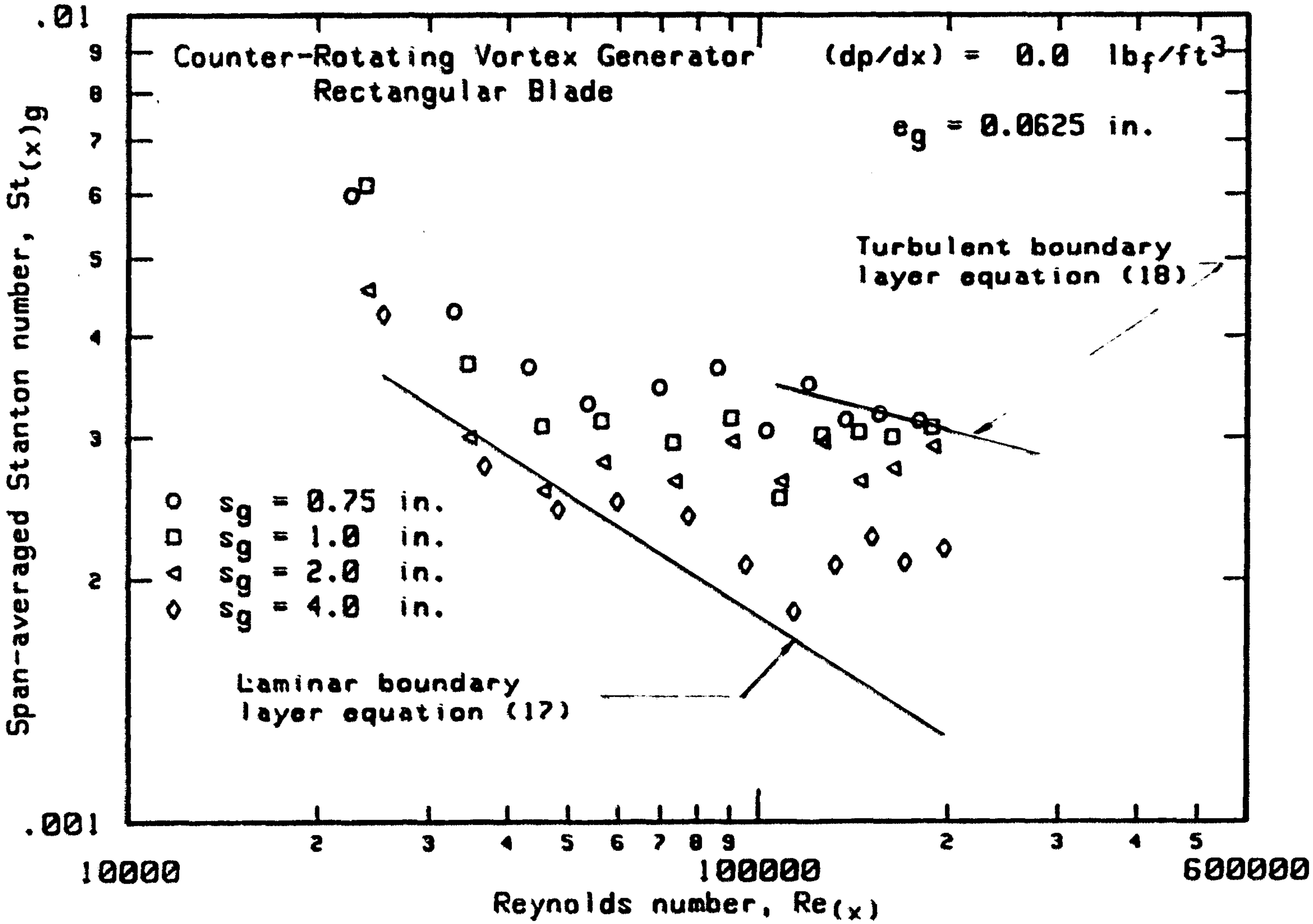

Figure 26. Heat transfer distribution with zero pressure gradient and e_g = 0.0625 in.

regions. For the larger spacings s_g = 4.0 and 2.0 in., values of $St_{(x)g}$ in the Reynolds number range from 3.2×10^4 to 5×10^4 decline below that for the laminar boundary layer flow over a plain surface, but rise to higher values at larger Reynolds numbers. For the smaller spacings s_g= 1.0 and 0.75 in., the local Stanton numbers $St_{(x)g}$ lie above the smooth plate line and again move to higher values beginning at a Reynolds number of 5×10^4. Separation of the data points from the laminar correlation line occurs earlier than without vortex generators and varies depending on the space between the vortex generator blades. Generally, the heat trasfer data have a larger increase over the line representing laminar flows as the space between vortex blades decreases. The largest blade spacing, s_g= 4.0 in. does not appear to complete any transition to the turbulent correlation.

The magnitudes of the increases in Stanton number are shown in Figure 27 as distributions of the ratio $[h_{(x)g}/ h_{(x)o}]$ versus the distance downstream from the plate leading edge given as (x/L) where L is the length of the plate and $h_{(x)o}$ is that obtained from the prediction equation (17).

For all blade arrangements, Figure 27 indicates that the local span-averaged coefficients increase non-linearly with distance downstream of the vortex blades. Immediately behind the blades the enhancement of heat transfer coefficients is from 1.20 to 1.70 times, declining to minimum values at about x = 0.2 L and rising to larger values downstream.

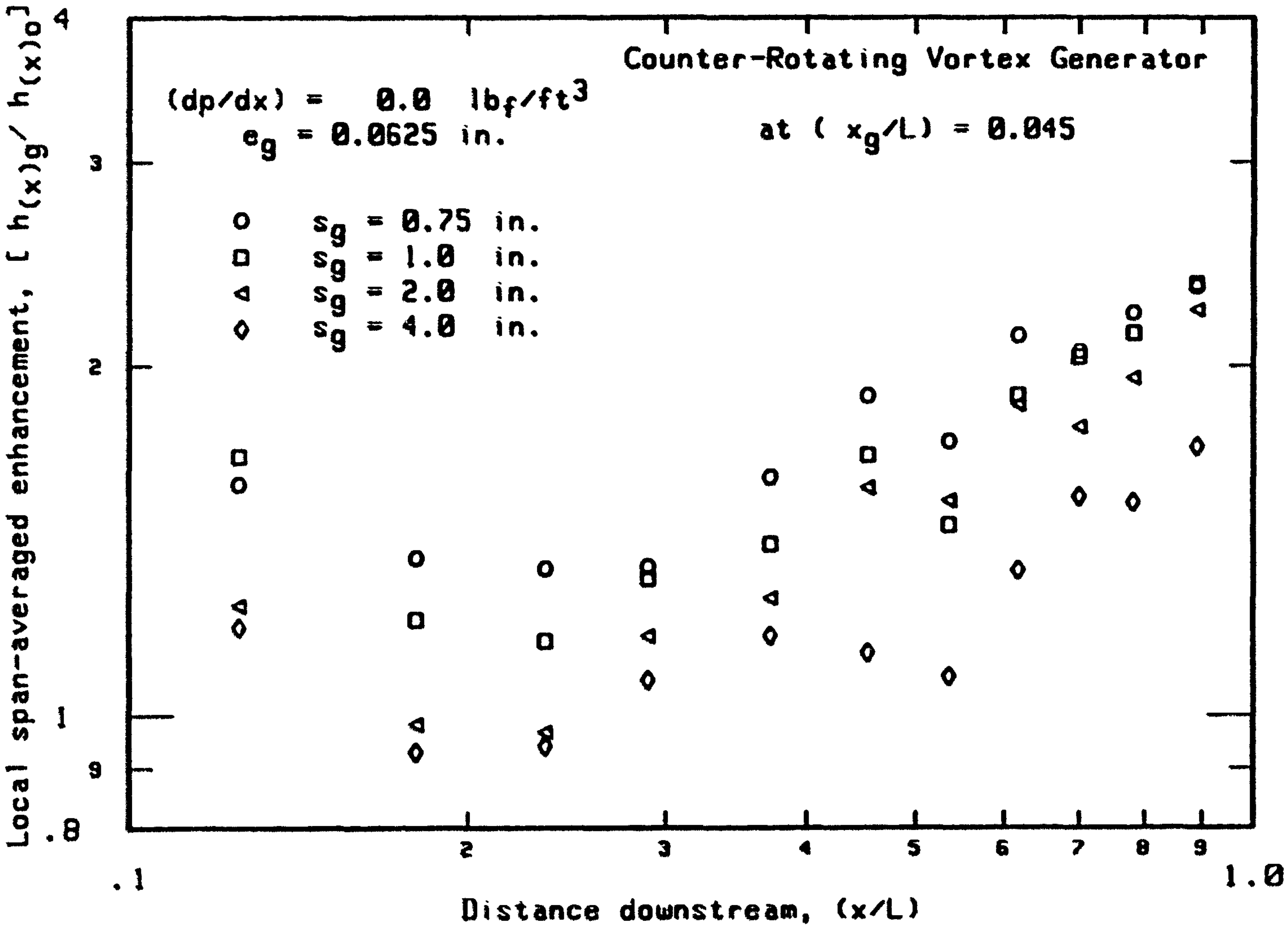

Figure 27. Enhancement of heat transfer coefficients with zero pressure gradient and e_g = 0.0625 in.

The minimum improvement varies depending on the spacing between the blades. In the case of larger spaces s_g = 4.0 and 2.0 in., the minimum improvement falls below unity to about 0.9 at about x = 0.20 L, and increases to about 1.9 to 2.0 at x = 0.9 L. For the smaller spacings s_g = 1.0 and 0.75 in. the minimum improvement of 1.15 to 1.35 percent occurs at about x = 0.23 L and increases to 2.35.

Figure 27 shows that the vortex generator with the smallest space between the blades s_g = 0.75 in. is more effective and gives higher local span-averaged enhancement of heat transfer coefficients than for larger spaces between the blades at the same free-stream conditions.

b. Effect of e_g = 0.125 in. Figure 28 shows the local span-averaged Stanton number as a function of Reynolds number for the different blade spacings with height e_g = 0.125 in.

The data do not deviate as far from the predicted laminar flow line nor do they approach the turbulent correlation as quickly when compared with the blades of e_g = 0.0625 in. The smallest space between blades s_g = 0.75 in. again provides the best local span-averaged Stanton number, but does not reach the values obtained for e_g = 0.0625 in. shown in Figure 26. The transition region moves to a slightly higher Reynolds number of about 6×10^4 compared with e_g = 0.0625 in.

Figure 29 shows the distribution of the enhancement of heat transfer coefficient $[h_{(x)g}/ h_{(x)o}]$ versus (x/L) downstream of the plate leading edge. In the range x = 0.12 L to x = 0.25 L, the improvement of heat transfer coefficient starts to decrease toward unity with only a

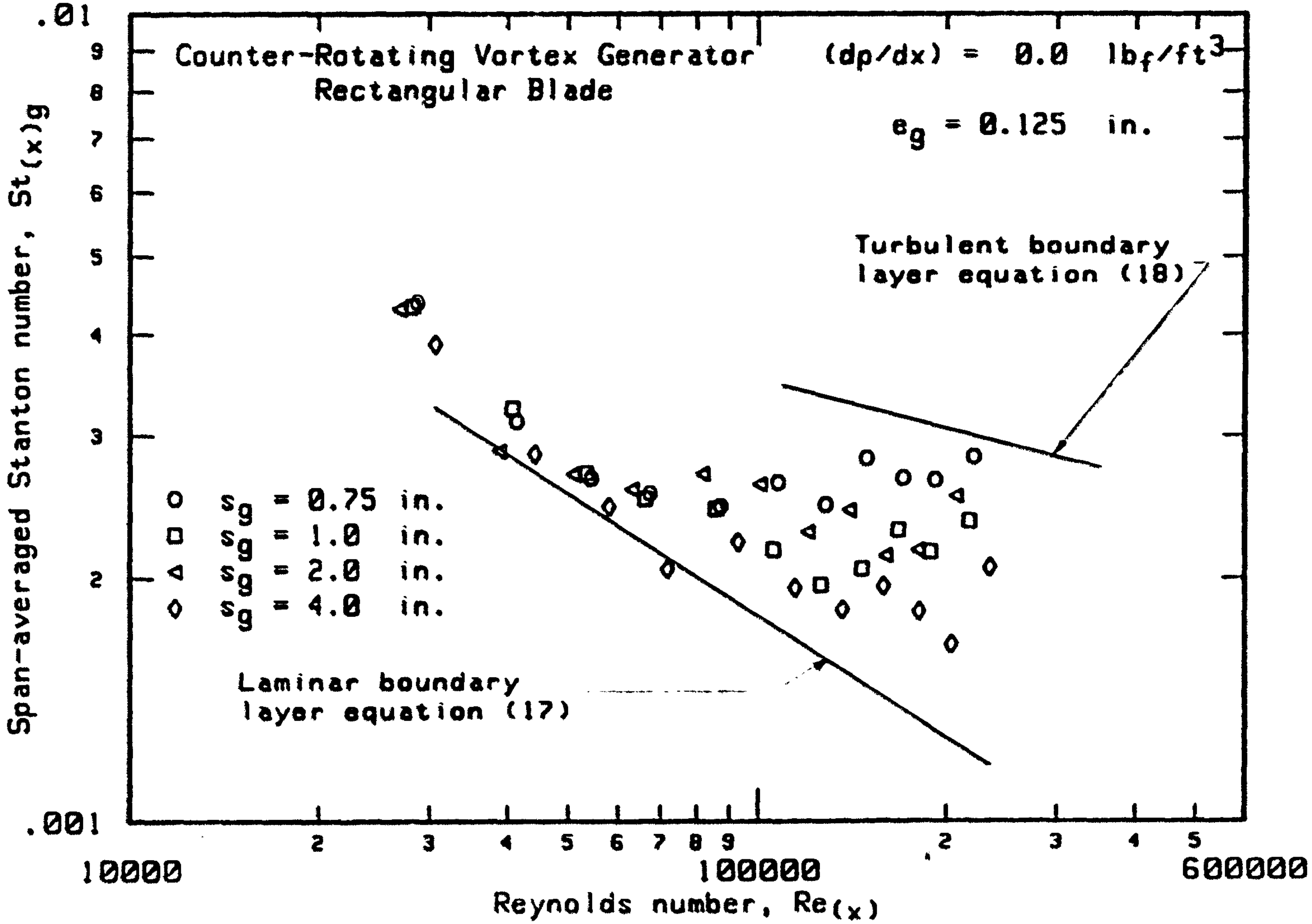

Figure 28. Heat transfer distribution with zero pressure gradient and $e_g = 0.125$ in.

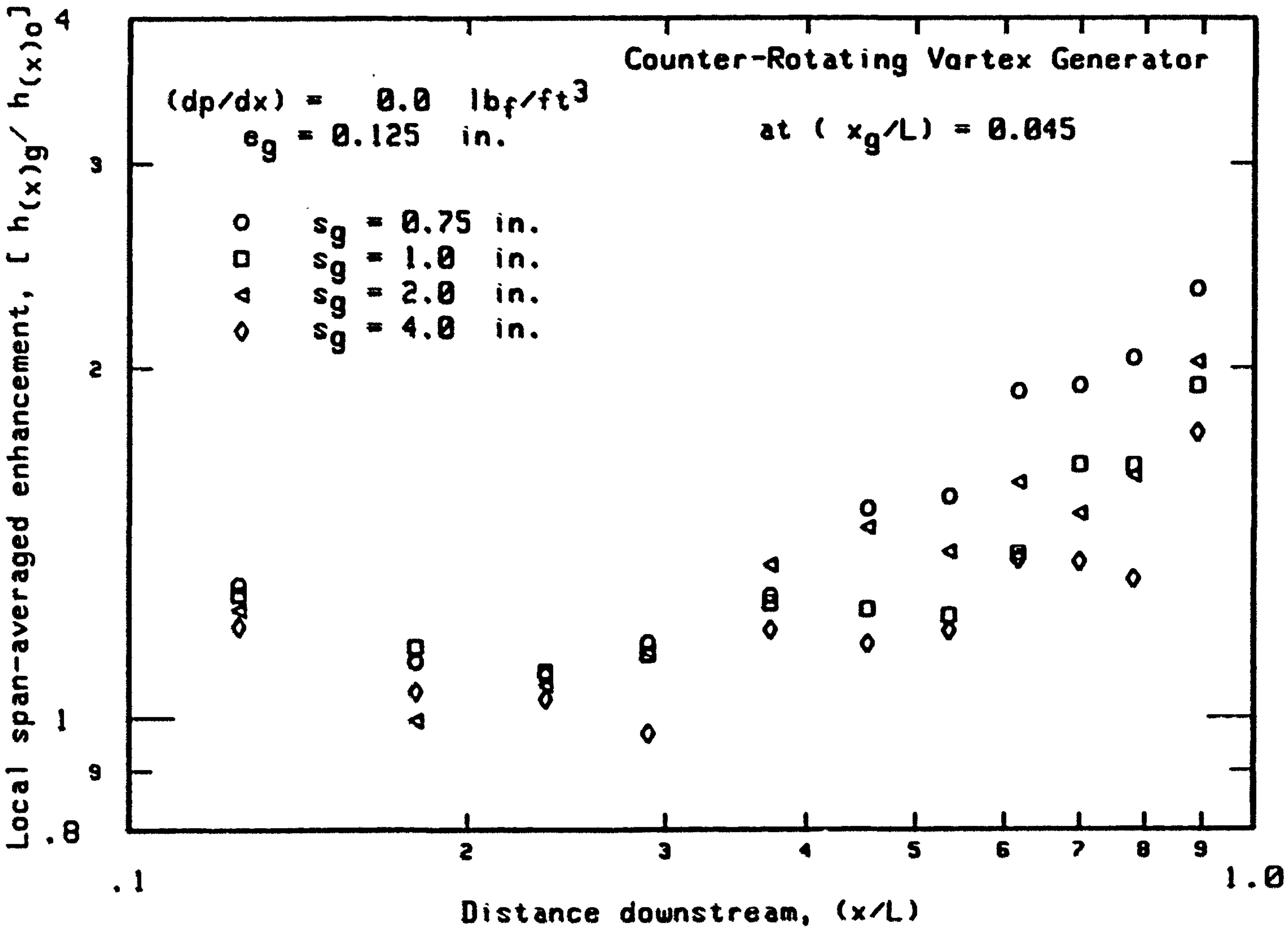

Figure 29. Enhancement of heat transfer coefficients with zero pressure gradient and $e_g = 0.125$ in.

small effect of s_g evident. In the region $x \geq 0.25$ L, the enhancement rises again with the smallest space between blades $s_g = 0.75$ in. indicating the greatest improvement, as was the case of $e_g = 0.0625$ in. Enhancement for $s_g = 1.0$ in. and 2.0 in., is roughly equal with the smallest improvement shown for $s_g = 4.0$ in.

c. Effect of $e_g = 0.25$ in. Figure 30 shows the Stanton number distribution versus the local Reynolds number for the different spaces with the largest height of vortex generator blades $e_g = 0.25$ in. The measured local span-averaged Stanton numbers are more closely grouped in the transition region than was observed for vortex blade heights $e_g =$ 0.0625 and 0.125 in. shown in Figures 26 and 28 respectively.

Once more the data for the $s_g = 0.75$ in. space between blades have generally higher local span-averaged Stanton numbers than for the larger spaces.

Figure 31 shows the magnitudes of the enhancement of heat transfer coefficients $[h_{(x)g}/ h_{(x)o}]$ versus (x/L). For the smaller spaces $s_g =$ 0.75, 1.0 and 2.0 in., Figure 31 indicates that the values obtained for the local span-averaged enhancement of heat transfer coefficient are less than that obtained with the smaller heights of vortex blades at the same free-stream conditions shown in Figures 27 and 29.

It was not possible to establish a Reynolds number range for a transition with $e_g = 0.25$ in. due to the erratic values obtained for different arrangements of the space between vortex blades. For the smaller spaces $s_g = 0.75$, 1.0 and 2.0 in., the minimum local span-

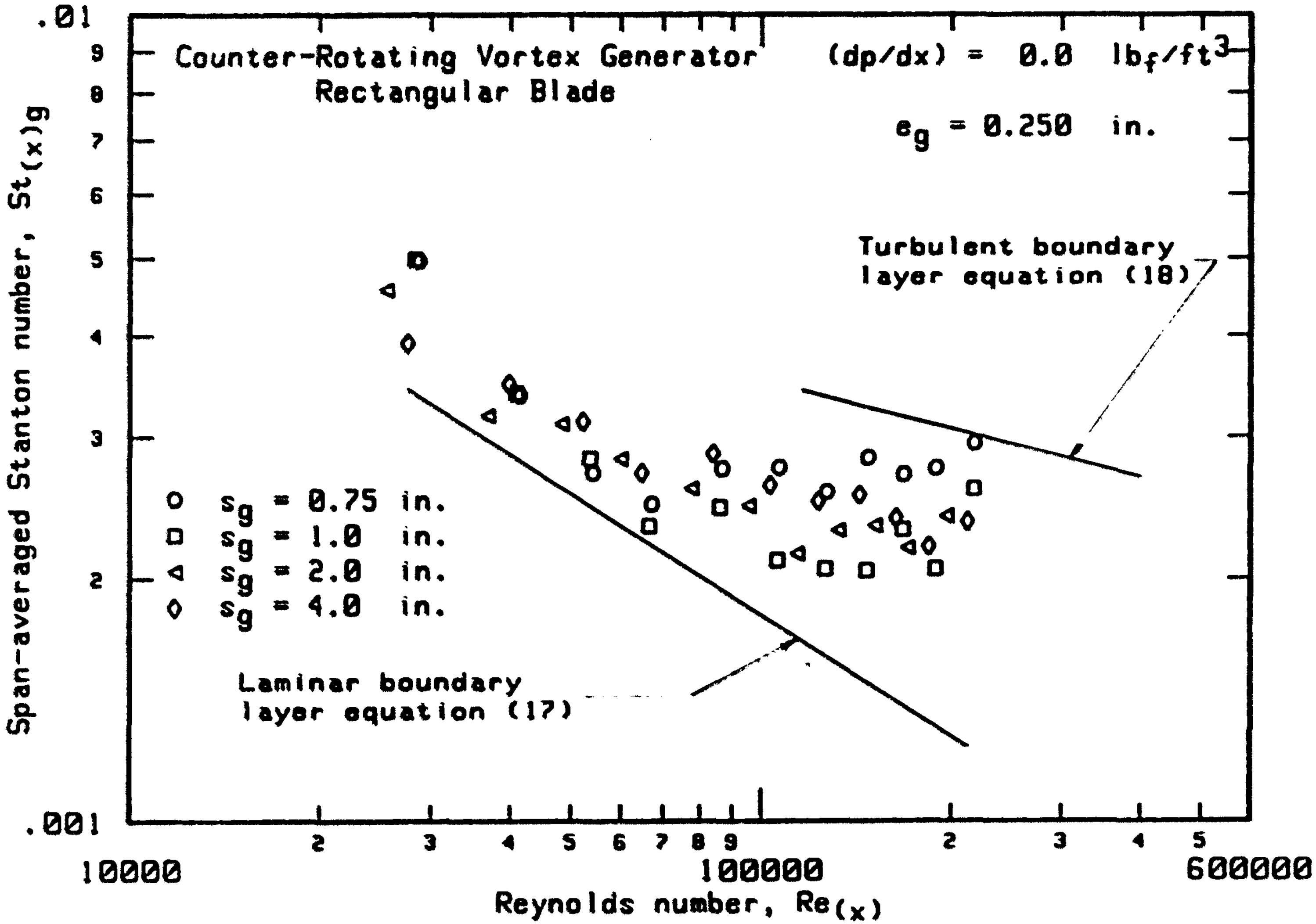

Figure 30. Heat transfer distribution with zero pressure gradient and e_g = 0.25 in.

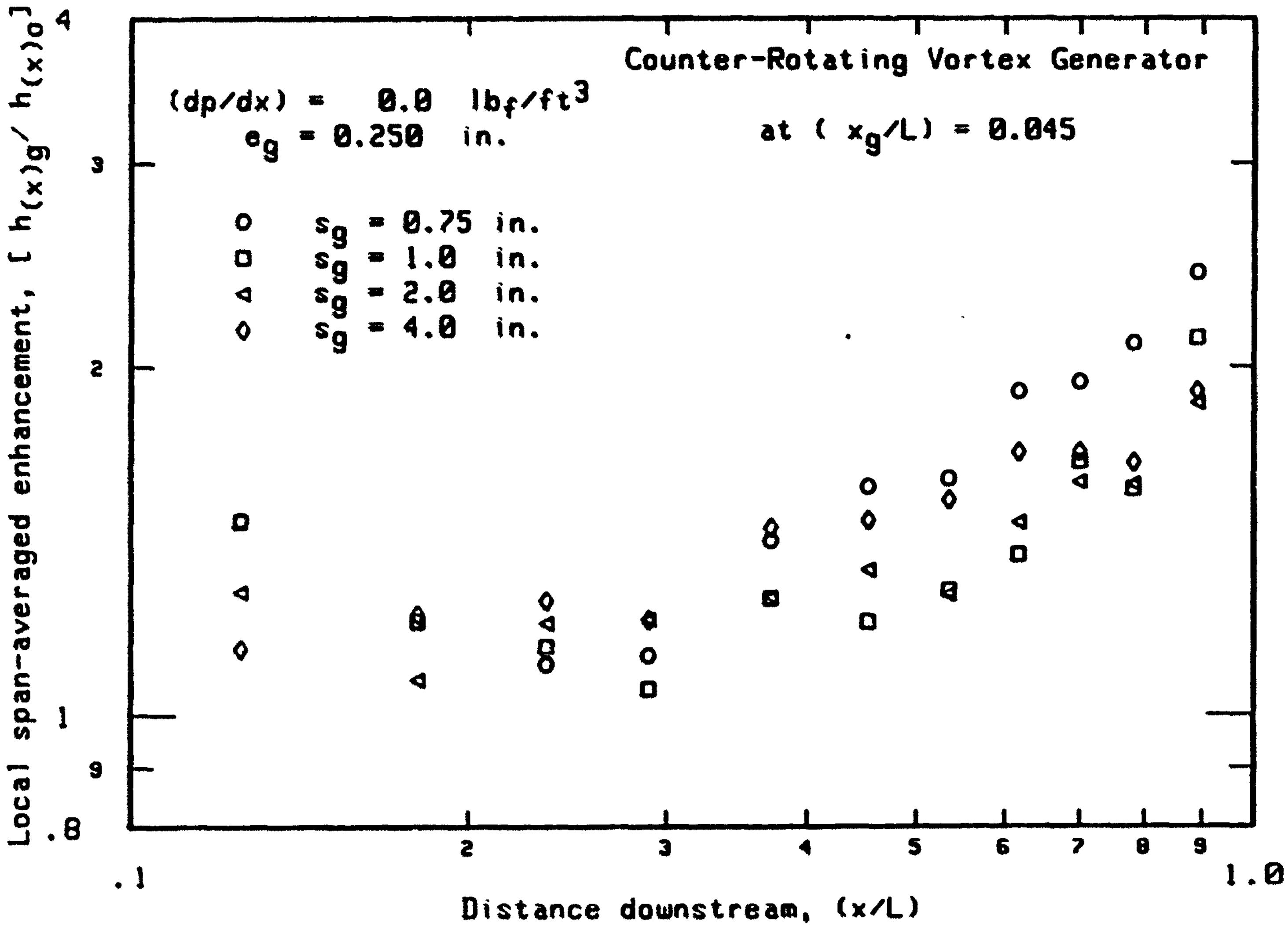

Figure 31. Enhancement of heat transfer coefficients with zero pressure gradient and e_g = 0.25 in.

averaged enhancement of heat transfer coefficient occurs at about x = 0.2 L and is higher than unity.

2. Overall heat transfer results

The enhancement of the overall heat transfer coefficient is presented as a ratio of the measured overall heat transfer coefficient over the plate surface with vortex generators $\bar{h}_g$ to the overall heat transfer coefficient with no vortex blades attached to the plate $\bar{h}_o$. The measured overall heat transfer coefficient $\bar{h}_g$ was obtained by numerically integrating of the measured local span-averaged heat transfer coefficient distribution $h_{(x)g}$ over the plate surface with respect to the distance downstream of the plate leading edge. The predicted overall heat transfer coefficient $\bar{h}_o$ was obtained by integrating the predicted heat transfer coefficient distribution $h_{(x)o}$ with respect to distance downstream for a laminar boundary layer obtained from equation (17) at the same free-stream conditions.

Figure 32 shows the enhancement of the overall heat transfer coefficient as a function of the space/height ratio of vortex blades for different blade vortex heights. Figure 32 also shows the enhancement of the overall heat transfer coefficient as a function of (e_g/δ_g) for various spaces between vortex blades, where δ_g is the predicted laminar boundary layer thickness estimated at the location of the row of vortex blades x_g measured downstream of the leading edge of the plate.

An equation of the form

$$(\bar{h}_g/\bar{h}_o) = c_o\ (s_g/e_g)^{c1} \qquad (22)$$

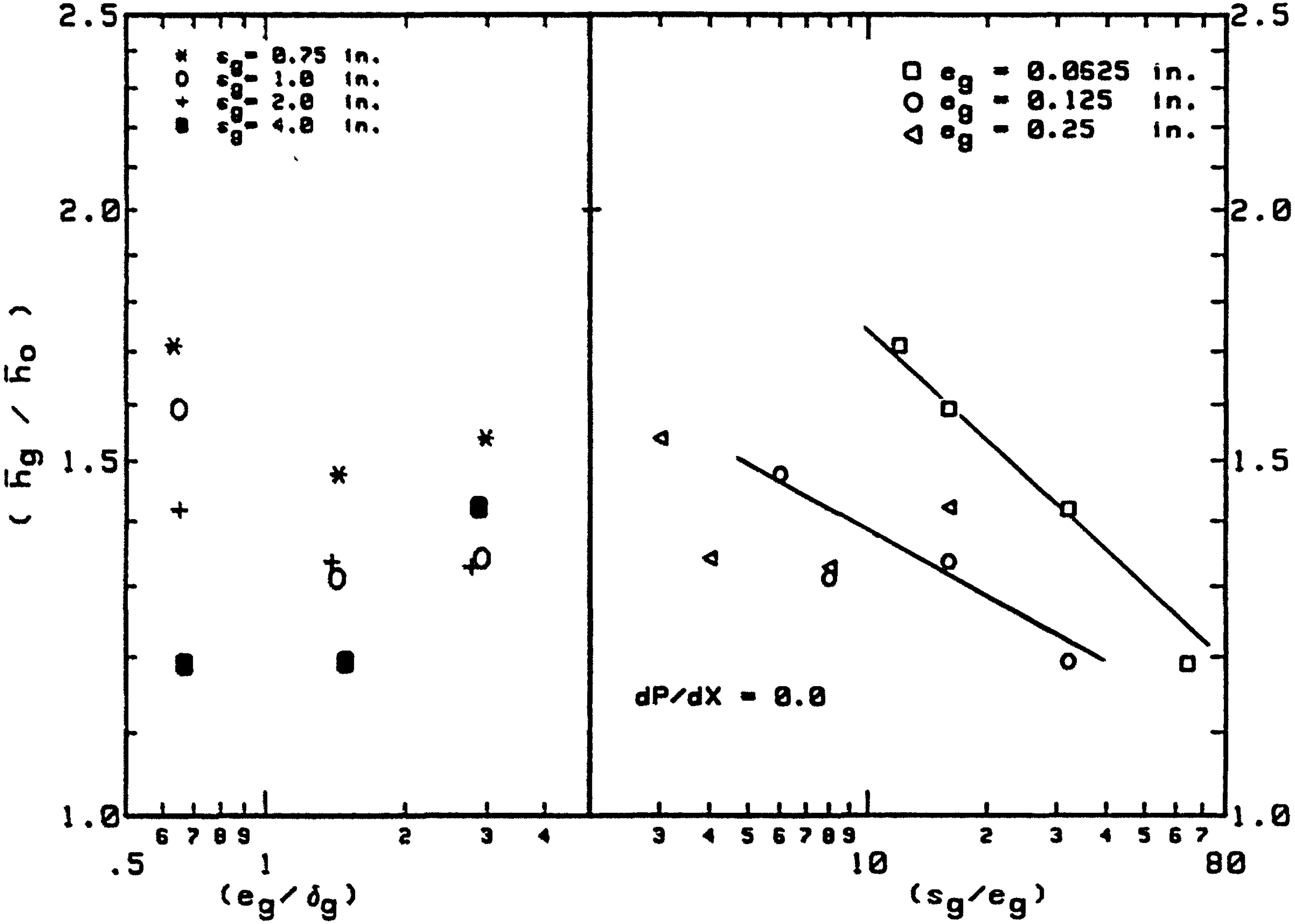

Figure 32. Enhancement of the overall heat transfer coefficient with zero pressure gradient

may be written for each vortex blade height. A linear regression analysis was used to obtain the constants c_o and c1. It is found that the values of the constants c_o and c1 vary with the height of the vortex blades. The lines representing equation (22) for the tested heights of the vortex blades are shown in Figure 32.

From the data shown in Figure 32, it can be observed that the amount of the enhancement of the overall heat transfer coefficient depends on the ratios of (s_g/e_g) and (e_g/δ_g). The enhancement of the overall heat transfer coefficient at a constant space/height ratio increases with decreasing blade height. Figure 32 shows that the best improvement of the overall heat coefficient at a constant space between the vortex blades is obtained at a vortex blade height smaller than the estimated boundary layer thickness at the location of the vortex generator blades except for the largest space between the vortex blades $s_g = 4.0$ in.

It is observed that the behavior of the arrangement of vortex generator blades with the largest space and height, $s_g = 4.0$ in. and $e_g = 0.25$ in., is different than that obtained for all other configurations and arrangements of vortex generator blades. When these blades are installed, only four blades are present and the distance from the tunnel wall to the nearest blade is 1.0 in. There is a possible interaction between the vorticity produced by the nearest blade and the wind tunnel wall. Although some interaction possibly occurs with all blades, the small number of blades present in this case may permit only the two blades near the centerline to operate without side wall effects.

B. Heat Transfer Performance at $(dp/dx) = -0.02\ lb_f/ft^3$

The data below are given in the same format as for the the zero pressure gradient case.

1. Local span-averaged heat transfer results

The blade heights and spacings used are the same as for the zero pressure gradient.

a. Effect of $e_g = 0.0625$ in. Figure 33 shows local span-averaged Stanton number distribution $St_{(x)g}$ as a function of the local Reynolds number $Re_{(x)}$ for different spaces s_g with the smallest height of the vortex blades $e_g = 0.0625$ in. For all spacings between blades, the measured local span-averaged Stanton numbers are higher than those obtained from equation (17) for a smooth plate with a laminar boundary layer. The value of the local span-averaged Stanton number at a constant Reynolds number increases with decreasing space between vortex blades.

Figure 34 shows the distributions of local span-averaged enhancement of heat transfer coefficient over the plate surface given as the ratio of $[h_{(x)g}/ h_{(x)o}]$ versus the distance downstream measured from the plate leading edge given as (x/L). For all arrangements of vortex blades, the local span-averaged enhancement of heat transfer coefficient is about 1.4 times immediately behind the vortex blades and then falls to a minimum improvement at about x = 0.20 L and then starts to rise further downstream. The minimum improvement varies depending on the

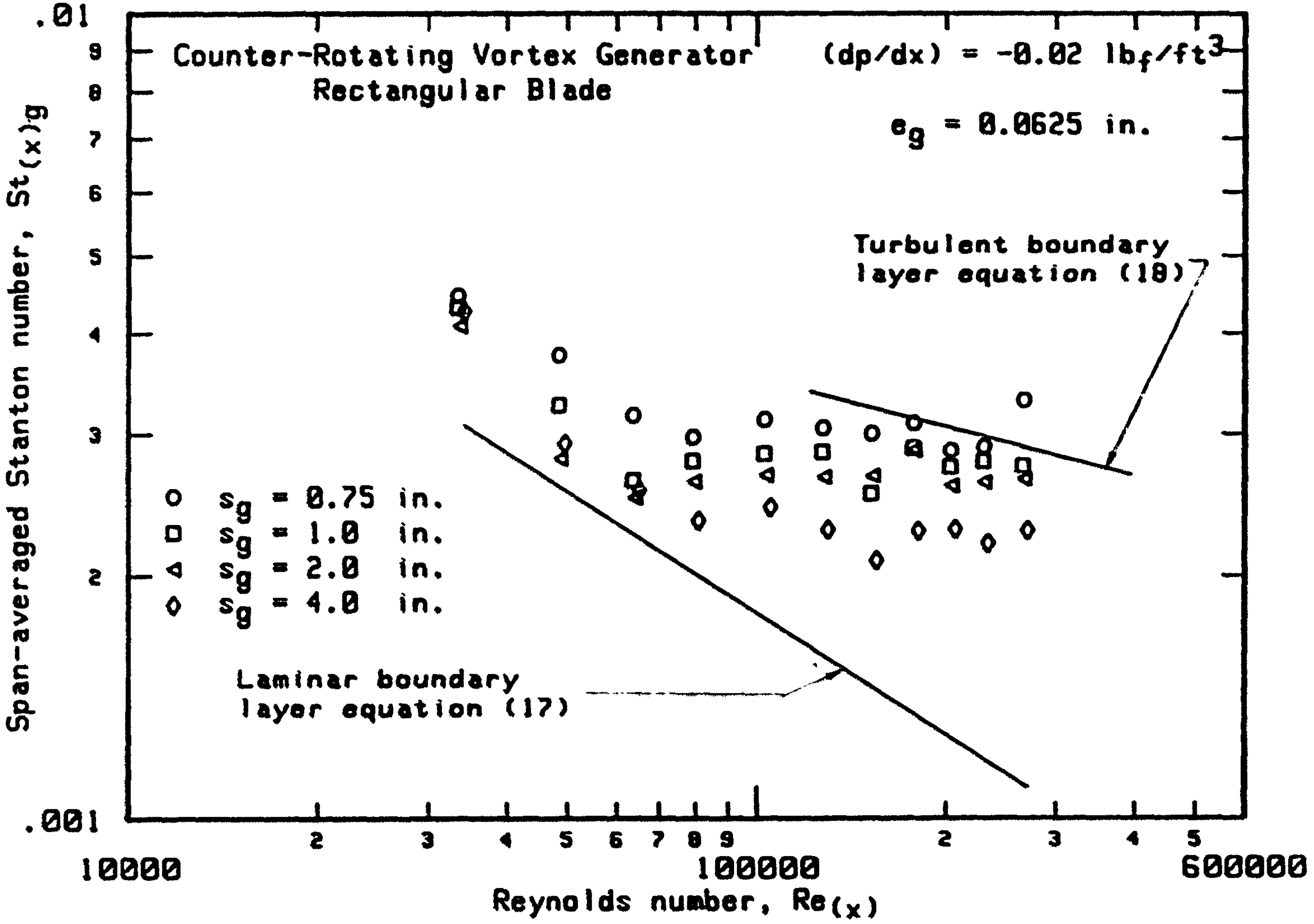

Figure 33. Heat transfer distribution with $(dp/dx) = -0.02\ lb_f/ft^3$ and $e_g = 0.0625$ in.

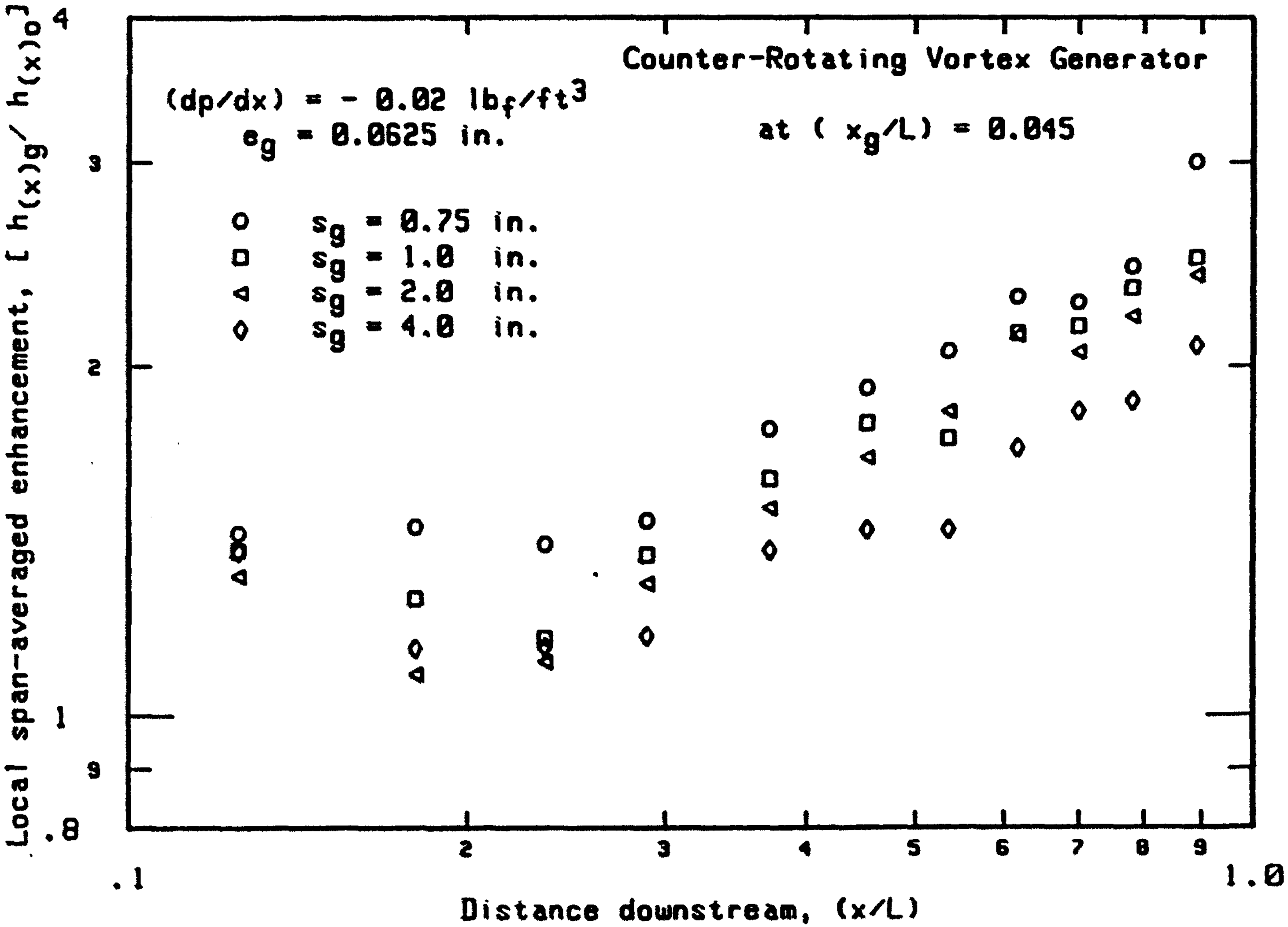

Figure 34. Enhancement of local heat transfer coefficient with $(dp/dx) = -0.02\ lb_f/ft^3$ and $e_g = 0.0625$ in.

space between vortex blades with the minimum improvement at about x = 0.25 L and 0.23 L for the smaller spacing between vortex blades s_g = 0.75 and 1.0 in. respectively. For the larger spacings s_g = 2.0 and 4.0 in., the minimum improvement is about 10 percent higher than that for a plain plate, and occurs at location x equal to about 0.20 L from the plate leading edge.

A comparison of Figures 27 and 34 shows that the local span-averaged enhancement of heat transfer coefficients increases with increasing level of free-stream pressure gradient for the larger spacings s_g = 2.0 and 4.0 in.

b. Effect of e_g = 0.125 in. Figure 35 shows distributions of the local span-averaged Stanton number versus Reynolds number for different arrangements of vortex blades with height e_g = 0.125 in. The distributions have the same trends as those obtained at zero pressure gradient shown in Figure 28. The results shown in Figure 35 are presented in Figure 36 in terms of the local span-averaged enhancement of heat transfer coefficient versus distance (x/L) downstream of the plate leading edge. The effect of the free-stream pressure gradient on the local span-averaged enhancement appears small as shown by comparing Figures 36 and 29.

Figure 36 shows that the heat transfer coefficient distributions increase with decreasing space between the vortex blades, but the improvement is not generally as large as for the smallest height e_g = 0.0625 in. shown in Figure 34.

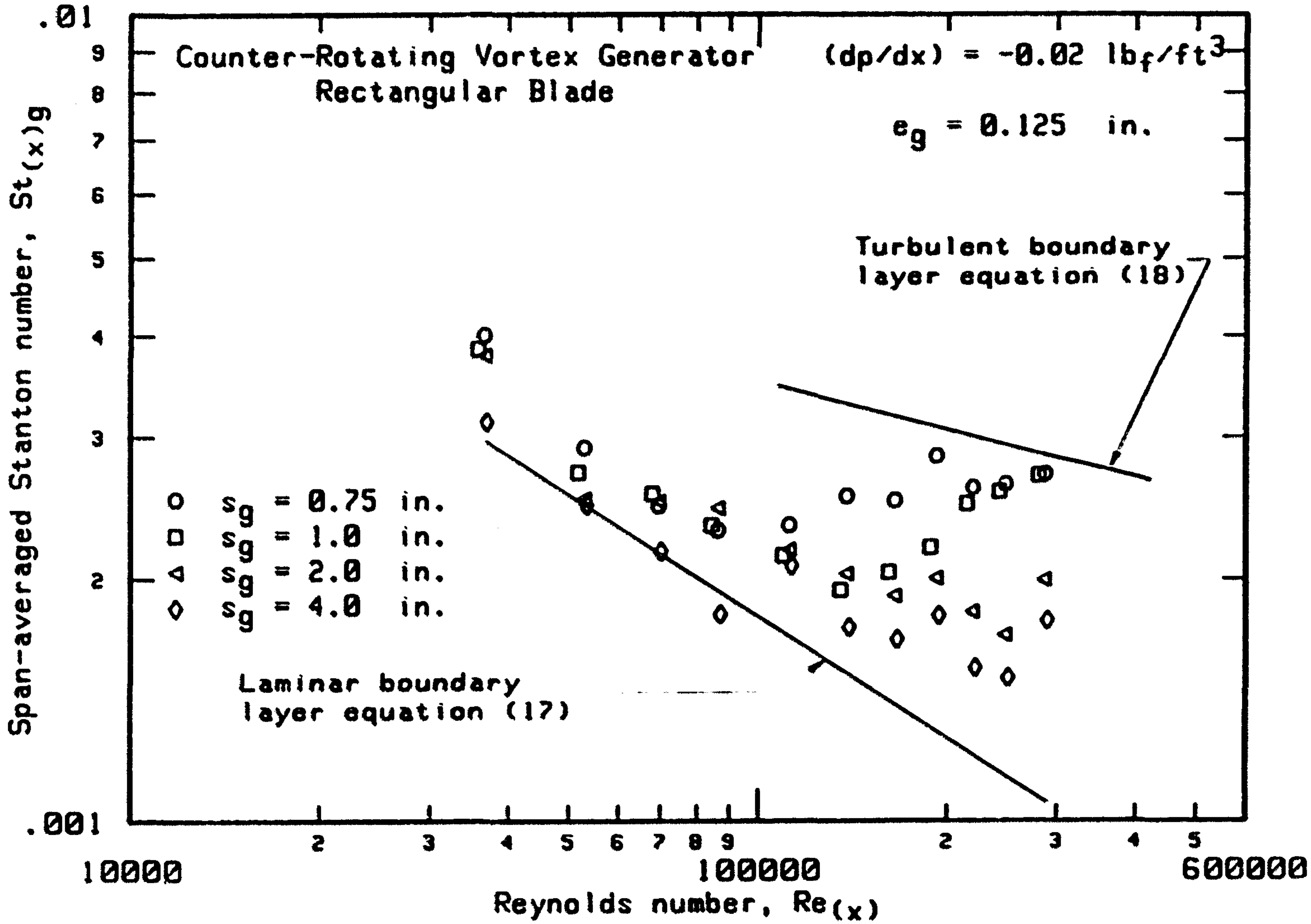

Figure 35. Heat transfer distribution with $(dp/dx) = -0.02\ lb_f/ft^3$ and $e_g = 0.125$ in.

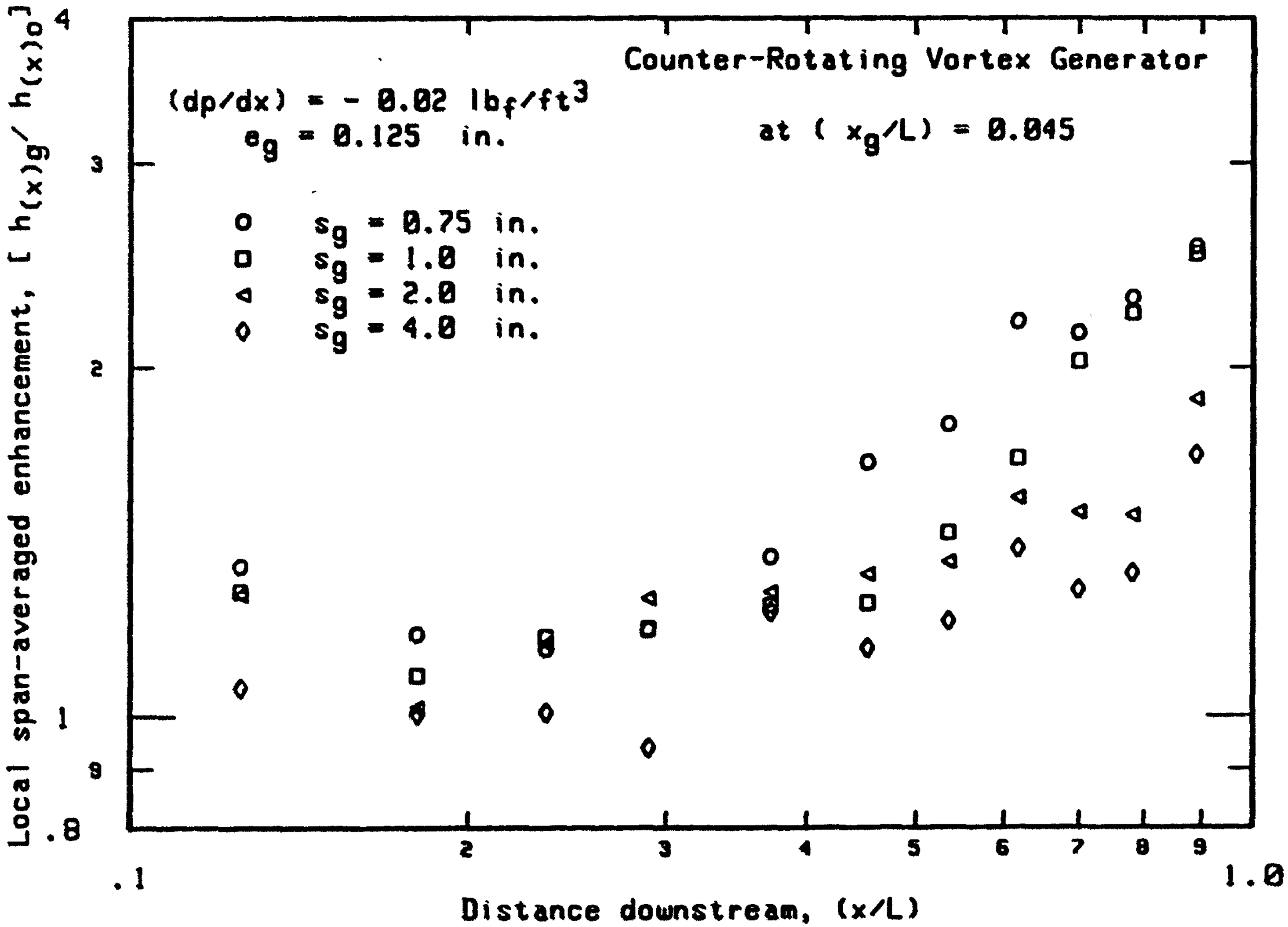

Figure 36. Enhancement of local heat transfer coefficient with $(dp/dx) = -0.02\ lb_f/ft^3$ and $e_g = 0.125$ in.

The minimum improvement occurs at about x = 0.20 L for the spacings s_g= 0.75, 1.0 and 2.0 in. shown in Figure 36.

c. Effect of e_g= 0.25 in. Figure 37 shows the span-averaged Stanton number versus the local Reynolds number for the same arrangements of vortex blades as before, but with the largest height of vortex blade e_g = 0.25 in. The data are more closely grouped than with the blade height e_g= 0.125 in. The smallest blade spacing again has higher local span-averaged Stanton numbers than those obtained for the larger spacing. At Reynolds numbers below $2x10^5$, an apperant laminar to turbulent transition occurs for each of the two smallest spacings but not for the two largest spacings, which exhibit no clear transition to the turbulent correlation.

Figure 38 gives the enhancement of heat transfer coefficient versus distance downstream from the plate leading edge. For the smaller spacings s_g= 0.75 and 1.0 in., the improvement of the local span-averaged heat transfer coefficients fall to minimum values at about x = 0.27 L but the larger spacings s_g= 2.0 and 4.0 in. do not appear to have a minimum enhancement and increase almost linearly with the distance x. This behavior is similar to that obtained for the same arrangements and height of vortex blades at zero free-stream pressure gradient shown in Figure 31.

2. Overall heat transfer results

Figure 39 shows the enhancement of the overall heat transfer coefficient as a function of space/height ratio of vortex blades and the

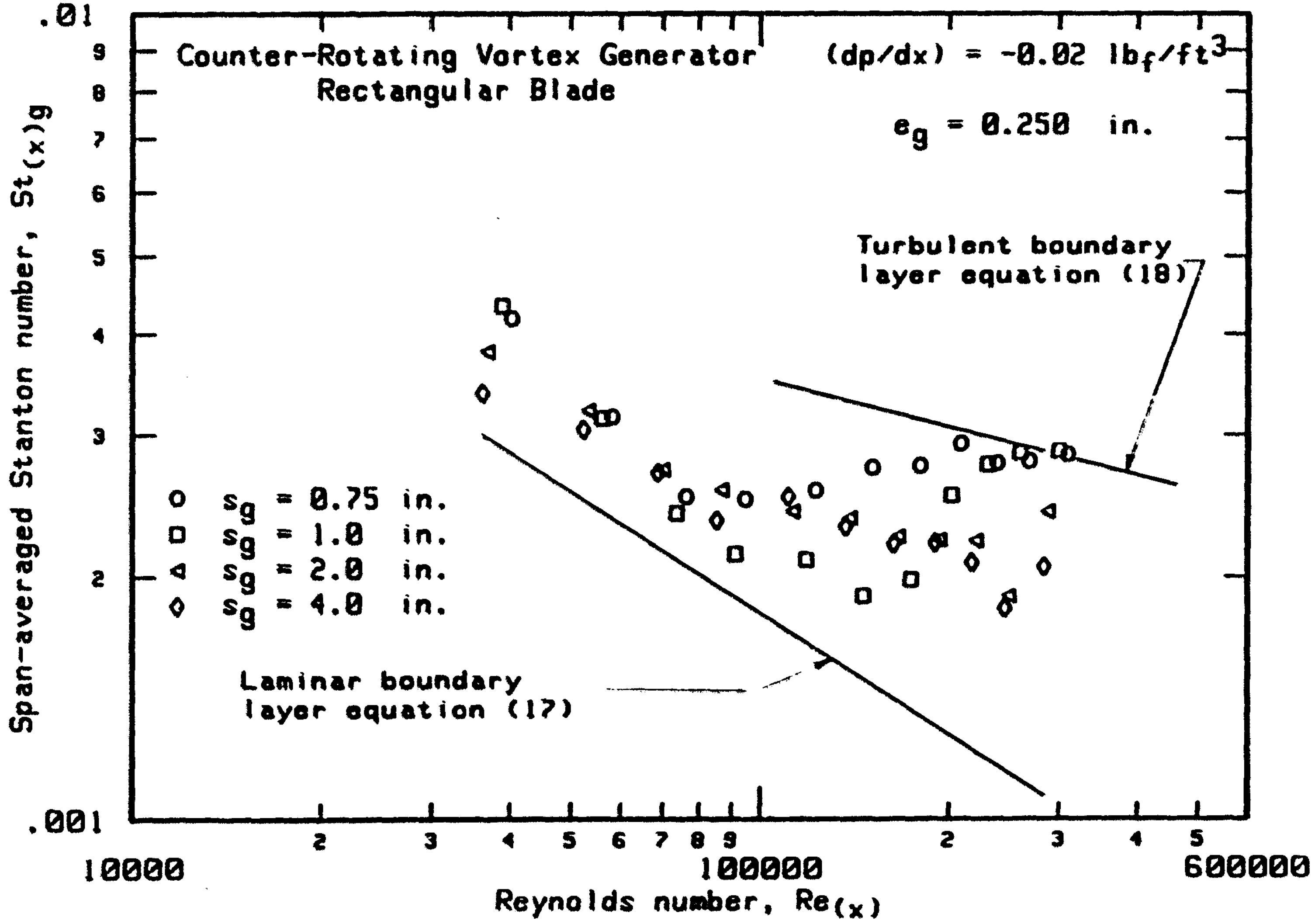

Figure 37. Heat transfer distribution with $(dp/dx) = -0.02\ lb_f/ft^3$ and $e_g = 0.25$ in.

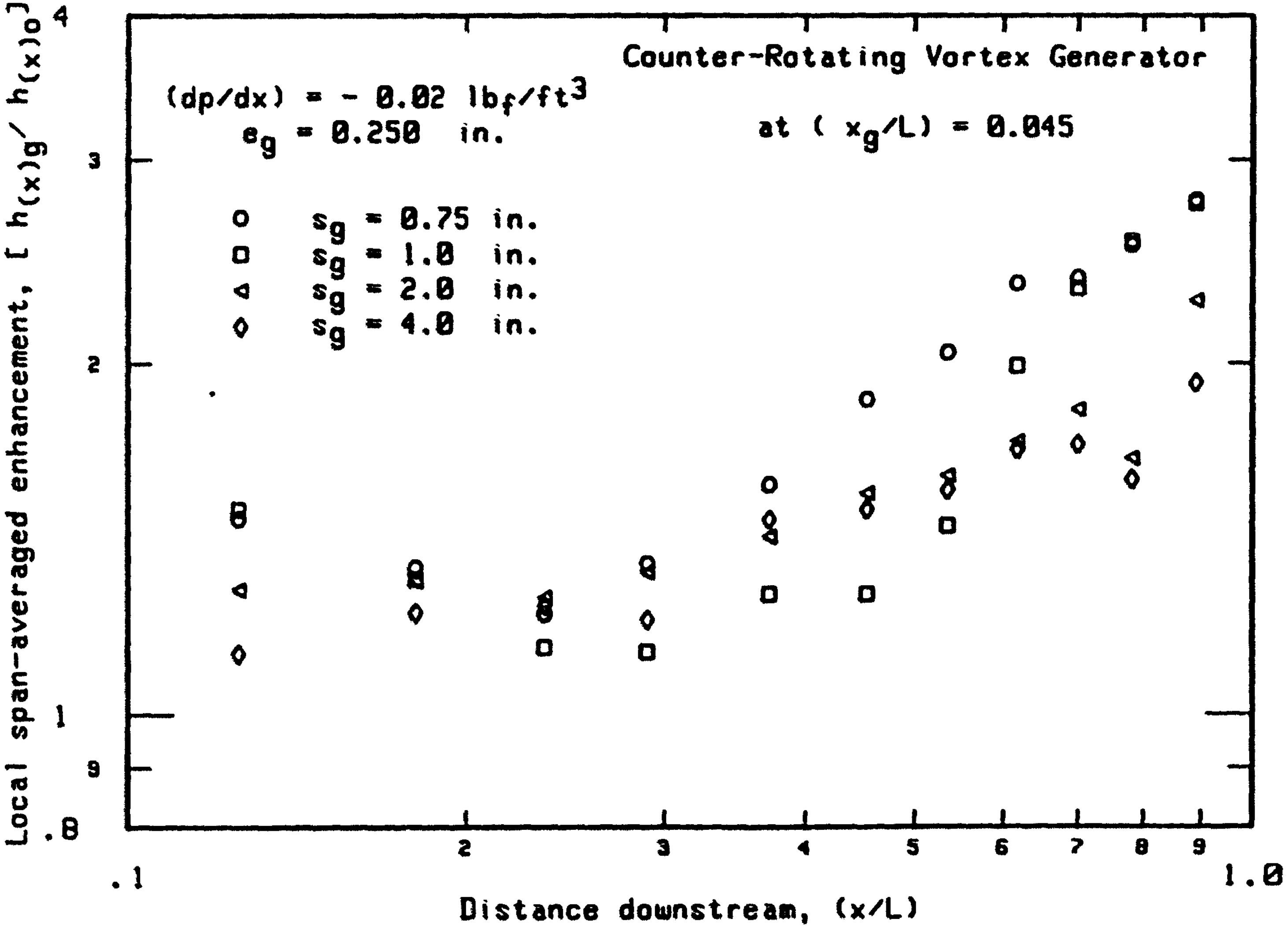

Figure 38. Enhancement of local heat transfer coefficient with $(dp/dx) = -0.02\ lb_f/ft^3$ and $e_g = 0.25$ in.

lines representing equation (22) for the three heights of vortex blades at $(dp/dx) = -0.02\ lb_f/ft^3$. For the smallest blade height, the amount of enhancement of the overall heat transfer coefficients at a constant space/height ratio of vortex blades is higher than that obtained with the larger blade heights. For the blade heights of vortex blades $e_g =$ 0.125 and 0.25 in. at a constant (s_g/e_g), Figure 39 shows that they are of roughly equal strength on improvement of the overall heat transfer coefficient.

It is clear that the enhancement of the overall heat transfer coefficients at a constant (e_g/δ_g) increase with decreasing the space between the vortex blades. Figure 39 also shows that the best improvement of the overall heat transfer coefficient at a constant space between vortex blades is obtained with a ratio (e_g/δ_g) of about 0.77. The enhancement falls to minimum values at a blade height e_g equal to about 1.6 δ_g, then starts to rise to higher improvement values with increasing the ratio (e_g/δ_g) but does not reach that obtained at $(e_g/\delta_g) < 1.0$.

The effect of the free-stream pressure gradients on the enhancement of the overall heat transfer coefficients can be obtained by comparing the data shown in Figure 39 with that presented at zero pressure gradient shown in Figure 32. A small increase of the level of the pressure gradient appears to have a small effect on the improvement of the overall heat transfer coefficients, especially for the arrangements of vortex generator blades with smaller spacing between blades and smallest height of blade.

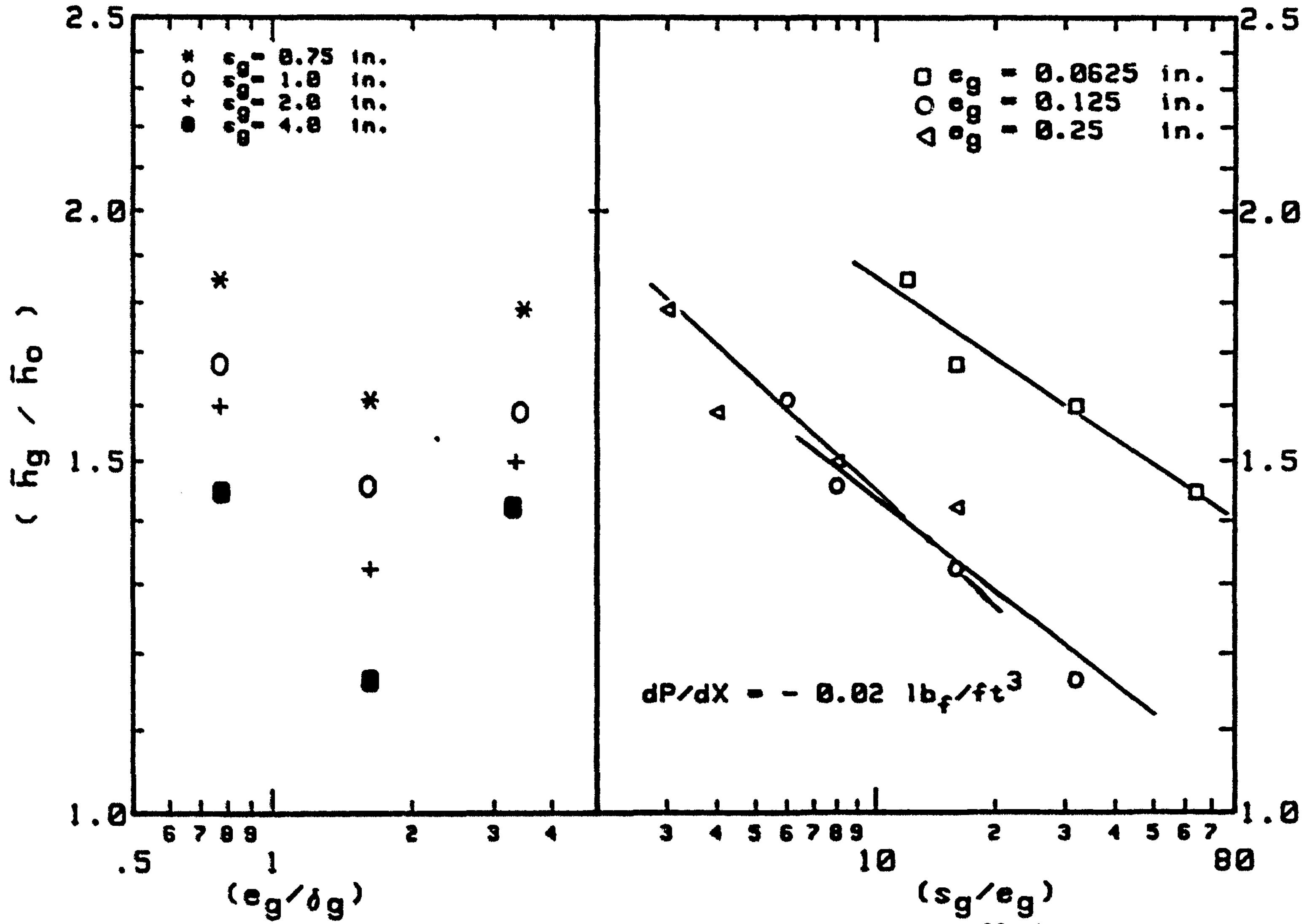

Figure 39. Enhancement of the overall heat transfer coefficient with $(dp/dx) = -0.02\ lb_f/ft^3$

C. Heat Transfer Performance at $(dp/dx) = -0.04\ lb_f/ft^3$

Data are presented below for a row of counter-rotating vortex blades in four different arrangements of the space between the vortex blades, s_g = 0.75, 1.0, 2.0 and 4.0 in. Each arrangement was tested for the three different heights of the vortex blades.

1. Local span-averaged heat transfer results

The blade heights and spacings used are the same as for $(dp/dx) = -0.02\ lb_f/ft^3$ and the zero pressure gradient.

a. Effect of e_g = 0.0625 in. Figure 40 shows the distributions of the measured local span-averaged Stanton number versus Reynolds number for the different spaces s_g with the smallest height of vortex blades e_g = 0.0625 in. For blade spacings s_g = 0.75 in. and 1.0 in., the local span-averaged Stanton number is larger than for the spacings s_g = 2.0 in. and 4.0 in. at Reynolds numbers below about 3×10^5. The data for all spacings appear to go through a transition from the laminar correlation to the turbulent correlation. The two smallest spacings have several points on the turbulent correlation. In the case of the largest spacing s_g = 4.0 in., the values of the measured local span-averaged Stanton number in the Reynolds number range from 5×10^4 to 1.2×10^5 are on the laminar correlation line, indicating no enhancement was obtained in this region.

Figure 41 shows the distributions of the local span-averaged enhancement of heat transfer coefficient over the plate surfaces versus

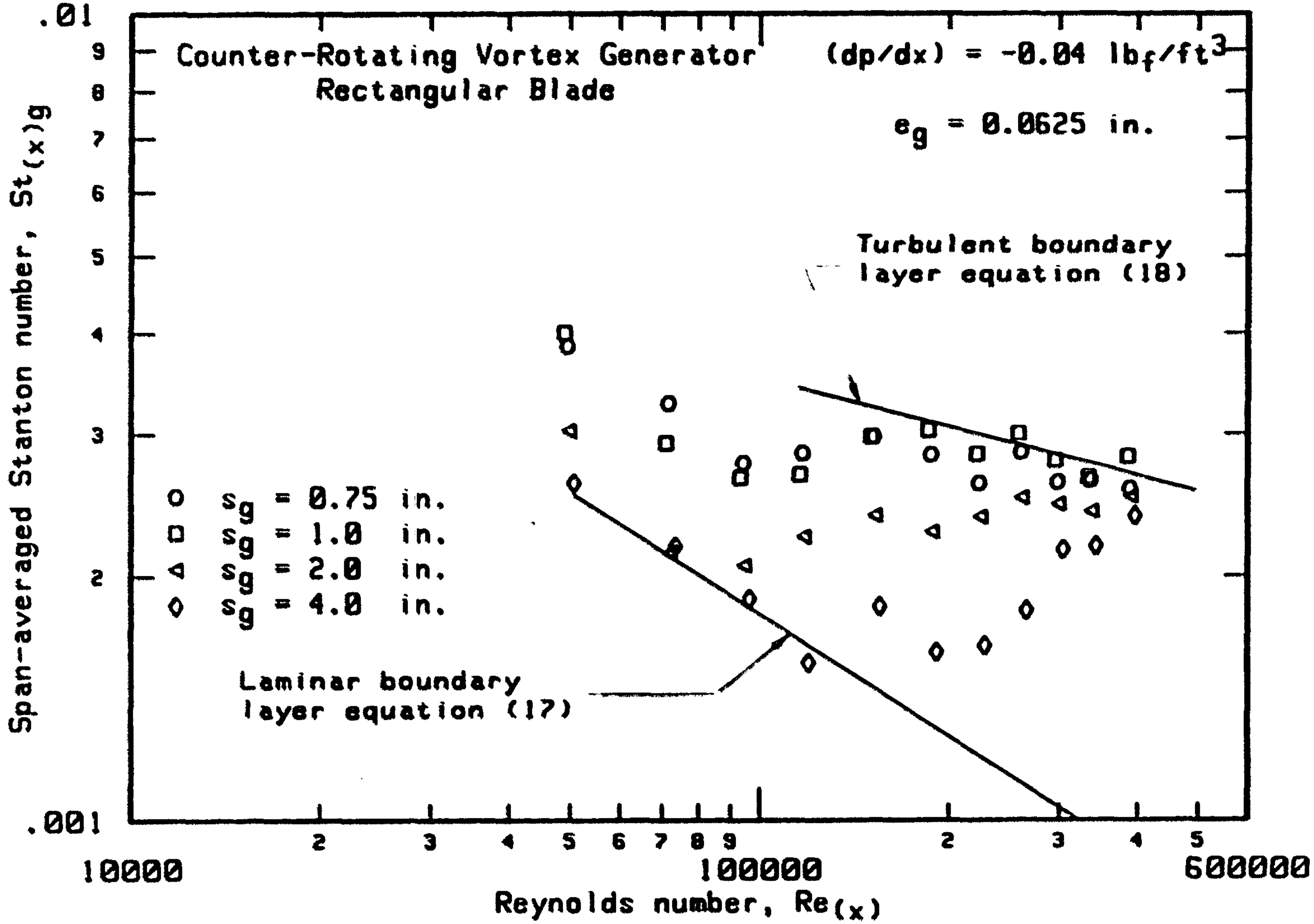

Figure 40. Heat transfer distribution with $(dp/dx) = -0.04\ lb_f/ft^3$ and $e_g = 0.0625$ in.

the distance x downstream measured from the plate leading edge referenced to the plate length L. The enhancement ratio $[h_{(x)g}/ h_{(x)}]$ at the same (x/L) values are larger than those obtained with (dp/dx) = $-0.02\ lb_f/ft^3$ in Figure 34 except for s_g = 4.0 in. which has lower values.

In Figure 41, the minimum improvement of the span-averaged heat transfer coefficients are obtained at about x = 0.2 L for both s_g = 0.75 and 1.0 in., and at about x = 0.18 L for s_g = 2.0 in. It is apparent that the arrangements of the vortex blades with spacings s_g = 0.75 and 1.0 in. have an equal effect on the enhancement of the local span-averaged heat transfer coefficients.

b. Effect of e_g = 0.125 in. Figure 42 shows the data for local span-averaged Stanton number as a function of Reynolds number with a vortex blade height e_g = 0.125 in. In Figure 42, the span-averaged Stanton numbers at the same Reynolds number are less than those obtained with a blade height e_g = 0.0625 in.

Figure 42 shows that the smallest blade spacings make a complete transition to the region of the turbulent correlation before $Re_{(x)} = 4x10^5$, while the larger spacings are still between the laminar and turbulent correlations at $Re_{(x)} = 4x10^5$.

Figure 43 shows the distributions of the local span-averaged enhancement ratio $[h_{(x)g}/ h_{(x)o}]$ versus the distance downstream (x/L). For both s_g = 0.75 and 1.0 in., the minimum improvement of the local span-averaged heat transfer coefficients is observed at about x =

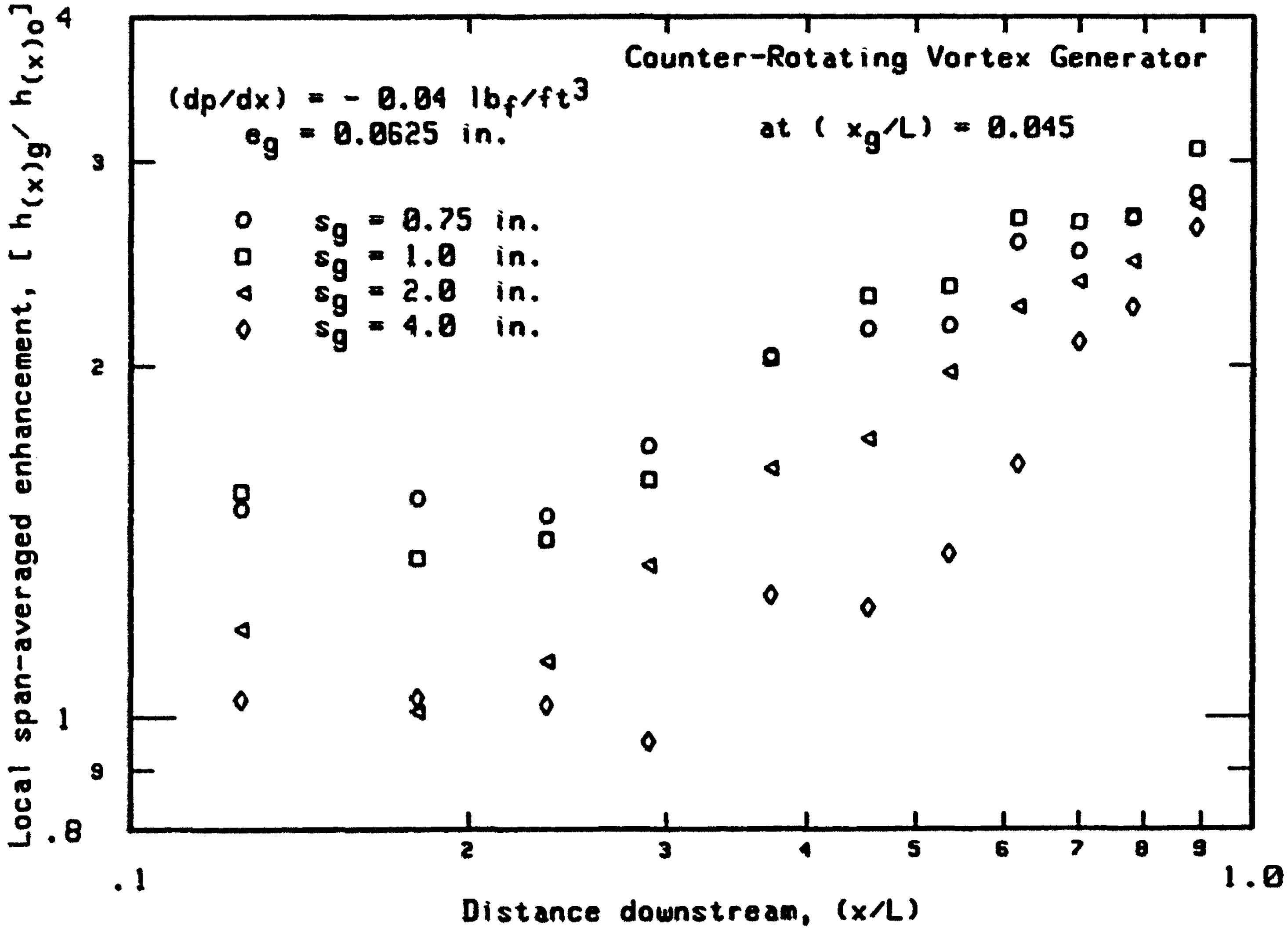

Figure 41. Enhancement of local heat transfer coefficient with $(dp/dx) = -0.04\ lb_f/ft^3$ and $e_g = 0.0625$ in.

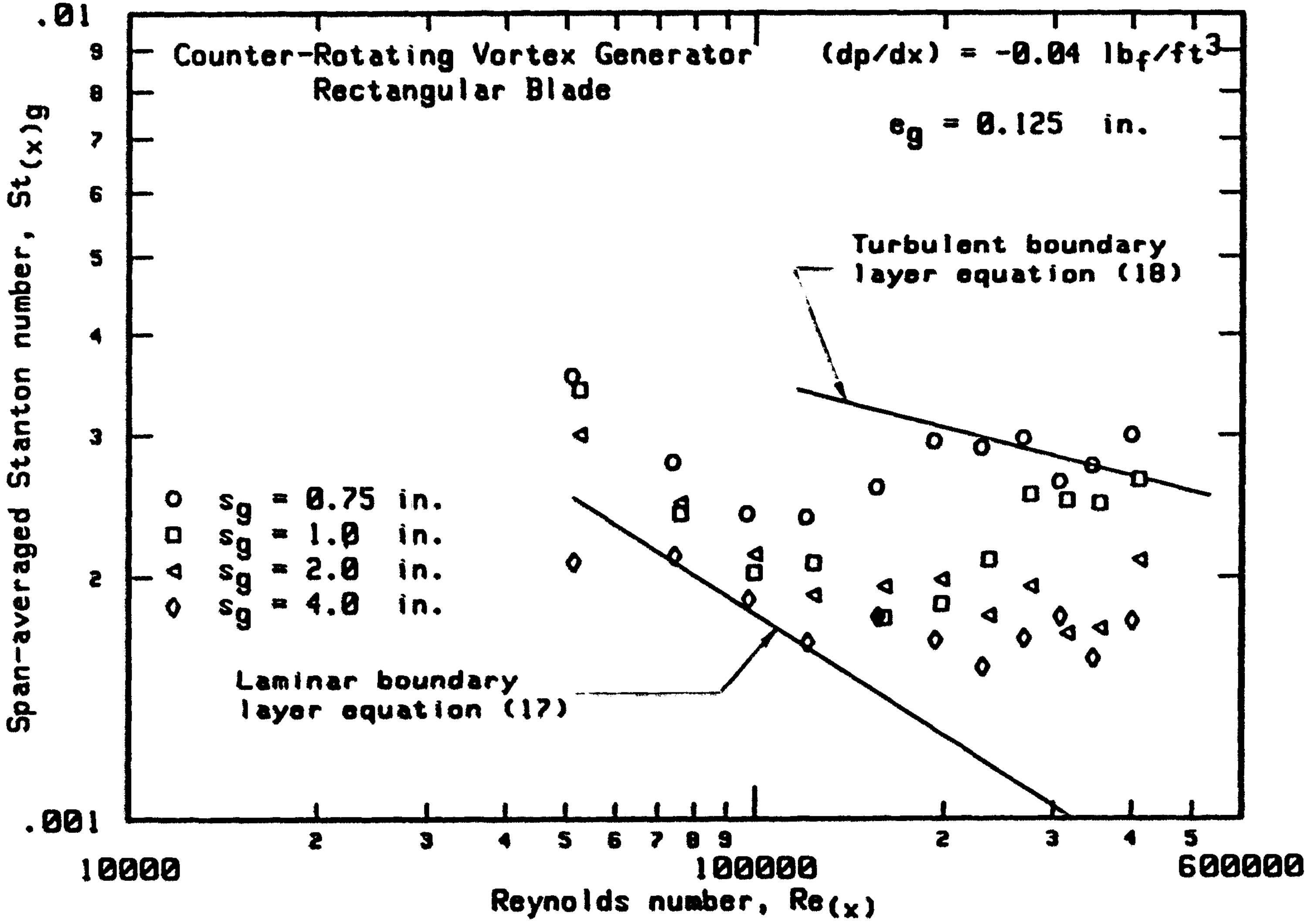

Figure 42. Heat transfer distribution with (dp/dx) = -0.04 lb_f/ft^3 and e_g = 0.125 in.

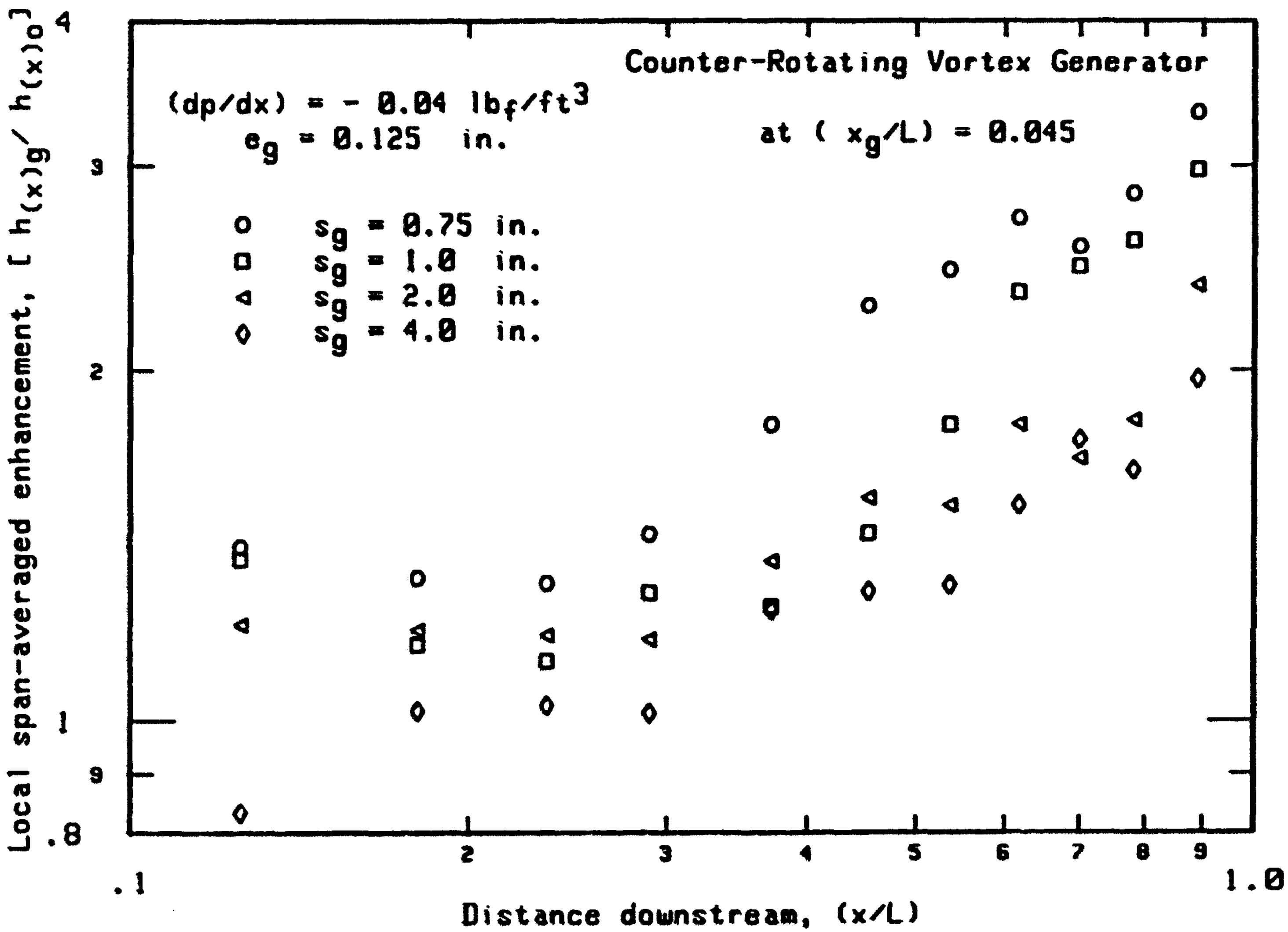

Figure 43. Enhancement of local heat transfer coefficient with (dp/dx) = -0.04 lb_f/ft^3 and e_g = 0.125 in.

0.22 L. The blades with s_g = 2.0 and 4.0 in. do not show any obvious minimum.

The effect of different levels of free-stream pressure gradient on the local span-averaged enhancement with the same arrangements of vortex generator blades can be observed by comparing Figures 43 and 36. Improvement of the local span-averaged heat transfer coefficient for s_g = 0.75 in. and s_g = 1.0 in. increases by increasing free-stream pressure gradient from -0.02 lb_f/ft^3 to -0.04 lb_f/ft^3.

c. Effect of e_g = 0.25 in. Figure 44 gives the local span-averaged Stanton number data versus local Reynolds number for vortex blade height e_g = 0.25 in. As with the previous data, the local span-averaged Stanton number at the same Reynolds number increases with decreasing space between the vortex blades. The data diverge from the the lines representing the laminar boundary layer correlation and again the two smallest blade spacings make a transition to turbulent regime while the others do not. High Reynolds number data for both s_g = 0.75 in. and s_g = 1.0 in. are significantly above the turbulent correlation line.

Figure 45 shows the distributions of the local span-averaged enhancement of heat transfer coefficient over the plate surface as a function of the distance x measured downstream from the plate leading edge. Comparison of Figure 45 and 43 show that for small spacings, larger enhancement exists at larger (x/L) with e_g = 0.25 in. Comparison of Figure 45 and Figure 38 shows a significant increase in enhancement at high Reynolds numbers with e_g = 0.25 in.

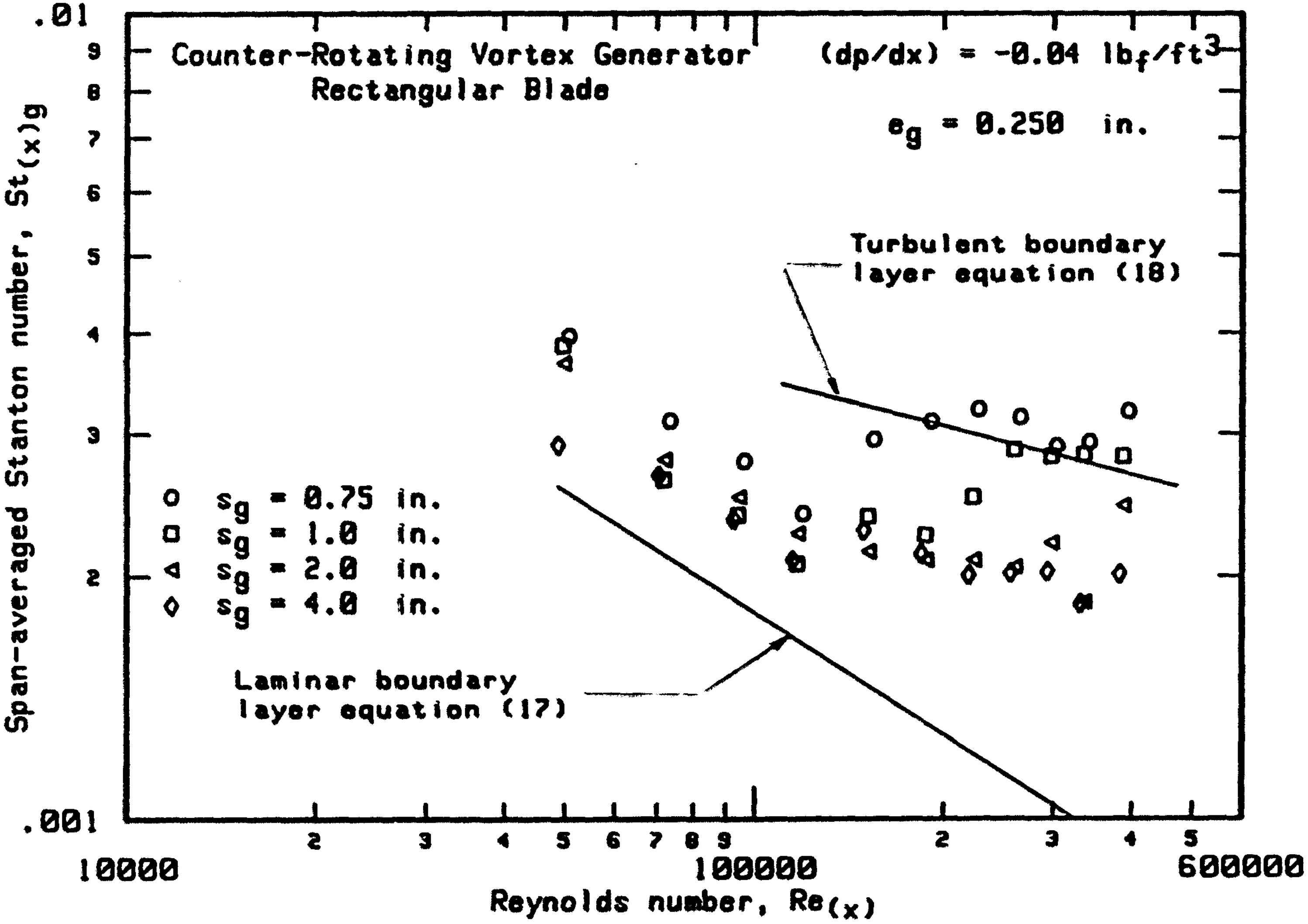

Figure 44. Heat transfer distribution with $(dp/dx) = -0.04\ lb_f/ft^3$ and $e_g = 0.25$ in.

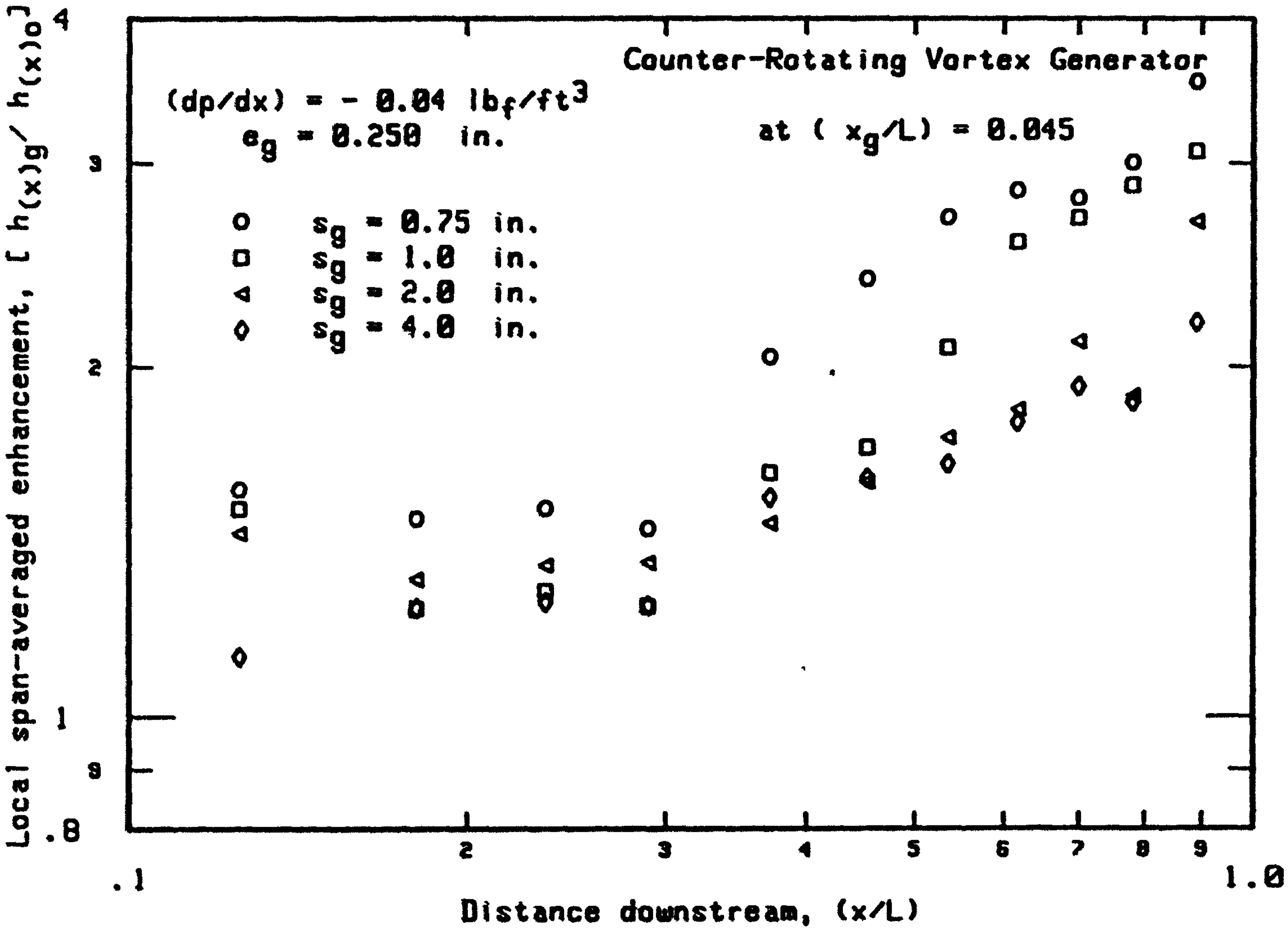

Figure 45. Enhancement of local heat transfer coefficient with $(dp/dx) = -0.04\ lb_f/ft^3$ and $e_g = 0.25$ in.

2. Overall heat transfer results

Figure 46 shows the enhancement of the overall heat transfer coefficients versus the space/height ratio of vortex blades for the three different heights of vortex blades. Also, it shows overall enhancement as a function of the heights of vortex blades referenced to the thickness of the laminar boundary layer at the location of the blades downstream of the plate leading edge. For all three blade heights and arrangements of the blades, the enhancement of the overall heat transfer coefficients is higher than those obtained at lower levels of the free-stream pressure gradients shown in Figures 32 and 39. The trend of the distributions of the enhancement of the overall heat transfer coefficient are quite similar for all the three levels of the free-stream pressure gradients. As shown in Figure 46, the enhancement of the overall heat transfer coefficients at a constant (s_g/e_g) increases with decreasing the height of the vortex blades. Also, it is clear that the enhancement of the overall heat transfer coefficients at a constant (e_g/δ_g) increase with decreasing the space between the vortex blades.

For all the spacing between the vortex blades, the minimum enhancement of the overall heat transfer coefficients is obtained at a height of vortex blade about two times the laminar boundary layer thickness at the location of the vortex blades.

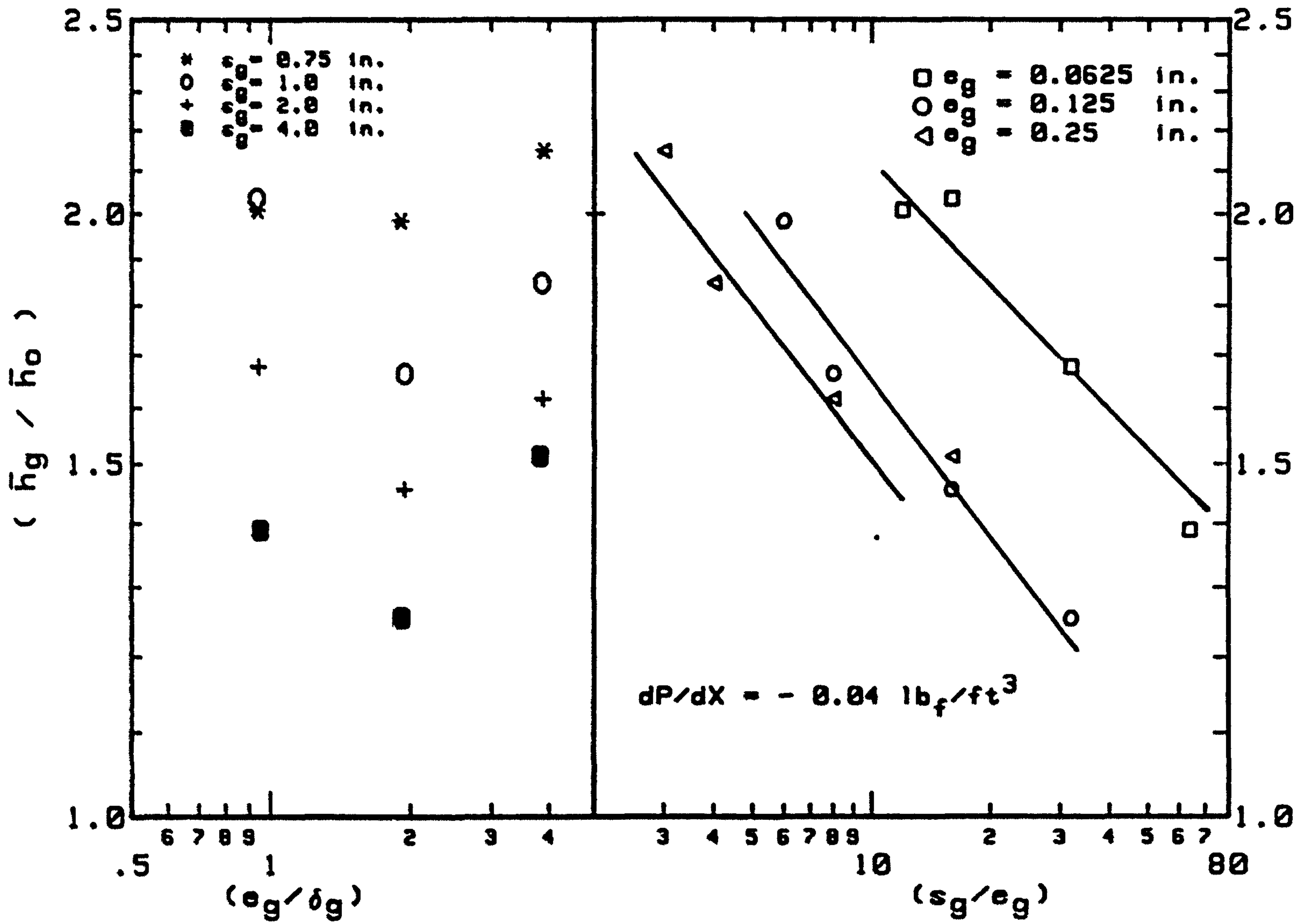

Figure 46. Enhancement of the overall heat transfer coefficient with $(dp/dx) = -0.04\ lb_f/ft^3$

D. Summary of the Effects of Vortex Generators on Overall Heat Transfer Coefficient

A correlation that explains how various configrations and arrangements of vortex generator blades are interrelated with the amount of enhancement over a flat plate surface can be obtained from the data. The correlation should useful for design purposes as well as an aid to understanding the complex thermal hydraulics involved in the flows studied. The data used are those from Figures 32, 39 and 46.

A regression analysis was used to aid in interpretation of the data and in obtaining a relationship between the variables involved. It was found that the best observed function may be made in the empirical form

$$(\bar{h}_g / \bar{h}_o) = m_o \quad (e_g/\delta_g)^{m1} \; (s_g/e_g)^{m2} \qquad (23)$$

where $(\bar{h}_g / \bar{h}_o)$ is the enhancement of the overall heat transfer coefficients, $\bar{h}_g$, referenced to that for laminar flow, $\bar{h}_o$, at the same range of Reynolds number. The ratio (s_g/e_g) is the space/height ratio for the vortex generator blades, δ_g is the boundary layer thickness estimated at the location of the row of vortex generator blades, x_g, on the plate surface measured from the plate leading edge. It was found that the constants m_o, m1 and m2 varied with the free-stream pressure gradients.

The variation of the parameter $(\bar{h}_g/\bar{h}_o)/(e_g/\delta_g)^{m1}$ with (s_g/e_g) is shown in Figures 47 through 49 for the three pressure gradients. These figures indicate that the enhancement of the overall heat transfer coefficient increases with decreasing (s_g/e_g) or (e_g/δ_g). On the other

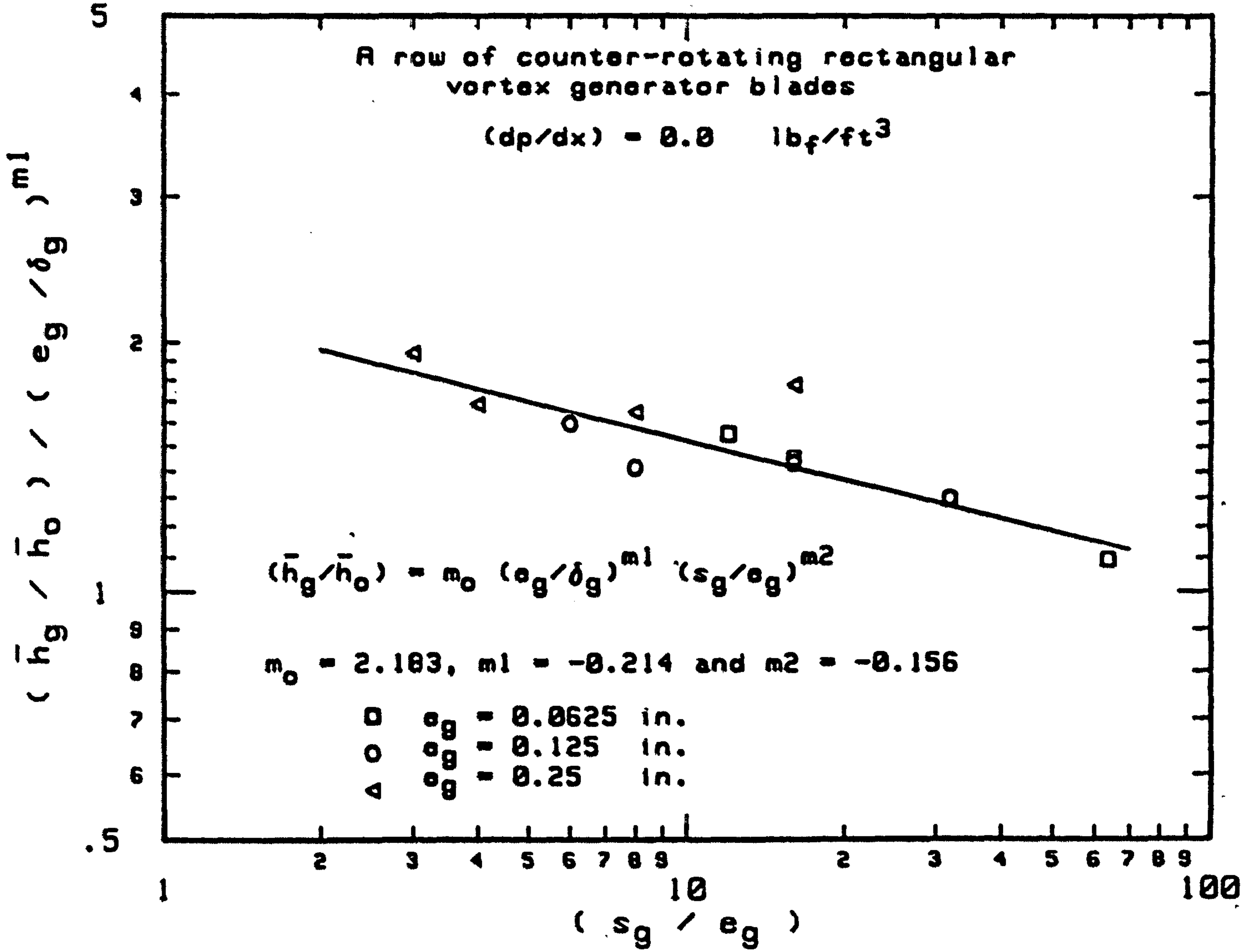

Figure 47. Variation in enhancement of the overall heat transfer coefficient behind row of counter-rotating vortex blades with zero pressure gradient

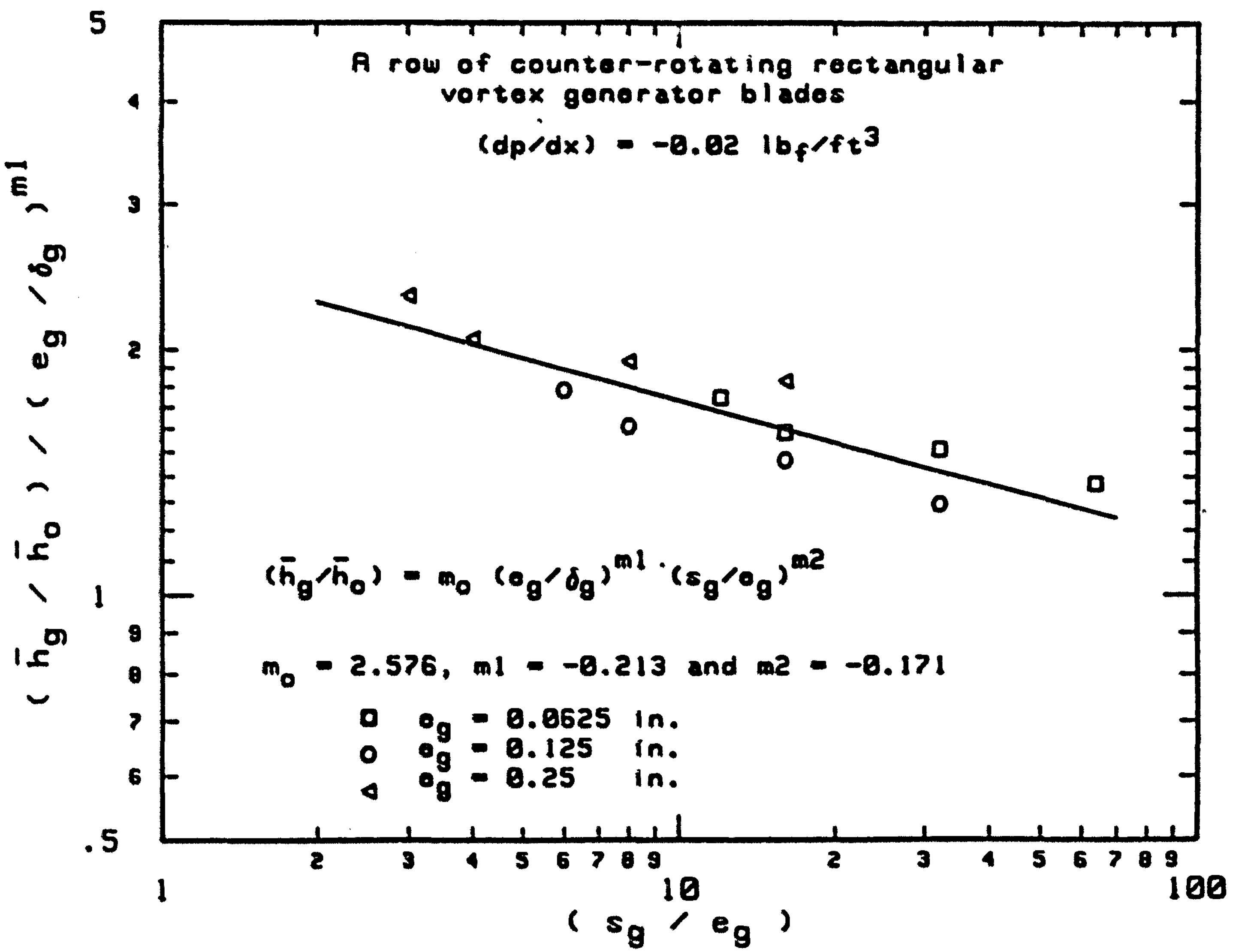

Figure 48. Variation in enhancement of the overall heat transfer coefficient behind row of counter-rotating vortex blades with (dp/dx) = -0.02 lb_f/ft^3

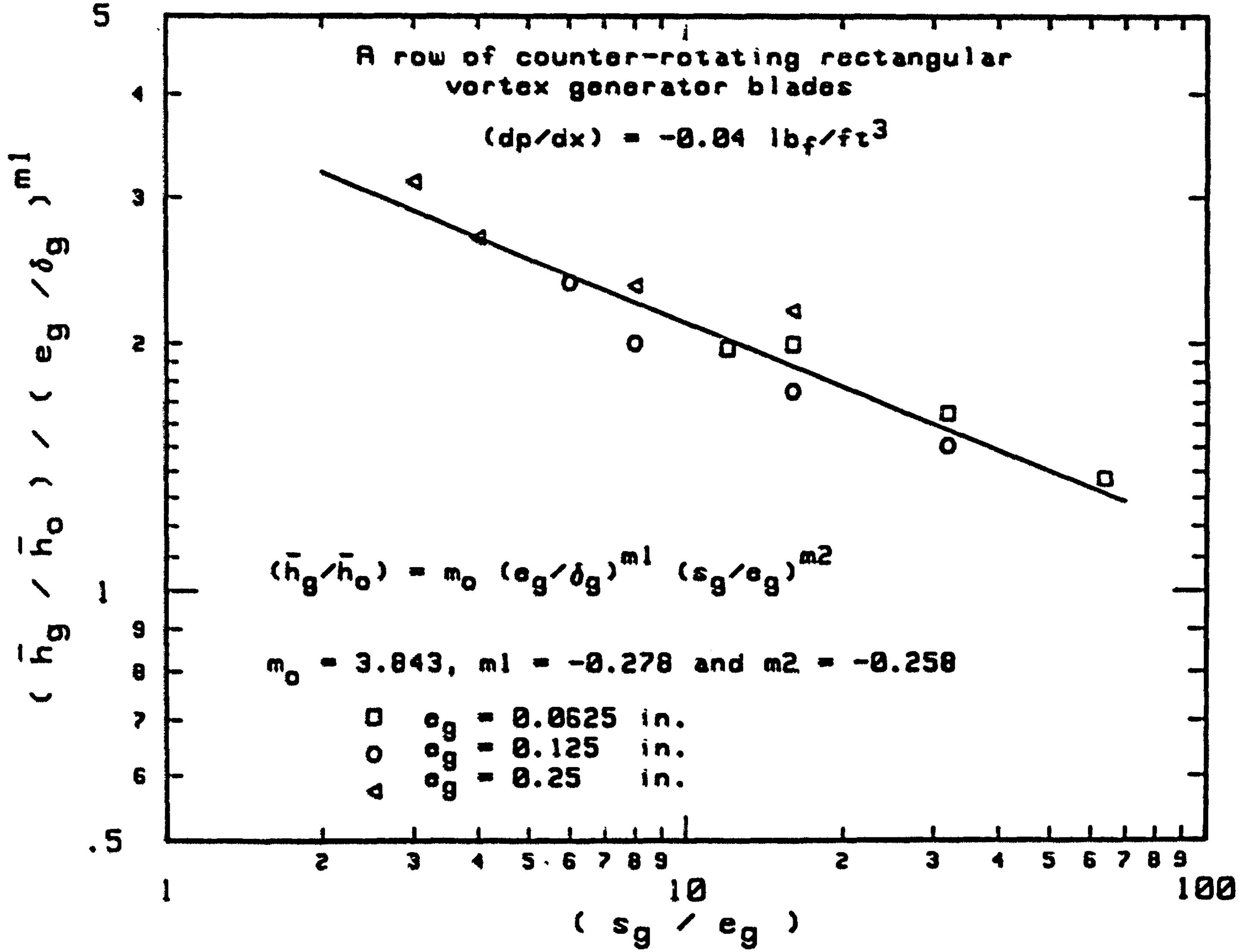

Figure 49. Variation in enhancement of the overall heat transfer coefficient behind row of counter-rotating vortex blades with $(dp/dx) = -0.04\ lb_f/ft^3$

hand, the general plate performance was significantly improved by using smaller space/height ratio of vortex blades especially when it was accomplished with smallest (e_g/δ_g) ratio.

These figures or equation (23) can be used to provide preliminary guidelines for the design of surfaces with vortex generators. It should be noted that these figures and the equation are valid only for a single row of blades oriented at ±20 degrees to the flow.

The free-stream velocity, pressure gradient and range of Reynolds number must be available or estimated for the plate surface to be designed. A location of the vortex blades at a distance x_g aft of the plate leading edge and a height of vortex blades e_g are selected. The appropriate constants m_o, m1 and m2 are selected according to the free-stream conditions. Then, either the transverse space is selected to obtain a desired enhancement from equation (23) or the enhancement is chosen and the spacing obtained by solving equation (23) for s_g. The results obtained in the preceding parametric study suggest that e_g be no larger than the boundary layer thickness expected without vortex generators at the chosen location.

E. Boundary Layer and Turbulence Development

The results of the span-averaged and overall enhancement do not provide details of the flow downstream of the blades. An in-depth study of these details is beyond the scope of this investigation, however, a series of measurements of mean velocity and longitudinal component of fluctuating velocity was made downstream of selected vortex generator configurations.

The first group of measurements was made with a blade spacing of 2.0 in. and the three heights of blades used previously. In order to find the vortex generator effects on the boundary layer, a plane 0.032 in. above and parallel to the plate surface was chosen for spanwise hot-film anemometer traverses at Reynolds numbers of 6×10^4, 1.2×10^5 and 1.8×10^5.

The decay of the vortices downstream of the blades may be described by a mean velocity decay factor defined as

$$D_{u(x,z)} = | U_{o(x)} - u_{(x,z)} | / U_{o(x)} \qquad (24)$$

Note that fully-diffused wakes would have a decay factor of zero. The decay factor, longitudinal turbulence intensity and local enhancement ratio $| h_{(x,z)g} / h_{(x)o} |$ were plotted and compared for each plate height. In the figures discussed below, the blade locations and sense of vortex rotation are shown along the abscissa and just below it. The span averaged parameters for the blade pair on the longitudinal plate centerline were also calculated for the central pair of blades at the centerline. The data given in Figure 50 for $e_g = 0.25$ in. show that the wake areas at this Reynolds number just downstream of the vortex generators are outlined clearly by the data for the turbulence intensity and the decay factor. The peak-to-peak variation in the enhancement ratio is about 0.30 and the span-averaged enhancement ratio is 1.23. The span-averaged decay factor is 0.042. Figure 51 is for the same flow

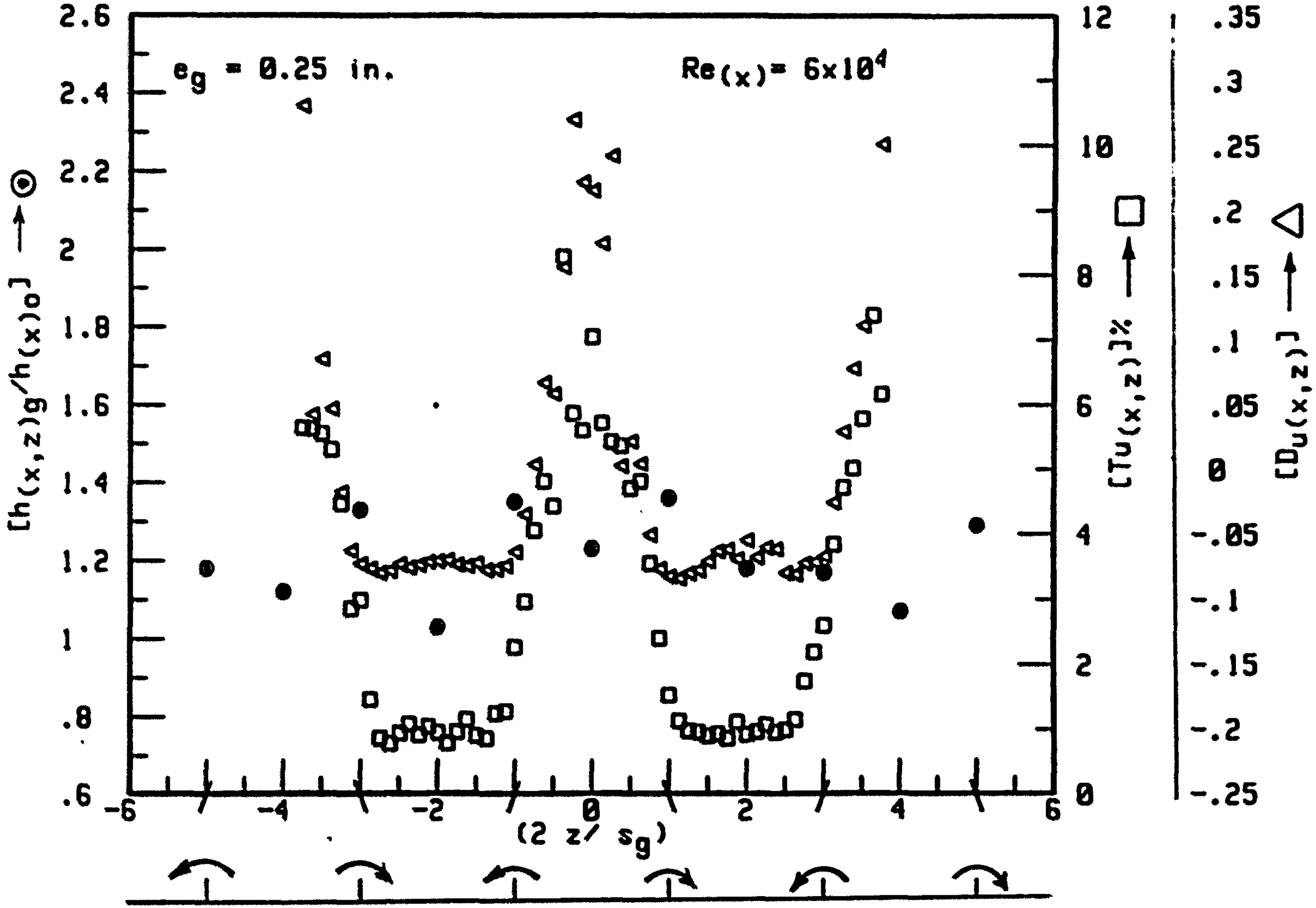

Figure 50. Spanwise variation in $[h_{(x,z)g}/h_{(x)o}]$, $Tu_{(x,z)}$ and $D_{u(x,z)}$ behind row of counter-rotating vortex blades with e_g = 0.25 in. at $Re_{(x)}$ = 6x10^4

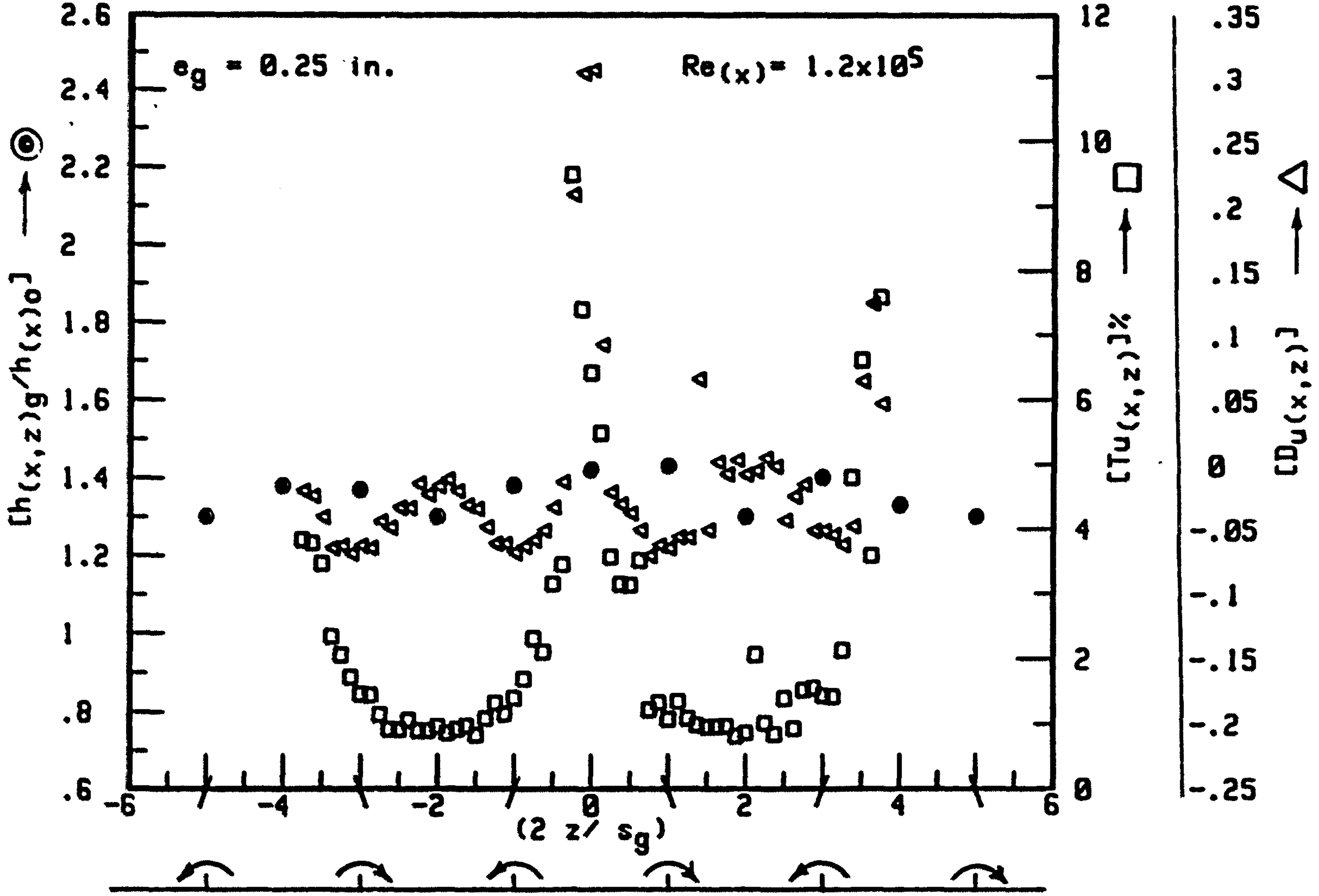

Figure 51. Spanwise variation in $[h_{(x,z)g}/h_{(x)o}]$, $Tu_{(x,z)}$ and $D_{u(x,z)}$ behind row of counter-rotating vortex blades with $e_g = 0.25$ in. at $Re_{(x)} = 1.2\times10^5$

conditions but at a Reynolds number of $1.2x10^5$. The decay factor and turbulence intensity data here show that the wakes are less sharply defined than in Figure 50. The local decay factor $D_{u(x,z)}$ at $(2z/s_g)$ = ±2.0 is increased over $D_{u(x,z)}$ at $(2z/s_g)$ = ±1.0 and $(2z/s_g)$ = ±3.0 but the span-averaged decay factor is 0.031, less than at $Re_{(x)} = 6x10^4$. The span-averaged enhancement ratio has increased to 1.37. Figure 52 shows further diffusion of the wakes, with the span-averaged decay factor increasing to 0.026 and a continuing increase in enhancement ratio to 1.77.

Figures 53, 54 and 55 for e_g = 0.125 in. show the same general trends. However, the wakes are more sharply defined for all Reynolds numbers and for corresponding Reynolds numbers have lower span-averaged enhancement ratios. Moreover, enhancement is not as uniform along the span as for e_g = 0.25 in.

The data for e_g = 0.0625 in. in Figure 56 show relatively much steeper peaks and valleys for the turbulence intensity and widely oscillating values of enhancement ratio. The span-averaged enhancement ratio is 1.08. Figure 57 shows a large variation in enhancement ratio with span-averaged value of 1.22. Some spanwise spreading of the turbulence intensity is evident. In Figure 58, one vortex at $(2z/s_g)$ = +2.0 has nearly disappeared and the enhancement ratio, while still appreciable, is much less than for the region near $(2z/s_g)$ = -2.0. The span-averaged enhancement ratio is 2.03.

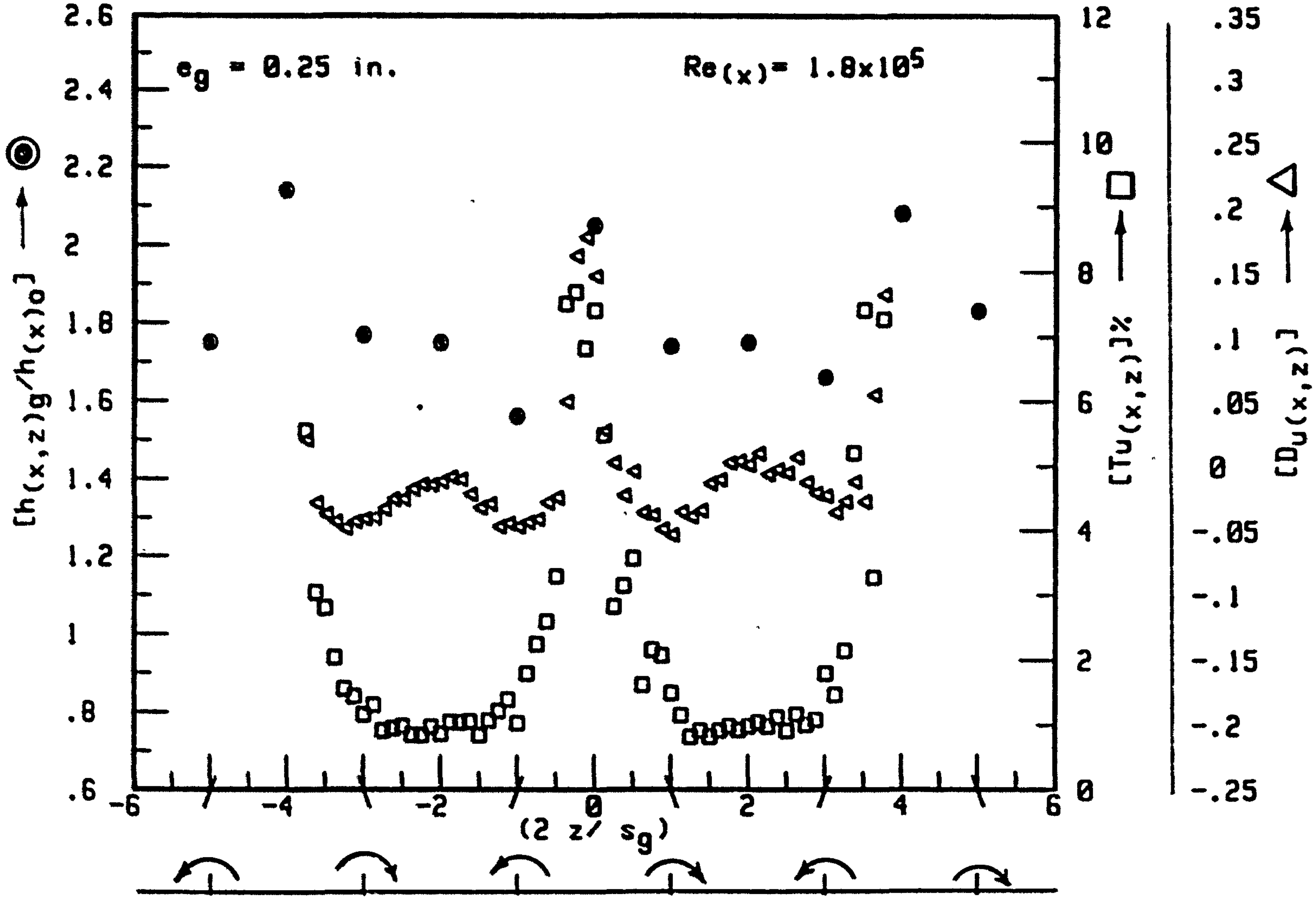

Figure 52. Spanwise variation in $[h_{(x,z)g}/h_{(x)o}]$, $Tu_{(x,z)}$ and $D_{u(x,z)}$ behind row of counter-rotating vortex blades with e_g = 0.25 in. at $Re_{(x)}$ = 1.8x10^5

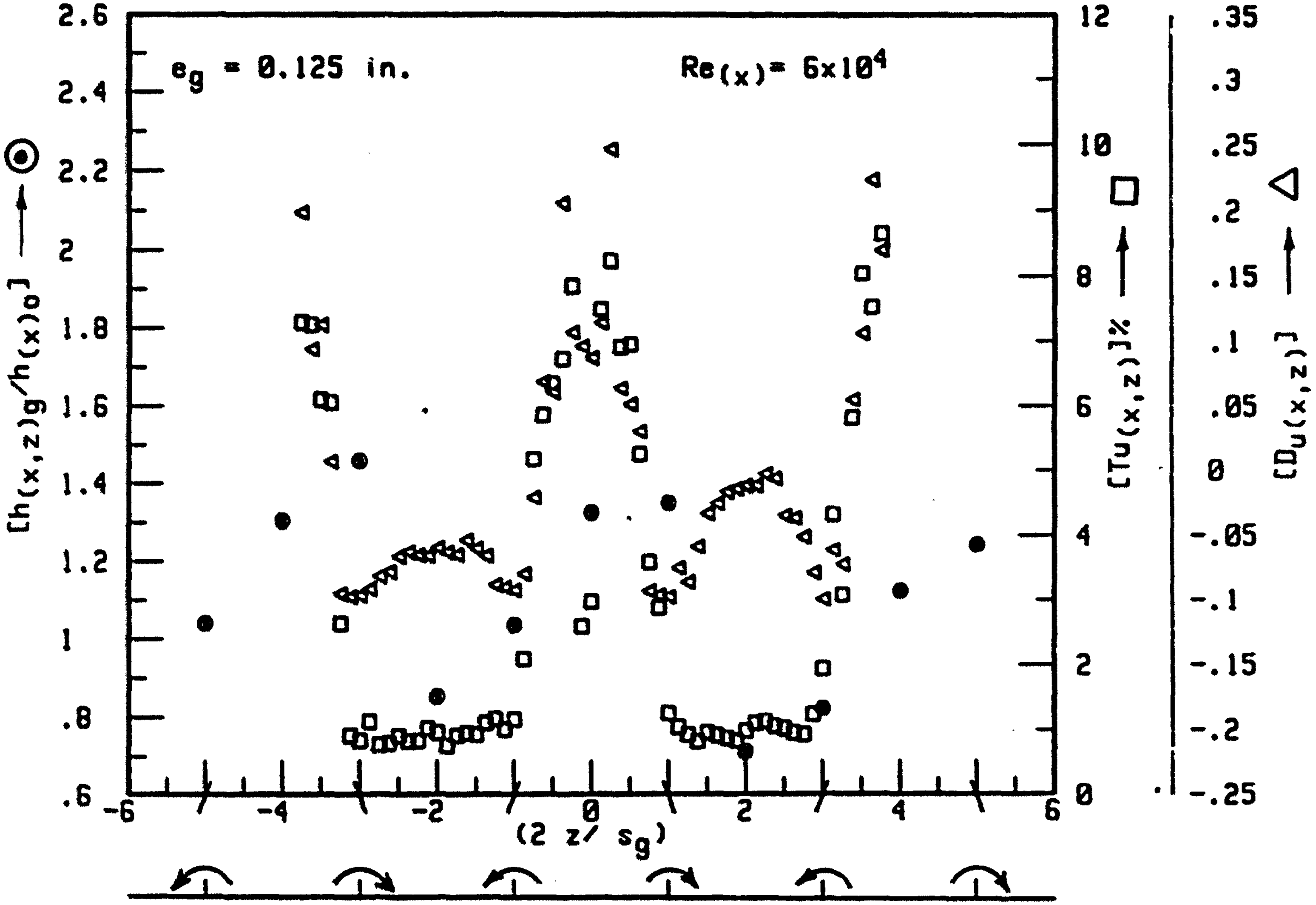

Figure 53. Spanwise variation in $[h_{(x,z)g}/h_{(x)o}]$, $Tu_{(x,z)}$ and $D_{u(x,z)}$ behind row of counter-rotating vortex blades with e_g = 0.125 in. at $Re_{(x)}$ = $6x10^4$

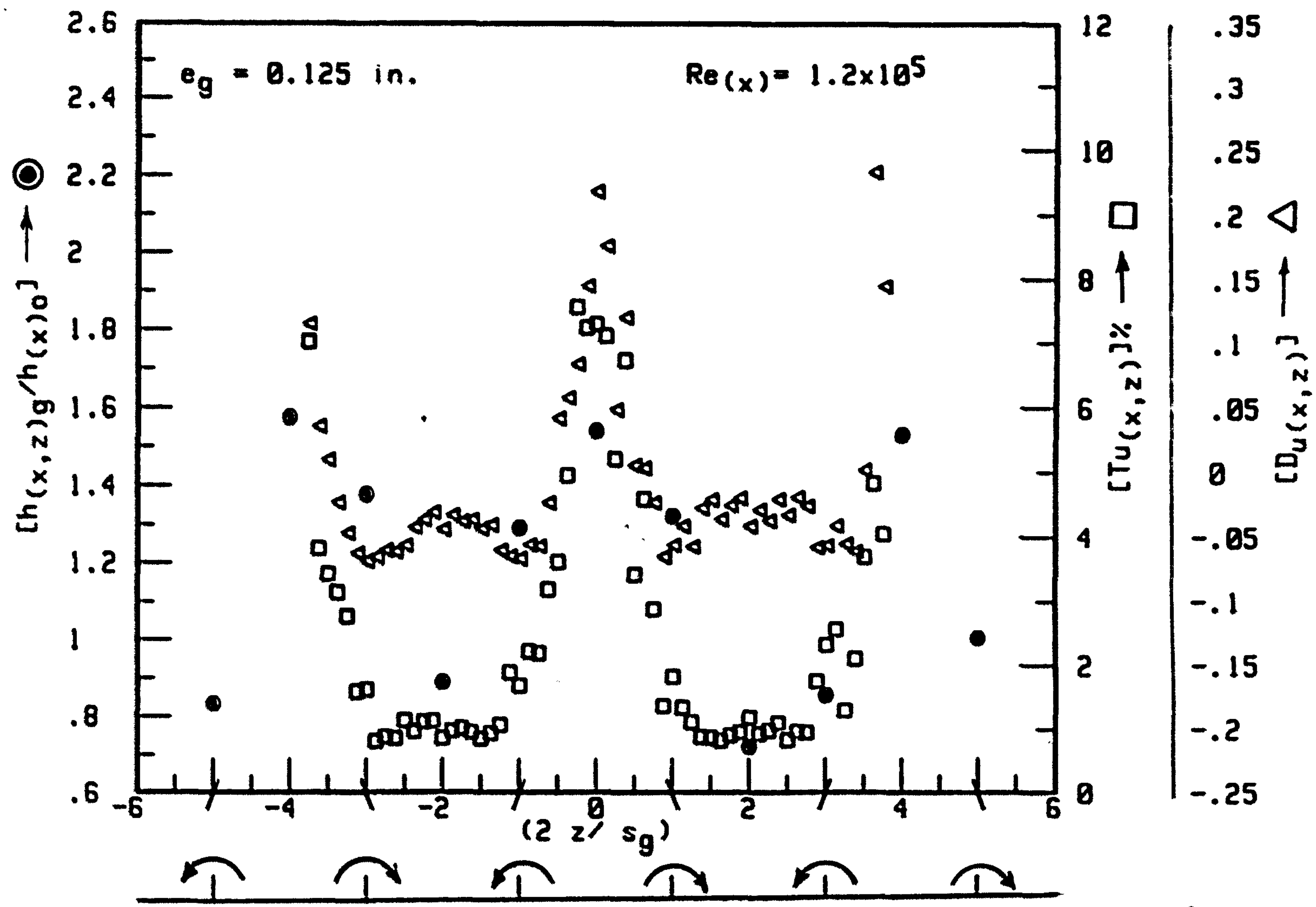

Figure 54. Spanwise variation in $[h_{(x,z)g}/h_{(x)o}]$, $Tu_{(x,z)}$ and $D_{u(x,z)}$ behind row of counter-rotating vortex blades with e_g = 0.125 in. at $Re_{(x)}$ = 1.2x10^5

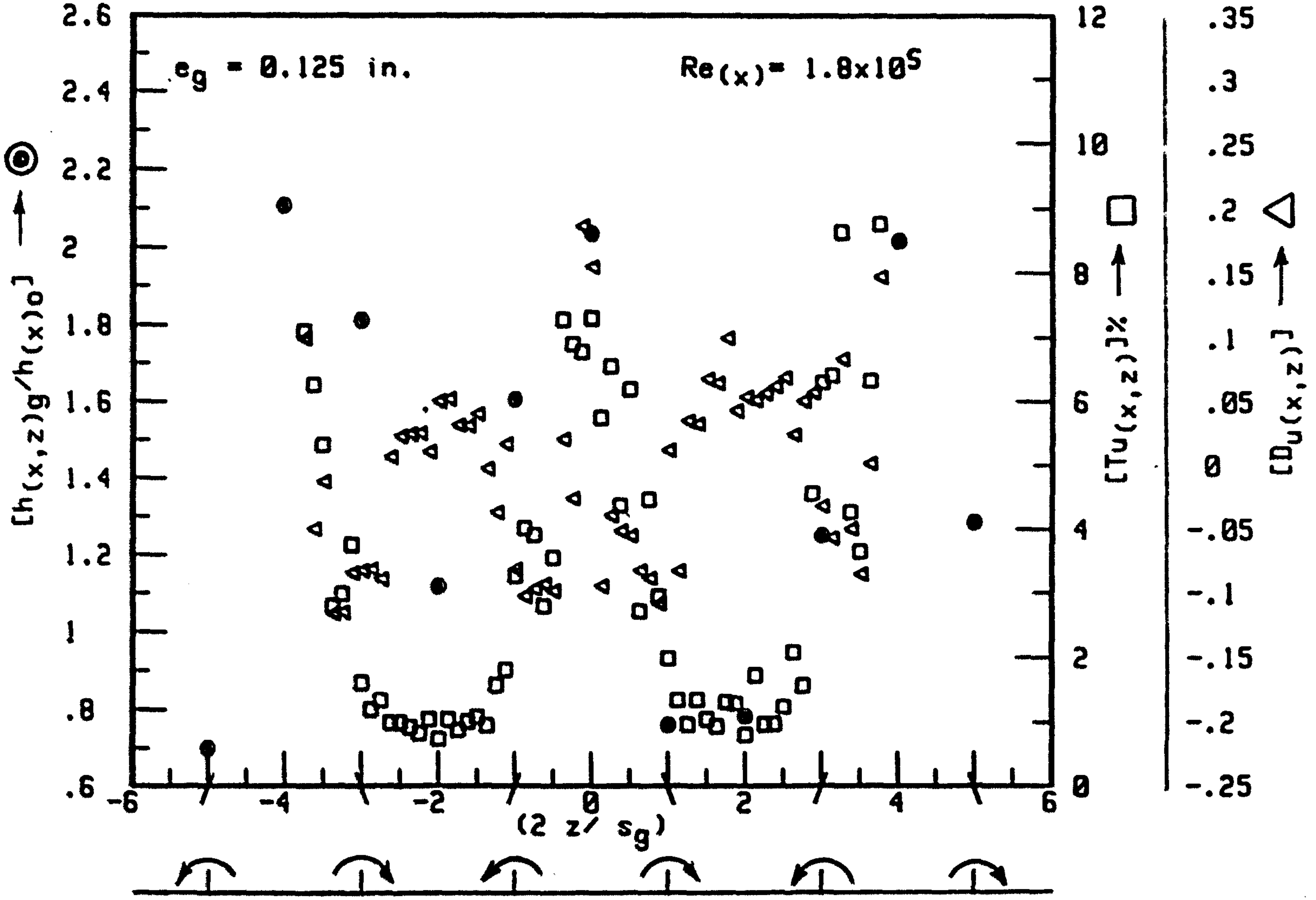

Figure 55. Spanwise variation in $[h_{(x,z)g}/h_{(x)o}]$, $Tu_{(x,z)}$ and $D_{u(x,z)}$ behind row of counter-rotating vortex blades with e_g = 0.125 in. at $Re_{(x)}$ = 1.8x10^5

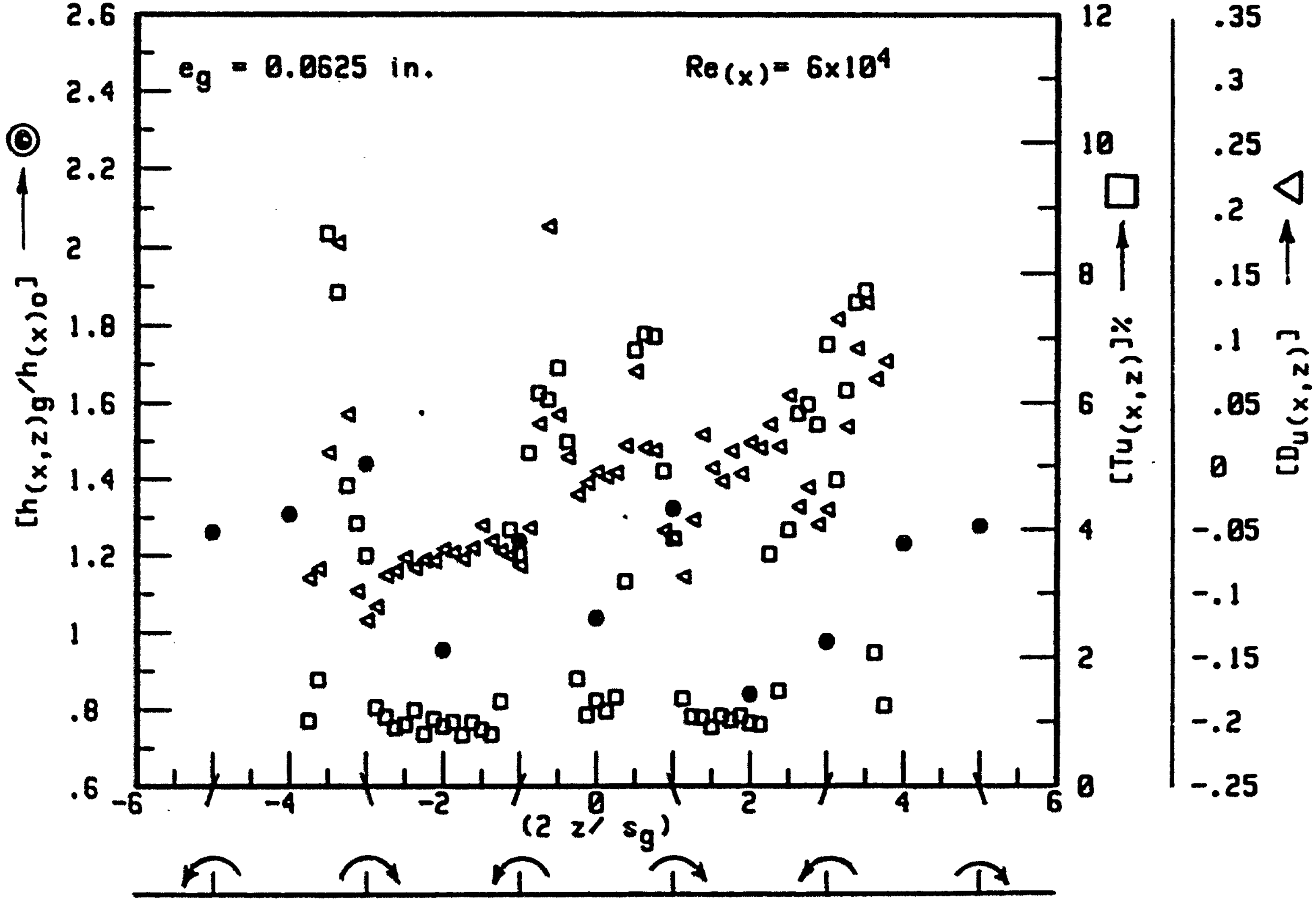

Figure 56. Spanwise variation in $[h_{(x,z)g}/h_{(x)o}]$, $Tu_{(x,z)}$ and $D_{u(x,z)}$ behind row of counter-rotating vortex blades with e_g = 0.0625 in. at $Re_{(x)}$ = 6x10^4

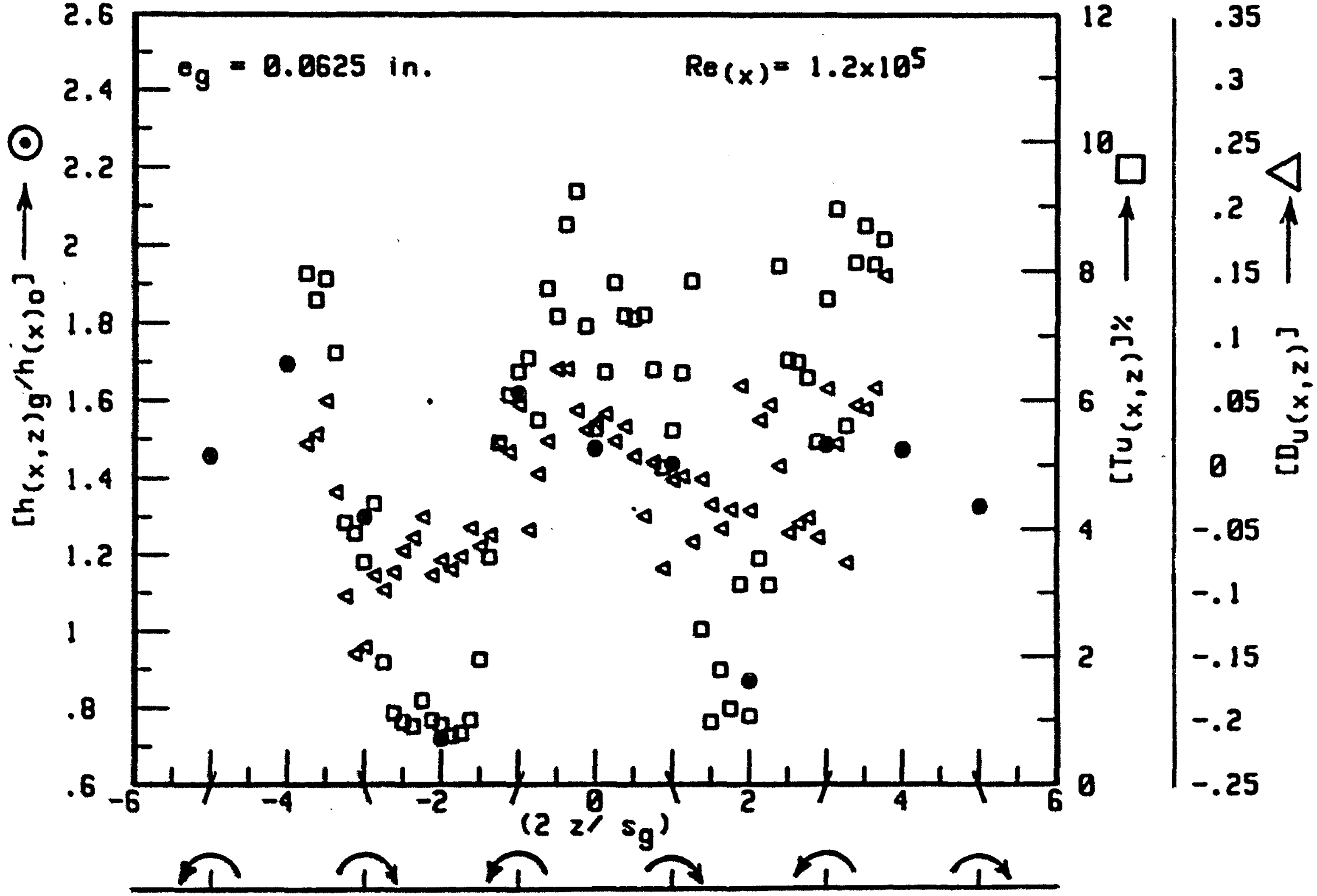

Figure 57. Spanwise variation in $[h_{(x,z)g}/h_{(x)o}]$, $Tu_{(x,z)}$ and $D_{u(x,z)}$ behind row of counter-rotating vortex blades with e_g = 0.0625 in. at $Re_{(x)}$ = 1.2×10^5

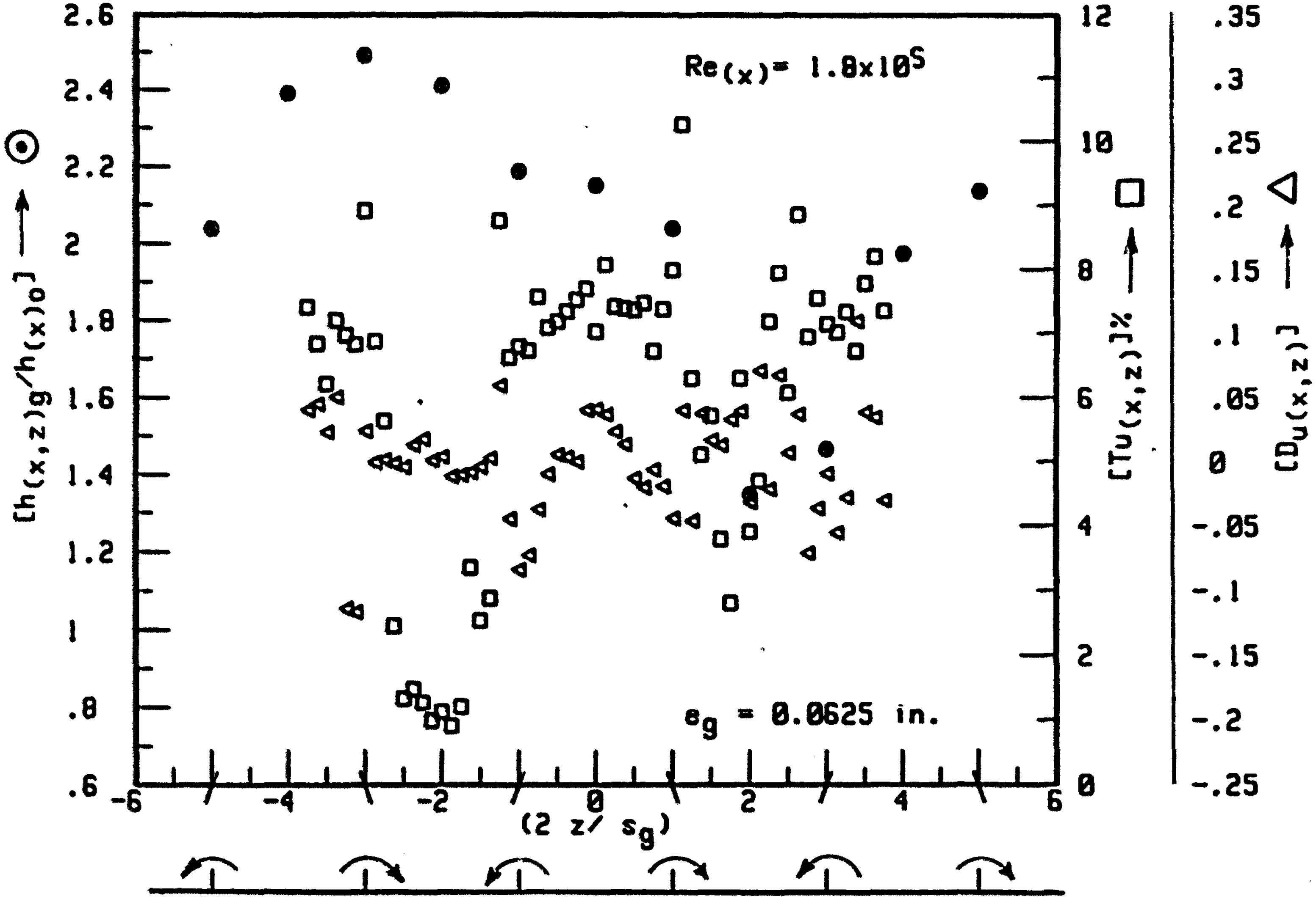

Figure 58. Spanwise variation in $[h_{(x,z)g}/h_{(x)o}]$, $Tu_{(x,z)}$ and $D_{u(x,z)}$ behind row of counter-rotating vortex blades with $e_g = 0.0625$ in. at $Re_{(x)} = 1.8\text{x}10^5$

In general, the span-averaged enhancement is lower for e_g= 0.125in. than for the other blade heights.

The span-averaged data for the single blade pair are given in Table 1 and are plotted in Figure 59. The decay factors for e_g= 0.25 in. decreases from about 0.04 to the range 0.02 to 0.025 as Reynolds number increases, whereas the decay factor for e_g= 0.0625 in. remains fairly constant at about 0.025. The x-component of the turbulence intensity does not have a large change for e_g= 0.125 in. or e_g= 0.25 in., but for e_g= 0.0625 in., the turbulence intensity nearly doubles over the Reynolds number range. Apparently, when the decay factor is declining, the x-component of the turbulence intensity remains relatively stable, but when the decay factor is nearly constant, the turbulence component increases markedly. Although only this single plane was surveyed, the data suggest that vortex generator blades with heights larger than the boundary layer thickness create vortices which dissipate their energy so as to disturb the free stream as well as the boundary layer. Conversely, vortices formed by blades only within the boundary layer diffuse close to the plate surface, increasing the x-component of the turbulence intensity in the boundary layer as they decay. The enhancement of heat transfer is then improved over a larger range of Reynolds numbers.

A second group of measurements was made to determine the x-direction turbulence intensity and mean velocity profiles in the y-direction at several spanwise locations downstream of a vortex blade

Table 1. Span-averaged parameters for hot-wire surveys for s_g = 2.0 in. and (dp/dx) = -0.02 lb_f/ft^3

e_g, in.	$Re_{(x)}$	$Tu_{(x)}$	$D_{u(x)}$	$[h_{(x)g}/h_{(x)o}]$
0.25	$6x10^4$	2.54	0.042	1.23
	$1.2x10^5$	2.02	0.031	1.37
	$1.8x10^5$	2.11	0.026	1.77
0.125	$6x10^4$	2.73	0.037	1.05
	$1.2x10^5$	2.41	0.034	1.15
	$1.8x10^5$	2.58	0.017	1.26
0.0625	$6x10^4$	2.26	0.026	1.08
	$1.2x10^5$	4.04	0.024	1.22
	$1.8x10^5$	4.85	0.025	2.03

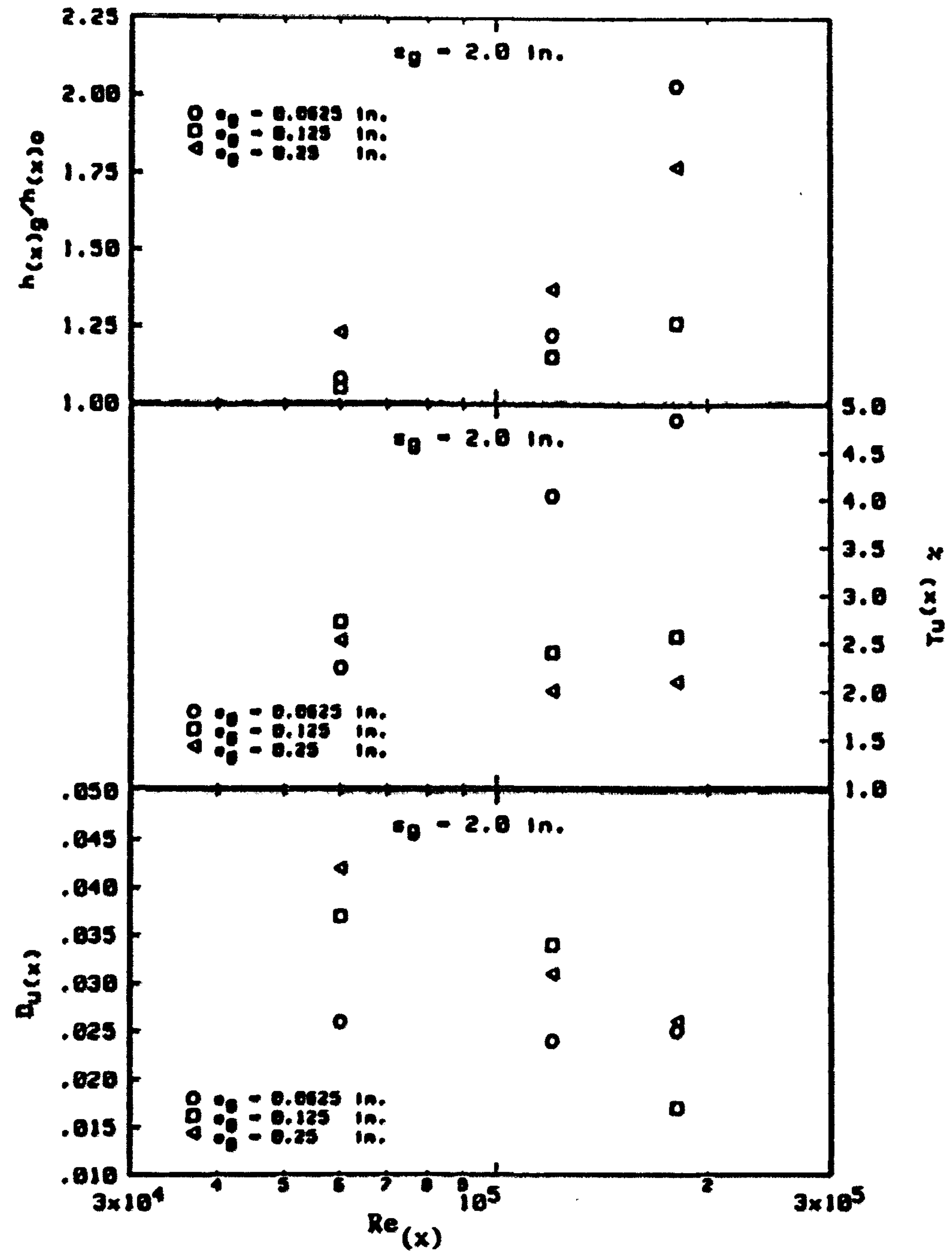

Figure 59. Span-averaged variation in $[h_{(x)g}/h_{(x)o}]$, $Tu_{(x)}$ and $D_{u(x)}$ behind row of counter-rotating vortex blades with $s_g = 2.0$ in.

pair for the same Reynolds numbers as in the first group of experiments. The configuration chosen was $s_8 = 0.75$ in. and $e_8 = 0.0625$ in.

Results of the above group of measurements are given in Figures 60 through 62 for the turbulence intensity and in Figures 63 through 65 for the mean velocity.

Figure 60 shows the longitudinal component of the turbulence intensity data plotted against the vertical distance above the plate surface divided by the undisturbed laminar boundary layer thickness. The legend on the figure shows the survey location graphically with respect to the vortex blade pair and one additional blade. The data are dispersed for about 4 laminar boundary layer thicknesses out into the flow and all are above the line representing the x-component turbulence intensity for a two-dimensional turbulent boundary layer taken from Schlichting [20]. The free-stream turbulence intensity for the tunnel conditions is about 0.5 percent.

Figure 61 shows less dispersion of the data at a Reynolds number of 1.2×10^5, and the data are again all significantly higher than the line representing conditions for a laminar boundary layer.

In Figure 62 for $Re_{(x)} = 1.8 \times 10^5$, the data are all grouped in a region laying several percent above the line and extend to about 3 laminar boundary layer thicknesses into the free-stream.

From Figures 63 through 65, it is clear that the spanwise mean velocity profiles move closer together with increasing distance downstream of the vortex blades until no significant spanwise change is observed.

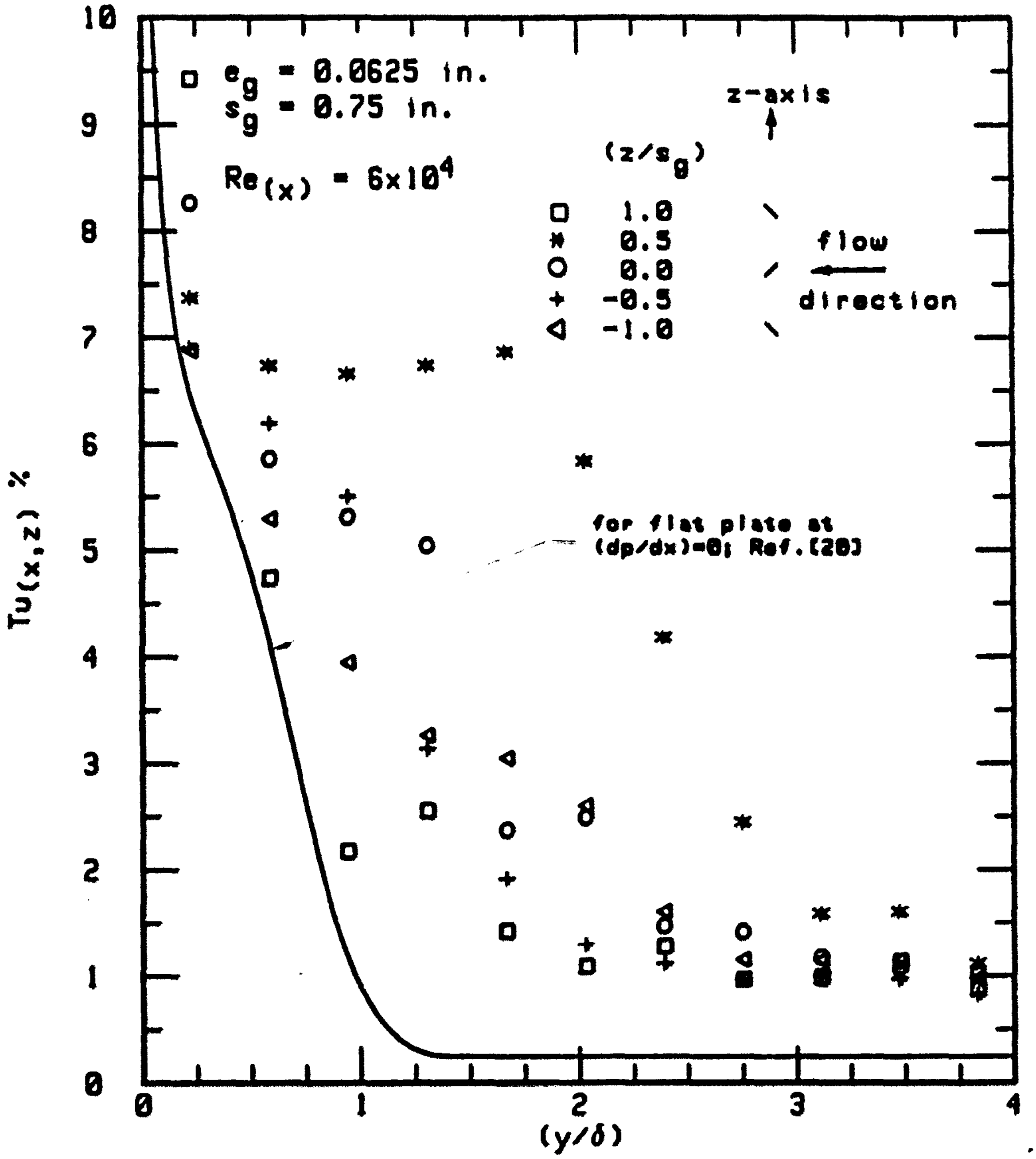

Figure 60. Longitudinal turbulence intensity distribution for $s_g = 0.75$ in. at $Re_{(x)} = 6x10^4$

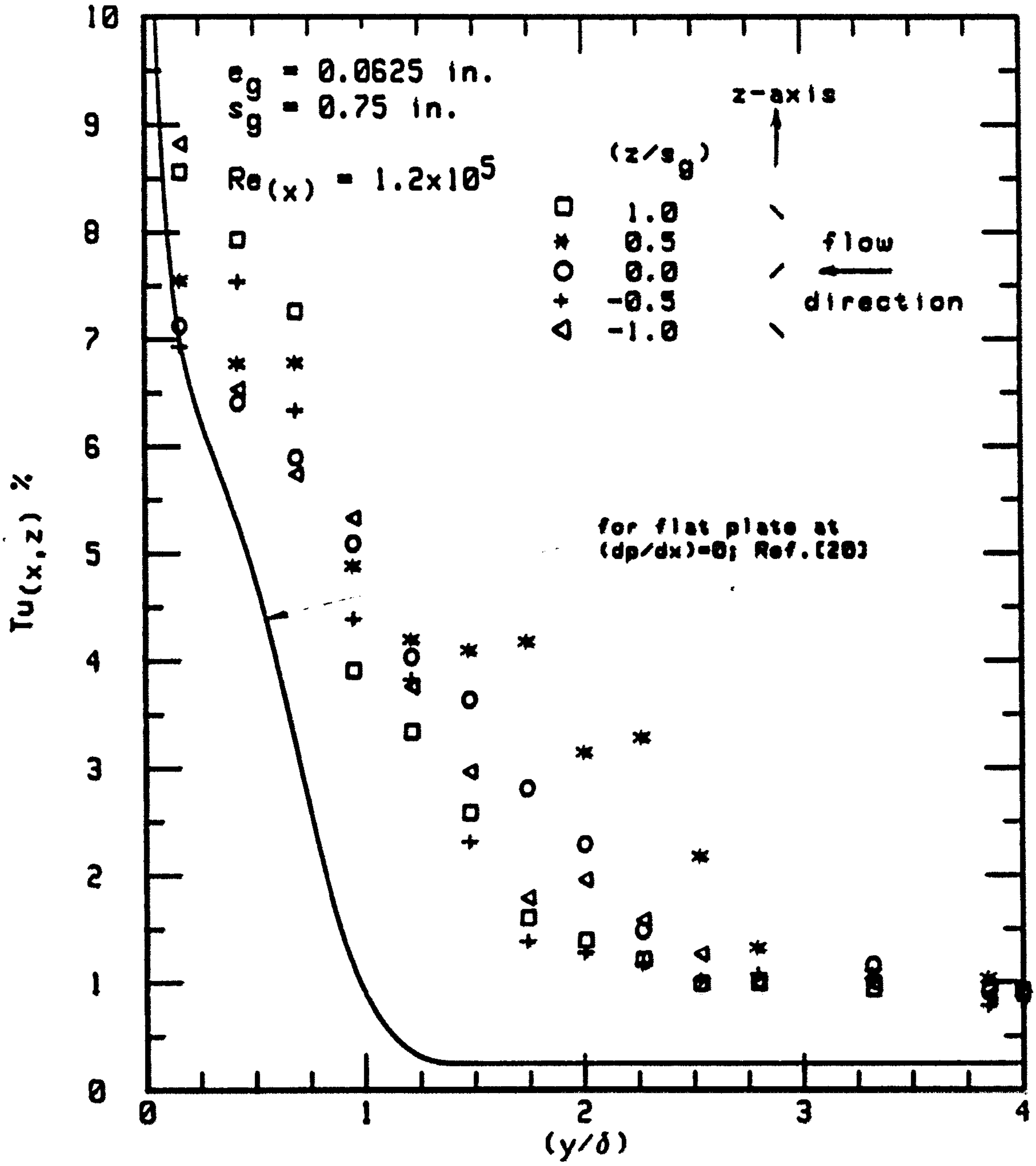

Figure 61. Longitudinal turbulence intensity distribution for s_g = 0.75 in. at $Re_{(x)} = 1.2\times10^5$

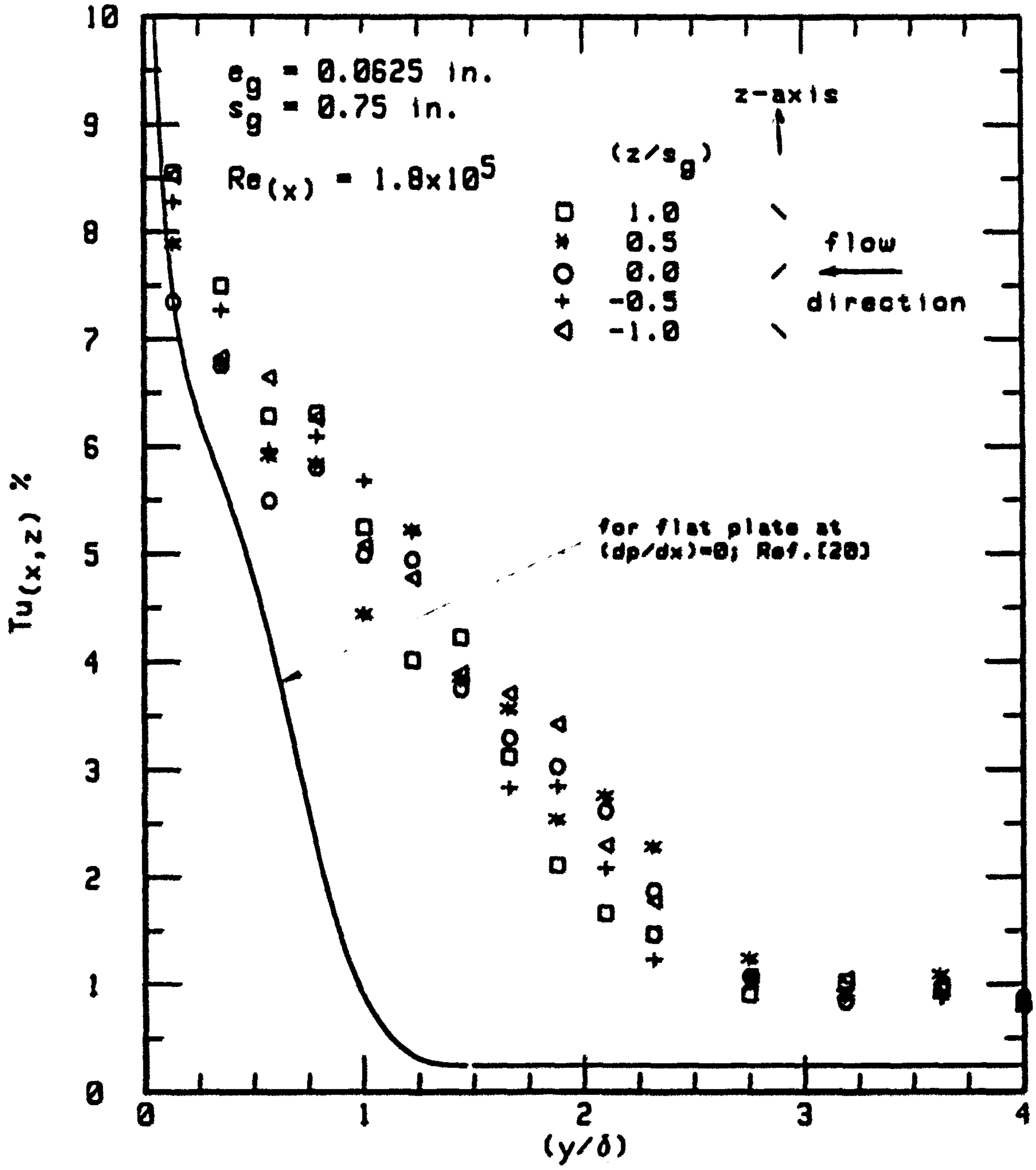

Figure 62. Longitudinal turbulence intensity distribution for s_g = 0.75 in. at $Re_{(x)}$ = 1.8×10^5

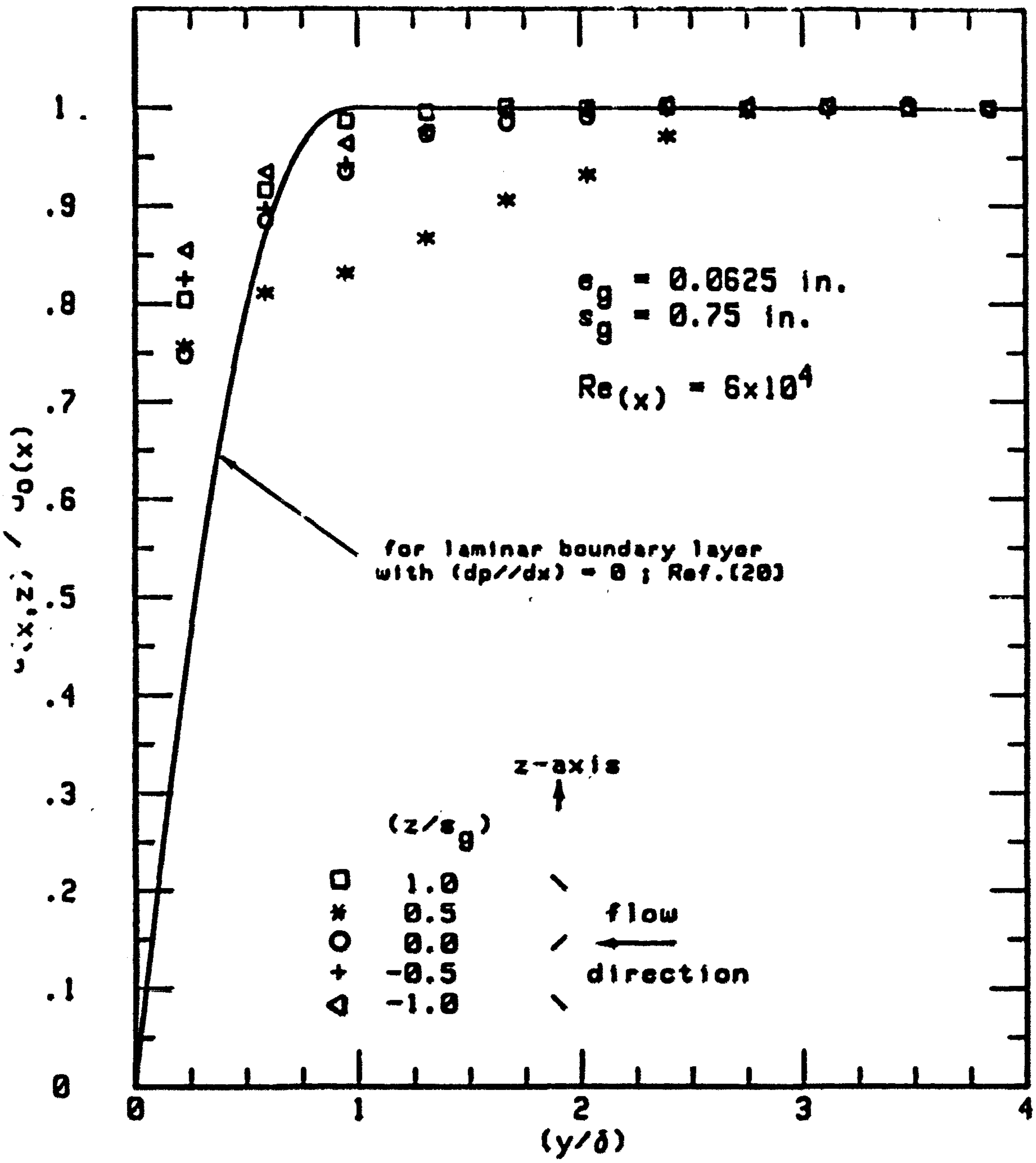

Figure 63. Spanwise distribution of velocity profiles for $s_g = 0.75$ in. and $e_g = 0.0625$ in. at $Re_{(x)} = 6x10^4$

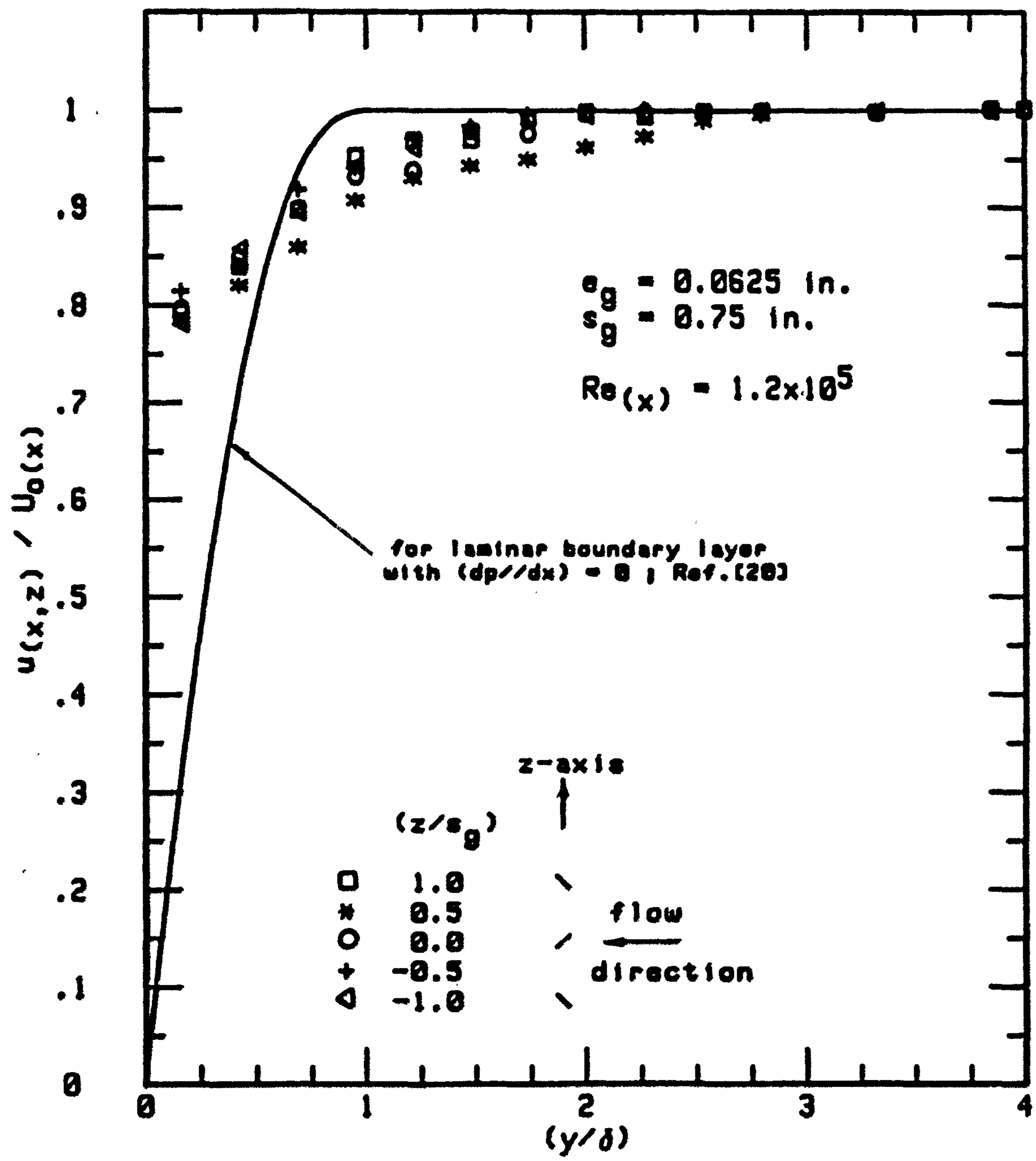

Figure 64. Spanwise distribution of velocity profiles for s_g = 0.75 in. and e_g = 0.0625 in. at $Re_{(x)}$ = 1.2×10^5

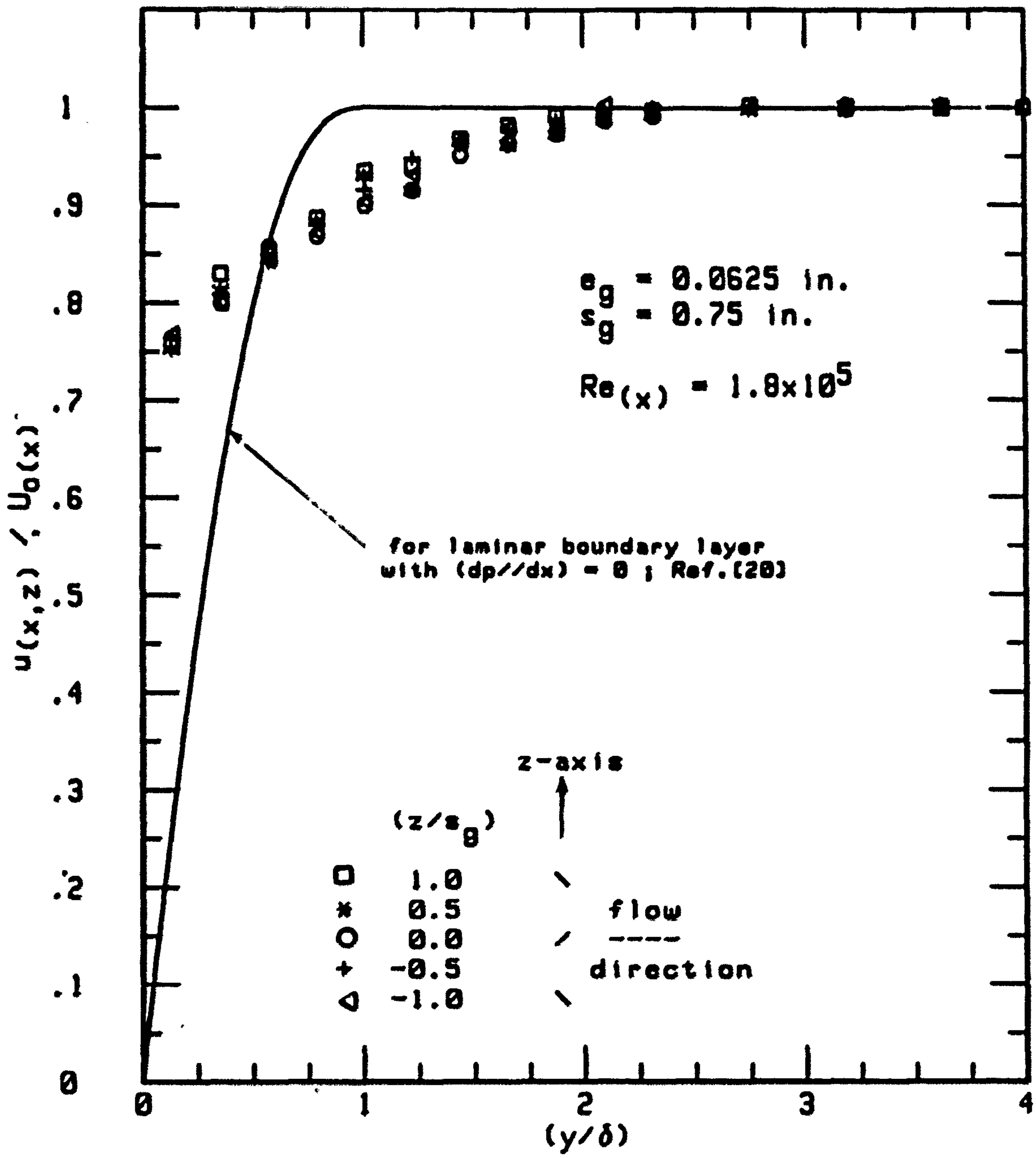

Figure 65. Spanwise distribution of velocity profiles for $s_g = 0.75$ in. and $e_g = 0.0625$ in. at $Re_{(x)} = 1.8 \times 10^5$

Figure 63 shows that the mean velocity at $(z/s_g) = +0.5$ is less than at $(z/s_g) = -0.5$ indicating lower and higher flow rate respectively displaced to those regions between the vortex blades. Figure 64 shows less dispersion of the data at $Re_{(x)} = 1.2 \times 10^5$, and the two mean velocity profiles become closer, as well as the velocity profiles at the locations behind the vortex blades. Moreover, all the mean velocity profiles shown in Figures 64 and 65 are in the transition region as determined from heat transfer data. In Figure 65, at $Re_{(x)} = 1.8 \times 10^5$ the data are grouped on one mean velocity profile.

The conclusion obtained from Figures 60 through 65 is that the wake region produced by each pair of vortex blades with the smallest spacing s_g and the smallest height e_g mixed rapidly downstream of the blades and produced higher local turbulence intensity.

The skin friction coefficient on the plate surface is expected increase where high velocities occur near the plate surface, as shown in Figures 60 through 65.

The free-stream pressure gradients did not vary with the vortex blade configurations and were the same as those obtained with no vortex generator blades attached to the plate surface.

F. Concluding Remarks

The only data available for heat transfer downstream of vortex generator blades on a flat surface are those obtained by Edwards and Alker [6] and Russell et al. [11]. However, a quantitative comparison of their work and the data obtained from this investigation can not be made. In the investigations of reference [6] and [11], the vortex blades were attached to the heated surface so that the vortex generator blades acted as extended surfaces and increased the surface area. The work of Edwards and Alker [6] adopted counter-rotating vortex blades with height e_g = 1.0 in. spaced with pitch $S_g = 3s_g$ and $4s_g$, and that their type of original boundary layer is unknown. Russell et al. [11] used a uniform temperature rather than a uniform heat flux with two rows of rectangular co-rotating blades.

The only qualitative comparison that could be made with data obtained by [6] and [11] is that with the behavior of the distribution of the local enhancement [$h_{(x,z)g}/h_{(x)o}$]. Their results indicated higher improvement of heat transfer coefficients in the regions located directly downstream of the vortex blades than in the regions between the blades. In Figures 50 through 58, similar behavior of the local enhancement was obtained and the regions between the blades indicated a small enhancement. From this point of view, similar results were obtained.

VI. CONCLUSIONS

The previous analysis of the results leads to several conclusions:

1. The new data presented in this investigation support using a vortex generator technique to provide an enhancement of heat transfer.

2. The amount of heat transfer enhancement depends on the vortex blade height and arrangement on the plate surface. The best improvement obtained was with the smallest space between the blades, especially if the blade height is not larger than the boundary layer thickness estimated at the blade location.

3. The overall heat transfer coefficients obtained at the three different pressure gradients have measureable increases with increasing the free-stream pressure gradient, contrary to that obtained with a smooth surface, indicating that the overall heat transfer coefficient is a function of pressure gradient in the presence of vortex generator blades.

4. The local enhancement of heat transfer coefficient was increased for this system over that for a plain flat plate mainly because of high turbulence produced over the region adjacent to the plate surface, resulting in increased mixing of the slower fluid near the plate surface with the free stream.

5. The most important factor in establishing an effective design of a vortex generator is the need to ensure that the effects of the vortices remain close to the plate surface and do not diffuse into the free-stream. Design guidelines were proposed on the basis of heat

transfer and the development of the boundary layer results. However, to set an optimum arrangement it would be necessary to do further heat transfer and boundary layer investigations over a wider range of vortex generator arrangements and configurations.

6. Skin-friction coefficients could not be determined from the distorted velocity profiles existing downstream from vortex generators; however, it is expected that they would increase where high velocities occur near the plate surface.

7. No experimental data were taken with an initially turbulent boundary layer at the vortex generator location. No conclusions can be made concerning whether or not the turbulent boundary layer heat transfer correlation represents an upper limit to the enhancement achievable with vortex generators.

VII. BIBLIOGRAPHY

1. Bergles, A. E. "Techniques to Augment Heat Transfer." In Handbook of Heat Transfer, pp. 10.1-10.32. New York: McGraw-Hill Book Company, 1973.

2. Chang, P. K. Control of Flow Separation. London: Hemisphere Publishing Company, 1976.

3. Pearcey, H. H. "Shock-induced separation and prevention by design and boundary layer control." In Boundary Layer and Flow Control, pp. 1166-1344. Edited by G. V. Lachmann. New York: Pergamon Press, 1961.

4. Schubauer, G. B.; and Spangenberg, W. G. "Forced Mixing in Boundary Layer." Journal of Fluid Mechanics 8 (1960): 10-32.

5. Johnson, T. R.; and Joubert, P. N. "The Inflence of Vortex Generators on Drag and Heat Transfer from a Circular Cylinder Normal to an Airstream." Journal of Heat Transfer 91 (1969): 91-99.

6. Edwards, F. J.; and Alker, C. J. R. "The Improvement of Forced Convection Heat Transfer Using Surface Protrusions in the Form of (a)- Cubes, and (b)- Vortex Generators." In Heat Transfer 1974, Fifth International Heat Transfer Conference, pp. 244-248. Vol. 2. Tokyo: Japan Society of Mechanical Engineers, 1974.

7. Lee, G. H. "Wind Tunnel Tests on Vortex Generators for cooling Fins." CE-Lummus Company Report HR-112, April 1976.

8. Lee, G. H. "Effect of Embossed Vortex Generators on Heat Transfer from Rectangular Aluminum Fins." CE-Lummus Company Report HR-118, August 1976.

9. Lee, G. H. "Heat Transfer and Pressure Drop from Rectangular Fintube Matrix." CE-Lummus Company Report HR-146, October 1978.

10. Lee, G. H. "Effect of Vortex Generators on Heat Transfer from Rectangular Plate Fins." CE-Lummus Company Report HR-159, December 1979.

11. Russell, C. M. B.; Jones, T. V.; and Lee, G. H. "Heat Transfer Enhancement Using Vortex Generators." In Heat Transfer 1982, Seventh International Heat Transfer Conference, pp. 283-288. Vol. 3. Munchen: Hemisphere Publishing Corporation, 1982.

12. Feiler, J.; and Yeager, E. B. "Effect of large-amplitude oscillations on heat transfer." U.S. National Aeronautics and Space Administration. Report NASA TRR-142, 1962.

13. Junkhan, G. H.; Serovy, G. K. "Effects of Free-Stream Turbulence and the Pressure Gradient on Flat-Plat Boundary-Layer Velocity Profiles and on Heat Transfer." Journal of Heat Transfer 89 (1967): 169-176.

14. Blair, M. F.; and Werle, M. J. "The Influence of Free-Stream Turbulence on the Zero Pressure Gradient Fully Turbulent Boundary Layer." United Technologies Corporation Research Center Report R80-914388-12, 1980.

15. Beckwith, T. G.; and Buck, N. L. Mechanical Measurements. 2nd ed. London: Addison-Wesley Publishing Company, 1973.

16. Wyler, J. "Practical Aspects of Hot-Wire Anemometry." Instruments and Control System 47, No. 1 (1974): 57-60.

17. Kline, S. J.; and McClintock, F. A. "Describing Uncertanities in Single-Sample Experiments." Mechanical Engineering 75 (1953): 3-8.

18. Kays, W. M.; and Crawford, M. E. Convective Heat and Mass Transfer. 2nd ed. New York: McGraw-Hill Book Company, 1980.

19. White, F. M. Viscous Fluid Flow. New York: McGraw-Hill Book Company, 1974.

20. Schlichting, H. Boundary Layer Theory. 4th ed. New York: McGraw-Hill Book Company, 1960.

VIII. ACKNOWLEDGEMENTS

The author wishes to express his deepest gratitude to his Major Professor, Prof. George H. Junkhan, for his guidance, assistance, and invaluable advice throughout the course of this study. He has patiently gone through the manuscript several times editing and contributing a great deal to its improvement.

The author also wishes to thank Prof. Arthur E. Bergles, Prof. Bruce R. Munson, Prof. Richard H. Pletcher, and Prof. William J. Cook, the members of his advisory committee, for their ready assistance and guidance throughout his Ph.D. program.

The author would like to express a very special thanks to Prof. Paul E. Morgan, Associate Dean of Engineering College, for making financial support available during many stages of this study.

The author is grateful for the technical assistance given him by Mr. Hap Steed and Mr. Gay Scandrett. The author would like to extend his sincere thanks to all his fellow graduate students.

Last, but not the least, the author is greatly indebted to his wife for her understanding and encouragement throughout the entire graduate program at Iowa State University.

IX. APPENDIX A

A. Computer Program For Reducing The Hot-Film Data

```
10   ! ************************************************************************
20   !
30   !                       Program Name is   " WAKE "
40   !
50   !   This programe is for :-
60   !             (1)- Calculation the velocity fluctuation in X-dir. u';
70   !                  and the velocity comp. u .  (inside B.L.).
80   !                  As well as,the Turbulence Intensity at this point
90   !                  based on the Free-Stream Velocity ; Ue(x).
100  !
110  !                The measurements took place at :-
120  !                   THREE location ;X; measured from the leading edge.
130  !
140  !                   * At each location :-
150  !                     -----------------
160  !                      61   Points on Z-dir.
170  !                                   each=.125 inch.
180  !                  at  ONE   Yo-Plane   located at distance equal to
190  !                                        the smallest Hight of the
200  !                                        Vortex Generator's Blade;
210  !                                          i.e.  Yo = .0625  inch.
220  !
230  !                The Free-Stream Velocity ; Ue(x) ; at each location was
240  !                   measured at  Y = ONE inch. from the plate surface
250  !                   at SEVEN differnt Z-direction , then the average
260  !                   Ue(x) was taken.
270  !
280  !
290  !  ### NOTE :-
300  !      =====      The DATA was obtained from this program is recorded
310  !                  on DISK as the File Name " W8 B8 P8 "
320  !
330  !                 To obtaine this DATA you can use the PROGRAM " G-WAKE "
340  !                 which gives the data and  plotting it on GRAPHS.
350  !
360  !
370  !
380  ! ************************************************************************
390  !
400  !
410  Key=701         !  The [ OUTPUT ] & [ WRITE BIN ] codes for the printer.
420  DISP " Set the printer at top of page"
430  PAUSE
440  OPTION BASE 1
450  WRITE BIN Key;32,32,32,32,32,32,32,32,32,32
460  WRITE BIN Key;27,77
470  WRITE BIN Key;27,84
480  WRITE BIN Key;27,70,INT(1056/64),INT(1056)
490  WRITE BIN Key;27,76,INT(1056/64),INT(1056)
500  !
510 DIM A$(1),B$(1),E(10)
520  !
530 DIM A(10),C(8),X(3),Re(3)
540 DIM Ze(7),Ue(3,7),Uue(3,7),Te(3,7)          !  for Free-Stream
550 DIM Z(61),U(3,61),Uu(3,61),T(3,61)          !  ( inside the B.Layer)
560  !
570  BEEP
580    INPUT "The Operater Name ? ",A$(1)
590    INPUT "The Date  ? ",B$(1)
600    INPUT " Atmesphric Pressure  ; inch Hg   ? ",Patm
```

```
610   A=3                            ! Information for Free-Stream Temperature.
620   B=5
630   Aa=43536.3205                  !    --!
640                                  !      !---)  Calibration's Constants
650   Bb=150.5536                    !    --!
660   !
670   ! ~~~~~~~~~~~~~~~~~~~~~~~~~~~~~~~~~~~~~~~~~~~~~~~~~~~~~~~~~~~~~~~~~~~~~~~~~~~~~~~~
680   !
690 Turbulence:     !
700  ! =========
710   !
720   !
730   !          (II)-   Calculation the Velocity Flucuation  u' in X-dir.;
740   !                  (outside and inside B.L.)and Turbulence Intensity.
750   !                  ==================================================
760   BEEP
770     INPUT "Input Run No. as (70.####) ?",A(1)
780     INPUT " Are you going to heat the plate ? (Yes=1,No=0) ",N
790     IF N=0 THEN GOTO Set_speed
800 Heated_plate:   !
810 ! ============
820   BEEP
830   DISP " Switch the D.C Power Supply On . Then  CONT  "
840   PAUSE
850   GOSUB Amper
860   BEEP
870   DISP " Io  ; amper ; =",A(10)            !  Check the input current.
880   PAUSE
890     INPUT " Is the current  Io  ; OK  ?? , Yes=1,No=0",N
900     IF N=0 THEN GOTO Heated_plate
910   !
920 Set_speed:  !
930 ! =========
940  !
950   BEEP
960   DISP " New measure  Pressure values @x'1 ,@x'2 ;and P.atm. Then  CONT "
970   PAUSE
980   A(2)=Patm                               ! Atmospheric pressure; in Hg.
990   BEEP
1000    INPUT " [ Pa - P.static ] @ x'=1.25  ??",Ps1
1010    INPUT " [ Pa - P stagn. ] @ x'=1.25  ??",Po
1020    INPUT " [ Pa - P.static ] @ x'=23.4  ??",Ps2
1030  !
1040  !
1050  DISP " Measuring the Ambient and Free-Stream Temperature. Then  CONT  "
1060  PAUSE
1070  A=1
1080  B=2
1090  GOSUB Thermo
1100  A(3)=(E(1)+E(2))/2                  ! Ambient temperature ; oF
1110  !
1120  A=3
1130  B=5
1140  GOSUB Thermo
1150  A(4)=(E(3)+E(4)+E(5))/3             ! Free-Stream Temperature.
1160  BEEP
1170  DISP "Amb. Temp.;oF =",A(3);" and  Free-Stream Temp. ; oF ; =";A(4)
1180  PAUSE
1190  !
1200  A(6)=4.375                          ! Plate Unheated Length ; inch.
```

```
1210  X1=1.25+A(6)
1220  X2=23.4+A(6)
1230  Dh1=Ps1-Po
1240  Dh2=Ps2-Po
1250  Tav=(A(3)+A(4))/2                            ! Air Average Temperature ; deg F
1260  Tavr=Tav+459.67                              !   "      "          "     ; deg.R
1270  A(5)=(70.731*A(2)-5.2024*Ps1)/(53.35*Tavr)  ! Air density     ; Ibm/Ft3
1280  Uo1=SQR(2*32.174*62.43*Dh1/(12*A(5)))        ! Ue(x1)=[2g Rw Dhw/Reir]^1/2
1290  Uo2=SQR(2*32.174*62.43*Dh2/(12*A(5)))        ! Ue(x2)=[                 ]^1/2
1300  A(8)=(Uo2-Uo1)/((X2-X1)/12)                  ! Velocity Gradient ; dUe(x)/dX
1310  A(7)=Uo2-A(8)*X2/12                          ! Velocity @ X=0    ; Ue(o)
1320  A(9)=-(A(5)*A(7)*A(8)/32.1739)               ! Pressure Gradient ; dP/dX
1330                                               ! dP/dX= -Re.air Ue (dU/dX)/gc
1340  GOSUB Air_prop
1350  !
1360  BEEP
1370  DISP " Ue ,fps, =",A(7)
1380  PAUSE
1390  DISP " (dU/dX)  , 1/Sec , =",A(8)
1400  PAUSE
1410  DISP " (dP/dX)  , Ibf/Ft3 , =",A(9)
1420  PAUSE
1430    INPUT "Is Ue , dUe/dX & dP/dX  OK ?? , Yes=1,No=0",N
1440    IF N=0 THEN GOTO Set_speed
1450  !
1460  BEEP
1470  INPUT " Have you used the Vortex Generators ? ,Yes=1,No=0 ",N
1480  IF N=1 THEN GOSUB Vortex
1490  !
1500  OUTPUT Key;""
1510  OUTPUT Key USING Fmta1;A(1)
1520  OUTPUT Key;"      Date       : ",B$(1)
1530  OUTPUT Key;"      Operator   : ",A$(1)
1540  WRITE BIN Key;10,10
1550  OUTPUT Key;"  Running Condition  :-"
1560  OUTPUT Key;"  ================"
1570  OUTPUT Key USING Fmta2;A(2)
1580  OUTPUT Key USING Fmta3;A(3)
1590  OUTPUT Key USING Fmta4;A(4)
1600  OUTPUT Key USING Fmta5;A(5)
1610  OUTPUT Key USING Fmta6;A(6)
1620  OUTPUT Key USING Fmta7;A(7)
1630  OUTPUT Key USING Fmta8;A(8)
1640  OUTPUT Key USING Fmta9;A(9)
1650  OUTPUT Key USING Fmta10;A(10)
1660 Fmta1:  IMAGE //,"              "," Run No. ",2D.4D,//
1670 Fmta2:  IMAGE /," Atmospher Pressure (Pa)           ; inch Hg ; = ",M3D.3D
1680 Fmta3:  IMAGE   " Ambient Temperature (Ta)          ;   oF    ; = ",M3D.2D
1690 Fmta4:  IMAGE   " Free-Stream Temperature (Te)      ;   oF    ; = ",M3D.2D
1700 Fmta5:  IMAGE   " Air Density  (Re.air)             ; Ibm/Ft3 ; = ",M3D.4D
1710 Fmta6:  IMAGE   " Unheated Length                   ;  inch   ; = ",M3D.3D
1720 Fmta7:  IMAGE   " Free-Stream Velocity @X=0  (Ue)   ;  Ft/Sec ; = ",M3D.2D
1730 Fmta8:  IMAGE   " Velocity Gradient ( dU/dX )       ;  1/Sec  ; = ",M3D.4D
1740 Fmta9:  IMAGE   " Pressure Gradient ( dP/dX )       ; Ibf/Ft3 ; = ",M3D.4D
1750 Fmta10: IMAGE " Input Current (Io)                 ;  amper  ; = ",M3D.4D,//
1760  IF G(1)=20 THEN GOSUB Write_vgs
1770  !
1780  ! --------------------------
1790  ! Hot - Wires Specification:-
1800  ! --------------------------
```

```
1810  !
1820  OUTPUT Key;"                    The Specification of Hot-Wire Probes"
1830  OUTPUT Key;"                   ======================================="
1840  WRITE BIN Key;10
1850  !
1860 INPUT " Input type of the hot_wire?,( Norm = 1 ,Slant =2 ;both=11",Hot
1870   IF Hot=11 THEN GOSUB Normal_probe
1880   IF Hot=11 THEN GOSUB Slant_probe
1890   IF Hot=1 THEN GOSUB Normal_probe
1900   IF Hot=2 THEN GOSUB Slant_probe
1910  !
1920  ! ------------------------
1930  !   MEASURED THE RUN DATA.
1940  ! ------------------------
1950  !
1960        Channel=10              ! Hot-Wire Channel.
1970        Hot_wire_sen=.3357      ! Hot-Wire Sensitivity ; from Calibration.
1980       X(1)=2.5+A(6)            !  X(I) = Xo + Unheated Length
1990       X(2)=8.7+A(6)
2000       X(3)=15.11+A(6)
2010  !
2020     FOR I=1 TO 3
2030      WRITE BIN Key;12
2040      BEEP
2050      DISP " Move to Position   X     ; inch ; =  ",X(I)
2060      PAUSE
2070  !
2080        U=A(7)+A(8)*X(I)/12           ! Ue(x) = Ue(0) + [dUe/dX] * x/12
2090  !
2100         BEEP
2110         DISP " Hot-Wire inside Free-Stream  ~ ONE in from surface"
2120         PAUSE
2130        FOR Number=1 TO 7           !  Measurment for Free-Stream.
2140         BEEP
2150         Zo(Number)=(4-Number)*1
2160         DISP " Hot-Wire inside Free-Stream  at   Zo  ;inch = ",Zo(Numbe
r)
2170         PAUSE
2180         GOSUB Dc_volt
2190         GOSUB Rms_volt
2200         Ue(I,Number)=E/Hot_wire_sen
2210         Uue(I,Number)=Ee/Hot_wire_sen
2220         To(I,Number)=Ee/E*100
2230        NEXT Number
2240        !
2250        Ue=0
2260        Uue=0
2270        To=0
2280         !
2290         FOR Number=1 TO 7            ! Average Ue(x),u'(x) and Tu%
2300         Ue=Ue+Ue(I,Number)           !  for Free-Stream
2310         Uue=Uue+Uue(I,Number)
2320         To=To+To(I,Number)
2330         NEXT Number
2340         Ue=Ue/7
2350         Uue=Uue/7
2360         To=To/7
2370        DISP "By Hot-Wire =";Ue,"By Pitot  =";U
2380        PAUSE
2390        DISP " CHECK the Hot-Wire Calibration"
```

```
2400          PAUSE
2410          OUTPUT 16;"Is it OK ?, if YES then CONT ,If NO then CHECK "
2420          OUTPUT 16;"the CONNECTIONS and STOP , Start from the beginning"
2430          PAUSE
2440          !
2450          B_layer=5*X(I)/SQR(Ue*(X(I)/12)/Kvis)  ! Est Laminar B.L. thick
2460          Re(I)=Ue*(X(I)/12)/Kvis                ! Re(x)= Ue(x)*X/K.Vis
2470          !
2480            OUTPUT Key USING 2490;X(I)
2490 IMAGE //," Distance downstream the leading edge.  X ; inch ; = ",2D.4D
2500            OUTPUT Key USING 2510;Ue
2510 IMAGE      " Free-Stream Velocity @ Location X.  Ue(X);  fps ; = ",2D.4D
2520            OUTPUT Key USING 2530;Re(I)
2530 IMAGE      " Reynolds Number ; Re(x)    @ Location X.           = ",7D,//
2540            OUTPUT Key USING 2550;Uue
2550 IMAGE      " Free-Stream flucuation Velocity     u'(x);  fps ; = ",2D.4D
2560            OUTPUT Key USING 2570;Te
2570 IMAGE      " Free-Stream Turbulence Intensity;Tu % =(u'/U)*100 = ",2D.4D
2580                                   Ee=Ue*Hot_wire_sen
2590            OUTPUT Key USING 2600;Ee
2600 IMAGE      " Dc. output Voltage of Free-Stream  Ue(X) ; volt ; = ",2D.4D,//
2610            OUTPUT Key USING 2620;B_layer
2620 IMAGE      " Estimated Laminar B.Layer thickness @ X  ; inch ; = ",2D.4D
2630            OUTPUT Key USING 2640;G(3)/2/B_layer
2640 IMAGE      " Measurement @ Y=Fvg./2 ; where  (Y/B.layer)       = ",2D.4D,//
2650               M=10
2660               GOSUB Line
2670 OUTPUT Key;"   Z          E          RMS            u          u'          (u'/u)
     (u'/Ue)       (Ue-u)"
2680 OUTPUT Key;" inch                volt                        Ft/Sec     "
2690               GOSUB Line
2700               WRITE BIN Key;10
2710  !
2720                  BEEP
2730                  DISP " Move to Position   Z(1) =3.75   inch "
2740                  PAUSE
2750                  Ye=.0625        !  Ye= Height of smallest V.G's blades.
2760                  BEEP
2770                  DISP " Move to Ye-Plane Position ;  Ye  ; inch ",Ye
2780                  PAUSE
2790  !
2800            FOR J=1 TO 61
2810             Z(J)=(31-J)*.125
2820               BEEP
2830               DISP " Move to Position   Z   ; inch ; =  ",Z(J)
2840               PAUSE
2850  !
2860                    GOSUB Dc_volt
2870                    GOSUB Rms_volt
2880                    !
2890                    U(I,J)=E/Hot_wire_sen
2900                    Uu(I,J)=Ee/Hot_wire_sen
2910                    T(I,J)=Ee/F*100
2920                    !
2930  OUTPUT Key USING 2940;Z(J),E,Ee,U(I,J),Uu(I,J),T(I,J),Ee/Ee*100,Ue-U(I,J)
2940 IMAGE 2X,MD.3D,5X,2D.3D,3X,M2D.3D,7X,2D.3D,4X,2D.3D,7X,2D.3D,4X,2D.3D,7X,2D
.3D
2950  !
2960            NEXT J
2970            WRITE BIN Key;10
```

```
2980            GOSUB Line
2990            OUTPUT Key;"      Measurement for Free-Stream     "
3000            WRITE BIN Key;10
3010            OUTPUT Key;"    Zo         Uo          u'o          TuoX        Uo(x,z)
/Uo(x)"
3020            OUTPUT Key;" inch              Ft/Sec                "
3030            M=7
3040            GOSUB Line
3050              FOR K=1 TO 7
3060            OUTPUT Key USING 3070;Zo(K),Uo(I,K),Uuo(I,K),To(I,K),Uo(I,K)/Uo
3070            IMAGE ,2X,MD.3D,5X,2D.3D,3X,2D.3D,7X,2D.4D,7X,D.4D
3080              NEXT K
3090            GOSUB Line
3100      NEXT I
3110   !
3120            WRITE BIN Key;10,10,10
3130   ! --------------------------------
3140   !   RECORDING OF RUN DATA ON DISK.
3150   ! --------------------------------
3160   !
3170 Recording_data: !
3180 ! =============
3190  BEEP
3200  INPUT " Are you going to record the data ? Yes=1 , No=0 ",N
3210          IF N=0 THEN GOTO 3680
3220  DISP " DATA Ready to be recorded on disk , if O.K   CONT  "
3230  PAUSE
3240  DISP " Insert Disk into the disk drive   and        CONT  "
3250  PAUSE
3260            IF G(3)=.0625 THEN Name1=1
3270            IF G(3)=.125 THEN Name1=2
3280            IF G(3)=.25 THEN Name1=3
3290        Name2=INT(G(2))
3300        IF G(2)=.75 THEN Name2=0
3310            IF ABS(A(9))<.015 THEN Name3=1
3320            IF (ABS(A(9))>.015) AND (ABS(A(9))<.025) THEN Name3=2
3330            IF ABS(A(9))>.030 THEN Name3=3
3340  !
3350  File$="W"&VAL$(Name1)&"G"&VAL$(Name2)&"P"&VAL$(Name3)
3360  OUTPUT 16;" File Name is ",File$
3370  DISP "If O.K  CONT  ;otherwise INPUT File$ as TEMP$, EXEC. &  CONT
 "
3380   PAUSE
3390   !
3400   MASS STORAGE IS ":F 8,0"
3410 Mass_storage: !
3420 ! ==========
3430   CREATE File$,25
3440   OUTPUT 16;" File Created for Recording the data is   ",File$
3450   DISP " Is the created File O.K , Press  CONT  "
3460   PAUSE
3470  !
3480  ASSIGN #1 TO File$
3490  PRINT #1;A(*),G(*),X(*),Re(*)
3500  PRINT #1;Zo(*),Uo(*),Uuo(*),To(*)
3510  PRINT #1;Z(*),U(*),Uu(*),T(*)
3520  !
3530  CHECK READ #1
3540  PROTECT File$,"DATA"
3550  !
```

```
3560  OUTPUT Key USING Fmt_file;File$
3570 Fmt_file:IMAGE L, " Data recorded on disk , file name is  ",6A
3580  INPUT " Would you like to store it on another disk ? Yes=1,No=0",N
3590  IF N=0 THEN GOTO Change_dim
3600   MASS STORAGE IS ":F 8,1"
3610   GOTO Mass_storage
3620  !
3630  WRITE BIN Key;12
3640  ! -------------------------------------------------------------
3650  !
3660 Change_dim: !
3670 ! ========
3680     INPUT " Is any of  [ (Ue) or (dP/dX) ] chanqged ? ,Yes=1, No=0",N
3690     IF N=1 THEN GOTO Turbulence
3700  DISP " Turn the D.C. power supply OFF !!!!! "
3710  PAUSE
3720  DISP " The CLOSED position & turn OFF the A.C Power of Wind Tunnel"
3730  PAUSE
3740  !
3750  !
3760  STOP   !                  **************************
3770  END    ! ***************! End of the Main Program !***************
3780  !                         **************************
3790  !
3800  ! ------------------------------------------------
3810  !   The next subprogram is for measuring the Current .
3820  ! ------------------------------------------------
3830 Amper:   !
3840 ! =====
3850  !
3860  OUTPUT 722;"F1R3T2M3A1H1"
3870  OUTPUT 709 USING 3880;9
3880  IMAGE #,"C",ZZ,"E"
3890  Sum=0
3900  !
3910    FOR N=1 TO 10
3920        TRIGGER 722
3930        ENTER 722 BINT;E
3940        Sum=Sum+E
3950    NEXT N
3960  !
3970  E=Sum/10
3980  A(10)=5/.05*E      !  Current Ie ,amp ,[ Using Shunt Resis.]
3990  !
4000  RETURN
4010  !
4020  ! ---------------------------------------------------
4030  !   The next Subprogram is for measuring the Temperaturs .
4040  ! ---------------------------------------------------
4050 Thermo:  !
4060 ! =======
4070  !
4080  OUTPUT 722;"F1R3T2M3A1H1"
4090  !
4100  FOR Ch=A TO B
4110    OUTPUT 709 USING 4120;Ch
4120    IMAGE #,"C",ZZ,"E"
4130    Sum=0
4140      FOR N=1 TO 10
4150       TRIGGER 722
```

```
4160        ENTER 722 BINT;E
4170        Sum=Sum+E
4180       NEXT N
4190     E=Sum/10
4200     E(Ch)=Aa*E+Bb
4210  NEXT Ch
4220  !
4230  RETURN
4240  !
4250  !   ---------------------------------------------------
4260  !   The next subprogram is for Hot-Wires Specification.
4270  !   ---------------------------------------------------
4280 Normal_probe:  !
4290  ! ==========
4300  !
4310  OUTPUT Key;" For Standard Straight Hot-Wire Probe"
4320  OUTPUT Key;"                     TSI  Model 1227 (-10) :-"
4330  Rc1=5
4340  Rh1=8
4350  Ohr1=Rh1/Rc1
4360  OUTPUT Key USING F_c;Rc1
4370 F_c: IMAGE /," Cold Resistance of Probe.        ; ohms ; = ",2D.3D
4380  OUTPUT Key USING F_h;Rh1
4390 F_h: IMAGE   " Operated Resistance of Probe.   ; ohms ; = ",2D.3D
4400  OUTPUT Key USING F_r;Ohr1
4410 F_r: IMAGE   " Over Heat Ratio of Probe.       ; ohms ; = ",2D.3D
4420  IF Estand_by=0 THEN 4450
4430  OUTPUT Key USING F_s;Estand_by
4440  !
4450  RETURN
4460  ! ~~~~~~~~~~~~~~~~~~~~~~~~~~~~~~~~~~
4470  !
4480 Slant_probe:  !
4490  ! =========
4500  !
4510  OUTPUT Key;" For the Slant Single  Hot-Wire Probe"
4520  OUTPUT Key;"                     TSI  Model 1213 (-10) :-"
4530  WRITE BIN Key;10
4540  Rc2=7
4550  Rh2=10.85
4560  Ohr2=Rh2/Rc2
4570  OUTPUT Key USING F_c;Rc2
4580  OUTPUT Key USING F_h;Rh2
4590  OUTPUT Key USING F_r;Ohr2
4600  IF Estand_by2=0 THEN GOTO 4630
4610  OUTPUT Key USING F_s;Estand_by2
4620  !
4630  RETURN
4640  !
4650  ! ------------------------------------------------------------------------
4660  !  The next subprogram is for Measuring the o/p D.C. volt of the Hot Wire.
4670  ! ------------------------------------------------------------------------
4680 Dc_volt:     !
4690 ! =======
4700  !
4710  TRIGGER 722
4720  OUTPUT 722;"F1R7T2M3A1H1"
4730  OUTPUT 709 USING 4740;Channel
4740  IMAGE #,"C",ZZ,"E"
4750  Sum=0
```

```
4760      FOR N=1 TO 20
4770          TRIGGER 722
4780          ENTER 722 BINT;E
4790          Sum=Sum+E
4800      NEXT N
4810  E=Sum/20
4820  !
4830  RETURN
4840  !
4850  ! ----------------------------------------------------------------------
4860  !  The next subprogram is for Measuring the RMS D.C. volt of the Hot Wire
4870  ! ----------------------------------------------------------------------
4880 Rms_volt:    !
4890 ! =======
4900  !
4910  TRIGGER 722
4920  OUTPUT 722;"F3R7A1M3T2H1"
4930  OUTPUT 709 USING 4940;Channel
4940  IMAGE #,"C",ZZ,"E"
4950  Sum=0
4960       FOR N=1 TO 20
4970           TRIGGER 722
4980           ENTER 722 BINT;Ee
4990           Sum=Sum+Ee
5000       NEXT N
5010  Ee=Sum/20
5020  !
5030  RETURN
5040  !
5050  ! ------------------------------------------------------
5060  !  The next subprogram is for the Properties of Air.
5070  ! ------------------------------------------------------
5080 Air_prop:      !
5090 ! ========
5100  !
5110  Cp=.2231+3.42*10^(-5)*Tavr-2.93*10^(-9)*Tavr^2  ! BTU/(Ibm.hr.oF)
5120  Ka=.0020493+2.43*10^(-5)*Tavr                   ! BTU/(hr.Ft.oF)
5130  Vis=.0118205+6.09*10^(-5)*Tavr                  ! Ibm/(hr.Ft)
5140  Kvis=(.00202*Tavr-.47862)/3600                  ! Ft2/Sec
5150  Pra=.78586-.00014*Tavr                          ! Prandtl Number.
5160  !
5170  RETURN
5180  !
5190  ! ---------------------------------------------------------------
5200  !  The next subprogram is the vertex generators' cefiguration .
5210  ! ---------------------------------------------------------------
5220 Vertex:  !
5230 ! ======
5240  !
5250  G(1)=20                       !  Angle of incidence          ; degree
5260  INPUT "  Transverse Pitch of V.G's blades   ; inch.",G(2)
5270  INPUT "  Height of a protrusion ; (V.G's)   ; inch.",G(3)
5280  G(4)=1                        !  Length of a protrusion      ; inch.
5290  G(5)=.0625                    !  Protrusion's  thickness     ; inch.
5300  INPUT "  The number of Vertex Generators Blades # ",G(6)
5310  !
5320  Xvg=1.75                      !  Location of Vertex Generators ; inch.
5330  Uvg=A(7)+A(8)*Xvg/12          !  Air Velocity at V. Generators ; Ft/Sec.
5340  Kvis=(.00202*Tavr-.47862)/3600
5350  Revg=Uvg*(Xvg/12)/Kvis        !  Reynolds Number at Vertex Generators.
```

```
5360  Delta=Xvg*5/SQR(Revg)      !  Laminar B.Layer thickness @ VG's  ; inch
5370  C(7)=Delta/C(3)
5380  Delta1=Xvg*.664/SQR(Revg) !  Laminar Momentum thickness @ VG's ; inch.
5390  C(8)=Delta1/C(3)
5400  RETURN
5410   !
5420 ! ~~~~~~~~~~~~~~~~~~~~~~~~~~~~~~~~~~~~
5430 Write_vgs:  !
5440 ! ========
5450  !
5460  OUTPUT Key;"  Using Rectangular Counter-Rotating Vortex Generators."
5470  OUTPUT Key;" ========================================================="
5480  OUTPUT Key USING Fmtg1;C(1)
5490  OUTPUT Key USING Fmtg2;C(2)
5500  OUTPUT Key USING Fmtg3;C(3)
5510  OUTPUT Key USING Fmtg4;C(4)
5520  OUTPUT Key USING Fmtg5;C(5)
5530  OUTPUT Key USING Fmtg6;C(6)
5540  OUTPUT Key USING Fmtg7;C(7)
5550  OUTPUT Key USING Fmtg8;C(8)
5560 Fmtg1:   IMAGE /,"Angle betn. a V.G's and  plate axis ; degree ; =",2D
5570 Fmtg2:   IMAGE   "Transverse pitch betn. V.G's blades ;  inch  ; =",2D.2D
5580 Fmtg3:   IMAGE   "Height of V.G's blades              ;  inch  ; =",2D.4D
5590 Fmtg4:   IMAGE   "Length of V.G's blades              ;  inch  ; =",2D
5600 Fmtg5:   IMAGE   "Thickness of V.G's blades           ;  inch  ; =",2D.4D
5610 Fmtg6:   IMAGE   "The number of Vortex Generators                =",2D
5620 Fmtg7:   IMAGE   "B-Layer thickness / Height of Vg's blade.      =",2D.4D
5630 Fmtg8:   IMAGE   "Momentum thickness / Height of Vg's blade.     =",2D.4D,//
5640   !
5650  RETURN
5660   !
5670   ! ~~~~~~~~~~~~~~~~~~~~~~~~~~
5680 Line:  !
5690 ! ===
5700   !
5710     FOR No=1 TO M
5720  OUTPUT Key USING 5730
5730  IMAGE #,"======="
5740     NEXT No
5750  OUTPUT Key USING 5760
5760  IMAGE "====="
5770   !
5780  RETURN
5790   !
5800   ! ~~~~~~~~~~~~~~~~~~~~~~~~~~
```

X. APPENDIX B

A. Computer Program For Reducing Heat Transfer Data

```
10    ! ==================================================================
20    !                   Program Name " HEAT "
30    !
40    !    For measuring :-
50    !    ---------------
60    !                 1-  Velocities, pressure and velocity gradients.
70    !                 2-  Local temeratures and heated current
80    !                 3-  Local heat transfer rates
90    !                      ( conduction, radiation and convection)
100   !                 4-  Local and Span-averaged Stanton numbers.
110   !                 5-  Compre measured Stanton number by the
120   !                      predicted for laminar and turbulent
130   !                      boundary layer flow.
140   ! ==================================================================
150   !
160   Key=701          !  The ( OUTPUT ) & ( WRITE BIN ) codes for the printer.
170   PRINTER IS 7,1
180   OPTION BASE 1
190   DIM Total(12,14)
200   DIM A$(1),B$(1),A(12),G(12)
210   DIM X(12),Ts(12),Tb(12),U(12),Re(12),Qia(12),Qca(12),Qra(12),Qna(12)
220   DIM Tsa(12),Sle(12),Ste(12),Sta(12),Rav(12)
230   DIM T(12,11),B(12,11),Qi(12,11),Qc(12,11),Qr(12,11),Qn(12,11),Tse(12,11)
240   DIM St(12,11),Ra(12,11),Z(12,11)
250   DIM E(40),P(4),Cp(4)
260   WRITE BIN Key;32,32,32,32,32,32,32,32,32,32
270   WRITE BIN Key;27,77
280   !
290   DISP " Set the printer at top of page"
300   PAUSE
310   WRITE BIN Key;27,84
320   WRITE BIN Key;27,70,INT(1056/64),INT(1056)
330   WRITE BIN Key;27,76,INT(1056/64),INT(1056)
340   INPUT "May you check thermocouples & the system ?,Yes=1,No=0",N
350   IF N=0 THEN GOTO 560
360   FOR J=1 TO 4
370   BEEP
380   DISP " Switch the Thermocouples Group in order.   ;  J = ",J
390   PAUSE
400   A=10
410   IF J=1 THEN B=39
420   IF J=2 THEN B=39
430   IF J=3 THEN B=37
440   IF J=4 THEN B=37
450   Aa=43536.3285
460   Bb=150.5536
470   GOSUB Therms
480   FOR I=A TO B
490   OUTPUT Key USING 500;J,I,E(I)
500   IMAGE 5X,2D,3X,2D,5X,M6D.2D
510   NEXT I
520   WRITE BIN Key;10,10
530   DISP "  Check the none working thermocouples !!! "
540   PAUSE
550   NEXT J
560   BEEP
570   INPUT "Input Run No.as(**.**) ?",A(1),"Operator?",A$(1),"Date ?",B$(1)
580   A(6)=4.375                          ! A(6)  = plate unheated length; inch.
590   INPUT " Atm. Pressure ;in.Hg; ?",A(2)       ! Atmospheric pressure; in.Hg.
600   !
```

```
610    A=1
620    B=2
630    Aa=43536.3205
640    Bb=150.5536
650    GOSUB Thermo
660    A(3)=(E(1)+E(2))/2                         ! Ambient temperature ; oF
670    BEEP
680    DISP "Amb. Temp  ; oF ; =",A(3)
690    PAUSE
700    !
710    BEEP
720    INPUT " [ Pa - P.static ] @ x'=1.25  ??",Ps1
730    INPUT " [ Pa - P.stagn. ] @ x'=1.25  ??",Po
740    INPUT " [ Pa - P.static ] @ x'=23.4  ??",Ps2
750    X1=1.25+A(6)
760    X2=23.4+A(6)
770    Dh1=Ps1-Po
780    Dh2=Ps2-Po
790    A(5)=(70.731*A(2)-5.2024*Ps1)/(53.35*(A(3)+459.67))         ! Air density
800    Ue1=SQR(2*32.174*62.43*Dh1/(12*A(5)))      ! Ue(x1)=[2g Rw Dhw/Rair]^1/2
810    Ue2=SQR(2*32.174*62.43*Dh2/(12*A(5)))      ! Ue(x2)=[             ]^1/2
820    A(8)=(Ue2-Ue1)/((X2-X1)/12)                ! Velocity Gradient ; dUe(x)/dX
830    A(7)=Ue2-A(8)*X2/12                        ! Velocity @ X=0    ; Ue(o)
840    A(9)=-(A(5)*A(7)*A(8)/32.1739)             ! Pressure Gradient ; dP/dX
850                                               ! dP/dX= -Ro.air Ue (dU/dX)/gc
860    BEEP
870    DISP " Ue ,fps, =",A(7)
880    PAUSE
890    DISP " (dU/dX)  , 1/Sec , =",A(8)
900    PAUSE
910    DISP " (dP/dX)  , lbf/Ft3 , =",A(9)
920    PAUSE
930    INPUT "Is Ue , dUe/dX & dP/dX  OK ?? , Yes=1,No=0",N
940    IF N=0 THEN GOTO 610
950    BEEP
960    DISP " Switch the power on !!! "
970    PAUSE
980    GOSUB Amper
990    BEEP
1000   DISP " Io  ; amper ; =",A(10)              !  Check the input current.
1010   PAUSE
1020   INPUT " Is the current  Io  ; OK  ?? , Yes=1,No=0",N
1030   IF N=0 THEN GOTO 960
1040   INPUT " Are Vertex Generators used ?? ,Yes=1,No=0",N
1050   IF N=1 THEN GOSUB Vertex
1060   IMAGE #,"C",ZZ,"E"
1070   IMAGE "F1R3T2M3A1H1"
1080   BEEP      ! The next part for pressure measurement on the plate surface.
1090   !         ===============================================================
1100   DISP " Pressure Gradint on the Plate "
1110   PAUSE
1120   DISP " Set Scanivalve at CHANNEL  6  "
1130   PAUSE
1140   OUTPUT 709 USING 1060;0
1150   OUTPUT 722 USING 1070
1160   K=0
1170   FOR N=1 TO 20
1180   TRIGGER 722
1190   ENTER 722 BINT;E
1200   K=K+E
```

```
1210  NEXT N
1220  E=K/20
1230  C=-1.139*E           ! Calibration const. for the pres. transducer.
1240  BEEP
1250  DISP " Set Scanivalve at Channel 5 "
1260  PAUSE
1270  OUTPUT 722 USING 1070
1280  K=0
1290  FOR N=1 TO 20
1300  TRIGGER 722
1310  ENTER 722 BINT;E
1320  K=K+E
1330  NEXT N
1340  E=K/20
1350  Pseg=C+1.139*E            ! Stagnation pressure on the plate nose ;in.H20
1360  FOR I=1 TO 4
1370  BEEP
1380  DISP " Set Scanivalve at Channel  ",I
1390  PAUSE
1400  OUTPUT 722 USING 1070
1410  K=0
1420  FOR N=1 TO 20
1430  TRIGGER 722
1440  ENTER 722 BINT;E
1450  K=K+E
1460  NEXT N
1470  E=K/20
1480  P(I)=C+1.139*E            ! Static Pressures on  Plate Surfase ; in.H20
1490  Cp(I)=1-(P(I)-Pseg)/(P(1)-Pseg)       ! Cp(x)=[Ps(x)-Ps(x1)/(.5Ro.air Ue^2)
1500  NEXT I
1510  !
1520  A=3
1530  B=5
1540  Aa=43536.3205
1550  Bb=150.5536
1560  GOSUB Thermo
1570  A(4)=(E(3)+E(4)+E(5))/3              ! Free-Stream Temperature.
1580  !
1590  OUTPUT Key USING Fmta1;A(1)
1600  OUTPUT Key;"       Date       : ",B$(1)
1610  OUTPUT Key;"       Operator  : ",A$(1)
1620  WRITE BIN Key;10,10
1630  OUTPUT Key;"  Running Condition  :-"
1640  OUTPUT Key;"  *****************"
1650  OUTPUT Key USING Fmta2;A(2)
1660  OUTPUT Key USING Fmta3;A(3)
1670  OUTPUT Key USING Fmta4;A(4)
1680  OUTPUT Key USING Fmta5;A(5)
1690  OUTPUT Key USING Fmta6;A(6)
1700  OUTPUT Key USING Fmta7;A(7)
1710  OUTPUT Key USING Fmta8;A(8)
1720  OUTPUT Key USING Fmta9;A(9)
1730  OUTPUT Key USING Fmta10;A(10)
1740  IF G(4)=1 THEN GOSUB Write_vgs
1750 Fmta1:  IMAGE //,"              "," Run No. ",2D.3D,//
1760 Fmta2:  IMAGE /," Atmospher Pressure (Pa)         ; inch Hg ; = ",M3D.3D
1770 Fmta3:  IMAGE   " Ambient Temperature (Ta)        ;   oF    ; = ",M3D.2D
1780 Fmta4:  IMAGE   " Free-Stream Temperature (Te)    ;   oF    ; = ",M3D.2D
1790 Fmta5:  IMAGE   " Air Density  (Ro.air)           ; Ibm/Ft3 ; = ",M3D.4D
1800 Fmta6:  IMAGE   " Unheated Length                 ;   inch  ; = ",M3D.3D
```

```
1810 Fmta7:  IMAGE   " Free-Stream Velocity @X=0  (Uo)    ;  Ft/Sec ; = ",M3D.2D
1820 Fmta8:  IMAGE   " Velocity Gradient ( dU/dX )        ;  1/Sec  ; = ",M3D.4D
1830 Fmta9:  IMAGE   " Pressure Gradient ( dP/dX )        ; lbf/Ft3 ; = ",M3D.4D
1840 Fmta10: IMAGE " Input Current (Io)                 ;  amper  ; = ",M3D.4D,//
1850  WRITE BIN Key;10,10
1860  WRITE BIN Key;12
1870  WRITE BIN Key;10,10,10,10,10
1880  OUTPUT Key USING Fmta1;A(1)
1890  OUTPUT Key;"       Pressure Measurements on the Plate Surface  "
1900  OUTPUT Key;"       ===========================================  "
1910  OUTPUT Key USING Fmta2;A(2)
1920  OUTPUT Key USING Fmtpo;Po
1930  OUTPUT Key USING Fmtp1;Ps1
1940  OUTPUT Key USING Fmtp2;Ps2
1950  OUTPUT Key;"        ========================================  "
1960  OUTPUT Key;"              X         (Patm - Ps.x)      Cp(I)   "
1970  OUTPUT Key;"             inch         inch H2o                 "
1980  OUTPUT Key;"        ========================================  "
1990  FOR I=1 TO 4
2000  IF I=1 THEN Xp=A(6)                 ! Location of Press. Tape #1
2010  IF I=2 THEN Xp=A(6)+5.25            ! Location of Press. Tape #2
2020  IF I=3 THEN Xp=A(6)+10.5625         ! Location of Press. Tape #3
2030  IF I=4 THEN Xp=A(6)+24.375          ! Location of Press. Tape #4
2040  OUTPUT Key USING Fmtpp;Xp,P(I),Cp(I)
2050 Fmtpp:  IMAGE /,9X,2D.4D,7X,MD.4D,8X,MD.4D
2060  NEXT I
2070  WRITE BIN Key;10
2080  OUTPUT Key;"        ========================================  "
2090  OUTPUT Key USING Fmtps;Pseg
2100 Fmtpo:   IMAGE " ( Patm. - Pstag )                ; in.H2O  ; ="M2D.4D
2110 Fmtp1:   IMAGE " ( Patm. - Pstat ) @x'=1.25       ; in.H2O  ; ="M2D.4D
2120 Fmtp2:   IMAGE " ( Patm. - Pstat ) @x'=23.4       ; in.H2O  ; ="M2D.4D,/
2130 Fmtps:   IMAGE /," ( Patm. - Pstag ) on plate's nose ;in.H2O; ="M2D.4D
2140  !
2150  !
2160 Measuring_tempe: !
2170 ! --------------
2180  DISP " Now For Heat Calculation , Check the values of ( Io ) & ( To ) "
2190  PAUSE
2200  WRITE BIN Key;12
2210  GOSUB Line
2220  OUTPUT Key;"      J   I      Ts(J,I)   Tb(J,I)    Ts-Tb      Ts-To    "
2230  OUTPUT Key;" ------------------------------------------------------------- "
2240  GOSUB Line
2250  WRITE BIN Key;10
2260  BEEP
2270  DISP " HEAT TRANSFER MEASUREMENT & CALCULATION "
2280  PAUSE !========================================
2290  !
2300  A=3
2310  B=5
2320  Aa=43536.3205
2330  Bb=150.5536
2340  GOSUB Thermo
2350  A(4)=(E(3)+E(4)+E(5))/3             ! Free-Stream Temperature , oF .
2360  !
2370  WAIT 500
2380  ! Check the Current
2390  GOSUB Amper                         ! A(10)= The Current      ,amper.
2400  DISP " Io    ; amper ; =",A(10)
```

```
2410  PAUSE
2420  !
2430  BEEP
2440  DISP " Switch on position (A - 1)" ! First Group of thermocouples.
2450  PAUSE !--------------------------
2460  A=10
2470  B=39
2480  Aa=43407.0727
2490  Bb=150.57144
2500  GOSUB Thermo
2510  !
2520  !
2530  J=1                          ! STRIP # 1
2540                               ! ---------
2550  Ks=0
2560  X(J)=.5+A(6)
2570  FOR I=10 TO 20
2580  T(J,I-9)=E(I)                          ! Surface Temps.
2590  Ks=Ks+E(I)
2600  NEXT I
2610  Ts(J)=Ks/11                            ! Av.  "      "
2620  B=21
2630  GOSUB Back_temp1                       ! Back Temps.
2640  Tb(J)=(E(21)+E(22)+E(23)+E(24))/4      ! Av."    "
2650  FOR I=1 TO 11
2660  GOSUB Temp
2670  !
2680  J=4                          ! STRIP # 7
2690                               ! ---------
2700  Ks=0
2710  X(J)=6.875+A(6)
2720  FOR I=25 TO 35
2730  T(J,I-24)=E(I)                         ! Surface Temps.
2740  Ks=Ks+E(I)
2750  NEXT I
2760  Ts(J)=Ks/11                            ! Av.  "     "
2770  B=36
2780  GOSUB Back_temp1                       ! Back Temps.
2790  Tb(J)=(E(36)+E(37)+E(38)+E(39))/4      ! Av."    "
2800  FOR I=1 TO 11
2810  GOSUB Temp
2820  !
2830  !
2840  BEEP
2850  DISP " Switch on position (A - 2)" ! Second Group of thermocouples.
2860  PAUSE !--------------------------
2870  A=10
2880  B=39
2890  Aa=43751.4371
2900  Bb=150.67595
2910  GOSUB Thermo
2920  !
2930  !
2940  E(31)=(E(30)+E(32))/2                  ! Thermocouple #31 (A-2) is not good.
2950  !
2960  !
2970  J=9                          ! STRIP # 22
2980                               ! ----------
2990  Ks=0
3000  X(J)=22.8125+A(6)
```

```
3010  FOR I=10 TO 20
3020  T(J,I-9)=E(I)                         ! Surface Temps.
3030  Ks=Ks+E(I)
3040  NEXT I
3050  Ts(J)=Ks/11                           ! Av.  "     "
3060  B=21
3070  GOSUB Back_temp1                      ! Back Temp.
3080  Tb(J)=(E(21)+E(22)+E(23)+E(24))/4    ! Av.  "  "
3090  FOR I=1 TO 11
3100  GOSUB Temp
3110  !
3120  J=12                 ! STRIP # 33
3130                       ! ----------
3140  Ks=0
3150  X(J)=34.5+A(6)
3160  FOR I=25 TO 35
3170  T(J,I-24)=E(I)                        ! Surface Temps.
3180  Ks=Ks+E(I)
3190  NEXT I
3200  Ts(J)=Ks/11                           ! Av.  "     "
3210  B=36
3220  GOSUB Back_temp1                      ! Back Temps.
3230  Tb(J)=(E(36)+E(37)+E(38)+E(39))/4    ! Av.  "  "
3240  FOR I=1 TO 11
3250  GOSUB Temp
3260  !
3270  !
3280  BEEP
3290  DISP " Switch on position (B - 1)" ! Third Group of thermocouples
3300  PAUSE !--------------------------
3310  A=10
3320  B=37
3330  Aa=43369.49115
3340  Bb=150.35391
3350  GOSUB Thermo
3360  !
3370  !
3380  J=2                  ! STRIP # 3
3390  Ks=0                 ! ---------
3400  X(J)=2.625+A(6)
3410  FOR I=10 TO 14
3420  T(J,I-9)=E(I)                         ! Surface Temps.
3430  Ks=Ks+E(I)
3440  NEXT I
3450  Ts(J)=Ks/5                            ! Av.  "     "
3460  B(J,2)=E(16)                          ! Back Temps.
3470  B(J,4)=E(15)
3480  GOSUB Back_temp2
3490  Tb(J)=(E(15)+E(16))/2                 ! Av.  "   "
3500  FOR I=1 TO 5
3510  GOSUB Temp
3520  !
3530  J=3                  ! STRIP # 5
3540  Ks=0                 ! ---------
3550  X(J)=4.75+A(6)
3560  FOR I=17 TO 21
3570  T(J,I-16)=E(I)                        ! Surface Temps.
3580  Ks=Ks+E(I)
3590  NEXT I
3600  Ts(J)=Ks/5                            ! Av.  "     "
```

```
3610  B(J,2)=E(23)                        ! Back Temps.
3620  B(J,4)=E(22)
3630  GOSUB Back_temp2
3640  Tb(J)=(E(22)+E(23))/2               ! Av.  "    "
3650  FOR I=1 TO 5
3660  GOSUB Temp
3670  !
3680  J=5                   ! STRIP # 10
3690  Ks=0                  ! ----------
3700  X(J)=10.0625+A(6)
3710  FOR I=24 TO 28
3720  T(J,I-23)=E(I)                      ! Surface Temps.
3730  Ks=Ks+E(I)
3740  NEXT I
3750  Ts(J)=Ks/5                          ! Av.  "    "
3760  B(J,3)=E(30)                        ! Back Temps.
3770  B(J,4)=E(29)
3780  GOSUB Back_temp2
3790  Tb(J)=(E(29)+E(30))/2               ! Av. "     "
3800  FOR I=1 TO 5
3810  GOSUB Temp
3820  !
3830  J=6                   ! STRIP # 13
3840  Ks=0                  ! ----------
3850  X(J)=13.25+A(6)
3860  FOR I=31 TO 35
3870  T(J,I-30)=E(I)                      ! Surface Temps.
3880  Ks=Ks+E(I)
3890  NEXT I
3900  Ts(J)=Ks/5                          ! Av.  "    "
3910  B(J,2)=E(37)                        ! Back Temps.
3920  B(J,4)=E(36)
3930  GOSUB Back_temp2
3940  Tb(J)=(E(36)+E(37))/2               ! Av.  "    "
3950  FOR I=1 TO 5
3960  GOSUB Temp
3970  !
3980  !
3990  BEEP
4000  DISP " Switch on position (B - 2)" ! Fourth Group of thermocouples
4010  PAUSE !--------------------------
4020  A=10
4030  B=37
4040  Aa=43617.29115
4050  Bb=150.6131
4060  GOSUB Thermo
4070  !
4080  !
4090  E(26)=(E(25)+E(27))/2               ! Thermocopule #26 is not good
4100  !
4110  !
4120  J=7                   ! STRIP # 16
4130  Ks=0                  ! ----------
4140  X(J)=16.4375+A(6)
4150  FOR I=10 TO 14
4160  T(J,I-9)=E(I)                       ! Surface Temps.
4170  Ks=Ks+E(I)
4180  NEXT I
4190  Ts(J)=Ks/5                          !  Av.  "    "
4200  B(J,2)=E(16)                        ! Back Temps.
```

```
4210  B(J,4)=E(15)
4220  GOSUB Back_temp2
4230  Tb(J)=(E(15)+E(16))/2                    ! Av.  "    "
4240  FOR I=1 TO 5
4250  GOSUB Temp
4260  !
4270  J=8                       ! STRIP # 19
4280  Ks=0                      ! ----------
4290  X(J)=19.625+A(6)
4300  FOR I=17 TO 21
4310  T(J,I-16)=E(I)                           ! Surface Temps.
4320  Ks=Ks+E(I)
4330  NEXT I
4340  Ts(J)=Ks/5                               ! Av.    "     "
4350  B(J,2)=E(23)                             ! Back Temps.
4360  B(J,4)=E(22)
4370  GOSUB Back_temp2
4380  Tb(J)=(E(22)+E(23))/2                    ! Av.    "     "
4390  FOR I=1 TO 5
4400  GOSUB Temp
4410  !
4420  J=10                      ! STRIP # 25
4430  Ks=0                      ! ----------
4440  X(J)=26+A(6)
4450  FOR I=24 TO 28
4460  T(J,I-23)=E(I)                           ! Surface Temps.
4470  Ks=Ks+E(I)
4480  NEXT I
4490  Ts(J)=Ks/5                               ! Av.    "     "
4500  B(J,2)=E(30)                             ! Back Temps.
4510  B(J,4)=E(29)
4520  GOSUB Back_temp2
4530  Tb(J)=(E(29)+E(30))/2                    ! Av.    "     "
4540  FOR I=1 TO 5
4550  GOSUB Temp
4560  !
4570  J=11                      ! STRIP # 29
4580  Ks=0                      ! ----------
4590  X(J)=30.25+A(6)
4600  FOR I=31 TO 35
4610  T(J,I-30)=E(I)                           ! Surface Temps.
4620  Ks=Ks+E(I)
4630  NEXT I
4640  Ts(J)=Ks/5                               ! Av.    "     "
4650  B(J,2)=E(37)                             ! Back Temp.
4660  B(J,4)=E(36)
4670  GOSUB Back_temp2
4680  Tb(J)=(E(36)+E(37))/2                    ! Av.    "     "
4690  FOR I=1 TO 5
4700  GOSUB Temp
4710  !
4720  !
4730  !
4740  WRITE BIN Key;12
4750  WRITE BIN Key;12
4760  !
4770  DISP " Check Thermocouples' Reading      ? "
4780  PAUSE
4790  INPUT " Is the STEADY STATE obtained ? Yes=1,No=0",Ans
4800  IF Ans=0 THEN Measurig_temps
```

```
4810  !
4820  !
4830  GOSUB Heat
4840  !
4850  !  Local span-averaged Stanton #
4860  !  based on heat rates measurements
4870  !  --------------------------------
4880  !
4890  FOR J=1 TO 12
4900  Qia=0
4910  Qca=0
4920  Qra=0
4930  Qna=0
4940  Sta=0
4950  Rav=0
4960  M=5
4970  IF (J=1) OR (J=4) OR (J=9) OR (J=12) THEN M=11
4980     FOR I=1 TO M
4990  Qia=Qia+Qi(J,I)
5000  Qca=Qca+Qc(J,I)
5010  Qra=Qra+Qr(J,I)
5020  Qna=Qna+Qn(J,I)
5030  Sta=Sta+St(J,I)
5040  Rav=Rav+Ra(J,I)
5050     NEXT I
5060  Qia(J)=Qia/M
5070  Qca(J)=Qca/M
5080  Qra(J)=Qra/M
5090  Qna(J)=Qna/M
5100  Sta(J)=Sta/M
5110  Rav(J)=Rav/M
5120  NEXT J
5130  !
5140  !
5150  OUTPUT Key USING Fmta1;A(1)
5160  OUTPUT Key;" Date      : ",B$(1)
5170  OUTPUT Key;" Operator  : ",A$(1)
5180  WRITE BIN Key;10,10
5190  GOSUB Line
5200 Fmtw1: IMAGE #"  X       U(x)     Re(x)     Z     Ts      Tb     (Ts-Te)  "
5210 Fmtw2: IMAGE #"(Ts-Tb)  Qin      Qc       Qr    Q.net    Stn(x,z) "
5220 Fmtw3: IMAGE  "Stn/Ste"
5230  OUTPUT Key USING Fmtw1
5240  OUTPUT Key USING Fmtw2
5250  OUTPUT Key USING Fmtw3
5260  OUTPUT Key;" in.     fps              in.              degree F.    "
5270  GOSUB Line
5280  !
5290  FOR J=1 TO 12
5300  !
5310  WRITE BIN Key;10
5320  OUTPUT Key USING Fmth1;X(J),U(J),Re(J)
5330 Fmth1:  IMAGE  #,2D.4D,2X,2D.2D,2X,7D,2X
5340  !
5350  M=5
5360  IF (J=1) OR (J=4) OR (J=9) OR (J=12) THEN M=11
5370  !
5380     FOR I=1 TO M
5390  IF M=11 THEN Z(J,I)=6-I
5400  IF M=5 THEN Z(J,I)=2*(3-I)
```

```
5410  OUTPUT Key USING Fmth2;Z(J,I),T(J,I),B(J,I),Tse(J,I),T(J,I)-B(J,I)
5420 Fmth2:  IMAGE #,M2D,2X,3D.2D,2X,3D.2D,2X,3D.2D,2X,3D.3D,2X
5430  OUTPUT Key USING Fmth3;Qi(J,I),Qc(J,I),Qr(J,I),Qn(J,I),St(J,I),Re(J,I)
5440 Fmth3:  IMAGE   2D.3D,2X,2D.3D,2X,2D.3D,2X,2D.3D,2X,D.6D,2X,2D.3D
5450  IF I=M THEN GOTO 5500
5460  OUTPUT Key USING Fmth4
5470 Fmth4: IMAGE #,25X
5480        NEXT I
5490  !
5500  NEXT J
5510  !
5520  !
5530  WRITE BIN Key;10
5540  GOSUB Line
5550  WRITE BIN Key;10,10,10
5560  OUTPUT Key USING Fmtal;A(1)
5570  !
5580  ! Now for "  Reduced Run Data "
5590  ! -------------------------
5600  !
5610  WRITE BIN Key;12
5620  OUTPUT Key USING Fmtal;A(1)
5630  OUTPUT Key;" Date      : ",B$(1)
5640  OUTPUT Key;" Operator : ",A$(1)
5650  WRITE BIN Key;10,10
5660  OUTPUT Key;"================================================================"
5670  OUTPUT Key;"                         Reduced Run Data                       "
5680  OUTPUT Key;"----------------------------------------------------------------"
5690  OUTPUT Key;"  x        Ts-To   Qin       Rex       St(x)      St(x)     St(x)"
5700  OUTPUT Key;"  in.       oF     BTU/hr              Turb.      Lam.      Meas."
5710  OUTPUT Key;"================================================================"
5720  FOR J=1 TO 12
5730  OUTPUT Key USING Fmtr;X(J),Tsa(J),Qia(J),Re(J),Ste(J),Sle(J),Sta(J),Rav(J)
5740 Fmtr: IMAGE /,2D.4D,2X,3D.2D,2X,2D.3D,2X,7D,3(3D.6D),2X,2D.3D
5750  NEXT J
5760  WRITE BIN Key;10
5770  OUTPUT Key;"================================================================"
5780  !
5790  !
5800  DISP " Check the Temperatures, Heat Loss & Measurement "
5810  PAUSE
5820  INPUT "Are Temp. Measurement O.K and B.S cond. ? ,Yes=1 , No=0 ",N
5830  IF N=0 THEN GOTO 610
5840  !
5850      FOR J=1 TO 12
5860  Total(J,1)=A(J)
5870  Total(J,2)=G(J)
5880  Total(J,3)=X(J)
5890  Total(J,4)=U(J)
5900  Total(J,5)=Re(J)
5910  Total(J,6)=Qia(J)
5920  Total(J,7)=Qca(J)
5930  Total(J,8)=Qra(J)
5940  Total(J,9)=Qna(J)
5950  Total(J,10)=Tsa(J)
5960  Total(J,11)=Sta(J)
5970  Total(J,12)=Rav(J)
5980  Total(J,13)=Sle(J)
5990  Total(J,14)=Ste(J)
6000      NEXT J
```

```
6010  !
6020  !        Check the Array Total (*)
6030  !
6040  WRITE BIN Key;12
6050  OUTPUT Key USING Fmtel;A(1)
6060  OUTPUT Key;" Date      : ",B$(1)
6070  OUTPUT Key;" Operator  : ",A$(1)
6080  WRITE BIN Key;10,10
6090  GOSUB Line
6100  OUTPUT Key;"                          The average result ( Total(*) ) "
6110  OUTPUT Key;"                          ------------------------------- "
6120  IMAGE #"  X       U(x)     Re(x)   (Ts-To)  Qia      Qca      Qra     Qna   "
6130  IMAGE "Stn(x)   Ratio   Sto(x) "
6140  OUTPUT Key USING 6120
6150  OUTPUT Key USING 6130
6160  OUTPUT Key;" inch     fps                  oF                  BTU/hr "
6170  GOSUB Line
6180  FOR J=1 TO 12
6190  WRITE BIN Key;10
6200  OUTPUT Key USING 6210;X(J),U(J),Re(J),Tsa(J),Qia(J),Qca(J),Qra(J),Qna(J)
6210  IMAGE #,2D.4D,2X,3D.2D,2X,7D,2X,3D.2D,2X,2D.3D,2X,2D.3D,2X,2D.3D,2X,2D.3D
6220  OUTPUT Key USING 6230;Sta(J),Rav(J),Sle(J)
6230  IMAGE D.6D,2X,2D.3D,2X,D.6D
6240  NEXT J
6250  WRITE BIN Key;10
6260  GOSUB Line
6270  WRITE BIN Key;12
6280  !
6290  !
6300  DISP " Check the array Total(*) ! . If it's O.K. ,then  RECORD DATA ,Cont"
6310  PAUSE
6320  !
6330  !  *******    Recording Data    *******
6340  !
6350  ! File Name
6360  ! ----------     for pressure gradients
6370  IF ABS(A(9))<.015 THEN Name3=1
6380  IF (ABS(A(9))>.015) AND (ABS(A(9))<.025) THEN Name3=1
6390  IF ABS(A(9))>.030 THEN Name3=1
6400  !
6410  File$="A"&VAL$(Name1)&"B"&VAL$(Name2)&"P"&VAL$(Name3)
6420  IF G(1)=0 THEN File$="LAM-"&VAL$(Name3)   ! for no-vortex data
6430  !
6440  !   RECORDING DATA :    on  DISC
6450  !
6460        MASS STORAGE IS ":F8,0"
6470        FCREATE File$,9
6480        FPRINT File$,Total(*)
6490        PROTECT File$,"DATA"
6500  !
6510  BEEP
6520  DISP " Data recorded on DISC . Now , ins. TAPE to recorde on it too "
6530  PAUSE
6540  !
6550        MASS STORAGE IS ":T15 "
6560        CREATE File$,9
6570        ASSIGN #1 TO File$
6580        PRINT #1;Total(*)
6590        PROTECT File$,"DATA"
6600  BEEP
```

```
6610  DISP " Data recorded on TAPE too"
6620  PAUSE
6630  !
6640  DISP " If the Uo(o),(dU/dX),and (dP/dx) are changed , Change FILE NAME"
6650  PAUSE
6660  !
6670  !
6680  INPUT " Is any of  [ (Uo) or (dP/dX) ] changed ? ,Yes=1, No=0",N
6690  IF N=1 THEN GOTO 610
6700  DISP " Turn the D.C. power supply OFF !!!!! "
6710  PAUSE
6720  DISP " The CLOSED position & turn OFF the A.C Power of Wind Tunnel"
6730  PAUSE
6740  !
6750  !
6760  STOP      !                 **************************
6770  END       ! ***************! End of the Main Program !***************
6780  !                           **************************
6790  !
6800  ! ------------------------------------------------
6810  !  The next subprogram is for measuring the Current .
6820  ! ------------------------------------------------
6830 Amper:  !
6840  OUTPUT 722;"F1R3T2M3A1H1"
6850  OUTPUT 709 USING 6860;9
6860  IMAGE #,"C",ZZ,"E"
6870  K=0
6880  !
6890  FOR N=1 TO 20
6900  TRIGGER 722
6910  ENTER 722 BINT;E
6920  K=K+E
6930  NEXT N
6940  !
6950  E=K/20
6960  A(10)=5/.05*E                   !  Current Is ,amp.,[ Using Shunt Resis.]
6970  RETURN
6980  !
6990  ! ---------------------------------------------------
7000  !  The next Subprogram is for measuring the Temperature .
7010  ! ---------------------------------------------------
7020  !
7030 Thermo: !
7040  OUTPUT 722;"F1R3T2M3A1H1"
7050  !
7060  FOR I=A TO B
7070  OUTPUT 709 USING 7080;I
7080  IMAGE #,"C",ZZ,"E"
7090  K=0
7100  FOR N=1 TO 10
7110  TRIGGER 722
7120  ENTER 722 BINT;F
7130  K=K+E
7140  NEXT N
7150  E=K/10
7160  E(I)=Aa*E+Bb
7170  NEXT I
7180  !
7190  RETURN
7200  !
```

```
7210  ! ------------------------------------------------------------------
7220  !  The next subprogram is renumbered back temp.for strips # 1,7,22&33
7230  ! ------------------------------------------------------------------
7240 Back_temp1:  I=0
7250  Slop=(E(I+2)-E(I+3))/6
7260  A=E(I+3)
7270  B(J,1)=A-Slop
7280  B(J,2)=A+Slop
7290  B(J,3)=A+3*Slop
7300  B(J,4)=A+5*Slop
7310  Slop=(E(I+1)-E(I+2))/6
7320  A=E(I+2)
7330  B(J,5)=A+Slop
7340  B(J,6)=A+3*Slop
7350  B(J,7)=A+5*Slop
7360  Slop=(E(I)-E(I+1))/6
7370  A=E(I+1)
7380  B(J,8)=A+Slop
7390  B(J,9)=A+3*Slop
7400  B(J,10)=A+5*Slop
7410  B(J,11)=A+7*Slop
7420  RETURN
7430  !
7440  ! ----------------------------------------------------------------------
7450  !  The next subprogram is for back temp. strips'#3,5,10,13,,16,19,25&29
7460  ! ----------------------------------------------------------------------
7470 Back_temp2: !
7480  B(J,1)=T(J,1)-(T(J,2)-B(J,2))
7490  B(J,3)=(B(J,2)+B(J,4))/2
7500  B(J,5)=T(J,5)-(T(J,4)-B(J,4))
7510  RETURN
7520  ! ..........
7530 Temp:  !
7540  OUTPUT Key USING 7550;J,I,T(J,I),B(J,I),T(J,I)-B(J,I),T(J,I)-A(4)
7550  IMAGE 5X,2D,2X,2D,4X,M4D.2D,2X,M4D.2D,2X,M4D.2D,2X,M4D.2D
7560  NEXT I
7570  WRITE BIN Key;10
7580  OUTPUT Key USING 7590;Ts(J)
7590  IMAGE 5X," Ts*(J) = ",M4D.2D
7600  OUTPUT Key USING 7610;Tb(J)
7610  IMAGE 5X," Tb*(J) = ",M4D.2D
7620  WRITE BIN Key;10,10
7630  RETURN
7640  ! ..........
7650  ! ----------------------------------------------------------------------
7660  !  The next subprogram is for the heat equations & St(x,z) calculation
7670  ! ----------------------------------------------------------------------
7680 Heat: !
7690  !
7700  Tavr=(A(3)+A(4))/2
7710  !
7720  !                    PROPERTIES OF AIR
7730  !                    =================
7740  Cp=.2231+3.42*10^(-5)*(Tavr+459.67)-2.93*10^(-9)*(Tavr+459.67)^2
7750  Ka=.0020493+2.43*10^(-5)*(Tavr+459.67)          !  BTU/(hr.Ft.oF)
7760  Vis=.0118205+6.09*10^(-5)*(Tavr+459.67)         !  Ibm/(hr.Ft)
7770  !
7780  !
7790  FOR J=1 TO 12
7800  !
```

```
7810 U(J)=A(7)+A(8)*X(J)/12                            ! U(x)=Uo+[dU/dX]*X  ; fps
7820 Kvis=(.00202*(Tavr+459.67)-.47862)/3600          !    Ft2/Sec
7830 Pra=.78586-.00014*(Tavr+459.67)                  !    Pr.#.
7840 Re(J)=U(J)*(X(J)/12)/Kvis                        ! Reynolds Number
7850 Tsa(J)=Ts(J)-A(4)
7860 Slo(J)=.453*(1-(A(6)/X(J))^.75)^(-.333)/(Re(J)^.5*Pra^.666)  ! Laminar
7870 Sto(J)=.0307*(1-(A(6)/X(J))^.9)^(-.111)/(Re(J)^.2*Pra^.400)  ! Turbulent
7880 ! ....................................................................
7890 !  The Span-averaged Measured STANTON # for each Strip ; St(x)m.av
7900 !          based on the span-averaged surface temperature
7910 !          ( for the plate without vortex generators)
7920 ! ....................................................................
7930 !
7940 ! R=.25*(1+.00023*(Ts(J)-68))
7950 ! Qia(J)=A(10)^2*R*3.413
7960 ! Qca(J)=.10155*.083*(Ts(J)-Tb(J))*(12/.227)
7970 ! Dtr=(Ts(J)+460)^4-(A(3)+460)^4
7980 ! Qra(J)=.147*10^(-8)*.45*.083*Dtr
7990 ! Qna(J)=Qia(J)-Qca(J)-Qra(J)
8000 ! Sta(J)=Qna(J)*(X(J)/12)/(.083*Tsa(J)*Ka*Re(J)*Pra)   ! Meas. Av. St. #
8010 ! Rav(J)=Sta(J)/Slo(J)                  ! [ St(x)VG / St(x)o ] <-- Av. Ratio
8020 !
8030 ! ....................................................................
8040 !  The Local Measured STANTON #'s for each Strip  ;   St(x,z)m
8050 ! ....................................................................
8060 !
8070 IF J=1 THEN M=11
8080 IF J=2 THEN M=5
8090 IF J=3 THEN M=5
8100 IF J=4 THEN M=11
8110 IF J=5 THEN M=5
8120 IF J=6 THEN M=5
8130 IF J=7 THEN M=5
8140 IF J=8 THEN M=5
8150 IF J=9 THEN M=11
8160 IF J=10 THEN M=5
8170 IF J=11 THEN M=5
8180 IF J=12 THEN M=11
8190 !
8200      FOR I=1 TO M
8210 !
8220 R=.25*(1+.00023*(T(J,I)-68))              ! Strip Reis. function of Temp
8230 Qi(J,I)=A(10)^2*R*3.413                   ! Heat input = I^2*R(t)*Con ;BTU/hr
8240 IF T(J,I)<B(J,I) THEN B(J,I)=T(J,I)-.2
8250 Qc(J,I)=.10*.083*(T(J,I)-B(J,I))*(12/.227)  !  Conduction loss ;BTU/hr
8260 Dtr=(T(J,I)+460)^4-(A(3)+460)^4              ! Radiation's Temp. diff.
8270 Qr(J,I)=.174*10^(-8)*.45*.083*Dtr       ! Radiation loss= c*e*A*Dtr ;BTU/hr
8280 Qn(J,I)=Qi(J,I)-Qc(J,I)-Qr(J,I)         ! Net Heat,(Forced Convection); "
8290 Tso(J,I)=T(J,I)-A(4)                    !  (Ts - To)               ; oF
8300 St(J,I)=Qn(J,I)*(X(J)/12)/(.083*Tso(J,I)*Ka*Pra*Re(J))
8310 ! * St(x,z)= [ Nu(x,z)/Re(x)*Pr] = [ h(x,z)/Ro*Cp*Uo(x) ]
8320 !                          where ;  h(x,z) = [ Qn/A*(Ts-To) ]
8330 !
8340 Ra(J,I)=St(J,I)/Slo(J)              ! Ratio = St(x,z)with VG /St(x)without
8350 !
8360      NEXT I
8370 !
8380 NEXT J
8390 !
8400 RETURN
```

```
8410  !
8420  ! ------------------------------------------------------------
8430  !  The next subprogram is the vortex generators' cofiguration .
8440  ! ------------------------------------------------------------
8450 Vortex:  !
8460  INPUT " Angle of incidence                     ?",G(1)
8470  INPUT " Transverse Pitch          , inch , ?",G(2)
8480  INPUT " Height of a protrusion   , inch , ?",G(3)
8490  INPUT " Length of a protrusion   , inch , ?",G(4)
8500  INPUT " Protrusion's  thickness , inch , ?",G(5)
8510  INPUT " The number of V.Generators.        ?",G(6)
8520  !     Order for the Recoding Files
8530  !     --------------------------
8540     IF G(3)=.0625 THEN Name1=1
8550     IF G(3)=.125 THEN Name1=2
8560     IF G(3)=.25 THEN Name1=3
8570     IF G(2)=4 THEN Name2=4
8580     IF G(2)=3 THEN Name2=3
8590     IF G(2)=2 THEN Name2=2
8600     IF G(2)=1 THEN Name2=1
8610     IF G(2)=.75 THEN Name2=0
8620  RETURN
8630  !
8640 Write_vgs:  !
8650  OUTPUT Key;"  Using Rectangular Counter Rotating Vortex Generators "
8660  OUTPUT Key;" ======================================================= "
8670  OUTPUT Key USING Fmtg1;G(1)
8680  OUTPUT Key USING Fmtg2;G(2)
8690  OUTPUT Key USING Fmtg3;G(3)
8700  OUTPUT Key USING Fmtg4;G(4)
8710  OUTPUT Key USING Fmtg5;G(5)
8720  OUTPUT Key USING Fmtg6;G(6)
8730 Fmtg1:  IMAGE /,"Angle betn. a V.G's and  plate axis ; degree ; =",2D.2D
8740 Fmtg2:  IMAGE   "Transverse pitch betn. V.G's blades ;  inch  ; =",2D.2D
8750 Fmtg3:  IMAGE   "Height of V.G's blades              ;  inch  ; =",2D.3D
8760 Fmtg4:  IMAGE   "Length of V.G's blades              ;  inch  ; =",2D.2D
8770 Fmtg5:  IMAGE   "Thickness of V.G's blades           ;  inch  ; =",2D.3D
8780 Fmtg6:  IMAGE   "The number of Vortex Generators                =",2D
8790  RETURN
8800  !
8810  ! ------------------
8820 Line:  !
8830  FOR N=1 TO 15
8840  OUTPUT Key USING 8850
8850  IMAGE #,"======="
8860  NEXT N
8870  OUTPUT Key USING 8880
8880  IMAGE "======="
8890  RETURN
8900  ! ------------------
```

XI. APPENDIX C

A. Error Analysis

In any experiment, uncertainties in the raw data can occur due to two types of errors: systematic and random. By careful operating procedure, random errors can be avoided or minimized. Systematic errors always exist in data acquisition but can be minimized by proper experimental design. Hence, to estimate the accuracy of experimental data, it is necessary to quantify the total uncertainty through the use of statistics in a propagation-of-error analysis for single sample experiments, such as that proposed by Kline and McClintock [19].

The expression of the uncertainty in a calculated results found from a linear function of variables is

$$W_\phi = \left\{ \sum_{i=1}^{n} \left[\frac{\partial \phi}{\partial X_i} W_{X_i} \right]^2 \right\}^{1/2} \tag{25}$$

where W_ϕ is the uncertainty in any quantity ϕ, X_i is any of n parameters of which quantity ϕ is a function, and W_{X_i} are the uncertainty limits placed on the several variable parameters by the experimenter.

In the following calculations, it has been assumed that the uncertainties in the properties of air are negligible. Uncertainties given below for the instruments used in this investigation were obtained from the manufacturers' catalogs for instruments.

The uncertainty in the dc voltage reading for voltage measurements of thermocouples and the hot-film anemometer is, for W_E = 0.003% of reading + 0.0004 of range,

$$W_E = \left(\frac{0.003}{100} \times 0.002\right) + \left(\frac{0.0004}{100} \times 1\right) V = 0.000004\ V$$

The uncertainty in the dc voltage measurement of the pressure transducer is for W_E = 0.002% of reading + 0.001% of range,

$$W_{E_p} = \left(\frac{0.002}{100} \times 3\right) + \left(\frac{0.001}{100} \times 10\right) V$$

$$W_{E_p} = 0.00016\ V$$

The uncertainty in the resistance measurement is, for W_R = 0.0025% of reading + 0.0004% of range,

$$W_R = \left(\frac{0.0025}{100} \times 0.15\right) + \left(\frac{0.0004}{100} \times 1\right)$$

$$W_R = 0.000008\ \text{kr}$$

The uncertainty in ac voltage measurement is, for W_e = 0.04% of reading + 40 digits

$$W_e = \left(\frac{0.04}{100} \times 0.1\right) + \left(\frac{0.04}{100} \times 1\right)$$

$$W_e = 0.00008\ V$$

Uncertainties for the following cases were obtained from the calibration data:

Temperature measurement using thermocouples = 0.2°F

Pressure measurement using pressure transducer = 0.01 in. water

Uncertainty in the mercury barometer = 0.01 in. Hg.

Current measurement using shunt resistance = 0.02 amp.

The free-stream density ρ_a was calculated from equation (12). The uncertainty in ρ_a using equation (25) is given by

$$W_{\rho_a} = \frac{1}{53.35\ T_o}\left\{\left[70.731\ W_{p_{atm}}\right]^2 + \left[5.2024\ W_{p_{s(x)}}\right]^2 + \left[\frac{(70.731\ p_{atm} - 5.2024\ p_{s(x)})}{T_o}\ W_{T_o}\right]^2\right\}^{1/2}$$

p_{atm} = 29.011 in. Hg

$p_{s(x)}$ = 0.115 in. of water

T_o = 530.27°R

ρ_a = 0.0725 lb_m/ft^3

W_{ρ_a} = 0.000025 lb_m/ft^3 or ± 0.0345%

The local free-stream velocity was calculated from equation (13). Then, the uncertainty in $U_{o(x)}$ is calculated using equation (25), given by

$$W_{U_{o(x)}} = U_{o(x)}\left\{\left[\frac{W_{\Delta p}}{2\Delta p}\right]^2 + \left[\frac{W_{\rho_a}}{2\rho_a}\right]^2\right\}^{1/2}$$

where $\Delta p = p_o - p_{s(x)}$

Δp = 0.047 in. of water

ρ_a = 0.0725 lb_m/ft^3

$U_{o(x)} = 14.03$ fps

$W_{U_{o(x)}} = 0.14927$ fps or ± 1.064%

The local Reynolds number was calculated from equation (15). The analysis showed that the uncertainty in the Reynolds number was dependent almost exclusively on the uncertainty in the velocity measurement. Because of small dependence on the kinematic viscosity ν_a, this variable was neglected in the computations. Then, from equation (25)

$$W_{Re_{(x)}} = Re_{(x)} \left\{ \left[\frac{W_{U_{o(x)}}}{U_{o(x)}} \right]^2 + \left[\frac{W_x}{x} \right]^2 \right\}^{\frac{1}{2}}$$

$x = 9.125$ in.

$U_{o(x)} = 14.03$ fps

$Re_{(x)} = 63646$

$W_{Re_{(x)}} = 691.37$ or ± 1.086%

The relation used to obtain the generated power on the local strip surface was given by equation (6). Then, the uncertainty in Q is

$$W_Q = Q \left\{ \left[\frac{2W_I}{I} \right]^2 + \left[\frac{W_{R_s}}{R_s} \right]^2 \right\}^{\frac{1}{2}}$$

$I = 3.0991$ amp

$R_s = 0.2512$ ohm

$Q = 8.235$ Btu/hr

$W_Q = 0.345$ Btu/hr or ± 4.185%

The local conduction loss was calculated from equation (8). Then, the uncertainty in Q_c is

$$W_{Q_c} = Q_c\left\{\left[\frac{W_{A_s}}{A_s}\right]^2 + \left[\frac{W_{y_p}}{y_p}\right]^2 + \left[\frac{W_{(t_s - t_b)}}{(t_s - t_b)}\right]^2\right\}^{1/2}$$

$A_s = 0.083\ ft^2$

$y_p = 0.227$ in.

$(t_s - t_b) = 1.622°F$

$Q_c = 1.284$ Btu/hr

$W_{Q_c} = 0.1952$ Btu/hr or ± 15.20%

From equation (9), the uncertainty in Q_r is

$$W_{Q_r} = Q_r\left\{\left[\frac{4T_s^3}{(T_s^4 - T_a^4)}\right]^2 + \left[\frac{4T_a^3}{(T_s^4 - T_a^4)}\right]^2 + \left[\frac{W_{A_s}}{A_s}\right]^2\right\}^{1/2}$$

$T_a = 530.27°R$

$T_s = 563.01°R$

$Q_r = 1.399$ Btu/hr

$W_{Q_r} = 0.0207$ Btu/hr or ± 1.485 %

Noting that, it has been assumed that k_p, σ and ε_s all have small enough variations in their true values that the contribution of each and total contribution of their aggregate uncertainty will be negligible. Thus from equation (10), the uncertainty in Q_n is

$$W_{Q_n} = Q_n \left\{ \left[\frac{W_Q}{Q_n} \right]^2 + \left[\frac{W_{Q_c}}{Q_c} \right]^2 + \left[\frac{W_{Q_r}}{Q_n} \right]^2 \right\}^{1/2}$$

$$Q_n = 5.551 \text{ Btu/hr}$$

$$W_{Q_n} = 0.3969 \text{ Btu/hr or } \pm 7.15\%$$

The specific heat of air was evaluated at the mean boundary layer temperature, where

$$C_p = 0.2231 + 3.42 \times 10^{-5}\, T_m - 2.93 \times 10^{-9}\, T_m^{\,2}$$

Then, the uncertainty in C_p is

$$W_{C_p} = \left\{ \left[3.42\ 10^{-5}\, W_{T_m} \right]^2 + \left[5.86 + 10^{-9}\, T_m\, W_{T_m} \right]^2 \right\}^{1/2}$$

$$T_m = 573.71°R$$

$$C_p = 0.2417 \text{ Btu/lb}_m°F$$

$$W_{C_p} = 7 \times 10^{-6} \text{ Btu/lb}_m°F \text{ or } \pm 0.0028\%$$

The local Stanton number was obtained from equation (16), and the local heat transfer coefficient was calculated from equation (11). Substituting from equation (11) into equation (16) for $h_{(x)}$, the local Stanton number is given by

$$St_{(x)} = \frac{Q_n}{A_s(t_s - t_o)\, \rho_a\, C_p\, U_{o(x)}}$$

The uncertainty in $St_{(x)}$ is

$$W_{St_{(x,z)}} = St_{(x,z)} \left\{ \left[\frac{W_{Q_n}}{Q_n}\right]^2 + \left[\frac{W_{A_s}}{A_s}\right]^2 + \left[\frac{W_{(t_s - t_o)}}{(t_s - t_o)}\right]^2 + \left[\frac{W_{\rho_a}}{\rho_a}\right]^2 + \left[\frac{W_{U_{o(x)}}}{U_{o(x)}}\right]^2 + \left[\frac{W_{C_p}}{C_p}\right]^2 \right\}^{\frac{1}{2}}$$

$Q_n = 5.551$ Btu/hr

$(t_s - t_o) = 21.36°F$

$\rho_a = 0.0725\ lb_m/ft^3$

$U_{o(x)} = 14.03$ fps

$C_p = 0.2417\ Btu/lb_m°F$

$St_{(x)} = 0.003499$

$W_{St_{(x)}} = 0.000259$ or $\pm$ 7.395%

The uncertainty for the sensitivity factor of the hot-film was determined from the calibration data. The effective mean air velocity was obtained from equation (4). The uncertainty in U_m is

$$W_{U_m} = U_m\left[\left(\frac{W_{E_m}}{E_m}\right)^2 + \left(\frac{W_S}{S}\right)^2\right]^{\frac{1}{2}}$$

$S_m = 0.3357$

$W_S = 0.0084$

$E_m = 6.339$ Volt

$U_m = 18.883$ fps

$W_{U_m} = 0.4725$ fps or ± 2.5%

The uncertainty in u' is

$$W_{u'} = u'\left[\left(\frac{W_e}{e'}\right)^2 + \left(\frac{W_S}{S}\right)^2\right]^{\frac{1}{2}}$$

$e' = 0.05$ Volt

$u' = 0.1489$ fps

$W_{u'} = 0.0037$ fps or ± 2.5%

The local turbulence intensity was obtained from

$$Tu = \frac{u'}{U_m}$$

Then the uncertainty in Tu is given by

$$W_{Tu} = Tu\left\{\left(\frac{W_{u'}}{u'}\right)^2 + \left(\frac{W_{U_m}}{U_m}\right)^2\right\}^{\frac{1}{2}} \qquad (26)$$

Inside the boundary layer, close to the plate surface, for a measurement point the data were

$U_m = 14.3582$ fps

$u' = 1.618$ fps

$Tu = 0.1127$

$W_{Tu} = 0.00448$ or ± 3.331%

For the free-stream turbulence, the data were

U_m = 18.883 fps

u' = 0.1489 fps

Tu = 0.0079

Then, from equation (26)

Tu = 0.0002 or ± 2.497%

XII. APPENDIX D

A. Tabular Data

Table D.1. Measured span-averaged Stanton number behind a row of counter-rotating vortex generator blades

Free-stream pressure gradient = 0.0
Height of vortex blade = 0.0625 in.

X	Space between vortex blades, in.							
	0.75		1.0		2.0		4.0	
in.	Re(x)	St(x)	Re(x)	St(x)	Re(x)	St(x)	Re(x)	St(x)
4.88	22629	0.00598	23836	0.00616	23955	0.00457	25341	0.00425
7.00	32769	0.00430	34505	0.00370	34670	0.00300	36634	0.00276
9.13	43076	0.00367	45342	0.00310	45552	0.00258	48076	0.00244
11.25	53551	0.00330	56349	0.00314	56599	0.00280	59668	0.00250
14.44	69577	0.00346	73176	0.00296	73482	0.00265	77337	0.00240
17.63	85980	0.00366	90382	0.00317	90738	0.00297	95342	0.00209
20.81	102760	0.00306	107970	0.00253	108367	0.00265	113684	0.00182
24.00	119916	0.00349	125937	0.00302	126370	0.00296	132363	0.00209
27.19	137450	0.00316	144284	0.00305	144747	0.00265	151378	0.00226
30.38	155360	0.00321	163012	0.00301	163497	0.00275	170731	0.00210
34.63	179826	0.00315	188574	0.00309	189079	0.00292	197057	0.00218

Table D.2. Measured span-averaged Stanton number behind a row of counter-rotating vortex generator blades

Free-stream pressure gradient = 0.0
Height of vortex blade = 0.125 in.

X	Space between vortex blades, in.							
	0.75		1.0		2.0		4.0	
in.	Re(x)	St(x)	Re(x)	St(x)	Re(x)	St(x)	Re(x)	St(x)
4.88	28635	0.00437	28185	0.00433	26830	0.00430	30628	0.00389
7.00	41376	0.00312	40720	0.00324	38767	0.00287	44224	0.00285
9.13	54275	0.00266	53407	0.00270	50850	0.00269	57969	0.00245
11.25	67332	0.00254	66246	0.00251	.63080	0.00258	71863	0.00206
14.44	87212	0.00245	85788	0.00244	81699	0.00269	92983	0.00222
17.63	107447	0.00263	105670	0.00217	100649	0.00261	114439	0.00195
20.81	128036	0.00247	125894	0.00196	119928	0.00228	136229	0.00183
24.00	148980	0.00281	146459	0.00206	139537	0.00243	158354	0.00196
27.19	170278	0.00266	167365	0.00230	159476	0.00213	180314	0.00182
30.38	191931	0.00265	188611	0.00216	179744	0.00217	203610	0.00166
34.63	221353	0.00283	217471	0.00236	207283	0.00253	234525	0.00207

Table D.3. Measured span-averaged Stanton number behind a row of counter-rotating vortex generator blades

Free-stream pressure gradient = 0.0
Height of vortex blade = 0.25 in.

X	Space between vortex blades, in.							
	0.75		1.0		2.0		4.0	
in.	Re(x)	St(x)	Re(x)	St(x)	Re(x)	St(x)	Re(x)	St(x)
4.88	28727	0.00496	28354	0.00499	25511	0.00456	27581	0.00392
7.00	41452	0.00338	40951	0.00340	36857	0.00319	39846	0.00349
9.13	54298	0.00271	53692	0.00282	48340	0.00312	52257	0.00313
11.25	67268	0.00248	66577	0.00233	59959	0.00282	64815	0.00271
14.44	86952	0.00274	86175	0.00245	77645	0.00259	83928	0.00286
17.63	106912	0.00275	106097	0.00211	95638	0.00246	103372	0.00262
20.81	127147	0.00256	126343	0.00206	113939	0.00215	123146	0.00250
24.00	147659	0.00283	146914	0.00205	132549	0.00230	143251	0.00254
27.19	168446	0.00270	167810	0.00231	151466	0.00233	163686	0.00238
30.38	189510	0.00275	189029	0.00206	170691	0.00219	184452	0.00220
34.63	218023	0.00295	217827	0.00259	196803	0.00239	212655	0.00236

Table D.4. Measured span-averaged Stanton number behind a row of counter-rotating vortex generator blades

Free-stream pressure gradient = - 0.02 lb_f/ft^3
Height of vortex blade = 0.0625 in.

X	Space between vortex blades, in.							
	0.75		1.0		2.0		4.0	
in.	Re(x)	St(x)	Re(x)	St(x)	Re(x)	St(x)	Re(x)	St(x)
4.88	33443	0.00446	33431	0.00432	33657	0.00409	34242	0.00426
7.00	48447	0.00376	48414	0.00326	48734	0.00280	49565	0.00292
9.13	63709	0.00317	63646	0.00263	64057	0.00250	65130	0.00255
11.25	79230	0.00298	79128	0.00278	79626	0.00262	80935	0.00234
14.44	102996	0.00313	102817	0.00284	103442	0.00267	105096	0.00244
17.63	127344	0.00306	127066	0.00285	127812	0.00266	129799	0.00228
20.81	152273	0.00301	151876	0.00253	152735	0.00266	155045	0.00209
24.00	177784	0.00310	177246	0.00288	178213	0.00287	180834	0.00228
27.19	203877	0.00286	203177	0.00273	204244	0.00259	207165	0.00229
30.38	230551	0.00289	229669	0.00277	230830	0.00261	234039	0.00220
34.63	267022	0.00331	265863	0.00274	267140	0.00264	270715	0.00228

Table D.5. Measured span-averaged Stanton number behind a row of counter-rotating vortex generator blades

Free-stream pressure gradient = - 0.02 lb_f/ft^3
Height of vortex blade = 0.125 in.

X	Space between vortex blades, in.							
	0.75		1.0		2.0		4.0	
in.	Re(x)	St(x)	Re(x)	St(x)	Re(x)	St(x)	Re(x)	St(x)
4.88	36574	0.00400	35763	0.00385	36581	0.00379	36921	0.00313
7.00	52914	0.00291	51739	0.00271	52903	0.00252	53412	0.00247
9.13	69496	0.00247	67951	0.00255	69454	0.00250	70143	0.00217
11.25	86319	0.00230	84398	0.00233	86233	0.00245	87115	0.00181
14.44	112005	0.00234	109510	0.00214	111831	0.00218	113025	0.00208
17.63	138235	0.00254	135151	0.00194	137943	0.00203	139476	0.00174
20.81	165008	0.00251	161321	0.00204	164570	0.00191	166470	0.00168
24.00	192323	0.00284	188021	0.00219	191711	0.00201	194005	0.00180
27.19	220182	0.00260	215250	0.00248	219367	0.00182	222082	0.00155
30.38	248584	0.00262	243008	0.00257	247537	0.00170	250701	0.00151
34.63	287298	0.00270	280843	0.00269	285897	0.00200	289703	0.00178

Table D.6. Measured span-averaged Stanton number behind a row of counter-rotating vortex generator blades

Free-stream pressure gradient = - 0.02 lb_f/ft^3
Height of vortex blade = 0.25 in.

X	Space between vortex blades, in.							
	0.75		1.0		2.0		4.0	
in.	Re(x)	St(x)	Re(x)	St(x)	Re(x)	St(x)	Re(x)	St(x)
4.88	40278	0.00418	38882	0.00434	36821	0.00380	36175	0.00338
7.00	58185	0.00316	55177	0.00315	53250	0.00322	52333	0.00305
9.13	76304	0.00252	73682	0.00240	69909	0.00272	68727	0.00270
11.25	94636	0.00250	91398	0.00214	86798	0.00257	85358	0.00235
14.44	122532	0.00256	118367	0.00210	112563	0.00242	110747	0.00252
17.63	150905	0.00274	145809	0.00189	138845	0.00237	136668	0.00231
20.81	179756	0.00275	173725	0.00199	165645	0.00225	163120	0.00220
24.00	209085	0.00293	202114	0.00253	192963	0.00223	190105	0.00221
27.19	238892	0.00277	230977	0.00276	220798	0.00222	217621	0.00208
30.38	269177	0.00279	260314	0.00285	249150	0.00190	245669	0.00183
34.63	310300	0.00284	300166	0.00287	287758	0.00241	283894	0.00206

Table D.7. Measured span-averaged Stanton number behind a row of counter-rotating vortex generator blades

Free-stream pressure gradient = $-0.04\ lb_f/ft^3$
Height of vortex blade = 0.0625 in.

X	Space between vortex blades, in.							
	0.75		1.0		2.0		4.0	
in.	Re(x)	St(x)	Re(x)	St(x)	Re(x)	St(x)	Re(x)	St(x)
4.88	49502	0.00385	49020	0.00401	49780	0.00303	50746	0.00261
7.00	71625	0.00328	70933	0.00293	72009	0.00214	73387	0.00218
9.13	94079	0.00276	93177	0.00265	94561	0.00206	96344	0.00188
11.25	116864	0.00284	115753	0.00267	117434	0.00224	119618	0.00157
14.44	151661	0.00298	150237	0.00298	152348	0.00238	155122	0.00184
17.63	187203	0.00283	185466	0.00304	187986	0.00227	191338	0.00161
20.81	223489	0.00261	221441	0.00283	224348	0.00237	228266	0.00164
24.00	260520	0.00285	258160	0.00300	261435	0.00250	265906	0.00182
27.19	298295	0.00262	295625	0.00278	299247	0.00246	304257	0.00216
30.38	336814	0.00263	333834	0.00265	337783	0.00241	343321	0.00218
34.63	389332	0.00257	385940	0.00281	390292	0.00251	396513	0.00238

Table D.8. Measured span-averaged Stanton number behind a row of counter-rotating vortex generator blades

Free-stream pressure gradient = - 0.04 lb_f/ft^3
Height of vortex blade = 0.125 in.

X	Space between vortex blades, in.							
	0.75		1.0		2.0		4.0	
in.	Re(x)	St(x)	Re(x)	St(x)	Re(x)	St(x)	Re(x)	St(x)
4.88	51047	0.00355	52526	0.00342	52458	0.00300	51395	0.00209
7.00	73826	0.00278	75964	0.00240	75882	0.00247	74318	0.00213
9.13	96924	0.00240	99731	0.00203	99645	0.00213	97556	0.00188
11.25	120343	0.00237	123827	0.00208	123747	0.00190	121110	0.00166
14.44	156070	0.00259	160588	0.00178	160535	0.00195	157033	0.00179
17.63	192517	0.00295	198090	0.00165	198086	0.00199	193666	0.00167
20.81	229684	0.00290	236332	0.00210	236399	0.00179	231008	0.00155
24.00	267571	0.00297	275314	0.00253	275475	0.00195	269061	0.00168
27.19	306178	0.00263	315036	0.00249	315313	0.00170	307824	0.00179
30.38	345505	0.00275	355499	0.00247	355913	0.00173	347297	0.00158
34.63	399060	0.00300	410601	0.00264	411233	0.00210	401032	0.00176

Table D.9. Measured span-averaged Stanton number behind a row of counter-rotating vortex generator blades

Free-stream pressure gradient = - 0.04 lb_f/ft^3
Height of vortex blade = 0.25 in.

X	Space between vortex blades, in.							
	0.75		1.0		2.0		4.0	
in.	Re(x)	St(x)	Re(x)	St(x)	Re(x)	St(x)	Re(x)	St(x)
4.88	50828	0.00396	49667	0.00386	49804	0.00367	48767	0.00291
7.00	73487	0.00311	71823	0.00264	72009	0.00279	70551	0.00266
9.13	96453	0.00278	94287	0.00238	94514	0.00250	92654	0.00235
11.25	119724	0.00239	117057	0.00207	117321	0.00226	115076	0.00210
14.44	155205	0.00296	151790	0.00238	152094	0.00215	149308	0.00228
17.63	191375	0.00311	187214	0.00225	187545	0.00210	184259	0.00213
20.81	228232	0.00322	223329	0.00251	223672	0.00210	219929	0.00201
24.00	265779	0.00315	260137	0.00287	260475	0.00206	256317	0.00202
27.19	304013	0.00290	297635	0.00282	297956	0.00220	293424	0.00203
30.38	342936	0.00293	335826	0.00283	336113	0.00186	331250	0.00185
34.63	395904	0.00320	387822	0.00282	388042	0.00245	382802	0.00201